RESOLUTION OF THE PAIR-WISE ALLOSTERIC INTERACTIONS FOUND IN PHOSPHOFRUCTOKINASE FROM *Bacillus stearothermophilus*

A Dissertation

by

ALLISON DAWN ORTIGOSA

Submitted to the Office of Graduate Studies of
Texas A&M University
in partial fulfillment of the requirements for the degree of

DOCTOR OF PHILOSOPHY

August 2003

Major Subject: Biochemistry

RESOLUTION OF THE PAIR-WISE ALLOSTERIC INTERACTIONS

FOUND IN PHOSPHOFRUCTOKINASE FROM *Bacillus stearothermophilus*

A Dissertation

by

ALLISON DAWN ORTIGOSA

Submitted to Texas A&M University
in partial fulfillment of the requirements
for the degree of

DOCTOR OF PHILOSOPHY

Approved as to style and content by:

Gregory D. Reinhart (Chair of Committee)	Arthur E. Johnson (Member)
Ryland Young (Member)	Andy C. LiWang (Member)
Gregory D. Reinhart (Head of Department)	

August 2003

Major Subject: Biochemistry

ABSTRACT

Resolution of the Pair-Wise Allosteric Interactions Found in Phosphofructokinase from *Bacillus stearothermophilus*. (August 2003)

Allison Dawn Ortigosa, B.A., Kalamazoo College

Chair of Advisory Committee: Dr. Gregory D. Reinhart

Phosphofructokinase from *Bacillus stearothermophilus* (BsPFK) is a homotetrameric enzyme with an average of one active site and one allosteric site per subunit. BsPFK is inhibited by phosphoenolpyruvate (PEP) and how this inhibitory signal is propagated throughout the enzyme is the main question we address through this investigation. By possessing a total of eight binding sites, a potential for twenty-eight total pair-wise allosteric interactions result within BsPFK, ten of which are unique. Of these ten interactions, four are heterotropic interactions, or interactions between unlike binding sites, while the remaining six interactions are homotropic interactions, or interactions between like binding sites. Thus, to address the question of how BsPFK is inhibited by PEP, each of these ten interactions needs to be quantified and their roles in the inhibition process assessed.

In order to quantify the roles of the 10 allosteric interactions, we created, purified and characterized several different hybrid enzymes by using site-directed mutagenesis to reduce the number of native active sites and native allosteric sites to permit the isolation of specific allosteric interaction(s). Through the creation and isolation of 1:3 hybrid enzymes, in which one native

active site and one native allosteric site remain, each of the four heterotropic interactions were characterized. Moreover, through the creation and isolation of the 2:2 hybrid enzymes, in which two native active sites and two native allosteric sites remain, characterization of the remaining six homotropic interactions was performed. Utilizing a linked function approach to quantify the heterotropic and homotropic effects for each hybrid enzyme, we determined that 5 to 6 of the ten pair-wise allosteric interactions found in BsPFK are involved in the inhibition process depending upon pH.

More importantly however, our data provides definitive results that the traditional two-state models used to describe an allosteric effect are not sufficient to describe the allosteric effect measured for BsPFK. Rather, our results show that the linked function approach is a more appropriate way to unambiguously measure the nature and magnitude of an allosteric effect. Moreover, this approach can also be used to explain the allosteric behavior of a dimeric enzyme.

DEDICATION

I would like to dedicate this work to many people, as my journey through life and this whole "Ph.D. process" has not been alone. First and foremost, to my Mom and Dad (mama and papa): at no point have you guys ever let me think I could not achieve anything I set my mind to, and I only hope that Jordan (and our other children…) will have that same unfailing resolve to do anything they want in their lifetimes. Thank you for all that you are and all that you have done for me. To Grandma: words cannot even explain how happy I am that you have not only seen me become a Dr., but also a mother. Your example will forever be something I will follow and I am sure Grandpa is looking down with a smile from above. Next, to Bisty: thanks for being such an inspiration to me all these years and showing me first-hand not only the power of science, but the power of faith. You continue to provide a love and friendship for me that is unending. To Jordan, my pumpkin-pie: you have made my world such a better place and words could never begin to express how much your smile, your laugh and your love have helped me through the end of this Ph.D. journey. And lastly, to Alex, my first and only true love: thank you for standing by me, helping me, and loving me through this whole thing, beginning to end. Having you by my side, both good times and bad, has enabled me to not only accomplish my goals, but to accomplish even more. I love you baby, more than I could ever explain on paper, and just know that I thank you for all that you have done not only for me but for our family (Payton Russell included).

ACKNOWLEDGMENTS

I would like to begin by thanking all the people in the Reinhart Lab both past and present. The Reinhart Lab is more like a family of brothers and sisters, and all of you have been instrumental in making my stay here both an enjoyable one and a memorable one. Dr. Michelle Riley-Lovingshimer, Dr. Mauricio "Chanchi" Lasagna, Dr. Aron Fenton, Dr. Jason Johnson, Dr. Jen Kimmel, Dr. Benjamin Lasseter, Monique Paricharttanakul, Jason Quinlan, and Libby Badgett, you guys are the greatest and thanks not only for your great scientific discussions but more importantly for the non-scientific ones as well. There are so many memories we have made, and I will cherish them all.

I would also like to thank those not in the Reinhart Lab, first of whom is Dr. Jonathan Sparks. Your friendship will forever be one of the greatest things I gained here at Texas A&M, and I thank you for all that you have done for me. The Pettigrew and Fitzpatrick labs for listening and providing insight into the "hybrid project" over the years at joint group meetings. Dr. Laura Busenlehner for keeping things "funny" rather than depressing as they sometimes seemed and for throwing such a great baby shower. Rachel Idol for being my resident pug lover. Mack Kuo for his assistance and expertise in solving the crystal structure of the R252A/D12A/R25E/K90E/K91E mutant protein. Kelly Vaughn and Sarah Aubert for the great times we shared living under the same roof and in the same kitchen. The ladies downstairs who saw me as a "Mom" rather than a "scientist", and shared in all my motherhood experiences. The BGA for providing such things as travel grants and the research competition,

which allows all of us to showcase our results to places outside the confines of our own lab walls. I would also like to thank my committee, Dr. Ry Young, Dr. Art Johnson, Dr. Andy LiWang, and Dr. Tom Baldwin for all your help, patience and scientific guidance over the years.

Next, I would like to thank the Reinhart family who has not only helped out with the care-taking of Jordan for the last 10 months, but the care-taking of both myself and Alex for the last six years. You have all made our family feel like your family and thank you for all that you have done for us. Last but not least, Dr. Reinhart, a.k.a "The Boss". I am not really sure where to begin. Thank you for being Dr. Reinhart in times when my experiments weren't working and providing insight into new things to try. Or those times when you would share in my excitement over a cool result I had just gotten and immediately go to "The Tome" to find the mathematical explanation for what I had just observed. And thank you for being a friend when my experiments weren't working and I needed words of encouragement to keep me going more than scientific insight. Or on all those Saturdays when we would just sit at the conference table and you would share all the "tales" of not only your scientific experiences, but your life experiences as well. And thank you for being like a father to me all these years. As much as you might not like it, you are stuck with the Ortigosa clan for a very long time. And just "Thank you" for everything you have done and the things I know you will continue to do.

NOMENCLATURE

Abbreviations

°	Degrees or denotes standard state
IIA^{Glc}	Factor IIA glucose
A	Generally denotes substrate or single letter code for alanine
Å	Angstroms
ADP	Adenosine 5′-diphosphate
AMP	Adenosine 5′-monophosphate
ATP	Adenosine 5′-triphosphate
BsPFK	Phosphofructokinase from *Bacillus stearothermophilus*
C	Single letter code for the nucleotide cytosine
ChiCPS	Chimera of Carbamoyl-phosphate synthetase from *Escherichia coli* and *Saccharomyces cerevisiae*
ChiPFK	Chimera of Phosphofructokinase from *Bacillus stearothermophilus* and *Escherichia coli*
CP	Carbamoyl-phosphate
D	Single letter code for aspartate
DTT	Dithiothreitol
E	Generally denotes enzyme or single letter code for glutamate
EcCPS	Carbamoyl-phosphate synthetase from *Escherichia coli*
EcGK	Glycerol kinase from *Escherichia coli*
EcPFK	Phosphofructokinase from *Escherichia coli*
EDTA	Ethylenediamine tetraacetic acid

EPPS	N-[2-Hydroxyethyl]piperazine-N′-3-propanesulfonic acid
FBP	Fructose-1,6-bisphosphate
FBPase	Fructose-1,6-bisphosphatase
Fru-1,6-P_2	Fructose-1,6-bisphosphate
Fru-2,6-P_2	Fructose-2,6-bisphosphate
Fru-6-P	Fructose-6-phosphate
G	Single letter code for the nucleotide guanine
GDP	Guanosine 5′-diphosphate
H	Single letter code for histidine
Hb	Hemoglobin
HiGK	Glycerol kinase from *Haemophilus influenzae*
I	Generally denotes inhibitor
IMP	Inosine monophosphate
K	Single letter code for lysine
KSCN	Potassium thiocyanate
L	Single letter code for leucine
LdPFK	Phosphofructokinase from *Lactobacillus delbrueckii*
Mg	Magnesium
MES	2-[N-Morpholino]ethanesulfonic acid
MOPS	3-[N-Morpholino]propanesulfonic acid
mPFK	Phosphofructokinase from mouse
MW	Molecular Weight
P	Generally denotes product

N	Single letter code for asparagine
NADH	Nicotinamide adenine dinucleotide, reduced form
NAD^+	Nicotinamide adenine dinucleotide, oxidized form
P	Generally denotes product
PAGE	Polyacrylamide gel electrophoresis
PEP	Phosphoenolpyruvate
PFK	Phosphofructokinase
PG	2-Phospoglycolate
Q	Single letter code for glutamine
R	Single letter code for arginine
RmPFK	Phosphofructokinase from rabbit muscle
S	Generally denotes substrate or the single letter code for serine
ScCPS	Carbamoyl-phosphate synthetase from *Saccharomyces cerevisiae*
SDS	Sodium dodecyl sulfate
Tris	Tris[hyroxymethyl]aminomethane
UMP	Uridine monophosphate
W	Single letter code for tryptophan
X	Generally denotes an allosteric ligand
Y	Denotes an inhibitor specifically PEP or the single letter code for tyrosine

Mathematical Terms

K_{ia}^{o}	Thermodynamic dissociation constant for A in the absence of effector
K_{ia}	Thermodynamic dissociation constant for A in the saturating presence of effector
K_{iy}^{o}	Thermodynamic dissociation constant for Y in the absence of substrate
K_{iy}	Thermodynamic dissociation constant for Y in the saturating presence of substrate
ε	Extinction coefficient
[A]	Concentration of ligand/substrate
[E]	Concentration of enzyme
[ES]	Concentration of enzyme substrate complex
ΔG	Coupling free energy
ΔG_{a}	Coupling free energy for A
ΔG_{aa}	Coupling free energy for the interaction between A and A
ΔG_{app}	The apparent coupling free energy
$\Delta G_{aa/yy}$	Coupling free energy for the interaction between A and A with two equivalents of Y bound
$\Delta G_{a/y}$	Coupling free energy for A in the saturating presence of Y
ΔG_{ay}	Coupling free energy for the interaction between A and Y
ΔG_{ay1}	Coupling free energy for the interaction between A and Y for one of two heterotropic interactions found in a dimer
ΔG_{ay2}	Coupling free energy for the interaction between A and Y for one of two heterotropic interactions found in a dimer
$\Delta G_{homo\text{-}allos}$	Coupling free energy for the homotropic interaction between allosteric sites

$\Delta G_{homo\text{-}active}$	Coupling free energy for the homotropic interaction between active sites
ΔG_{y}	Coupling free energy for Y
ΔG_{yy}	Coupling free energy for the interaction between Y and Y
$\Delta G_{yy/aa}$	Coupling free energy for the interaction between Y and Y with two equivalents of A bound
$\Delta G_{y/a}$	Coupling free energy for Y in the saturating presence of A
$\Delta\Delta G_{pH}$	The difference between the ΔG_{ay} at low and high pH
□M	Micromolar
□g	Microgram
IC_{50}	Inhibition constant at which 50% of the maximal activity is reduced
K	Dissociation constant
K_a	The association constant or the Michaelis constant for A
$K_{1/2}$	The concentration of ligand that produces half-maximal change
k_{cat}	The catalytic rate constant at saturating substrate concentrations
K_d	Dissociation constant
K_m	Michaelis constant
L	Allosteric constant
M	Molar
MaxΔ	Maximal change in activity or Hill number
mg	Milligram
mL	Milliliter
mM	Millimolar

n	Binding stoichiometry
n_H	Hill number
$n_{H_{1/2}}$	Concentration of PEP resulting in half-maximal Hill number value
nm	Nanometer
Q	Coupling constant for an allosteric interaction which alters binding affinity
Q_{aa}	Coupling constant for the interaction between A and A
$Q_{aa/yy}$	Coupling constant for the interaction between A and A with two equivalents of Y bound
Q_{app}	The apparent coupling constant
Q_{ay}	Coupling constant for the interaction between A and Y
Q_{ay1}	Coupling constant for the interaction between A and Y for one of two heterotropic interactions found in a dimer
Q_{ay2}	Coupling constant for the interaction between A and Y for one of two heterotropic interactions found in a dimer
Q_{homo}	Coupling constant for the homotropic interaction
Q_{yy}	Coupling constant for the interaction between Y and Y
$Q_{yy/a}$	Coupling constant for the interaction between Y and Y with one equivalent of A bound
$Q_{yy/aa}$	Coupling constant for the interaction between Y and Y with two equivalents of A bound
R	Gas constant
[S]	Concentration of substrate
T	Temperature
U	Units

v	Initial velocity
V_{max}	Maximal velocity
V_o	Initial rate of turnover
[Y]	Concentration of inhibitor
Y_S	Fractional saturation

TABLE OF CONTENTS

Page

ABSTRACT iii

DEDICATION v

ACKNOWLEDGMENTS vi

NOMENCLATURE viii

TABLE OF CONTENTS xv

LIST OF TABLES xvii

LIST OF FIGURES xx

CHAPTER

I INTRODUCTION 1

Models Commonly Used to Describe an Allosteric Effect 2
Phosphofructokinase Background 14
Methods Used to Probe the Possible Mechanism of Allosteric Regulation 28
Present Study 49

II GENERAL METHODS 51

Materials and Methods 51

III ISOLATION AND CHARACTERIZATION OF TWO OF THE FOUR POSSIBLE HETEROTROPIC INTERACTIONS FOUND WITHIN PHOSPHOFRUCTOKINASE FROM *Bacillus stearothermophilus* 75

Introduction 75
Materials and Methods 85
Results 86
Discussion 120

CHAPTER Page

IV COMPARING THE RELATIVE ALLOSTERIC CONTRIBUTIONS OF THE FOUR UNIQUE HETEROTROPIC INTERACTIONS FOUND WITHIN PHOSPHOFRUCTOKINASE FROM *Bacillus stearothermophilus* TO THE NATIVE HOMOTETRAMER 128

Introduction..... 128
Materials and Methods..... 132
Results..... 135
Discussion..... 157

V FORMATION AND ISOLATION OF THE 2:2 HYBRIDS 162

Introduction..... 162
Materials and Methods..... 168
Results..... 172
Discussion..... 204

VI THE ALLOSTERIC CHARACTERIZATIONS OF THE 2:2 HYBRIDS..... 211

Introduction..... 211
Materials and Methods..... 221
Results..... 227
Discussion..... 270

VII CONCLUSIONS 278

REFERENCES 285

VITA 293

LIST OF TABLES

TABLE		Page
2-1	Purification table for wild-type BsPFK	62
3-1	The BsPFK variants used in attempting to isolate the 30 Å and 32 Å interactions via their respective 1:3 hybrids	91
3-2	Steady-state kinetic and thermodynamic parameters for wild-type BsPFK and the individual active site and allosteric site mutants used in constructing the mutant parent protein(s)	103
3-3	Values obtained for the midpoint of stability in the KSCN denaturation profiles for several mutant proteins	106
3-4	Steady-state kinetic parameters for wild-type BsPFK and the two 1:3 hybrids which isolate the 30 Å interaction and the 32 Å interaction at 25°C, pH 6.0, 6.5, 7.0, 7.5 and 8.0, [MgATP] = 3 mM and [PEP] = 0 mM	110
3-5	Thermodynamic parameters for wild-type and the two individual allosteric interactions (control subtracted) at 25°C, pH 6.0, 6.5, 7.0, 7.5 and 8.0 and [MgATP] = 3 mM	118
3-6	Reduction in the allosteric complexity of a homotetramer containing one active site and one allosteric site per subunit upon reducing the number of wild-type subunits successively by one	121
4-1	List of the active site and allosteric site mutations used in the isolation of the four individual allosteric heterotropic interactions	136
4-2	Steady-state kinetic and thermodynamic coupling parameters for the wild-type, the active site mutants and the allosteric site mutants at 25°C and pH 7.0 with [MgATP] = 3 mM	140

TABLE Page

4-3 Steady-state kinetic parameters for wild-type BsPFK and the four 1:3 hybrids containing the four individual allosteric interactions within BsPFK at 25°C, pH 6.0, 7.0 and 8.0, [MgATP] = 3 mM and [PEP] = 0 mM 145

4-4 Thermodynamic parameters for wild-type and the four individual allosteric interactions (control subtracted) at 25°C, pH 6.0, 7.0 and 8.0 and [MgATP] = 3 mM 150

4-5 Thermodynamic parameters determined for the wild-type control hybrid (4 | 1) at 25°C, pH 6.0, 7.0 and 8.0 and [MgATP] = 3 mM 158

5-1 The 2:2 hybrids that were unable to be formed utilizing the [a,□] mutant protein with the K213E mutation in the allosteric site 181

5-2 Kinetic and thermodynamic parameters determined for the wild-type enzyme and the three charge tag proteins at 25°C, pH 7.0 and the [MgATP] = 3 mM 198

5-3 Kinetic and thermodynamic parameters determined for the two 2:2V(30&32) hybrids isolated via the [b,□] or [b,□] mutant proteins at 25°C, pH 6.0, 7.0, 8.0 and [MgATP] = 3 mM 204

6-1 A summary of the kinetic and thermodynamic parameters obtained for the 2:2V hybrids at 25°C, pH 6.0, 7.0 and 8.0 and [MgATP] = 3 mM 232

6-2 A summary of the kinetic and thermodynamic parameters obtained for the 2:2D hybrids at 25°C, pH 6.0, 7.0 and 8.0 and [MgATP] = 3 mM 244

6-3 A summary of the kinetic and thermodynamic parameters obtained in characterizing the 23 Å homotropic interaction between allosteric sites 252

6-4 A summary of the kinetic and thermodynamic parameters obtained for the 2:2H hybrids at 25°C, pH 6.0, 7.0 and 8.0 and [MgATP] = 3 mM 259

TABLE		Page
6-5	A summary of the kinetic and thermodynamic parameters obtained in characterizing the 40 Å homotropic interaction between allosteric sites	266
7-1	The coupling free energies (ΔG_{ay}, ΔG_{yy} or ΔG_{aa}) in kcal/mol determined from the allosteric characterizations of the 10 pair-wise allosteric interactions via the 1:3 and 2:2 hybrids at 25°C and [MgATP] = 3 mM	280

LIST OF FIGURES

FIGURE		Page
1-1	Schematic diagrams of the concerted (MWC) and sequential (KNF) models of allosteric regulation of a homotetramer	6
1-2	Three coupling free energy diagrams depicting either activation, inhibition or no allosteric effect at all for the binding of two individual ligands (A or Y) to an enzyme (E) in which ΔG_{ay} is the coupling free energy associated with binding A and Y	10
1-3	The thermodynamic box of an allosteric mechanism involving a single substrate (A) and a single modifier (Y) binding to the enzyme (E)	11
1-4	The reaction catalyzed by PFK and the metabolites responsible for either inhibiting (PEP) or activating (MgADP) PFK activity	15
1-5	The crystal structure of BsPFK solved to a resolution of 2.4 Å	18
1-6	Relating the crystal structure of BsPFK to a two-dimensional schematic in order to stress how the subunits are organized and the location of the active sites and allosteric sites	22
1-7	The identification of the 30 Å heterotropic interaction	24
1-8	The four unique heterotropic interactions in BsPFK	25
1-9	The three unique homotropic interactions between active sites in BsPFK	26
1-10	The three unique homotropic interactions between allosteric sites in BsPFK	27
1-11	The three 2:2 FBPase hybrids (2:2p, 2:2q and 2:2r) examined to address both the inhibition of the enzyme by AMP and the cooperative effects observed in AMP binding for the native enzyme	39

FIGURE		Page
1-12	The 10 hybrid hemoglobin species	41
1-13	A model for the evolution of a monomer of mammalian PFK from a dimer of a bacterial predecessor	48
2-1	The coupling enzyme system used to assay BsPFK activity	56
2-2	Elution profile of a mutant BsPFK (R252A/R25A/K90E/K91E) from the Matrex Blue-A column	59
2-3	12% SDS-polyacrylamide gel of a typical BsPFK purification	61
2-4	Elution profile of hybrids made via monomer exchange from the Mono-Q anion exchange column	65
2-5	10% native polyacrylamide gel identifying the hybrids obtained via monomer exchange and isolated from the Mono-Q column	66
2-6	The apparent dissociation constant measured for Fru-6-P versus PEP concentration for wild-type BsPFK at pH 8.0, 25°C and [MgATP] = 3 mM	70
2-7	A schematic depicting the pair-wise allosteric interactions possible in either a symmetrical dimer or a 2:2 hybrid	72
3-1	A two-dimensional schematic of the concerted and sequential models representing contrasting predictions regarding the influence of the binding of a single allosteric ligand upon the binding of the substrate at a single active site	76
3-2	A two-dimensional schematic of the concerted and sequential models representing contrasting predictions regarding the influence of the binding of a single allosteric ligand upon the binding of the substrate at a single active site as it pertains to the measured allosteric effect for each of the four heterotropic interactions	78
3-3	A two-dimensional schematic of BsPFK	80

FIGURE Page

3-4 A diagram showing the various steps involved in isolating the 1:3 hybrid as determined by Kimmel and Reinhart (2001) for isolating the 22 Å heterotropic interaction 84

3-5 Schematic of the positively charged residues that line the active site and allosteric site binding pockets 87

3-6 An illustration of the two 1:3 hybrid combinations used to isolate the 30 Å and 32 Å heterotropic interactions 89

3-7 Fru-6-P saturation profiles for wild-type BsPFK and the active site mutants proteins R252A and R252E 92

3-8 Dependence of the apparent $K_{1/2}$ for Fru-6-P on increasing concentrations of the inhibitor PEP for wild-type BsPFK and the allosteric site mutant protein R25E 94

3-9 A 10% native PAGE gel showing the inability to form hybrids between wild-type and the R252A/R25E/K90E/K91E mutant 96

3-10 Fru-6-P saturation profiles for wild-type BsPFK and the active site mutants proteins H249A, H249E and H249N 97

3-11 10% native PAGE gels showing the inability to form the 1:3 hybrid and sometimes other hybrids regardless of the conditions assayed and mutant constructs used 98

3-12 The x-ray crystal structure of the active site region highlighting the location of the R252, D12, and H160 residues 100

3-13 Fru-6-P saturation profiles for wild-type BsPFK and the active site mutant protein R252A/D12A 102

3-14 KSCN denaturation profiles for wild-type BsPFK and several mutant proteins 104

3-15 Fru-6-P saturation profiles for the 1:3 hybrids that isolate the 30 Å interaction and 32 Å interaction at pH 7.0, 25°C and in the absence of PEP 108

FIGURE Page

3-16 Two-dimensional schematics of the 1:3 hybrids corresponding to the 1|1 hybrid and 1|0 hybrid for the 30 Å interaction 112

3-17 Dependence on the apparent $K_{1/2}$ for Fru-6-P on increasing concentrations of the inhibitor PEP for the 1|1 hybrid, the 1|0 control hybrid, and the corrected 32 Å allosteric interaction 114

3-18 Dependence of the corrected apparent $K_{1/2}$ for Fru-6-P on increasing concentrations of the inhibitor PEP for the 30 Å interaction and the 32 Å interaction at pH 6.0, pH 6.5, pH 7.0, pH 7.5, and pH 8.0 115

3-19 Determining the extent to which ΔG_{ay} changes as a function of pH for the 30 Å and 32 Å interactions 119

3-20 Comparison of the relative binding affinities for the allosteric inhibitor PEP of wild-type BsPFK and the D12A/K90E/K91E mutant protein 124

4-1 Contrasting predictions of the concerted and sequential models regarding the influence of the binding of a single allosteric ligand to the binding of substrate at a single active site associated with the shaded subunit 129

4-2 The subunit and binding site organization of BsPFK and the heterotropic interactions possible between the eight binding sites 131

4-3 The two-dimensional schematics of the four possible 1:3 hybrids highlighting the binding site mutations used to isolate each of the four heterotropic interactions 138

4-4 The two-dimensional schematics of the four control hybrids (1|0) constructed in order to correct for the allosteric effect incurred upon the native active site by PEP binding to the mutated allosteric sites 143

4-5 The dependence of the corrected apparent $K_{1/2}$ for Fru-6-P on increasing concentrations of the inhibitor PEP for the 22 Å interaction, the 30 Å interaction, the 32 Å interaction and the 45 Å interaction 148

FIGURE Page

4-6 The dependence of the apparent $K_{1/2}$ for Fru-6-P determined for the 45 Å control hybrid (1|0) on increasing concentrations of the inhibitor PEP 152

4-7 Comparison of the sum of the individual coupling free energies determined for the four heterotropic interactions to the coupling free energy determined for the native tetramer at pH 6.0, 7.0 and 8.0 154

4-8 The dependence upon the Hill number (n_H) determined for PEP binding as a function of increasing concentrations of Fru-6-P for the wild-type enzyme..... 155

4-9 A two-dimensional schematic of the wild-type control hybrid (4|1) and the steady-state characterization of its allosteric properties at pH 6.0, 7.0 and 8.0..... 156

4-10 Comparison of the sum of the individual coupling free energies determined for the four heterotropic interactions to the coupling free energy determined for the wild-type control hybrid (4|1) and the wild-type enzyme (4|4) at pH 6.0, 7.0 and 8.0..... 159

5-1 Three schematics depicting the pair-wise allosteric interactions possible within BsPFK..... 163

5-2 A schematic of the twelve 2:2 hybrids..... 165

5-3 Elution profile for BsPFK hybrids made via dimer exchange from the Mono-Q column..... 170

5-4 10% native polyacrylamide gel identifying the hybrids obtained via dimer exchange and isolated from the Mono-Q column..... 171

5-5 The three 2:2 isomers that form between wild-type BsPFK and either the [b,□] or [b,□] mutant proteins when using monomer exchange..... 174

5-6 The elution profile for hybrids between wild-type and the [b,□] mutant protein (R252A/D12A/R25E/K90E/K91E) from the Mono-Q anion exchange column..... 175

FIGURE Page

5-7 Two elution profiles demonstrating the influence of the R211E/K213E mutations upon resolution of the 2:2 isomers 178

5-8 The dependence of the apparent $K_{1/2}$ for Fru-6-P on increasing concentrations of the inhibitor PEP for wild-type BsPFK and the R162E/K213E mutant protein 180

5-9 The positions of K90 and K91 in the 2:2D, 2:2H and 2:2V isomers in either the two-dimensional schematic or crystal structure 184

5-10 The positions of R232 and Q233 in the 2:2D, 2:2H and 2:2V isomers in either the two-dimensional schematic or crystal structure 186

5-11 The positions of N303 and K304 in the 2:2D, 2:2H and 2:2V isomers in either the two-dimensional schematic or crystal structure 188

5-12 Two elution profiles demonstrating the influence of the R232E/Q233E and N303E/K304E charge tags upon the resolution of the 2:2 isomers 189

5-13 The elution profile for the 2:2V hybrid (with some 2:2H contamination) from the Mono-Q anion exchange column 191

5-14 A 10% native PAGE gel illustrating the importance of PEP in the dimer exchange procedure 193

5-15 The nine of the twelve 2:2 hybrids that were able to be formed and isolated using strategically placed charge tags and either monomer exchange or dimer exchange with the wild-type enzyme 195

5-16 The dependence of the apparent $K_{1/2}$ for Fru-6-P upon increasing concentrations of the inhibitor PEP for wild-type BsPFK, the K90E/K91E charge tag mutant, the R232E/Q233E charge tag mutant and the N303E/K304E charge tag mutant at pH 7.0 197

FIGURE Page

5-17 A schematic showing the possible proteins that can form when performing dimer exchange between wild-type and the 2:2H(30&45) hybrid, and a 10% native PAGE gel verifying the expected results..... 200

5-18 The dependence of the apparent $K_{1/2}$ for Fru-6-P upon increasing concentrations of the inhibitor PEP for the 2:2V(30&32) hybrid obtained by monomer exchange utilizing the N303E/K304E charge tag and the 2:2V(30&32) hybrid obtained by dimer exchange utilizing the K90E/K91E charge tag at pH 6.0, 7.0 and 8.0..... 203

6-1 A schematic depicting the predictions regarding the observed allosteric effect in either the concerted or sequential models on the binding of one equivalent of Fru-6-P to the A site..... 218

6-2 The data predictions for the concerted, sequential and conformational free/linkage models as they pertain to the 2:2V(30&32) hybrid..... 220

6-3 The PEP saturation profiles determined for the 2:2D(22&30) hybrid at pH 7.0 and increasing concentrations of Fru-6-P 225

6-4 The two-dimensional schematics of the three 2:2V hybrids isolated and the steady-state characterization of their allosteric properties at pH 6.0, 7.0 and 8.0..... 230

6-5 The characterization of the 47 Å homotropic interaction between active sites by following the dependence of the Hill number (n_H) determined for Fru-6-P binding as a function of increasing concentrations of PEP for the 2:2V hybrids 234

6-6 The characterization of the 39.9 Å homotropic interaction between allosteric sites by following the dependence of the Hill number (n_H) determined for PEP binding as a function of increasing concentrations of Fru-6-P for the 2:2V hybrids 237

FIGURE Page

6-7 The comparison of the sum of the individual coupling free energies determined for the heterotropic interactions to the coupling free energy determined for the 2:2V hybrids at pH 6.0, 7.0 and 8.0 in the absence of any homotropic contribution 239

6-8 The two-dimensional schematics of the three 2:2D hybrids isolated and the steady-state characterization of their allosteric properties at pH 6.0, 7.0 and 8.0..... 243

6-9 The characterization of the 45 Å homotropic interaction between active sites by following the dependence of the Hill number (n_H) determined for Fru-6-P binding as a function of increasing concentrations of PEP for the 2:2D hybrids 248

6-10 The characterization of the 23 Å homotropic interaction between active sites by following the dependence of the Hill number (n_H) determined for PEP binding as a function of increasing concentrations of Fru-6-P for the 2:2D(22&30) hybrid..... 251

6-11 The comparison of the sum of the individual coupling free energies determined for the heterotropic interactions and the 23 Å homotropic contribution to the coupling free energy determined for the 2:2D hybrids at pH 6.0, 7.0 and 8.0..... 254

6-12 The two-dimensional schematics of the three 2:2H hybrids isolated and the steady-state characterization of their allosteric properties at pH 6.0, 7.0 and 8.0 258

6-13 The characterization of the 28 Å homotropic interaction between active sites by following the dependence of the Hill number (n_H) determined for Fru-6-P binding as a function of increasing concentrations of PEP for the 2:2H hybrids 262

6-14 The characterization of the 40 Å homotropic interaction between allosteric sites by following the dependence of the Hill number (n_H) determined for PEP binding as a function of increasing concentrations of Fru-6-P for two of the 2:2H hybrids 265

FIGURE Page

6-15 The comparison of the sum of the individual coupling free energies determined for the heterotropic interactions and the 40 Å homotropic contribution to the coupling free energy determined for the 2:2H hybrids at pH 6.0, 7.0 and 8.0..... 269

6-16 The dependence upon the apparent $K_{1/2}$ for Fru-6-P as a function of PEP concentration for the 2:2V(30&32) hybrid obtained from using the [b,□] mutant protein..... 275

CHAPTER I

INTRODUCTION

For all the diversity in life on our planet, ranging from prokaryotes to eukaryotes, regulation is one of the few things that is common to all of them. Of course, there are many different forms of regulation found in any given cell, proven by the number of "hits" received when the word "regulation" is entered into the Medline database (over 650,000 hits). However, for this investigation we are only going to focus upon the allosteric regulation of enzymes.

When the words "allosteric regulation" are entered into the Medline Database, over 4,000 "hits" are received. Thus, even though our investigation has been significantly narrowed, the field of allosteric regulation as a whole is still relatively large as is the number of opinions regarding *how* allosterism occurs in proteins. Over the past 40 years, many different models have been proposed to describe an allosteric effect, and many methods have been both developed and applied to identify specific residues and regions of proteins involved in the transmission of an allosteric signal. Furthermore, this allosteric signal, whether activating or inhibiting, is transmitted via all the different allosteric interactions found between the binding sites of a particular enzyme. Thus, to gain a better understanding of how an allosteric enzyme "works", we first want to quantify the roles each of the 10 unique pair-wise allosteric interactions found in the allosteric enzyme phosphofructokinase from *Bacillus*

This dissertation follows the style and format of *Biophysical Journal.*

stearothermophilus (BsPFK) plays in the inhibition of the enzyme by phosphoenolpyruvate (PEP) and second, apply these findings to gain a better understanding of how multiple allosteric interactions combine in an oligomer.

Allosterism literally derives from *allos* = other and *steoros* = space (Greek), but allosterism is defined more specifically as the binding of an effector molecule(s) to a site distinct from the substrate binding site that regulates enzyme activity either by activation or inhibition. This regulation can occur two ways: (1) by altering substrate affinity (K-type system) or (2) by altering the catalytic rate (V-type system). Since a greater percentage of allosteric enzymes are regulated via changes in substrate affinity (K-type system), including phosphofructokinase, we are going to focus on K-type regulation and the models used to account for these types of allosteric effects.

Models commonly used to describe an allosteric effect

The following models have all been formulated to describe the allosteric behavior of proteins. However before continuing, a few features common to most of the models need to be described. Cooperativity is a characteristic common to most oligomeric allosteric proteins and is a result of a change in ligand-binding affinity with increasing concentrations of a particular ligand. Thus, positive cooperativity is defined as an increase in ligand-binding affinity with increasing ligand concentration, while negative cooperativity is defined as a decrease in ligand-binding affinity with increasing ligand concentration. These phenomena result in a non-hyperbolic ligand-binding curve, which cannot be adequately described by Michaelis-Menten kinetics. Thus, Archibald

Hill formulated what we have now come to know as a Hill plot to describe the cooperative behavior of oxygen binding to hemoglobin (Hill, 1910).

We begin by first considering an enzyme E consisting of *n* subunits that can each bind ligand S:

$$E + nS \rightleftharpoons ES_n \qquad (1\text{-}1)$$

By assuming infinite cooperativity in which all or none of the ligand binding sites are occupied, we obtain the following dissociation constant, K, and fractional saturation, Y_s, for the above reaction:

$$K = \frac{[E] \cdot [S]^n}{[ES_n]} \qquad (1\text{-}2)$$

$$Y_s = \frac{[ES_n]}{([E] + [ES_n])} \qquad (1\text{-}3)$$

After combining Eqs. 1-2 and 1-3 and performing some algebraic rearrangement, the Hill equation is obtained:

$$Y_s = \frac{[S]^n}{K + [S]^n} \qquad (1\text{-}4)$$

Equation 1-4 can be applied to describe the degree of saturation for an oligomeric protein as a function of ligand concentration. Since the assumption of infinite cooperativity is physically impossible, *n* must be considered not as a number of subunits per protein, but rather as a measurement of the degree of cooperativity among interacting ligand-binding sites. Thus, if n = 1, ligand binding is non-cooperative and should follow Michaelis-Menten kinetics. However, for a positively cooperative ligand-binding curve, $n > 1$, and for a negatively cooperative ligand-binding curve, $n < 1$.

Also, in the realm of allosterism, the terms heterotropic and homotropic interactions (*effects*) are commonly used. A heterotropic interaction is defined as an interaction between unlike binding sites or ligands, while a homotropic interaction is defined as an interaction between like binding sites or ligands. Thus, a cooperative ligand-binding curve would reflect a homotropic effect since it involves the binding of one ligand influencing the binding of the same ligand to a different binding site, while an example of a heterotropic effect would be the binding of an inhibitor influencing the binding of substrate at a separate site.

The concerted and sequential models. Two of the most widely used models in the allosteric field are the concerted and sequential models and both were formulated to describe an allosteric response for a protein. The concerted model or Monod-Wyman-Changeux (MWC) model, was originally formulated to describe the allosteric effect observed for hemoglobin and simplified the allosteric transition into an all-or-none phenomenon (Monod et al., 1965). The concerted model begins by considering any allosteric enzyme existing in one of two functional/conformational states based upon the ligand(s) bound. The "R-state" or relaxed state preferentially binds substrates and activators with high affinity, and the "T-state" or taut state preferentially binds inhibitors and thus binds substrate with low affinity. According to the concerted model, the "R-state" and "T-state" are in equilibrium whether or not ligand is bound to the enzyme and the equilibrium constant for the R ↔ T transition is denoted "L". Thus, when the substrate binds the free enzyme form, the equilibrium is shifted towards the "R-state", and the enzyme undergoes a concerted transition making

more “R” sites accessible for substrate binding leading to a cooperative (positive) substrate binding profile. Activators also bind to the “R-state”, however, they too shift the equilibrium towards the “R-state”, but since the enzyme is already in the “R-state”, the substrate saturation profile lacks cooperativity. On the other hand, when inhibitor binds to the enzyme, the equilibrium is shifted towards the “T-state” in a concerted transition reducing the number of “R” sites available to bind substrate. Thus, when performing a substrate saturation profile at any given inhibitor concentration, positive cooperativity will always be observed because as the amount of substrate is increased, the equilibrium is shifted back towards the “R-state” increasing the number of accessible “R” sites. Thus, the major component of the concerted model is that when the protein goes from one state to another state after only one binding event, its molecular and conformational symmetry is conserved and this distinction is shown schematically for a homotetramer in Fig. 1-1. A major drawback to the concerted model is its inability to describe negative cooperativity, part of which was the motivation for the formulation of the sequential model.

The sequential model or Koshland-Nemethy-Filmer (KNF) model, also uses the “R-state”, “T-state” and “L” notation, but differs from the concerted model in several ways (Koshland et al., 1966). First, the sequential model does not restrict the enzyme to exist at equilibrium between two defined conformational states, but rather allows the ligand (substrate, activator or inhibitor) that binds to the enzyme to determine the conformation adopted by

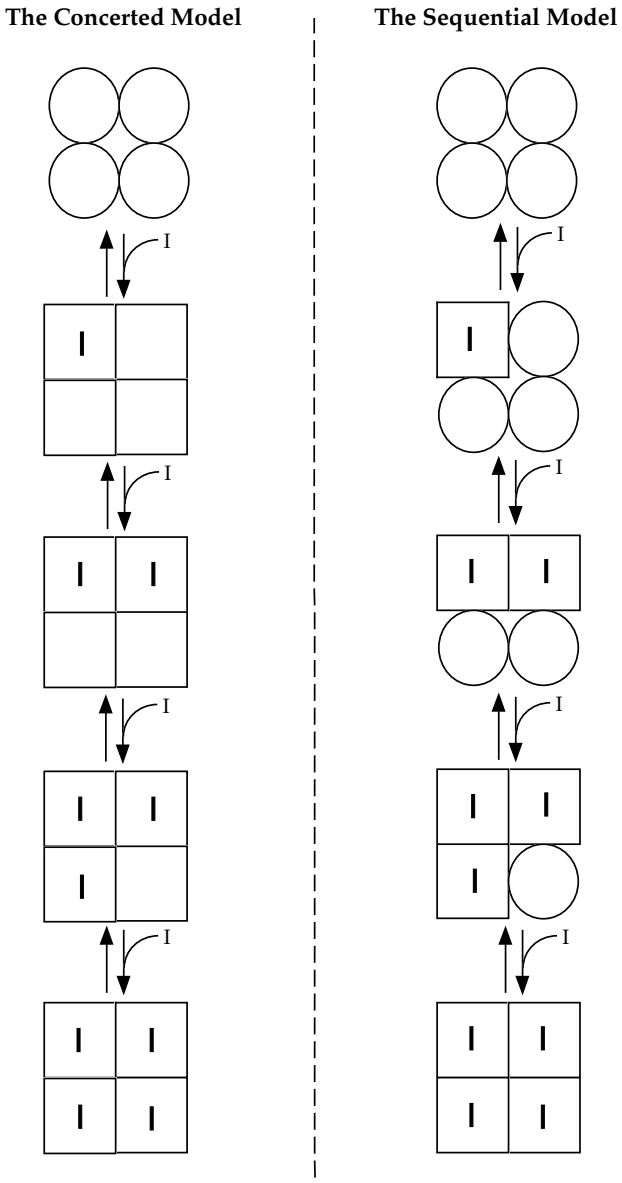

FIGURE 1-1 Schematic diagrams of the concerted (MWC) and sequential (KNF) models of allosteric regulation of a homotetramer. For the concerted model, only one equivalent of inhibitor (I) is required to bind for the enzyme to undergo the allosteric transition from the R-state (circles) to the T-state (squares – inhibited form) (Monod et al., 1965). The sequential model, on the other hand, requires four equivalents of inhibitor to bind for the enzyme to be converted from the R-state to the T-state (Koshland et al., 1966).

the protein. Furthermore, instead of a concerted allosteric transition upon ligand binding, only the subunit that binds the ligand undergoes the allosteric transition or conformational change. However, that one subunit also influences the neighboring subunits, giving rise to either positive or negative cooperativity. If the influence upon the neighboring subunits is favorable, positive cooperativity is observed, and if the influence is unfavorable, negative cooperativity is observed. Both activation and inhibition are easily rationalized by this phenomenon, as an activator would have a favorable influence upon substrate binding, whereas an inhibitor would have an unfavorable influence upon substrate binding. Most importantly however, the sequential model requires saturation to occur in order for the entire enzyme to adopt either the "R-state" or "T-state" forms (see Fig. 1-1). Thus, from examining Fig. 1-1, the biggest difference between the concerted and sequential models is the extent of conformational changes the enzyme experiences upon binding the first equivalent of ligand (the case of inhibitor binding in Fig. 1-1). Consequently, a great deal of information would be gained about the applicability of these two models if the first binding event could be isolated.

Several variations of the concerted and sequential models (two-state models) have been formulated in order to try to describe an observed allosteric effect that cannot be adequately described by either model. Eigen (1967) developed a unifying model that combines the extremes of both the concerted and sequential models, while a series of "nested" models have also been created which invoke different degrees of either the concerted or sequential models

simultaneously, depending upon the ligation state of the enzyme (Ackers et al., 2000; Ackers et al., 1992; Herzfeld and Stanley, 1974; Decker and Sterner, 1990). Common to all these secondary model formulations is the inability of the concerted or sequential models to adequately describe an allosteric effect on their own, mainly because the enzyme is restricted to two conformational states, the "R-state" or the "T-state". Thus, a third model or approach is warranted in which more "conformational freedom" is granted to the protein and which would permit any range of functionality to the various ligand-bound forms of the enzyme.

Linked-function analysis. The idea of linkage was first proposed by Wyman (1964 and 1967) and later adapted by Weber (1972 and 1975) to describe an observed allosteric effect between two ligands binding to two separate sites on a protein. Furthermore, linkage states that the interaction between these two ligands must be equivalent regardless of the order of ligand binding. When considering these effects of ligand binding in free energy terms, a thermodynamic basis is established that can successfully describe activation, inhibition or no allosteric effect at all (Weber, 1972, 1975; Reinhart, 1983, 1988).

Let's begin by considering an enzyme E that binds two different ligands, A and Y, to two different binding sites on the enzyme.

$$Y + E + A \sqcap Y \sqcap E \sqcap A \qquad (1\text{-}5)$$

Next, for the enzyme to proceed from its unbound form to having both A and Y bound (ternary complex), two binding events must occur, with the order of ligand binding generating a potential of four different binding events. First,

either A or Y can bind to E resulting in either a binding free energy of ΔG_a or ΔG_y respectively. After that, the remaining ligand, either Y or A binds to the enzyme resulting in two additional binding free energy terms, $\Delta G_{y/a}$ or $\Delta G_{a/y}$ which describe the binding free energy of either binding Y to E with A already bound or binding A to E with Y already bound respectively. Thus, the binding free energies of both ligand binding events, regardless of order, must equal the following (Weber 1972, 1975; Reinhart, 1983, 1988):

$$\Delta G_a + \Delta G_{y/a} = \Delta G_y + \Delta G_{a/y} \qquad (1\text{-}6)$$

Moreover, the magnitude of the interaction between the two ligands (ΔG_{ay}) can be defined by the following equation:

$$\Delta G_{ay} \equiv \Delta G_{a/y} - \Delta G_a = \Delta G_{y/a} - \Delta G_y \qquad (1\text{-}7)$$

Figure 1-2 illustrates the three cases possible upon both A and Y binding to E. First, if the binding of Y augments the binding of A and *vice versa*, a coupling free energy less than zero will be observed (activation; Fig. 1-2 *A*). Second, if the binding of Y antagonizes the binding of A and *vice versa*, a coupling free energy greater than zero will be observed (inhibition; Fig. 1-2 *B*). Finally, if the binding of Y has no effect upon the binding of A and *vice versa*, no allosteric regulation exists between the two ligands (Fig. 1-2 *C*). Figure 1-3 also illustrates the basic linkage idea in terms of a thermodynamic box, with the macromolecular dissociation constants for each binding event also included.

Reinhart (1983) applied these ideas to predict the observed allosteric response in a single substrate-single modifier system. Using linked function

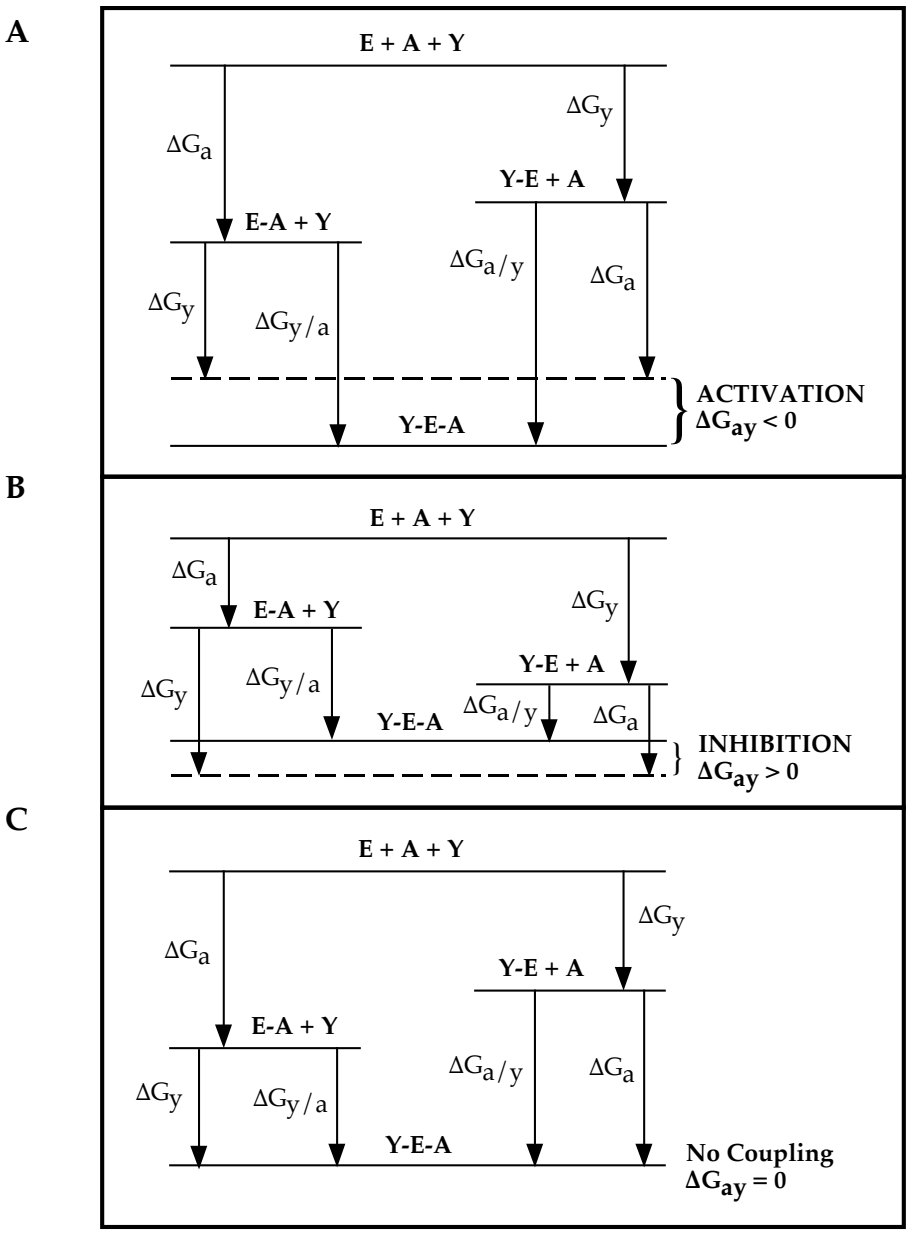

FIGURE 1-2 Three coupling free energy diagrams depicting either activation, inhibition or no allosteric effect at all for the binding of two individual ligands (A or Y) to an enzyme (E) in which ΔG_{ay} is the coupling free energy associated with binding A and Y. (*A*) When $\Delta G_{ay} < 0$, activation occurs. (*B*) When $\Delta G_{ay} > 0$, inhibition occurs. (*C*) When $\Delta G_{ay} = 0$, no allosteric effect is measured. Diagrams adapted from Weber (1972 and 1975).

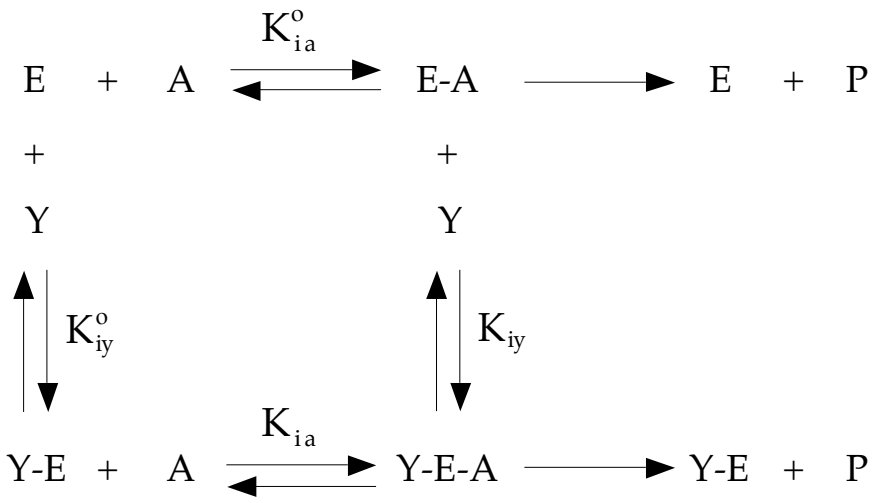

FIGURE 1-3 The thermodynamic box of an allosteric mechanism involving a single substrate (A) and a single modifier (Y) binding to the enzyme (E). The dissociation constants for each binding event are also shown.

analysis, both the nature (activation or inhibition) and magnitude of an allosteric effect can be determined by measuring the coupling constant (Q_{ay}) which is derived from the dissociation constants defined by the thermodynamic box shown in Fig. 1-3 (Botts and Morales, 1953; Freiden, 1964; Reinhart, 1983). Each binding event is governed by individual dissociation constants termed either K^o_{ia}, K_{ia}, K^o_{iy} or K_{iy} in which the subscript denotes the ligand bound and the superscript denotes the degree of saturation of the other ligand. Thus, K^o_{ia} is the dissociation constant for A in the absence of Y and K_{ia} is the dissociation constant for A in the saturating presence of Y, in which A is the substrate and Y is an inhibitor. The notation utilized here expands on the notation introduced by Cleland (1963a) in which the terms K_a and K_{ia} were used to distinguish between the Michaelis constant and the thermodynamic dissociation constant of the substrate A respectively. Thus, from Fig. 1-3 the dissociation constants are determined as follows:

$$K^o_{ia} = \frac{[E][A]}{[E - A]} \qquad (1\text{-}8)$$

$$K_{ia} = \frac{[Y - E][A]}{[Y - E - A]} \qquad (1\text{-}9)$$

$$K^o_{iy} = \frac{[E][Y]}{[Y - E]} \qquad (1\text{-}10)$$

$$K_{iy} = \frac{[E - A][Y]}{[Y - E - A]} \qquad (1\text{-}11)$$

The coupling constant, Q_{ay}, can then be calculated by taking the ratio of the dissociation constants determined for A or Y in the absence and saturating presence of Y or A respectively:

$$Q_{ay} = \frac{K_{ia}^{o}}{K_{ia}} = \frac{K_{iy}^{o}}{K_{iy}} \qquad (1\text{-}12)$$

Moreover, if $Q_{ay} < 1$ the allosteric ligand is an inhibitor, and if $Q_{ay} > 1$ the allosteric ligand is an activator. If $Q_{ay} = 1$ then the allosteric ligand has no effect on the binding of substrate or *vice versa*.

It should be noted that the thermodynamic parameters, K_{ia}^{o} and K_{ia}, are not necessarily interchangeable with their Michaelis constant counterparts, K_{a}^{o} and K_{a}. However, they are equivalent if the rapid equilibrium assumption is valid (Reinhart, 1983). Furthermore, Symcox and Reinhart (1992) developed a steady-state kinetic method to determine if in fact the rapid equilibrium assumption is valid. Essentially, independent determinations of K_{ia}^{o} / K_{ia} and K_{iy}^{o} / K_{iy} must be equivalent if the allosteric ligand has reached rapid equilibrium.

The coupling parameter can also be used to calculate the coupling free energy associated with the interaction between substrate and allosteric effector using the following equation:

$$\Delta G_{ay} = -RT\ln\left(Q_{ay}\right) \qquad (1\text{-}13)$$

where ΔG_{ay} is the coupling free energy between Fru-6-P and PEP as defined in Eq. 1-7, R is the gas constant which is equivalent to 1.987×10^{-3} kcal/deg·mol,

and T is absolute temperature in Kelvin. Allosteric inhibition is defined by $\Delta G_{ay} > 0$, allosteric activation by $\Delta G_{ay} < 0$, and if no coupling between the two ligands occurs, $\Delta G_{ay} = 0$ (see Fig. 1-2). A further elaboration of applying linked function analysis to a symmetrical dimer is discussed in both Chapter II and Chapter VI.

One shortcoming of using a linked-function approach to study allosterism is the lack of a model to describe an allosteric effect. Conceptualization via circles and squares for the two-state models is a big advantage, but with the linked-function approach, having only mathematical relationships to describe the allosteric effect makes describing an observed allosteric effect a bit more challenging.

Phosphofructokinase background

Phosphofructokinase (PFK) (EC 2.7.1.11) is the third enzyme found in the glycolytic pathway and catalyzes the phosphorylation of fructose-6-phosphate (Fru-6-P) to fructose-1,6-bisphosphate using MgATP as the phosphoryl donor (Fig. 1-4). For both the eukaryotic and prokaryotic forms of the enzyme, PFK is allosterically regulated by numerous metabolites in the glycolytic and energy production pathways (Bloxham and Lardy, 1973; Kolartz and Buc, 1982; Evans et al., 1981). However, for purposes of this investigation, our focus is on the regulatory behavior of phosphofructokinase from two well known bacterial sources, *Escherichia coli* (a mesophile) and *Bacillus stearothermophilus* (a moderate thermophile).

For both of the enzymes, several molecules have been found to regulate the activity of the enzyme, but the two main effector molecules are MgADP

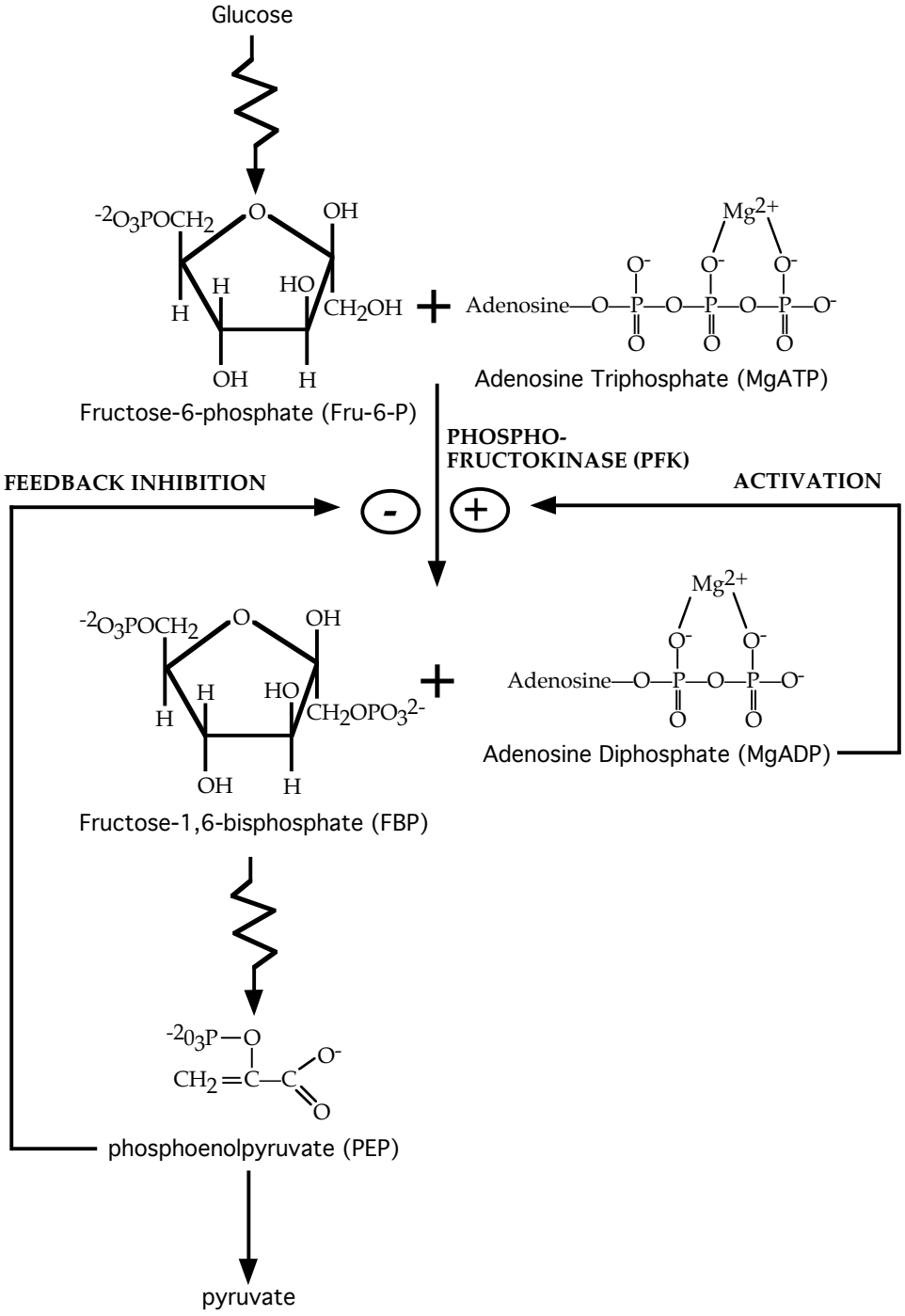

FIGURE 1-4 The reaction catalyzed by PFK and the metabolites responsible for either inhibiting (PEP) or activating (MgADP) PFK activity.

(activator) and phosphoenolpyruvate (PEP; inhibitor) (Uyeda, 1979; Evans et al., 1981 and Kolartz and Buc, 1982). In response to the energy requirements of the cell, MgADP has been shown to activate PFK activity by binding to the enzyme and increasing the enzyme's affinity for the substrate Fru-6-P. On the other hand, PEP inhibits PFK by binding to the same allosteric sites and decreasing the enzyme's affinity for Fru-6-P (feedback inhibition). Thus, PFK is subject to "K-type" regulation. Other molecules that have been shown to regulate PFK activity include MgGDP (activator), MgATP (inhibitor) and 2-phosphoglycolate (inhibitor) (Blangy et al., 1968; Bloxham and Lardy, 1973; Kolartz and Buc, 1981; Evans et al., 1981; Johnson and Reinhart, 1992 and 1994, Tlapak-Simmons and Reinhart, 1994).

With such a high degree of nucleotide (58%) and amino acid (55%) identity between PFK from *E. coli* (EcPFK) and *B. stearothermophilus* (BsPFK), it is not surprising that the allosteric properties of the two enzymes are similar (French and Chang, 1987). The biggest difference in the nucleotide sequence between the two species is the elevated guanine (G) and cytosine (C) content at the third position of BsPFK's codons (71.3% G or C for BsPFK compared to 57.5% G or C for EcPFK). This is consistent with other mesophilic and thermophilic bacteria and supports the idea that the higher G and C content increases the stability of the nucleic acid interactions in thermophiles (Kagawa et al., 1984 and Hellinga and Evans, 1985).

Based on crystal structures for both EcPFK and BsPFK in the presence of several ligand combinations, it is clear that the two enzymes are very similar.

Both enzymes are homotetramers (subunit MW ~34,000) arranged as a dimer of dimers with the crystal structure of BsPFK shown in Fig. 1-5 (Evans and Hudson, 1979; Evans et al., 1981; Evans et al., 1986; Schirmer and Evans, 1990). They share the same secondary structural elements, and, when comparing their α-carbon traces, the enzymes are nearly superimposable (Evans et al., 1981 and Shirakihara and Evans, 1988).

Each subunit is comprised of a large domain and a small domain, with each domain containing a central β-sheet sandwiched between several α-helices (Fig. 1-5 *B*). The Fru-6-P binding site is located at the cleft between the two domains and at the interface of the protein. Thus, residues from either side of the interface are involved in binding Fru-6-P, and it is this site that will be referred to as the active site. The MgATP binding site, located next to the Fru-6-P binding site, is located entirely in the large domain. The allosteric site, which is capable of binding both MgADP and PEP, is located at the interface of the protein in both the large and small domains. Therefore, each subunit contributes two half Fru-6-P (active) sites and two half allosteric sites, resulting in an average of each subunit containing one full active site and one full allosteric site. Moreover, all four active sites are arranged along one dimer-dimer interface, while all four allosteric sites are situated along the other dimer-dimer interface (Fig. 1-5).

With such a high degree of sequence and structural similarity between the two enzymes, one might expect the enzymes to perform and act identically with respect to ligand binding, allosteric behavior and protein stability, but this

A

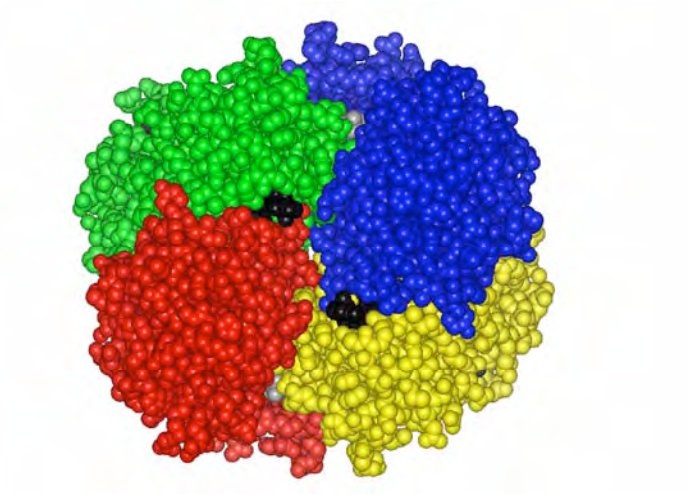

B

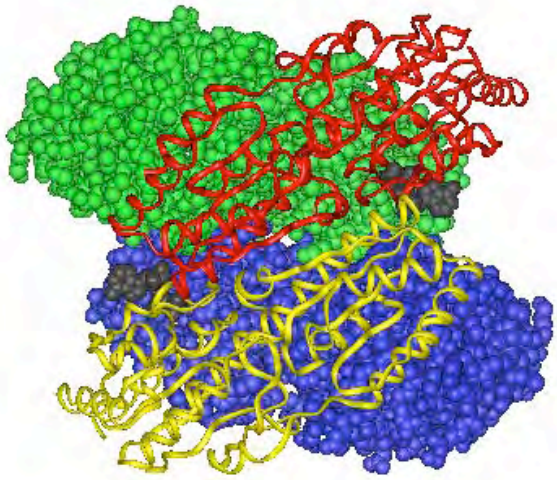

FIGURE 1-5 The crystal structure of BsPFK solved to a resolution of 2.4 Å (Schirmer and Evans, 1990). (*A*) A space-fill representation of BsPFK with each subunit colored green, blue, yellow or red. The ADP molecules bound in the allosteric sites are shown in black and the Fru-6-P molecules bound in the active sites are shown in gray. (*B*) A diagram of two of the four subunits shown as ribbons in order to show the two domains of each subunit.

is not the case. First, the two enzymes differ in their individual Fru-6-P saturation profiles. For EcPFK, the binding of Fru-6-P displays positive cooperativity in the presence of saturating MgATP. By contrast, Fru-6-P binding to BsPFK shows little to no cooperativity under the same conditions. However, Fru-6-P binding becomes cooperative in BsPFK in the presence of the inhibitor PEP, whereas cooperativity diminishes in the presence of inhibitor in EcPFK (Blangy et al., 1968 and Valdez et al., 1989).

Secondly, MgADP (or MgGDP) activates and PEP inhibits both EcPFK and BsPFK. However, the two enzymes differ in the degree of activation and inhibition measured at room temperature. For EcPFK activation is easily observed under normal assay conditions, but for BsPFK activation is practically undetectable under the same conditions. Fortunately, by altering the temperature and pH of the assay conditions, binding of MgADP can be detected and hence its effects upon Fru-6-P binding observed for BsPFK. What is more, MgADP has been shown to become an inhibitor of BsPFK at low temperatures. As for inhibition, PEP is a better inhibitor of BsPFK than EcPFK at room temperature (Braxton et al., 1994; Byrnes et al., 1994; Tlapak-Simmons and Reinhart, 1994 and 1998). Thus, although similar structurally, the kinetic behaviors of EcPFK and BsPFK are quite different.

A third difference between EcPFK and BsPFK involves the stability of the two enzymes at room temperature. EcPFK undergoes dimer exchange across the active site dimer-dimer interface quite readily (in the absence of Fru-6-P) at 25 °C (Fenton and Reinhart, 2002), while no exchange between dimers has been

observed under the same conditions in BsPFK (data not shown). Furthermore, exchange of the subunits at the monomer level has been observed for EcPFK with the addition of only 0.4 M KSCN, while BsPFK requires 2 M KSCN to achieve the same results (Deville-Bonne et al., 1989; Johnson et al., 2001; Fenton and Reinhart, 2002; Kimmel and Reinhart, 2001). Finally, when the two enzymes are subjected to hydrostatic pressure, EcPFK dissociates by approximately 1000 bar, while for BsPFK, no evidence for dissociation of the tetramer is observed up to 2500 bar (Johnson and Reinhart, 1996; Quinlan and Reinhart, unpublished results). Thus, at room temperature and in the absence of KSCN, the BsPFK enzyme is far more stable than the EcPFK enzyme.

For this investigation we have chosen to focus on the allosteric properties of BsPFK and more specifically, inhibition of BsPFK by PEP. As mentioned previously, a lot is known about BsPFK and its regulatory behavior, but *how* the enzyme is inhibited is the focus of this investigation. However, before addressing how the enzyme is inhibited, we have to first identify the potential allosteric interactions involved in the inhibition process.

Identifying the ten unique allosteric interactions in BsPFK. In order to get a better idea of how the subunits are organized in BsPFK as well as to emphasize the location of the binding sites, we have converted the crystal structure into a two-dimensional schematic (Figs. 1-6, *A* and *B*) (Schirmer and Evans, 1990). All four subunits are shown in a different color (green, blue, yellow and red) with the active site dimer-dimer interface located between the green and blue subunits and the red and yellow subunits (positioned vertically

in Fig. 1-6), and the allosteric site dimer-dimer interface located between the green and red subunits and the blue and yellow subunits (positioned horizontally in Fig. 1-6).

As mentioned previously, all eight of the binding sites are located at the subunit interfaces within the protein, with each subunit contributing two half-active sites and two half-allosteric sites per subunit. In order to differentiate between these four different half-sites within the two-dimensional schematic, different geometric shapes have been used to represent the different "sides" of the binding sites (see Fig. 1-6, *B* and *C*). The active sites are represented as being formed by a combination of a triangle and a half-hexagon, while the allosteric sites are represented by a combination of a semi-circle and a rectangle. Furthermore, specific residues that contribute to the binding sites have also been included in the schematic (Schirmer and Evans, 1990). For example, the active site is lined with R162 from one side (triangle) and R252 from the other side (half-hexagon), while the allosteric site is lined with R211 and K213 on one side (semi-circle) and R25 on the other side (rectangle).

With a total of four active sites and four allosteric sites, 28 total pair-wise allosteric interactions are possible between the eight binding sites. Of those 28 interactions, 16 are heterotropic interactions with the rest being homotropic interactions. Of the 28 total pair-wise allosteric interactions, only 10 are unique. Moreover, all of the interactions are shown in Fig. 1-6 *C* with each of the 10 unique interactions designated a distinct color.

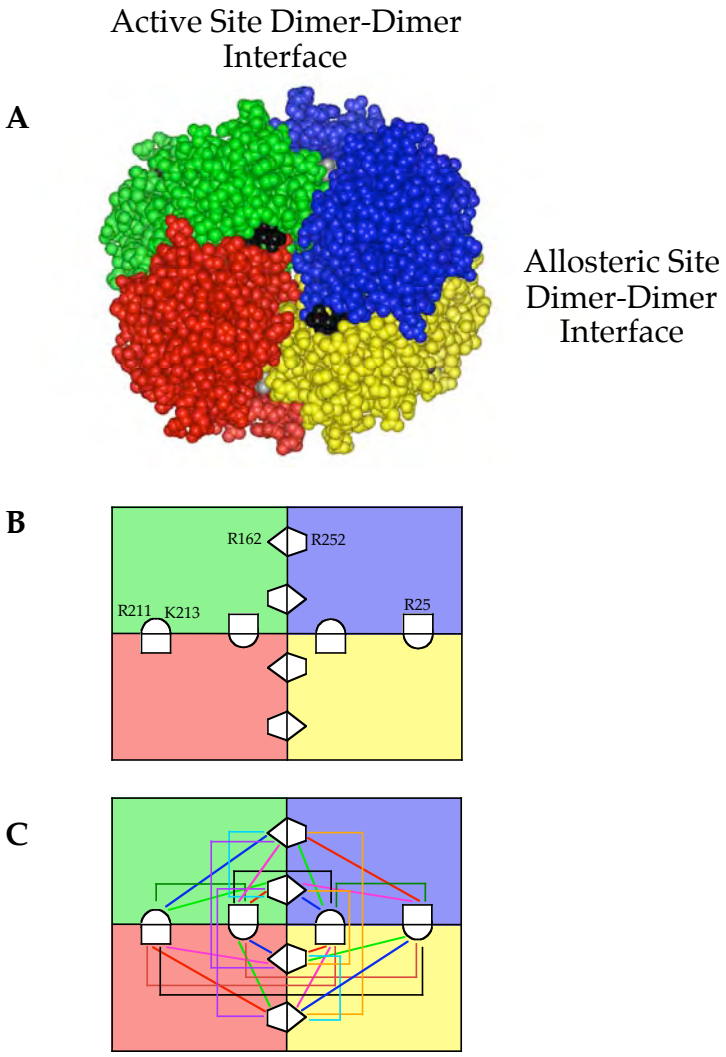

FIGURE 1-6 Relating the crystal structure of BsPFK to a two-dimensional schematic in order to stress how the subunits are organized and the location of the active sites and allosteric sites. (*A*) The crystal structure of BsPFK indicating both the active site dimer-dimer interface (vertical) and the allosteric site dimer-dimer interface (horizontal). (*B*) The two dimensional schematic of BsPFK with the "sides" of the binding sites represented by a different geometrical figure and the specific residues on either side of the binding sites shown. (*C*) The 28 potential pair-wise allosteric interactions found in BsPFK, 10 of which are unique with each one designated a different color.

In order to identify the structural relationships corresponding to each of the 10 pair-wise interactions, we simply use the aforementioned binding site residues (R162 and R252 at the active sites and R211/K213 and R25 at the allosteric sites) as "landmarks" within the crystal structure, and proceed to map each of the 10 allosteric interactions from the three-dimensional structure to the two-dimensional schematic. A unique distance is also measured between the different pairs of binding sites (depending upon the interaction of interest) and that distance is then used to identify that particular interaction. Fig. 1-7 walks through this process for identifying the 30 Å heterotropic interaction.

This process was performed for the remaining three heterotropic interactions resulting in distances of 22 Å, 32 Å and 45 Å. These distances were measured within the crystal structure from the phosphorous atom of one of the bound Fru-6-P molecules to the β-phosphorous atom on the bound ADP molecules in each of the four allosteric sites (Fig. 1-8).

The distances were then measured between the four active sites in order to distinguish the 3 unique homotropic interactions between active sites from one another (2 copies of each in the tetramer). Measuring from the phosphorous atom of one of the Fru-6-P molecules bound in the active site to the phosphorous atoms on each of the other three Fru-6-P molecules bound in the active sites generated the distances of 28 Å, 45 Å and 47 Å (Fig. 1-9).

The distances corresponding to the 3 homotropic interactions between allosteric sites were also measured within the crystal structure (2 copies of each in the tetramer). The distances were measured from the β-phosphorous atom on

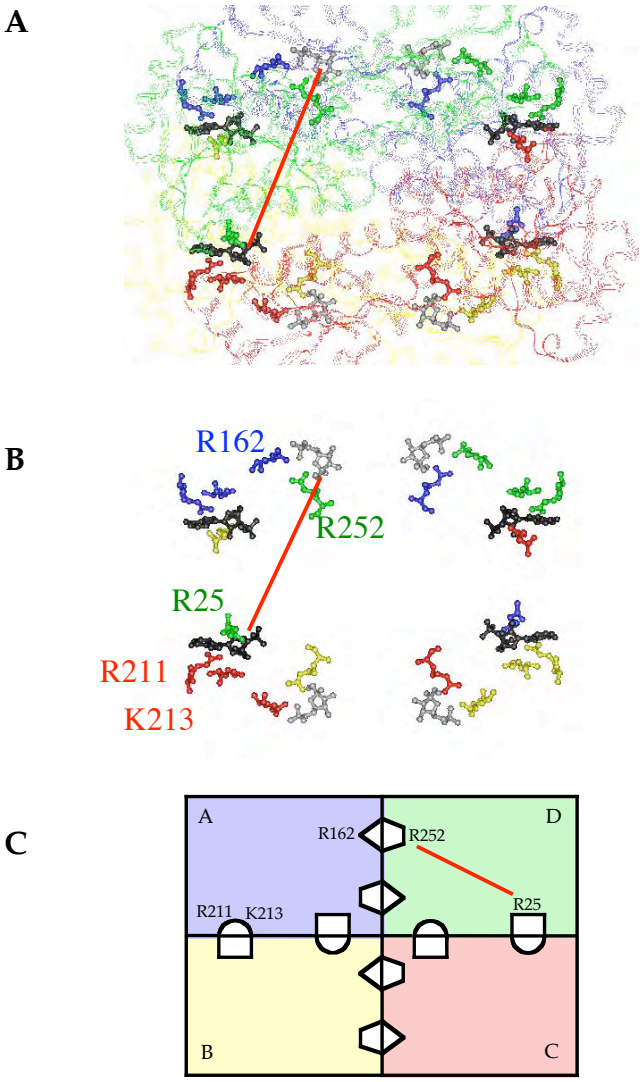

FIGURE 1-7 The identification of the 30 Å heterotropic interaction (red line in all three figures). (*A*) The crystal structure of BsPFK with the binding site residues R162, R252, R211, K213 and R25 (the "landmarks") shown in the color of the subunit from which they originate, the Fru-6-P molecules shown in gray and the ADP molecules shown in black. (*B*) Same as *A* except the protein "scaffold" is removed in order to see all the ligands and binding sites more easily. Moreover, the identities of the binding site residues are also shown. (*C*) The "mapping" of the 30 Å heterotropic interaction from the blue-R162/green-R252 binding site pair to the green-R25/red-R211/K213 binding site pair.

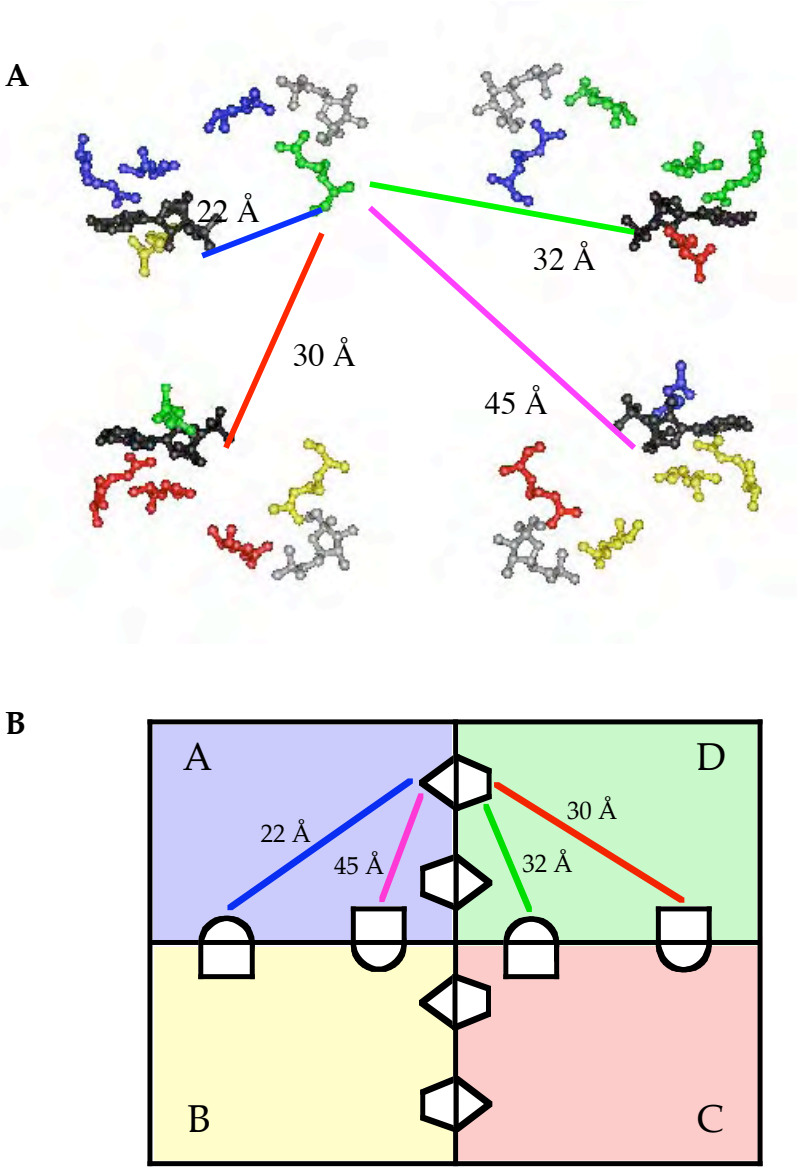

FIGURE 1-8 The four unique heterotropic interactions in BsPFK. The 22 Å heterotropic interaction is blue, the 30 Å heterotropic interaction is red, the 32 Å heterotropic interaction is green and the 45 Å heterotropic interaction is magenta. (*A*) The crystal structure of BsPFK showing just the "landmark" residues (in the color of the subunit from which they come from), Fru-6-P bound in the active sites (gray) and ADP bound in the allosteric sites (black). The four heterotropic interactions are also shown. (*B*) The two-dimensional schematic with the four heterotropic interactions mapped onto it.

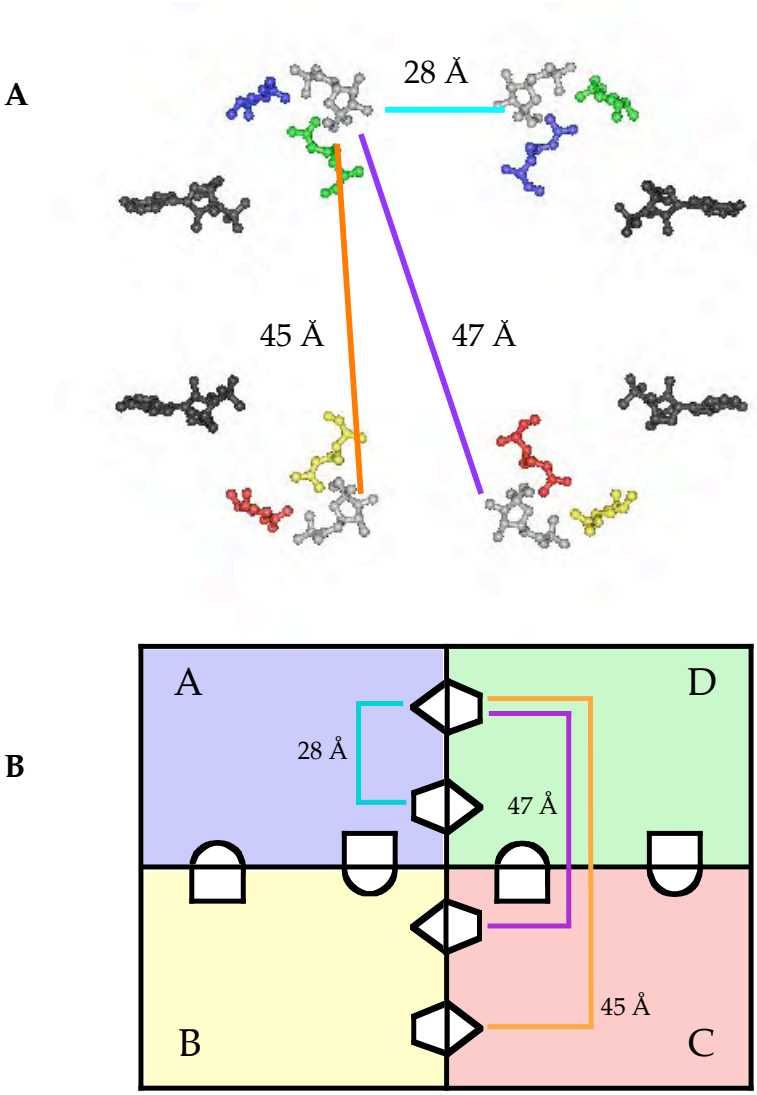

FIGURE 1-9 The three unique homotropic interactions between active sites in BsPFK. The 28 Å homotropic interaction is cyan, the 45 Å homotropic interaction is orange, and the 47 Å homotropic interaction is purple. (*A*) The crystal structure of BsPFK showing just the "landmark" residues (in the color of the subunit from which they come from), Fru-6-P bound in the active sites (gray) and ADP bound in the allosteric sites (black). The three homotropic interactions between active sites are also shown. (*B*) The two-dimensional schematic with the three homotropic interactions between active sites mapped onto it.

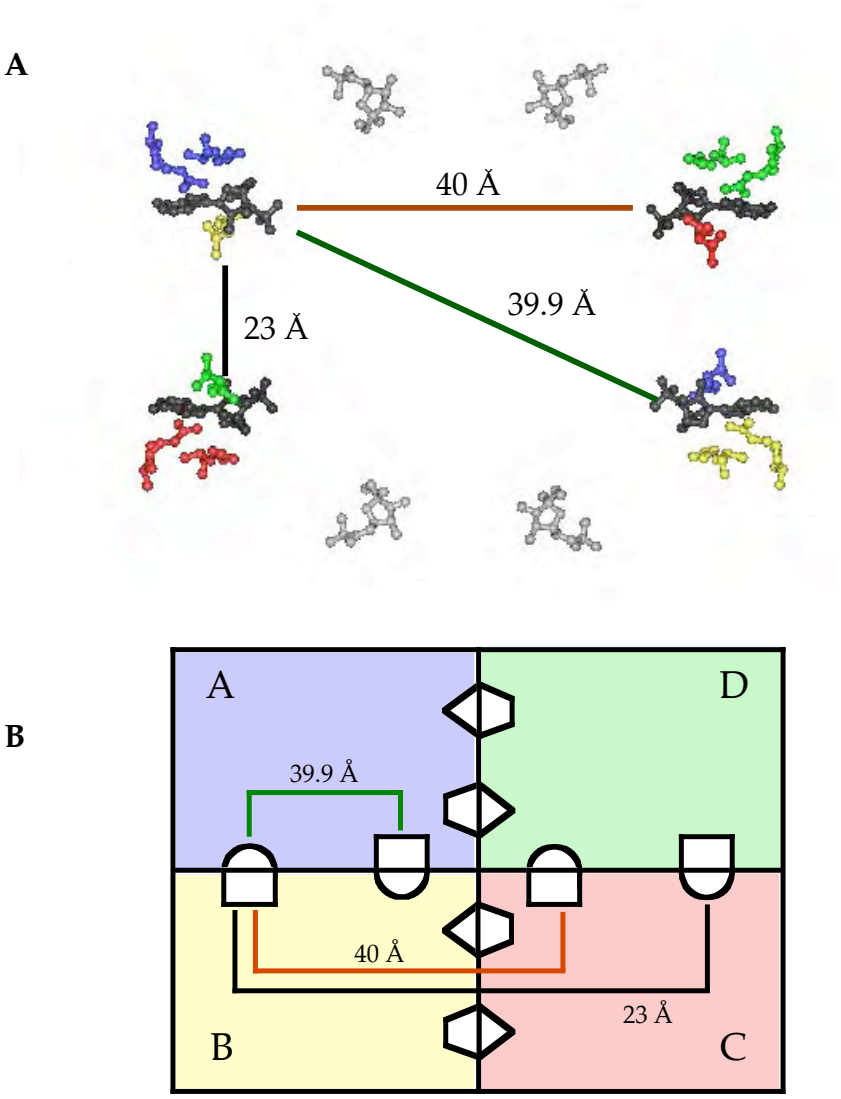

FIGURE 1-10 The three unique homotropic interactions between allosteric sites in BsPFK. The 23 Å homotropic interaction is black, the 39.9 Å homotropic interaction is dark green, and the 40 Å homotropic interaction is brown. (*A*) The crystal structure of BsPFK showing just the "landmark" residues (in the color of the subunit from which they come from), Fru-6-P bound in the active sites (gray) and ADP bound in the allosteric sites (black). The three homotropic interactions between allosteric sites are also shown. (*B*) The two-dimensional schematic with the three homotropic interactions between allosteric sites mapped onto it.

one of the ADP molecules bound in the allosteric site to the β-phosphorous atoms on each of the other three ADP molecules bound in the allosteric sites resulting in the 23 Å, 39.9 Å and 40 Å homotropic interactions (Fig. 1-10).

Methods used to probe the possible mechanism of allosteric regulation

The following text summarizes various approaches used to better understand the mechanism of allosteric regulation. Moreover, if a method or approach has been used for better understanding the allosteric regulation of PFK, it is included in this review.

The structural stability of proteins and its role in transmitting an allosteric signal. To identify the structural components involved in the transmission of an allosteric signal, Freire and colleagues (1999 and 2000; Pan et al., 2000) conducted a structure-based thermodynamic stability analysis of homologous enzymes for which high-resolution structures in various ligated states are available. Basically, they determine the structural stability constants for each residue found in an enzyme (based upon the comparison to other crystal structures and using the COREX algorithm; Hilser et al., 1998), and "map" these stability constants onto the structure of the protein to see what role protein stability plays in ligand binding and the transmission of the allosteric signal. For example, for any given protein it is postulated that the protein is dynamic and undergoes various local unfolding reactions scattered throughout the enzyme. Moreover, Freire and coworkers believe these unfolding reactions, occurring independently of one another, can involve only a few amino acids, or the entire protein, leading to a large number of potential conformational states a

given protein can "sample". Furthermore, this collection of states is termed "the native state ensemble", and by using the COREX algorithm, each residue of the protein is assigned a stability constant which reflects its probability of being either folded or unfolded within the native state ensemble.

Freire and coworkers have performed this analysis on over 20 structurally diverse proteins to date (16 of which are found in the Luque and Freire (2000) paper), and discovered some common themes in protein structure and stability. First, regions of both high stability and low stability were found distributed throughout each protein. Furthermore, the binding sites of the proteins were found to have "dual character", meaning the residues comprising the ligand binding pocket(s) were either highly stable or unstable. This phenomenon was attributed to the residues being involved in either catalysis and/or ligand binding specificity (stable) or in the transmission of an allosteric signal (less stable). Moreover, in the allosteric enzymes, the allosteric sites were found to be markedly unstable. Thus, based impart upon their results with glycerol kinase, Freire and coworkers conclude that transmission of the allosteric signal involves a unique set of residues connecting the active and allosteric sites that are unstable in the unbound form of the enzyme and become stabilized upon effector binding due to the cooperative interactions between the residues; this effectively constitutes the "mapping" of the residues involved in the transmission of the allosteric signal. Moreover, Pawlyk and Pettigrew (2002) have used these theoretical calculations to confirm the requirement of these "cooperative interactions" in transmitting the allosteric signal in glycerol kinase

(see Genetic approach – chimeric proteins section).

Structure determination of an enzyme in different ligated states. Obtaining numerous structures of a given allosteric enzyme in as many different ligation states as possible is a highly desired goal because of the information one could gain from these various "snap shots" of enzyme function and regulation. Schirmer and Evans (1990) were successful in crystallizing and solving two different ligation states of BsPFK, one with Fru-6-P and MgADP bound and the other with the non-physiological inhibitor 2-phosphoglycolate (PG) bound. Upon examining the two structures, the biggest difference was a 7° rotation of two of the four subunits (rigid dimers) about the active site interface. Thus, binding of PG at the effector sites (along the allosteric site dimer-dimer interface) causes a significant alteration of the active site dimer-dimer interface.

Another significant change involves the positions of E161 and R162. In the Fru6-P/MgADP structure, the side chain of R162 hydrogen bonds with the Fru-6-P molecule bound in the active site, while the side chain of E161 is positioned in the opposite direction. However, in the PG structure, the two residues switch positions as the side chain of E161 is now found in the active site and the side chain of R162 replaces the previous E161 position. From these results Schirmer and Evans formulated a model for PG inhibition: upon PG binding, E161 replaces R162, thus introducing a negative charge into the active site, resulting in a decrease in Fru-6-P affinity because of charge repulsion. Kimmel and Reinhart (2000) later provided evidence that this proposed mechanism is wrong using site-directed mutagenesis studies. Thus, although

crystal structures may provide insight into the conformational response of an enzyme upon ligand binding, crystal structures can also be misleading if superficial functional inferences are drawn. Thus, definitive experiments are necessary before any kind of functionality of an enzyme is assumed from a crystal structure.

Genetic approach — chimeric proteins. As mentioned initially, allosteric regulation is common to both eukaryotic and prokaryotic organisms. However, a specific enzyme found in two different organisms might be allosterically regulated in one but not the other. Due to this evolutionary divergence, a sequence comparison is commonly performed to determine which amino acids are different between the two enzymes. With the residues identified subsequent experiments are then performed to try to identify the conserved residue(s) or region(s) responsible for transmitting the allosteric signal. This identification involves making either chimeric proteins in which entire regions of the enzymes are "swapped" and their allosteric properties characterized, or by making single amino acid changes from one enzyme to the other and determining if the changes affect the allosteric properties of either enzyme.

The first example of the chimera-based approach is the formation of a chimeric phosphofructokinase between *E. coli* (EcPFK) and *B. stearothermophilus* (BsPFK) to investigate why MgATP is a much better inhibitor of EcPFK than BsPFK. Byrnes et al. (1995) hypothesized that this disparity could be a result of the structural response incurred by MgATP binding in EcPFK, but not in BsPFK. Thus, a chimeric protein (ChiPFK) was made to contain the MgATP binding

domain of BsPFK (residues 1-122 including part of the allosteric site) grafted onto the remainder of the EcPFK subunit (residues 123-319 containing the Fru-6-P binding site).

Upon characterizing ChiPFK and the two parent proteins (EcPFK and BsPFK), Byrnes et al. determined that the kinetic properties of the three enzymes are quite similar with respect to their catalytic activities and their affinities for MgATP. The major differences arose in their binding affinities for Fru-6-P and the degree of Fru-6-P cooperativity measured for the three proteins. ChiPFK was found to behave more like BsPFK with respect to both Fru-6-P binding and cooperativity, with the antagonism between MgATP and Fru-6-P still present in ChiPFK. Furthermore, and rather surprisingly, ChiPFK was also found to be insensitive to regulation by PEP binding leading to the conclusion that the structural components involved in the transmission of the allosteric signal are different for EcPFK and BsPFK.

Another example of using chimeric proteins to investigate the mechanism of allosteric regulation involves the enzyme carbamoyl-phosphate synthetase (CPS). Eroglu and Powers-Lee (2002) used a chimeric CPS to examine the possible structural basis to why *E. coli* CPS (EcCPS), which provides carbamoyl-phosphate (CP) for both arginine and pyrimidine biosynthesis, is allosterically regulated by UMP, IMP and ornithine, and *Saccharomyces cerevisiae* CPS (ScCPS), which provides CP for only arginine biosynthesis, is not. Thus, a chimera of EcCPS and ScCPS was made (ChiCPS) in which the C-terminal 136 residues of EcCPS (residues 937-1073 from the D domain which is termed the "allosteric

domain") are replaced by the corresponding residues of ScCPS (residues 959-1118) in an effort to define the structural basis for the allosteric unresponsiveness of ScCPS.

With the catalytic effectiveness of ChiCPS verified, the allosteric characterizations of the parental proteins and the chimera were performed. From the analysis it was determined that ornithine is unable to bind to ChiCPS and ScCPS, but that both UMP and IMP bind to ChiCPS and ScCPS without altering the activities of the respective enzymes. Thus, the residues involved in binding two of three allosteric effectors are intact for both ChiCPS and ScCPS. Nevertheless, the structural components found in the D domain of EcCPS involved in transmitting the heterotropic signal are different in ScCPS, rendering ScCPS and hence ChiCPS, unresponsive to UMP and IMP binding. Thus, with the D domain now identified as the region responsible for transmitting the allosteric signal, subsequent mutagenesis studies are necessary to pinpoint the responsible residues.

Glycerol kinase is another enzyme that displays different regulatory properties in different organisms. Pawlyk and Pettigrew (2002) have used the chimera-based approach to determine the possible structural components involved in binding and transmitting the allosteric signal in glycerol kinase from IIA^{Glc} binding in *E. col*i (EcGK). IIA^{Glc}, a phosphotransferase system protein, is known to inhibit EcGK activity, but glycerol kinase from *Haemophilus influenzae* (HiGK) neither binds IIA^{Glc} nor is inhibited by IIA^{Glc}, even though the primary structures of EcGK and HiGK are 87% similar (76% identical). Thus, a number

of successive chimeric proteins were made in order to determine the least amount of genetic information in EcGK required to confer not only IIA^{Glc} binding but inhibition of HiGK activity as well.

After making several chimeras, Pawlyk and Pettigrew found that by "transplanting" only 11 residues from EcGK to HiGK (8 residues that interact with IIA^{Glc} and 3 residues at the catalytic core of the protein) conferred both IIA^{Glc} binding and inhibition. Thus, a majority of the residues involved in the transmission of the allosteric signal incurred by IIA^{Glc} binding are already poised for inhibition, agreeing with the earlier data regarding EcCPS and ScCPS. Moreover, from using this chimera-based approach, Pawlyk and Pettigrew have been able to identify an allosteric locus that is essential for inhibition to occur. This finding is also consistent with the residues identified by Luque and Freire (2000), using the COREX algorithm, as being involved in the network of cooperative interactions found between the active site and the allosteric site.

Due to the potential of the chimera-based approach, our lab is currently using the amino acid sequence of a PFK from *Lactobacillus delbrueckii* (LdPFK) (47% sequence identity to EcPFK) as a chimeric partner to identify the residues responsible for transmitting the allosteric signal in EcPFK and BsPFK. In addition, the reverse experiment is also being performed in an attempt to make LdPFK allosterically responsive to either MgADP (activator) or PEP (inhibitor).

Genetic approach — site-directed mutagenesis. Site-directed mutagenesis is another approach used to elucidate the mechanism of allosteric regulation. Residues highlighted in sequence alignments or structural

considerations are changed and the allosteric properties of the mutant enzyme characterized. For this approach we will only focus on residues mutated in PFK.

Serre and coworkers (1990), using the crystal structure of EcPFK, chose L178 to mutate due to its location in an □-helix that "connects" one of the active sites and one of the allosteric sites (Shirakihara and Evans, 1988). L178 was changed to a tryptophan in hopes of destroying the "structural connection" between the two binding sites and rendering the enzyme unresponsive to allosteric regulation. Upon characterizing the L178W mutant protein, Serre et al. discovered that a majority of its binding properties are quite similar to wild-type EcPFK. The mutant binds both MgATP and Fru-6-P with wild-type affinity, and the Fru-6-P saturation profile is still cooperative (n_H mutant = 3.3, n_H EcPFK = 3.7) indicating that the homotropic interactions between the active sites are essentially conserved. Interestingly, however, the L178W mutant protein is virtually unresponsive to both MgGDP activation and PEP inhibition. Thermal denaturation protection experiments were performed in the presence and absence of the effector molecules (one at a time) to show that MgGDP and PEP were still able to bind to the mutant protein. Thus, Serre and coworkers conclude that the L178W mutation has disrupted the heterotropic communication between the active sites and allosteric sites, implicating □-helix 7 as playing a major role in transmitting both the activation and inhibition signals. Furthermore, these results also suggest a common pathway for the two allosteric signals, which is difficult to rationalize since the two effectors produce opposite effects upon Fru-6-P binding. However, a tree analogy can be made in which □-

helix 7 would serve as the "trunk" of the allosteric signal, and differentiation into either activation or inhibition would occur in the "branches" of the tree. Thus, by affecting the trunk (via the L178W mutation), the branches are affected as well (transmission of both allosteric signals).

Another example of using site-directed mutagenesis to probe the mechanism of allosteric regulation resulted in disproving a widely accepted mechanism for the inhibition of BsPFK by PEP. Kimmel and Reinhart (2000) tested the proposed charge-repulsion mechanism of Schirmer and Evans (1990) regarding the roles of E161 and R162 in the inhibition process of BsPFK by simply substituting either residue or both simultaneously with alanines.

Upon characterizing the steady-state kinetics of each of the three mutant proteins it was found that all three mutant proteins are still inhibited by PEP, although to varying degrees. The E161A mutant protein was least affected in its ability to be inhibited by PEP (~10% change in coupling free energy, ΔG_{ay}), while the R162A and R162A/E161A mutant proteins displayed an approximate 40% loss in PEP's inhibitory effects. However, regardless of the degree of PEP inhibition measured, what is important is that all three mutant proteins are *still* inhibited by PEP, thus eliminating Schirmer and Evans' proposed charge-repulsion model. Nevertheless, some loss in PEP's effects is observed in either case, thus, R162 and E161 may be involved in part of the transmission of the allosteric signal.

The final example of using site-directed mutagenesis to probe the allosteric properties of PFK involves the mutation of the residues lining the

putative Fru-2,6-P_2 activating site found in rabbit muscle PFK (RmPFK). Chang and Kemp (2002) constructed three mutant proteins S530D, R292A and H662A, to test their hypothesis regarding the evolutionary divergence of the duplicated active sites into allosteric sites specific for Fru-2,6-P_2 activation. In these proteins, S530 , R292 and H662 of RmPFK are analogous to D127, R243 and H249 of EcPFK.

Upon characterizing the three mutant proteins via steady-state kinetics, Chang and Kemp discovered that the binding affinity for Fru-6-P was nearly identical to wild-type, thus supporting the hypothesis that the duplicated active sites were no longer binding Fru-6-P, and had in fact evolved to bind Fru-2,6-P_2. Moreover, a significant change in the ability of Fru-2,6-P_2 to activate RmPFK was also observed. The S530D mutant protein did not respond to the concentrations of Fru-2,6-P_2 used, while the R292A and H662A mutant proteins were still activated by Fru-2,6-P_2, but to a lesser degree. Thus, from these mutational studies, Change and Kemp were able to confirm the identity of the Fru-2,6-P_2 allosteric activating sites in RmPFK.

Using hybrid enzymes to isolate and characterize specific allosteric interactions. Using hybrid enzymes to study the behavior of enzymes is not new to the field of enzymology, but using hybrid enzymes to isolate and characterize specific allosteric interactions found within a particular allosteric enzyme is. Four examples will be discussed: hybrid tetramers of porcine liver fructose-1,6-bisphosphatase; hybrid tetramers of human hemoglobin; and hybrid tetramers of EcPFK and BsPFK.

Fructose-1,6-bisphosphatase (FBPase) is a homotetramer that catalyzes the hydrolysis of Fru-1,6-P_2 to Fru-6-P and inorganic phosphate, and the reaction is inhibited by AMP binding 28 Å away from the nearest active site (Nelson et al., 2002). To address the mechanism by which AMP inhibits FBPase, Nelson et al. (2002) have created and isolated FBPase hybrids that contain either wild-type subunits or AMP-binding deficient subunits. Moreover, it was previously reported that AMP must bind to two subunits of FBPase to cause inhibition (Kelly-Loughnana and Kantrowitz, 2001). Thus, three different 2:2 hybrids of wild-type FBPase and AMP-binding deficient subunits were isolated to determine which two AMP-binding sites triggered inhibition, or if the identity of the two AMP-binding sites was insignificant (Fig. 1-11 illustrates the three 2:2 hybrids in question and their designations).

Unfortunately for Nelson et al., they were only able to separate the 2:2p hybrid away from the 2:2q and 2:2r hybrids using anion exchange chromatography and a glutamate tag on the c-terminus of the mutated subunits. Due to this inadequate degree of separation, their comparisons of AMP inhibition and AMP cooperativity are only between the 2:2p hybrid and a mixture of the 2:2p and 2:2r hybrids. Interestingly, upon characterizing the 2:2 hybrids via steady-state kinetics and fluorescence, it was found that an AMP molecule must bind to a top and bottom subunit to display cooperativity in AMP binding and inhibition of FBPase activity ($nH = 1.5 \pm 1$) (either 2:2q or 2:2r hybrids). However, AMP molecules bound to the same half (both top or both

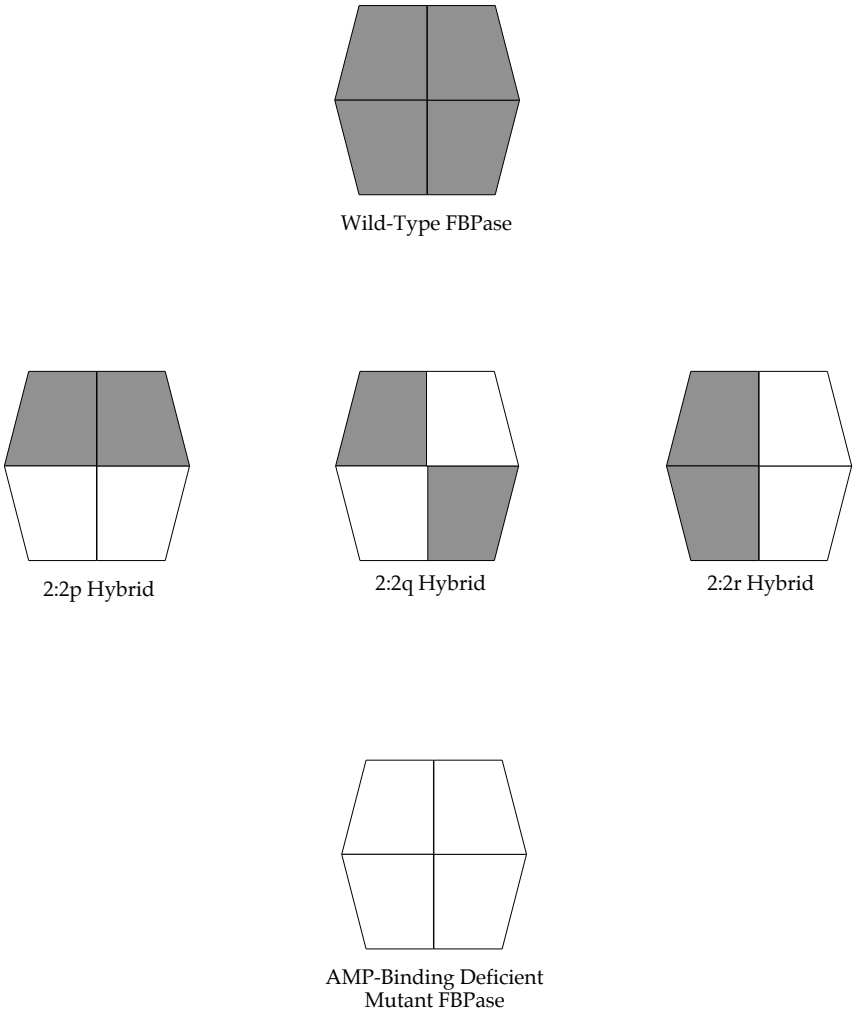

FIGURE 1-11 The three 2:2 FBPase hybrids (2:2p, 2:2q and 2:2r) examined to address both the inhibition of the enzyme by AMP and the cooperative effects observed in AMP binding for the native enzyme.

bottom – 2:2p hybrid) of the tetramer can still inhibit the enzyme (to a lesser degree, $IC_{50\text{-}AMP}$ 2:2q/2:2r = 6.8 ± 0.5 and $IC_{50\text{-}AMP}$ 2:2p = 43 ± 2), but in the absence of cooperativity in AMP binding to the enzyme (n_H = 0.99 ± 0.5). Thus, by characterizing the 2:2 hybrids, Nelson et al. (2002) have shown a variability in the contributions of both the heterotropic and homotropic interactions in AMP inhibiting FBPase, a result consistent with our own data.

Ackers and coworkers have used hybrids to gain insight into the possible mechanism of allosteric regulation of hemoglobin. Hemoglobin (Hb), a tetramer consisting of two □□ dimers, is the protein responsible for oxygen transport in blood. It displays positive cooperativity upon oxygen binding leading to the development of numerous models to explain the allosteric behavior of proteins and enzymes. By making various hybrid forms of hemoglobin which contain varied amounts of oxygenated subunits (resulting in the 10 possible hybrids shown in Fig. 1-12), Ackers et al. sought to identify the mechanism by which the cooperative signal is transmitted through the protein.

To summarize a great deal of work from the last 20 years involving hybrids, Ackers and coworkers have devised an alternative model to explain the positive cooperativity measured for oxygen binding in Hb. The model is called the Symmetry Rule and is based upon the cooperative free energies measured in each of the 10 species (Fig. 1-12) in which the cooperative free energy is the difference in the binding free energy measured for the hybrid tetramer and the two dimers that comprise that hybrid tetramer. For example, to determine the

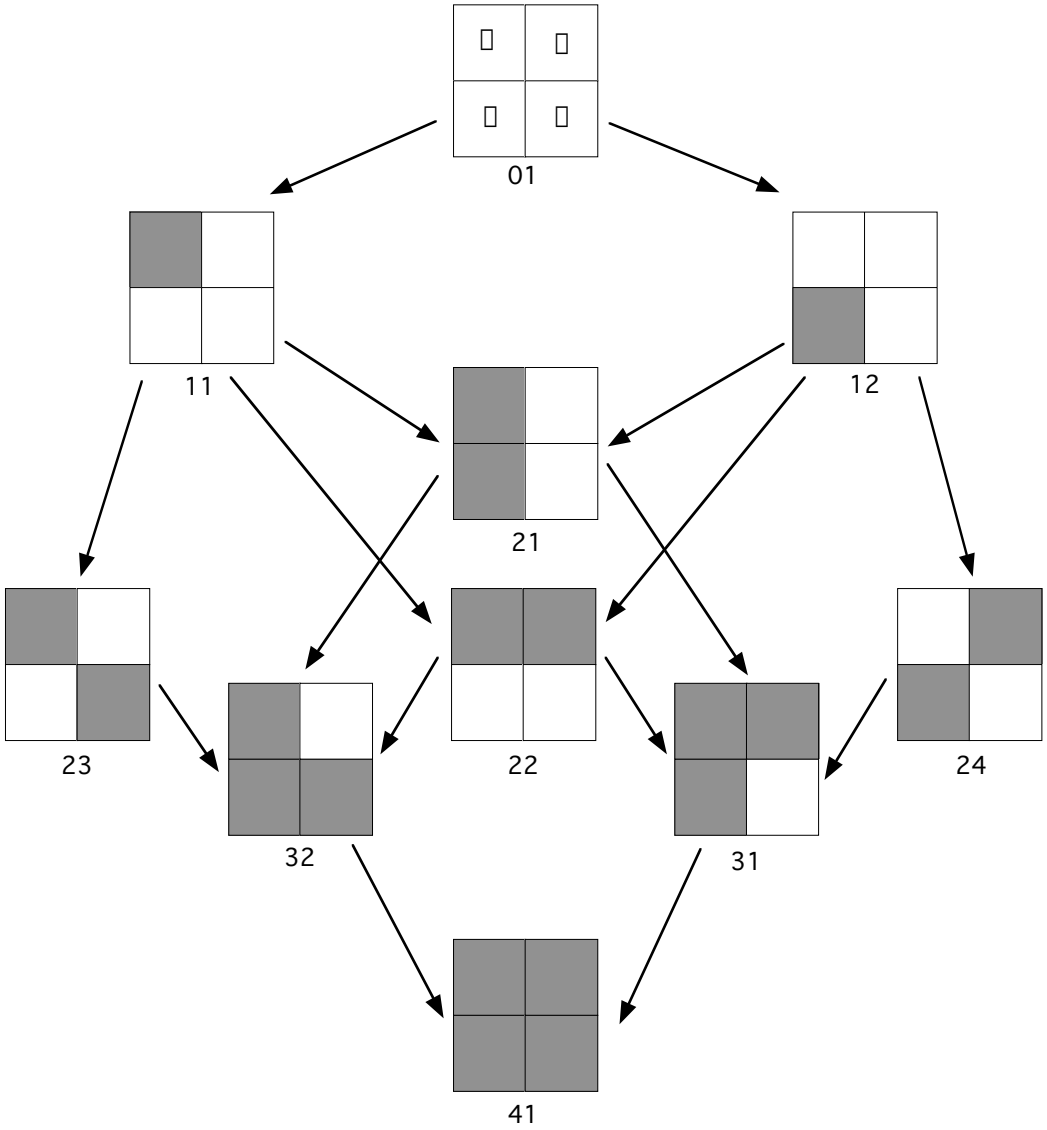

FIGURE 1-12 The 10 hybrid hemoglobin species (adapted from Ackers et al., 2000). Deoxygenated subunits are "open" while oxygenated subunits are "shaded". The different ligated species are also "named" in the figure with the first number indicating the number of oxygen molecules bound and the second number indicating what number species of the ligated form it is: fully deoxygenated = '01'; singly ligated = '11' or '12'; doubly ligated = '21', '22', '23' or '24'; triply ligated = '31' or '32'; fully oxygenated = '41'.

cooperative free energy for the '11' hybrid, the binding free energies are first determined for a singly ligated □□ dimer and an oxygen-free □□ dimer and those two values are added together. Next, that value is subtracted from the binding free energy measured for the '11' hybrid resulting in a cooperative free energy. Thus, if Hb was not cooperative, the binding free energy measured for the '11' hybrid would equal the sum of the binding free energies measured for the two dimers that comprise the '11' hybrid.

Utilizing this analysis, Ackers and coworkers found that the cooperative binding free energies determined for the 10 hybrid species were segregated into four unique energy levels. The unligated molecule (10) occupies the first energy level (zero), while the singly ligated molecules (11 and 12) occupy the next energy level (~3 kcal/mol). The '21' doubly ligated molecule occupies an energy level all its own at ~5 kcal/mol and the remaining species then comprise the final energy level (~6 kcal/mol) and includes the other three doubly ligated molecules (22, 23 and 24), the triply ligated molecules (31 and 32) and the fully ligated molecule (41). Since the '21' species is different than either the 11/12 or 22/23/24 species, each interface is suggested to have a different role in the transmission of the allosteric signal. Ackers and coworkers have also performed a great deal of site-directed mutagenesis and characterization of the residues in between the dimer-dimer interfaces supporting their observations that the two dimers act autonomously until an oxygen molecule binds to both dimers (Ackers et al., 1992, 2000 and 2002; Holt and Ackers, 1995).

Finally, Kimmel and Reinhart (2001) and Fenton and Reinhart (2002) have

successfully isolated one of four specific heterotropic interactions found in either the BsPFK or EcPFK enzymes utilizing the same hybrid approach. For both enzymes, mutations at both the active sites and allosteric sites were made to diminish both Fru-6P binding and PEP binding for BsPFK or MgADP binding for EcPFK. Two residues on the surface of the mutant protein were also mutated so that the various hybrid species could be separated via anion exchange chromatography. Hybrids were then made between the wild-type enzyme and the ligand binding deficient mutant protein and applied to an anion exchange column in order to separate the 1:3 hybrid (1 wild-type subunit:3 mutated subunits) from the other hybrid species. The method for the hybrid making procedure can be found in Chapter II. Thus, for both BsPFK and EcPFK, a hybrid enzyme containing one native active site and one native allosteric site was isolated, and more importantly contained only one of the 28 total native allosteric interactions found in the native enzymes.

For the BsPFK 1:3 hybrid, Kimmel and Reinhart chose to investigate the contribution the isolated heterotropic interaction made to the inhibition of BsPFK by PEP. After a thorough steady-state kinetic analysis was performed, it was determined that the isolated heterotropic interaction contributes about 41% to the inhibition measured for the wild-type enzyme. It was concluded that the diminished amount of inhibition measured for the 1:3 hybrid was either a result of the mutations made to isolate the 1:3 hybrid or that the one heterotropic interaction is one of many allosteric interactions involved in transmitting the inhibitory signal. Only further analysis of the other three possible 1:3 hybrids

can resolve this issue.

For the EcPFK 1:3 hybrid, Fenton and Reinhart examined the contribution the isolated heterotropic interaction made to the activation of EcPFK by MgADP. Consistent with the results of the BsPFK 1:3 hybrid, the 1:3 hybrid retained about 37% of the wild-type activation. However, comparison to the wild-type enzyme in this case was not appropriate due to the loss in Fru-6-P cooperativity in the 1:3 hybrid. Thus, an additional hybrid was constructed to contain one native active site and four native allosteric sites to eliminate any of the allosteric effects incurred by the homotropic interactions between the active sites (cooperativity) in the wild-type enzyme. After the characterization of this secondary hybrid was performed, the percent contribution of the isolated heterotropic interaction to MgADP activation was decreased from ~37% to ~20%. This reduction is explained by the increased activation measured in the secondary hybrid and the fact that the homotropic interactions between the active sites in the wild-type EcPFK enzyme diminish the allosteric effect incurred by MgADP binding. Again, like BsPFK, further analysis of the other three 1:3 hybrids is required to address if the strategy in isolating the heterotropic interaction is responsible for the less than 100% contribution or if the isolated heterotropic interaction is merely one of the many players involved in the activation process in EcPFK.

Gene duplication. The final section of this review concerns sequence alignments to identify gene duplication events, which in turn enables the identification of putative binding sites in enzymes for which structural

information is missing. Poorman et al. (1984) have postulated that rabbit muscle PFK (RmPFK) is a gene duplication of a bacterial PFK, based upon the sequence homology between the N and C-termini of RmPFK, EcPFK and BsPFK. Moreover, this duplication pattern has also been observed in several other eukaryotic PFK's (yeast, liver, brain and fruit fly) (Gehnrich et al., 1988; Li et al., 1994; Heinisch et al., 1989 and Currie and Sullivan, 1994). Unfortunately, no crystal structure is available for the mammalian enzyme.

The major differences between RmPFK, EcPFK and BsPFK are the relative sizes of the three proteins (RmPFK is about twice the size as EcPFK and BsPFK) and the number of effector molecules that regulate enzyme activity. Poorman et al. postulate that each monomer of RmPFK (tetramer) is composed of two monomers of bacterial PFK linked with approximately 30 amino acids, resulting in eight active sites and eight allosteric sites for RmPFK. Interestingly, experiments have only indicated four active sites in RmPFK; suggesting that four of the eight active sites have mutated into allosteric sites that are now capable of binding Fru-2,6-P_2 as an activator. This idea is substantiated by the sequence alignments of the Fru-6-P binding sites that show D127 mutated to a serine in four of the binding sites, a residue implicated for catalysis in BsPFK. Furthermore, by removing the negative charge of D127 in RmPFK, more room is provided for Fru-2,6-P_2 binding. Thus, rationalizing how Fru-2,6-P_2 is an activator of RmPFK is not difficult due to the significant amount of positive cooperativity measured for Fru-6-P binding in EcPFK. Furthermore, from this sequence comparison it is quite possible to believe that the structural

components involved in transmitting the allosteric signal between Fru-2,6-P_2 and Fru-6-P in RmPFK were previously established in the bacterial enzyme (EcPFK) via the homotropic interactions between Fru-6-P binding sites. It should be noted that Li et al. (1999) and Chang and Kemp (2002), using site-directed mutagenesis, have further substantiated that the four putative Fru-2,6-P_2 binding sites do in fact bind Fru-2,6-P_2.

Kemp and Gunasekera (2002) have built upon the ideas established by Poorman et al., using the same gene-duplication approach to identify the origins of the ATP and citrate allosteric sites in mouse PFK (mPFK). From the same sequence comparisons used by Poorman et al., it was proposed that the bacterial MgADP/PEP binding sites evolved to become the MgATP inhibitory sites and citrate inhibitory sites in mPFK. Based upon the sequence alignments of the N and C-termini with the sequences from EcPFK and BsPFK, residues from mPFK were selected as candidates (R47, R429 and R433) for site-directed mutagenesis to determine if inhibition by MgATP or citrate was diminished. Kemp and Gunasekera constructed three mutant proteins, R47L (N-terminus half; analogous to R25 in EcPFK and BsPFK), R429A and R433A (C-terminus half; analogous to R21 and R25 in EcPFK and BsPFK), and characterized their allosteric properties. The specific activities of all three mutant proteins were found to be virtually identical to wild-type as well their binding affinities for Fru-6-P and MgATP. The differences between the mutant proteins arose when comparing their allosteric properties. For the R47L mutant protein, MgATP was found to inhibit the enzyme while citrate was not, while the R429A and R433

mutant proteins were inhibited by citrate but not MgATP. Thus, from these results, Kemp and Gunasekera (2002) have proposed that the ancestral (bacterial) MgADP/PEP allosteric sites have evolved to become either a citrate inhibitory site (R47) or a MgATP inhibitory site (R429 and R433) in mammalian PFK.

Figure 1-13 summarizes the results of Kemp and Gunasekera, Poorman et al. (1984), Li et al. (1999) and Change and Kemp (2002) in a schematic of how the active and allosteric sites of the bacterial PFK enzyme evolved into the active and allosteric sites of the mammalian enzyme. Interestingly, the new inhibitory sites found in mPFK (citrate and MgATP) seem to have evolved from the duplicated MgADP/PEP allosteric sites, whereas the new activating sites (Fru-2,6-P_2 and MgADP or MgAMP) appear to have evolved from the duplicated active sites. Thus, by simply using a sequence alignment and simple mutagenesis, putative active sites and allosteric sites have been identified for the mammalian enzyme in the absence of any kind of structural data.

The results summarized here are representative examples of how the field of allosterism has benefited from the approaches taken by numerous labs and how each result provides additional information into answering the enigma of how allosterism "works". By using structural data, amino acid sequence comparisons, site-directed mutagenesis and hybrid enzymes, specific residues and regions of proteins have either been suggested or shown to be involved in the transmission of an allosteric signal. Thus, by using a combination of these

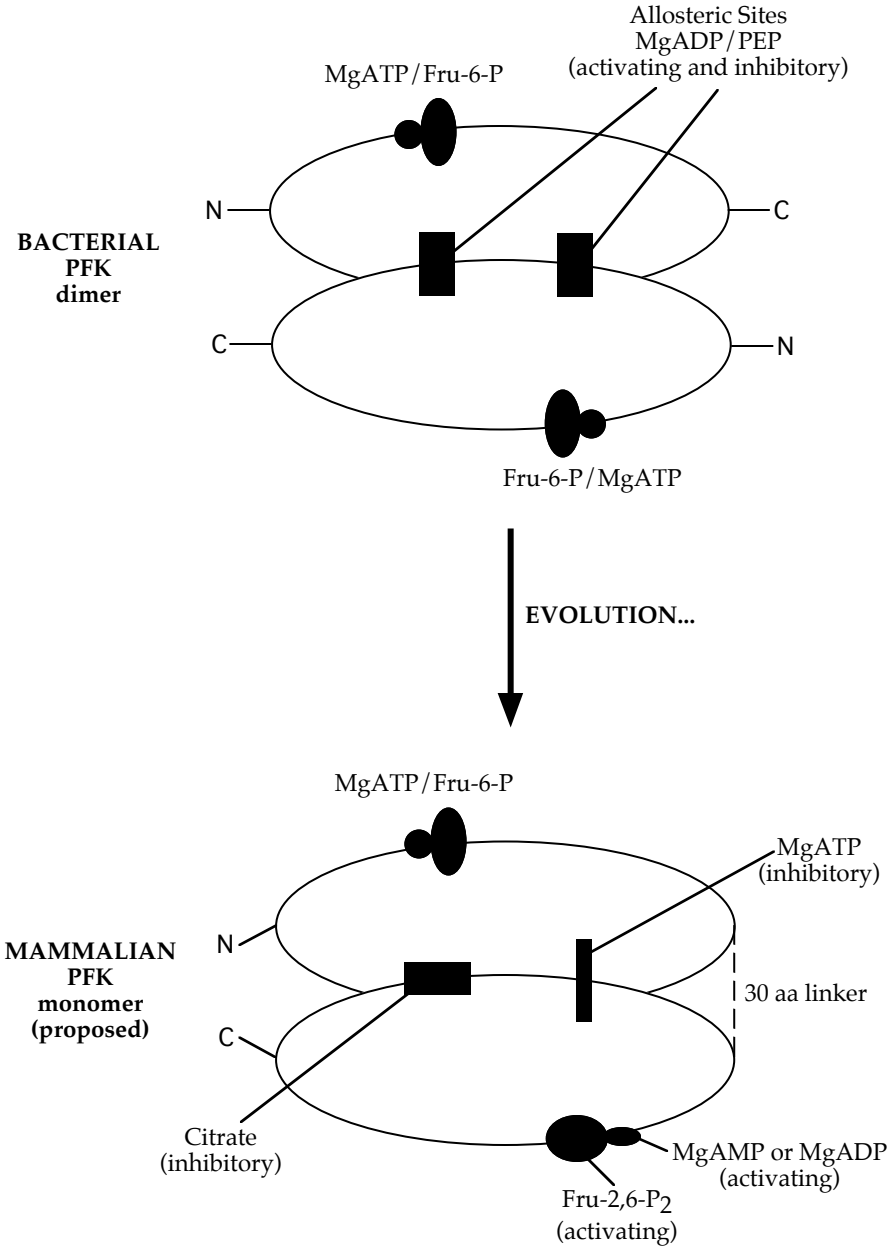

FIGURE 1-13 A model for the evolution of a monomer of mammalian PFK from a dimer of a bacterial predecessor (adapted from Kemp and Gunasekera (2002)). For the mammalian form, both inhibitory sites (citrate and MgATP) seem to have evolved from the MgADP/PEP allosteric sites, while the activating sites (Fru-2,6-P_2 and MgAMP or MgADP) appear to have evolved from the duplicated substrate binding/active sites.

approaches, we hope to elucidate the mechanism of allosteric regulation specifically in BsPFK by measuring the contributions of each of the 10 unique allosteric interactions found in the enzyme to the inhibition response. In turn, we will be able to better understand the basis for how PEP inhibits PFK activity and we will also be able to address the roles each interaction plays in transmitting the allosteric signal between the eight binding sites.

Present study

The main goal of our investigation is to gain a better understanding of how allosteric regulation occurs, and more specifically how inhibition by PEP occurs in BsPFK. The common link among all four data chapters (III, IV, V and VI) is the use of hybrid tetramers to take a divide-and-conquer approach in assessing the role of each interaction individually in order to address how they ultimately combine in the tetramer.

Chapter II provides a detailed explanation of most the materials and methods that were used to form, isolate, identify and characterize, utilizing linked-function analysis, all the different hybrid enzymes used in our investigation (1:3 hybrids and 2:2 hybrids). Chapter III explains the strategy as well as the trials and tribulations behind individually isolating two of the four unique heterotropic interactions (the 30 Å and 32 Å heterotropic interactions) via the 1:3 hybrids, and concludes with the results from the allosteric characterizations of the 30 Å and 32 Å heterotropic interactions to assess their roles in the inhibition process. Chapter IV is an extension of Chapter III as it discusses the contributions of all four heterotropic interactions to the inhibition

process, and also addresses how their contributions compare not only to one another, but to the overall inhibition measured in the native tetramer and a wild-type variant that lacks PEP cooperativity.

With four of the ten unique allosteric interactions characterized, the next step was to determine the roles each of the six homotropic interactions play in the inhibition process, and we addressed that question via the 2:2 hybrids. Thus, Chapter V discusses how nine different 2:2 hybrids were formed, isolated and identified using the same mutant proteins previously used in Chapters III and IV. Furthermore, the strategy of isolating and identifying the 2:2 hybrids with the use of strategically placed charge tag mutations on the surface of the protein is also described. Chapter VI discusses the allosteric characterizations of the nine 2:2 hybrids and also talks about the characterizations of the six unique homotropic interactions as well as how the allosteric interactions combine uniquely in each of the nine 2:2 hybrids. Finally, Chapter VII summarizes all of the results discussed in the previous chapters and elaborates upon possible future work.

CHAPTER II

GENERAL METHODS

Materials and methods

Materials. All chemical reagents used in buffers, protein purifications and enzymatic assays were of analytical grade, purchased from either Fisher or Sigma. The Matrex Gel Blue A-agarose resin for was purchased from Amicon Corporation. Creatine kinase and the coupling enzymes (aldolase, triosephosphate isomerase and glycerol-3-phosphate dehydrogenase in ammonium sulfate suspensions) were purchased from Roche. The coupling enzymes were dialyzed against buffer containing 50 mM MOPS-KOH, 100 mM KCl, 5 mM $MgCl_2$ and 0.1 mM EDTA at pH 7.0 before use. Creatine phosphate, NADH, and the sodium salts of Fru-6-P and PEP were purchased from Sigma. The sodium salt of ATP was obtained from either Sigma or Roche. Site-directed mutagenesis was performed using the Altered Sites *In Vitro* Mutagenesis System which was purchased from Promega and included the pALTER mutagenesis vector, the pALTER control vector, and ampicillin repair and control oligonucleotides. All other oligonucleotides were synthesized using an Applied Biosystems 392 DNA/RNA synthesizer at the Gene Technologies Laboratory at the Institute of Developmental and Molecular Biology at Texas A&M University. DNA modifying enzymes (T4 polynucleotide kinase, T4 DNA polymerase and T4 ligase) were purchased from Promega. The plasmid used for all mutagenesis reactions, pGDR26 (Riley-Lovingshimer et al., 2001), was derived from pBR322/Bs-pfk (French et al., 1987), a plasmid obtained from Dr. Simon Chang

(Louisiana State University). A glycerol stock of *E. coli* DF1020 cells, which were used to express both wild-type and mutant forms of BsPFK, was obtained from Dr. Robert Kemp (Chicago Medical School). Deionized distilled water was used throughout.

Nomenclature. In order to differentiate among all the different BsPFK hybrid species created for this investigation, several notations have been introduced for clarification. The first notation is used when identifying the different BsPFK hybrid enzymes, and refers to the number of subunits each parental enzyme contributes to the hybrid enzyme. For example, to isolate one of the four possible heterotropic interactions, a 1:3 hybrid is isolated. The 1:3 notation refers to 1 wild-type subunit and 3 mutant subunits. Thus, a 2:2 hybrid is 2 wild-type subunits and 2 mutant subunits.

The second notation, introduced by Fenton and Reinhart (2002), refers to the number of native binding sites a hybrid enzyme contains. Using the same example as above, the 1:3 hybrid can also be designated as a 1|1 hybrid where the left side of the slash refers to the number of native active sites and the right side of the slash refers to the number of native allosteric sites. Thus, wild-type BsPFK would be designated 4|4 and a mutant form of BsPFK where both the active sites and allosteric sites have been mutated to discourage ligand binding would be designated 0|0. Control hybrids or hybrids that contain only one native active and no native allosteric sites have also been made to assess the influence upon the observed allosteric effect in a 1:3 hybrid from the mutated allosteric sites, and its notation would be 1|0.

The last notation introduced by Ortigosa et al. (2003), refers to the sides of the binding sites mutated in the mutant parental protein used in making the BsPFK hybrids. As Chapter I introduced, all of the binding sites found in BsPFK are located along the dimer-dimer interfaces of the protein, thus two subunits are required to constitute a full binding site. To orientate ourselves within the structure, we have designated the two sides of the active site as the a-side (R162 and R243) and the b-side (R252), while the allosteric site has been divided into the □-side (R211,K213) and the □-side (R25). The amino acids in parentheses are the residues found on those respective sides of the interface, and are the residues mutated for this study. Thus, in order isolate the 30 Å heterotropic interaction via it's respective 1:3 hybrid, the mutant parental protein (0:4 or 0|0) must have the b-side of the active site mutated and the □-side of the allosteric site mutated generating the [b,□] mutant parental protein. Moreover, to isolate the 32 Å heterotropic interaction, the [b,□] mutant parental protein is required.

Site-directed mutagenesis. Mutagenesis was performed following the protocol for the Altered Sites in Vitro Mutagenesis System as provided by Promega. Single stranded DNA (ssDNA) of pGDR26 was made using the helper phage R408 (Hutchinson et al., 1978) and isolated. pGDR26 is a plasmid previously constructed containing the BsPFK gene ligated into the pALTER mutagenesis vector (Riley-Lovingshimer et al., 2001).

Prior to performing the mutagenesis, phosphorylation of the 5'-end of each oligonucleotide (both the mutant and ampicillin repair oligonucleotides) was performed using T4 polynucleotide kinase to increase the number of

mutants obtained, and subsequently annealed to the previously isolated ssDNA from pGDR26. A five to one ratio of mutant oligonucleotide to ampicillin repair oligonucleotide was used to increase the chance of creating a plasmid containing both the ampicillin repair oligonucleotide and the mutant oligonucleotide(s). Furthermore, a five to one ratio of ampicillin oligonucleotide to ssDNA was used to increase the probability of the oligonucleotide(s) annealing to the DNA. At this point, as long as oligonucleotide overlap was not a problem, all the desired mutant oligonucleotides were annealed at once. The oligonucleotides were extended and ligated using T4 DNA polymerase and T4 DNA ligase respectively. The resulting plasmids were transformed into competent BMH 71-18 mutS cells (thi, supE, Δ(lac-proAB), [mutS::Tn10] [F', $proA^{-}B^{-}$, $lacI^{q}Z\Delta M15$]) (Kramer et al., 1984), which are deficient in DNA mismatch repair functions (Zell et al., 1987), using the calcium chloride method (Cohen et al., 1972). The entire transformation reaction was then plated on a Luria-Bertani plate (10 g/L tryptone, 5 g/L yeast extract and 10 g/L sodium chloride) containing ampicillin (LB Amp) at a concentration of 100 □g/mL and incubated overnight at 37°C.

Ampicillin resistant plasmids were transformed into competent XL1-Blue cells, (endA1, recA1, gyrA96, thi-1, hsdR17, relA1, supE44, lac[F', $proA^{-}B^{-}$, $lacI^{q}Z\Delta M15$, Tn10 (Tet^{r})]) (Bullock et al., 1987) and the resulting ampicillin resistant plasmids sequenced. The entire BsPFK gene was sequenced to confirm the desired mutations by the Sanger dideoxy method using an Applied Biosystems sequencer and dye-labeled terminators (Sanger et al., 1977).

Wild-type BsPFK and all of the mutant proteins were expressed from the

pALTER mutagenesis vector that was transformed into competent DF1020 cells [a recA derivative of DF1010: pro-82, ΔpfkB201, recA56, Δ(rha-pfkA)200, endA1, hdsR17, supE44], a PFK-1 and PFK-2 deficient strain (Daldal, 1983).

Enzymatic activity assays. The activity of the various BsPFK enzyme species were measured by coupling the production of fructose-1,6-bisphosphate to the oxidation of NADH (Babul, 1978; Kolartz and Buc, 1982), and monitoring the corresponding decrease in absorbance at 340 nm. The entire coupled assay (enzymes and the intermediates necessary), as well as the MgATP regeneration system, is shown in Fig. 2-1. Assays were carried out in either a 1.0 mL or 0.6 mL reaction volume of 50 mM MES-KOH (pH 6.0), 50 mM MOPS-KOH (pH 7.0) or 50 mM EPPS-KOH (pH 8.0) buffer containing 100 mM KCl, 5 mM $MgCl_2$, 0.1 mM EDTA, 2 mM DTT, 0.2 mM NADH, 250 □g of aldolase, 50 □g of glycerol-3-phosphate dehydrogenase and 5 □g of triosephosphate isomerase adjusted to the pH of choice. MgATP was held constant at 3 mM and the concentrations of Fru-6-P and PEP were adjusted as indicated. Assays were initiated with $1/100^{th}$ of the reaction volume (10 □L or 6 □L) of appropriately diluted BsPFK so that the amount of activity would not result in a change of absorbance greater than 0.02 absorbance units/minute. For experiments involving the analysis of the effect of PEP on the binding affinity of Fru-6-P or *vice versa*, creatine kinase and creatine phosphate were added to regenerate MgATP from MgADP to prevent the accumulation of MgADP (shown in Fig. 2-1). All activity measurements were performed on Beckman Series 600 spectrophotometers using a linear regression calculation to convert the change in absorbance at 340 nm to enzyme activity.

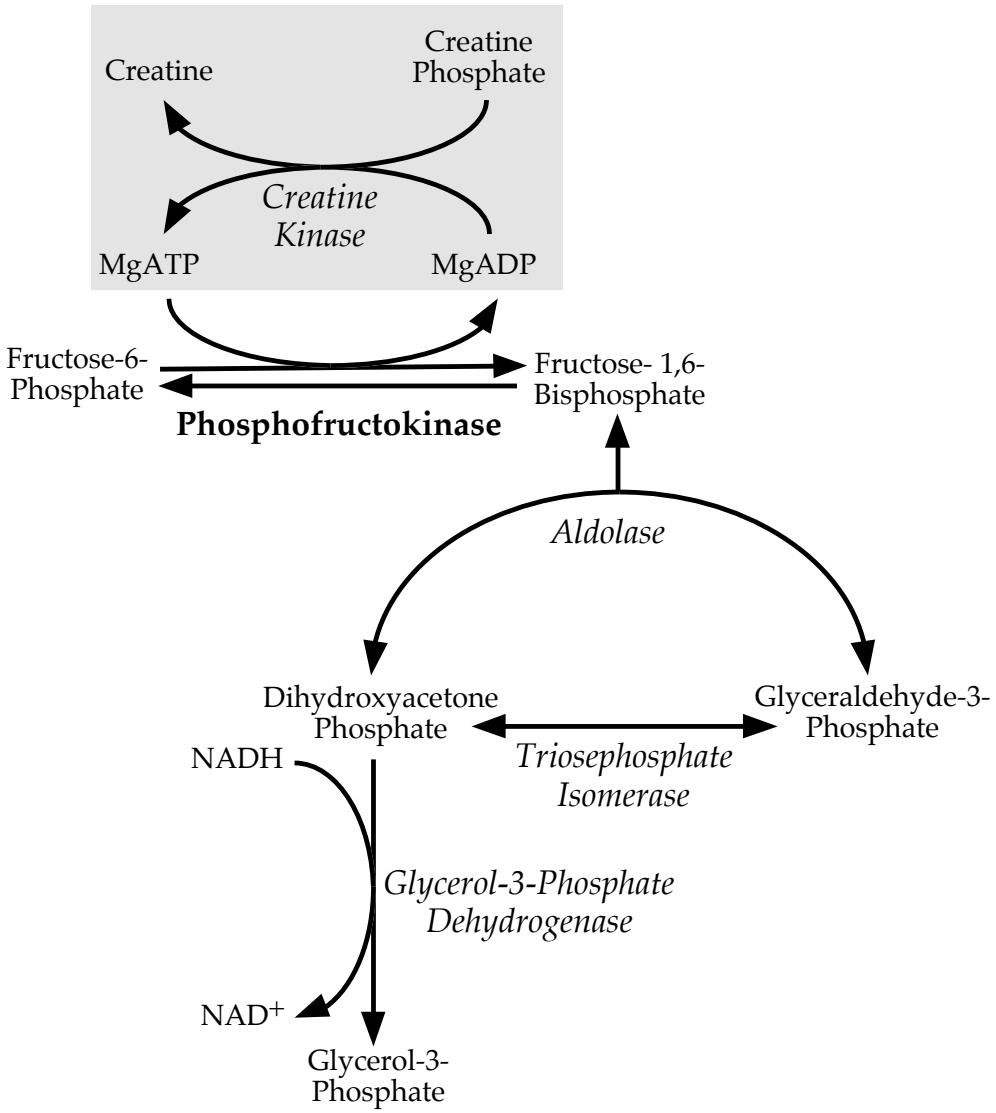

FIGURE 2-1 The coupling enzyme system used to assay BsPFK activity. The production of fructose-1,6-bisphosphate by phosphofructokinase is coupled via three enzymes (aldolase, triose phosphate isomerase and glycerol-3-phosphate dehydrogenase) to the oxidation of NADH to NAD^+, which is monitored spectroscopically at 340 nm. The enzymes involved in this process are in italics and the regeneration system used to regenerate ATP and avoid accumulation of ADP during the assay is shown in the gray box.

One unit (U) of activity is defined as the amount of enzyme needed to produce 1 μmol of fructose 1,6-bisphosphate per minute.

Protein purification. Purification of wild-type and mutant BsPFK proteins was performed as described by Valdez et al. (1989). DF1020 cells containing the plasmid of interest were grown to stationary phase (approximately 20-24 hours) in LB broth containing 100 □g/mL ampicillin at 37°C. Cells were harvested by centrifugation at 4,000 RPM using a Beckman Model J-6B centrifuge. Pelleted cells were either stored at 0°C for later use or stored at –80°C until the cells were frozen. The frozen cells were resuspended in approximately 30-40 mL of cell lysis buffer (50 mM Tris-HCl pH 7.5, 1 mM DTT and 1 mM EDTA) and set on ice. Cells were lysed by sonication using a Sonic Dismembrator Model 550 (Fisher Scientific). Fifteen-second pulses were used followed by a one-minute rest period to allow the cells to cool for a total time of at least 40 minutes. The crude lysate was clarified by centrifugation at 12,000 RPM for 1 hour in a Beckman J2-21 centrifuge equipped with a JA-20 rotor. The supernatant containing BsPFK and other soluble *E. coli* proteins was heated for 10-12 minutes at 70°C and then set on ice for 10-15 minutes to cool. Since BsPFK is from the thermophilic bacterium *B. stearothermophilus*, it survived the high temperature, while most of the host *E. coli* proteins denatured. The cooled sample was centrifuged as before, and the supernatant (~30 mL) applied to a 10-15 mL Matrex Blue-A agarose column previously equilibrated with wash buffer (50 mM Tris-HCl pH 7.5, 0.1 M NaCl, 1 mM DTT and 1 mM EDTA). After loading the supernatant, the column was washed with 5-10 bed volumes of

wash buffer. BsPFK was eluted using a linear salt gradient (0.1-1.5 M NaCl) and 3 mL fractions collected. Depending upon whether the protein being purified was wild-type BsPFK or a mutant, the protein eluted from the column between 0.2 M NaCl and 1 M NaCl. Variation in the elution was due to the introduction of mutations at the actives site of the protein and was not problematic as most of the contaminating proteins were either denatured during the heat step or were washed through the column during the load and wash steps. The absorbance of the fractions was monitored at 280 nm and the fractions assayed for BsPFK activity. Figure 2-2 shows a typical elution profile for a mutant BsPFK protein from the Matrex Blue-A agarose column. Fractions containing the greatest amount of BsPFK activity were pooled together and concentrated using an Amicon ultra-filtration apparatus equipped with a YM10 10,000 molecular weight cut-off membrane filter. Concentrated enzyme (7-13 mL typically) was dialyzed into MOPS storage buffer (50 mM MOPS-KOH pH 7.0, 5 mM $MgCl_2$, 100 mM KCl and 0.1 mM EDTA) and stored at 4°C.

Assessment of BsPFK purity was performed via SDS-PAGE analysis (Laemmli, 1970) using a 4% polyacrylamide stacking gel and a 12% polyacrylamide resolving gel. Prior to electrophoresis, 5-10 μL from each purification step and 1-2 μL of concentrated purified protein was suspended in a sample loading buffer that contained 12.5 mM Tris-HCl, 10% SDS, 50% glycerol, 2 mM DTT and bromphenol blue. All samples were heated at 100°C for 3-5 minutes to denature the protein(s) and loaded into their respective wells. Electrophoresis was performed using a Mini-PROTEAN 3 Cell system (BioRad)

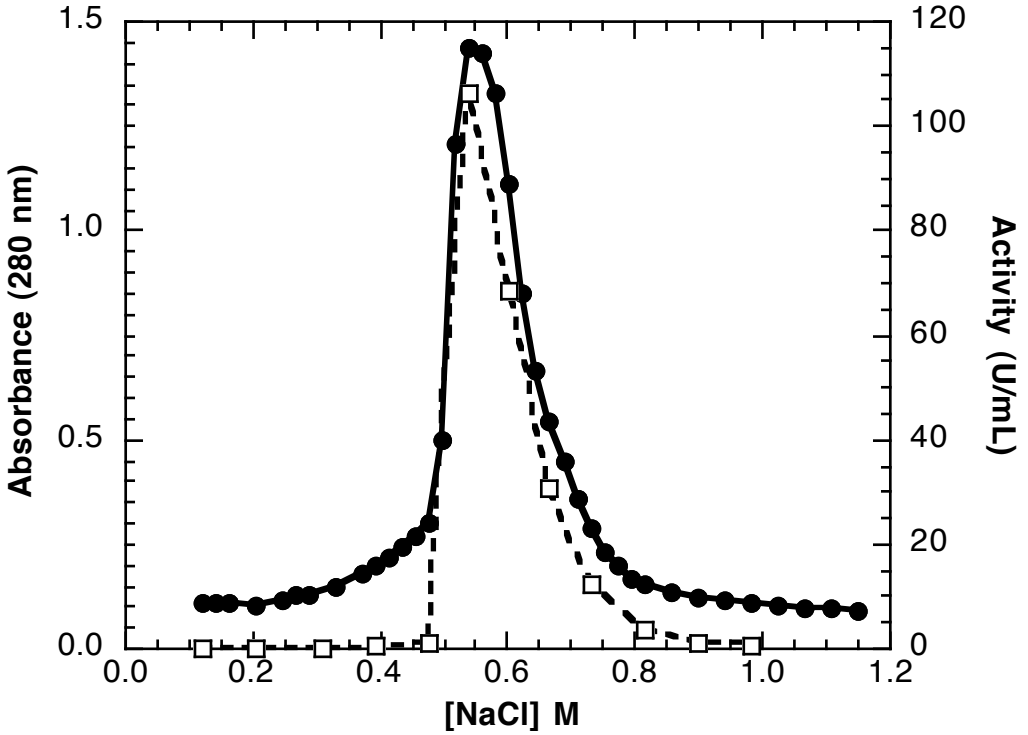

FIGURE 2-2 Elution profile of a mutant BsPFK (R252A/R25A/K90E/K91E) from the Matrex Blue-A column. Absorbance at 280 nm (●) and activity in U/mL (□) are plotted versus salt concentration for each 3 mL fraction. The elution of the protein was begun at 0.1 M NaCl (wash buffer contains 0.1 M NaCl) and activity measurements were performed at 20 mM Fru-6-P because of the R252A mutation in the active site.

set at a constant voltage of 220 V for the entire run. The gel was stained for approximately 1 hour using a solution of 40% methanol, 10% glacial acetic acid and 0.1% Coomassie brilliant blue, and destained for 2-3 hours using a solution of 40% methanol and 10% glacial acetic acid. Gels were documented using either a Polaroid Photo-Documentation Camera (Fisher) or an AlphaImager 950 Documentation System. A single band on the gel defined a "pure" sample, and an example of a typical SDS-PAGE gel showing the individual steps of purification is shown in Fig. 2-3.

Protein concentration was determined by using the bicinchoninic acid protein assay (Smith et al., 1985) or by using ε_{280} = 18910 M^{-1} cm^{-1} (Riley-Lovingshimer et al., 2001) where the extinction coefficient was determined using the method described by Pace et al. (1995). The concentrations calculated with either method were always in agreement. Moreover, whenever pure BsPFK protein was being used, the concentration of protein was always determined by the absorbance at 280 nm. Table 2-1 shows a typical purification for wild-type BsPFK.

Hybrid formation, isolation and identification via monomer exchange. Kimmel and Reinhart (2001) devised a method for dissociating BsPFK tetramers into their individual subunits by modifying a method described previously by Deville-Bonne et al. (1989) and later by Le Bras et al. (1995) for dissociating EcPFK tetramers into their individual subunits. The method involves incubating the two parental BsPFK proteins of interest simultaneously (usually

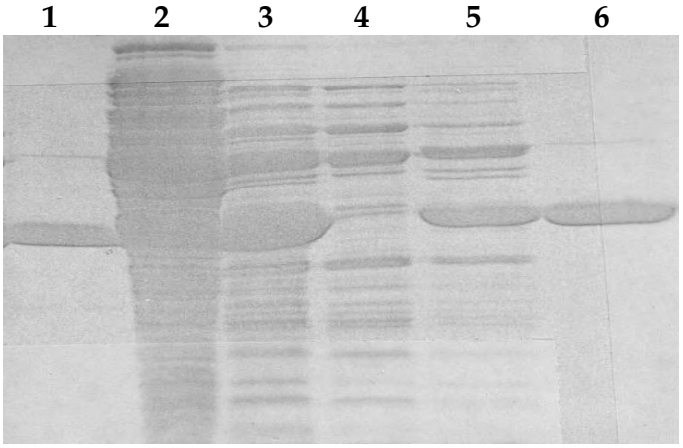

FIGURE 2-3 12% SDS-polyacrylamide gel of a typical BsPFK purification. Samples were taken at each step of the purification process and the lanes correspond to the following: Lane 1 shows the wild-type BsPFK standard previously purified (MW 34,000). Lane 2 shows a sample of the supernatant after the first centrifugation step (crude lysate). Lane 3 shows a sample of the supernatant after the second centrifugation step (post-heat step). Lane 4 shows a sample of the flow-through collected when loading the lane 3 sample. Lane 5 shows a sample of the wash collected prior to elution. Lane 6 shows the purified sample of BsPFK.

TABLE 2-1 Purification table for wild-type BsPFK

	Volume (mL)	Activity (U/mL)	Total Units	[Protein] (mg/mL)	Total Protein	Specific Activity (U/mg)	% Yield
1[a]	24.0	460	11000	18.5	444	24.8	100
2[b]	21.4	420	9000	9.2	197	45.4	81.3
3[c]	10.0	850	8500	7.6	76	111.7	77.1

[a]Supernatant from cell lysate.

[b]Supernatant after heat step.

[c]Concentrated protein.

wild-type BsPFK and a mutant) in 2 M KSCN and 20 mM Tris-HCl (pH8.5) for 30 minutes at room temperature to facilitate breakdown of the parental tetramers into their individual subunits. A final protein concentration of 2 mg/mL was used with a total volume between 7-10 mL. Furthermore, the relative ratio of the two parental proteins was varied depending upon the desired hybrid. For instance, if a 1:3 hybrid was desired, a greater amount of mutant protein was used relative to wild-type, whereas for isolating a 2:2 hybrid, equal amounts of the two parental proteins was used.

In order to separate the hybrid species, we needed a way to differentiate chromatographically between the two types of subunits; thus, a surface "charge tag" was added to one of the proteins to facilitate this separation via anion exchange chromatography. The surface "charge tag" is simply a mutation of two charged residues on the surface of the protein (or one charged and one neutral) to the opposite charge, e.g. two lysines at positions 90 and 91 on the surface of the protein mutated to glutamates. In all cases, as Chapter V describes, these charge changes on the surface of the protein have no dramatic effect upon the allosteric properties of the enzymes.

After incubating the two proteins in KSCN, the hybrid mixture was dialyzed at room temperature into 20 mM Tris-HCl (pH 8.5) for 4 1/2 hours replacing the buffer every 90 minutes. Next, the protein mixture was passed through a 0.22 □M membrane filter and loaded onto a Pharmacia Mono-Q HR 10/10 FPLC anion-exchange column previously equilibrated with 20 mM Tris-HCl (pH 8.5). After washing the column with 3-5 bed volumes, the hybrid

proteins were eluted with a linear NaCl gradient (1.77 mM NaCl/mL) and 1.5 mL fractions collected.

The absorbance of the fractions was monitored at 280 nm and the fractions assayed for activity. Figure 2-4 shows a typical elution profile for hybrids between wild-type and the K90E/K91E charge tag protein from the Mono-Q HR 10/10 column. Six peaks are observed in Fig. 2-4 but, depending upon the location of the charge tag mutation, one can observe between 5 to 7 peaks. This difference is due to the variable separation of the three 2:2 hybrids (isomers) that form when monomers recombine.

To identify the different hybrid species, the fractions exhibiting the greatest absorbance at 280 nm were pooled together and a 10-15 μL sample was suspended into a solution containing 12.5 mM Tris-HCl, 50% glycerol, 2 mM DTT and bromphenol blue. Next, 20-25 μL of each sample was loaded onto a native PAGE gel consisting of a 4% polyacrylamide stacking gel and 10% polyacrylamide resolving gel (Laemmli, 1970), and run for 3 hours using a constant voltage of 100 V. The electrophoresis system was also set on ice during the run to prohibit any dissociation of the hybrid tetramers. After electrophoresis, the gel was stained in a solution containing 40% methanol, 10% glacial acetic acid and 0.1% Coomassie brilliant blue for approximately 1 hour prior to destaining and analysis. Figure 2-5 shows a typical native-PAGE gel used to identify the various hybrids isolated. The isolated hybrids were then stored at 4°C to prevent re-hybridization.

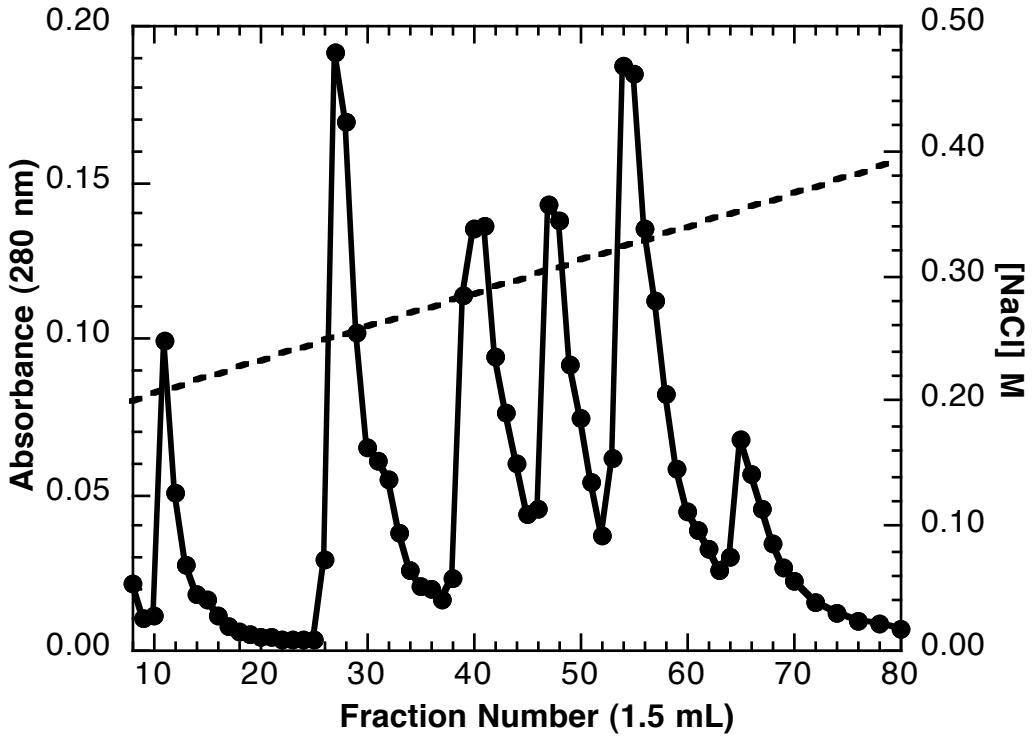

FIGURE 2-4 Elution profile of hybrids made via monomer exchange from the Mono-Q anion exchange column. Equal amounts of wild-type BsPFK and the K90E/K91E mutant were mixed together with 2 M KSCN and incubated for 30 minutes. The proteins were dialyzed and loaded onto the Mono-Q column. A linear salt gradient was used to elute the proteins (1.77 mM NaCl/mL) and 1.5 mL fractions collected. Since the K90E/K91E mutant has more net negative charge than wild-type BsPFK at pH 8.5, the K90E/K91E mutant binds to the column longer. Absorbance at 280 nm (●) is plotted versus fraction number, and the dashed line (---) indicates the salt gradient used to elute the hybrid proteins from the column. Six peaks are observed and each peak was identified as the following: Peak 1: Wild-type BsPFK (4:0). Peak 2: The 3:1 hybrid. Peaks 3 and 4: The 2:2 hybrids. Peak 5: The 1:3 hybrid. Peak 6: The K90E/K91E mutant (0:4).

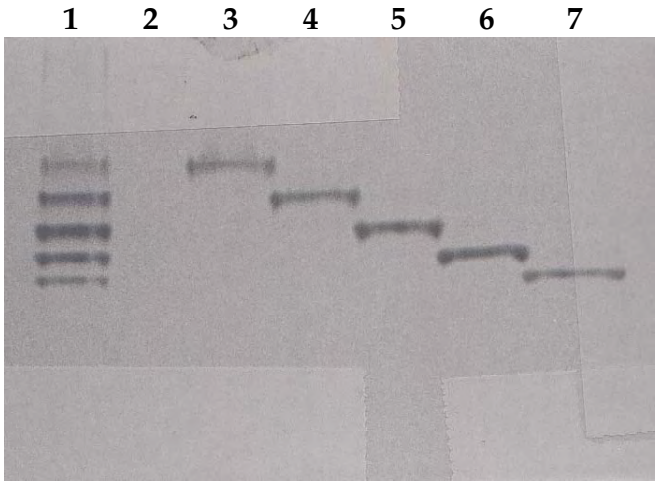

FIGURE 2-5 10% native polyacrylamide gel identifying the hybrids obtained via monomer exchange and isolated from the Mono-Q column. Samples were taken from each of the six peaks (Fig. 2-3) and the lanes correspond to the following: Lane 1 shows the hybrid mix prior to separation. Lane 2 is empty. Lane 3 shows peak 1 corresponding to wild-type BsPFK (4:0). Lane 4 shows peak 2 corresponding to the 3:1 hybrid. Lane 5 shows peak 4 corresponding to one of the 2:2 hybrids. Lane 6 shows peak 5 corresponding to the 1:3 hybrid. Lane 7 shows peak 6 corresponding to the K90E/K91E mutant (0:4).

Data analysis. All data analysis was performed on either a Power Macintosh 7100/80AV or a Macintosh G4 using Kaleidagraph 3.08 or 3.51 (Synergy Software). Initial velocity activity as a function of Fru-6-P concentration was fit to the Hill equation (Hill, 1910):

$$v = \frac{V_{max}[A]^{n_H}}{K_{1/2}^{n_H} + [A]^{n_H}} \qquad (2\text{-}1)$$

where v equals the steady-state rate of turnover, V_{max} represents the maximal specific activity, [A] equals the concentration of Fru-6-P, $K_{1/2}$ is the concentration of Fru-6-P resulting in half maximal specific activity, and n_H is the Hill coefficient. Furthermore, all the above terms refer to the kinetic parameters obtained for the high affinity (native) binding sites.

Data obtained from hybrid enzymes, which exhibited two distinct affinities for Fru-6-P, were fit to either Eq. 2-2 or Eq. 2-3 depending upon the necessity of the Hill coefficient (n_H) to improve the fit:

$$v = \left[\frac{V_{max}[A]}{K_{1/2} + [A]}\right] + \left[\frac{V'_{max}[A]}{K'_{1/2} + [A]}\right] \qquad (2\text{-}2)$$

$$v = \left[\frac{V_{max}[A]^{n_H}}{K_{1/2}^{\ n_H} + [A]^{n_H}}\right] + \left[\frac{V'_{max}[A]^{n'_H}}{K'^{\ n'_H}_{1/2} + [A]^{n'_H}}\right] \qquad (2\text{-}3)$$

where V'_{max}, $K'_{1/2}$ and n'_H refer to the maximal specific activity, apparent dissociation parameter and the Hill coefficient for the low affinity (mutated) binding site population, respectively.

The variation in $K_{1/2}$ as a function of PEP concentration was fit to the following equation:

$$K_{1/2} = K_{ia}^{o}\left[\frac{K_{iy}^{o} + [Y]}{K_{iy}^{o} + Q_{ay}[Y]}\right] \qquad (2\text{-}4)$$

where $K_{1/2}$ is the concentration of Fru-6-P resulting in half-maximal activity for the high affinity site obtained from either Eqs. 2-1, 2-2 or 2-3. To be consistent with previously adopted notation (Cleland, 1963a, 1963b; Tlapak-Simmons and Reinhart, 1994, 1998; Johnson and Reinhart, 1994, 1997), A refers to the substrate Fru-6-P and Y represents the allosteric inhibitor PEP. Furthermore, K_{ia}^{o} is the apparent dissociation constant for the substrate Fru-6-P in the absence of PEP, K_{iy}^{o} is the dissociation constant for PEP in the absence of Fru-6-P, and Q_{ay} is the coupling parameter describing the extent to which the binding of PEP affects the binding of Fru-6-P and *vice versa* as defined by the following equation:

$$\frac{K_{ia}^{o}}{K_{ia}} = \frac{K_{iy}^{o}}{K_{iy}} = Q_{ay} \qquad (2\text{-}5)$$

where K_{ia} and K_{iy} represent the dissociation constants for Fru-6-P and PEP, respectively, in the saturating presence of the other ligand. By resolving both the terms K_{iy}^{o} and Q_{ay}, Eq. 2-4 allows the separate quantification of both PEP binding affinity and its allosteric effect once bound, respectively.

The coupling parameter, Q_{ay}, describes both the nature and magnitude of the effect the allosteric ligand has upon the binding of the substrate. If $Q_{ay} < 1$ the allosteric ligand is an inhibitor, and if $Q_{ay} > 1$ the allosteric ligand is an activator. If $Q_{ay} = 1$ then the allosteric ligand has no effect on the binding of substrate. In the case of the inhibitor PEP, the smaller the value of Q_{ay}, the

greater the extent of inhibition by PEP upon substrate binding. Figure 2-6 shows an example of the inhibition of wild-type BsPFK by PEP at pH 8.0 and 25°C, where Q_{ay} is the ratio of the two plateaus.

The coupling parameter can also be used to calculate the free energy associated with the interaction between substrate and allosteric effector, provided the rapid equilibrium assumption is valid as it is for BsPFK (Tlapak-Simmons and Reinhart, 1998) using the following equation:

$$\Delta G_{ay} = -RT\ln\left(Q_{ay}\right) \qquad (2\text{-}6)$$

where ΔG_{ay} is the coupling free energy of inhibition by PEP, R is the gas constant which is equivalent to 1.987×10^{-3} kcal/deg·mol, and T is absolute temperature in Kelvin. Allosteric inhibition is defined by a ΔG_{ay} value greater than zero, while allosteric activation results in a ΔG_{ay} value less than zero. When no coupling between the ligands occurs, $\Delta G_{ay} = 0$.

When using a single substrate, single modifier model, the coupling measured, Q_{ay}, is a composite of all the possible allosteric interactions (both heterotropic and homotropic) that may exist regardless of the number of active and allosteric sites. Thus, for the native BsPFK tetramer, individual quantification of each of the ten unique allosteric interactions is impossible. However, if the number of functional binding sites is reduced, as it is in a 2:2 hybrid, we can assess the individual allosteric interactions directly using the following equation (Reinhart, 1988):

$$Q = Q_{ay1} \cdot Q_{ay2} \cdot \left[\frac{Q_{yy/a}}{Q_{yy}} \cdot \frac{Q_{aa/yy}}{Q_{aa}}\right]^{1/2} \qquad (2\text{-}7)$$

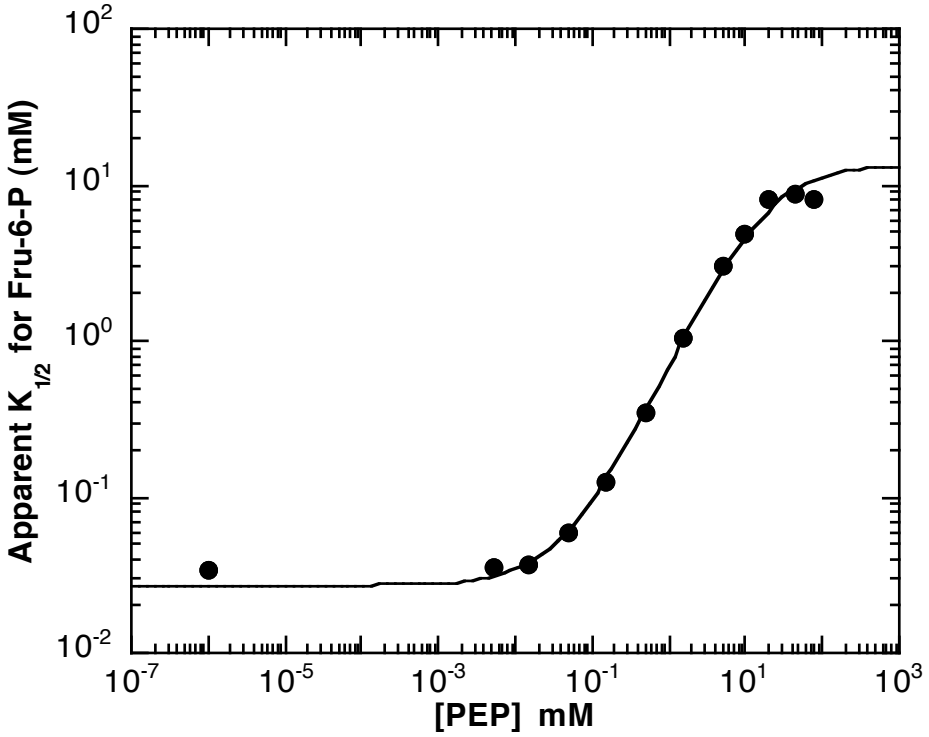

FIGURE 2-6 The apparent dissociation constant measured for Fru-6-P versus PEP concentration for wild-type BsPFK at pH 8.0, 25°C and [MgATP] = 3 mM. The $K_{1/2}$ values were obtained from individual Fru-6-P saturation profiles (data fit to Eq. 2-1) at varying concentrations of PEP. The error for each of the points is plotted, but the error is smaller than the points so they cannot be seen. The solid line represents the best fit to Eq. 2-4.

where Q is the overall coupling measured for the 2:2 hybrid, Q_{ay1} and Q_{ay2} are the couplings for the two heterotropic interactions where the values of Q_{ay1} and Q_{ay2} are obtained from the characterization of their respective 1:3 hybrids (Ortigosa et al. (2003)). Q_{yy} and Q_{aa} are the couplings for the homotropic interactions between allosteric sites and active sites respectively. Figure 2-7 shows schematically these four individual allosteric interactions in both a symmetrical dimer and a 2:2 hybrid (Reinhart, 1988). $Q_{yy/a}$ is the coupling for the homotropic interaction between allosteric sites with a single equivalent of Fru-6-P bound, and $Q_{aa/yy}$ is the coupling for the homotropic interaction between active sites with both equivalents of PEP bound. Thus, Eq. 2-7 states that besides the individual heterotropic interactions (Q_{ay1} and Q_{ay2}) contributing to the apparent coupling for the 2:2 hybrid (Q), the homotropic interactions also contribute to the magnitude of the apparent coupling only when the homotropic couplings change in response to the binding of the heterotropic ligand.

Unfortunately, $Q_{yy/a}$ cannot be determined explicitly, thus we need to consider the two extremes that are possible upon binding each equivalent of Fru-6-P to the two native active sites found within the 2:2 hybrid. First, we can imagine that the entire change in the homotropic interactions is realized upon the first binding event (i.e. $Q_{yy} \neq Q_{yy/a} = Q_{yy/aa}$) or second, that both equivalents are required to bind before any change in the homotropic interactions is observed (i.e. $Q_{yy} = Q_{yy/a} \neq Q_{yy/aa}$). However, a third case can also be imagined as an "average" between these two extremes. This means that the binding of

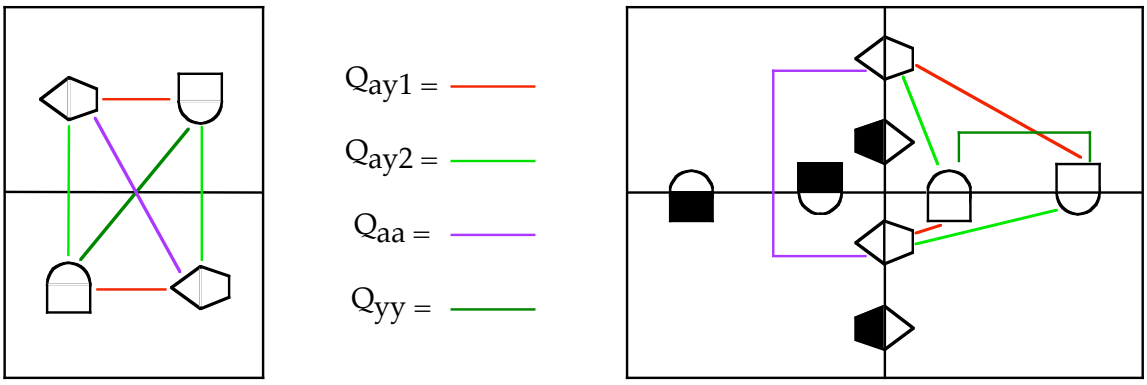

FIGURE 2-7 A schematic depicting the pair-wise allosteric interactions possible in either a symmetrical dimer (left) or a 2:2 hybrid (right). The active sites consist of the triangle and half-hexagon, and the allosteric sites consist of the rectangle and semi-circle. For the 2:2 hybrid, to indicate the presence of a mutation, a closed shape is used, while the native, non-substituted binding sites remain open. There are two copies of two unique heterotropic interactions shown in red (Q_{ay1}) and green (Q_{ay2}), and two homotropic interactions, one between active sites shown in purple (Q_{aa}) and one between allosteric sites shown in dark green (Q_{yy}). The coupling constants correspond those described in the text.

each equivalent of Fru-6-P contributes equally to the observed allosteric effect, and this case is how we will be considering the allosteric behavior of the 2:2 hybrids (Reinhart, 1988). This would result in:

$$\left(\frac{Q_{yy/a}}{Q_{yy}}\right)^2 = \left[\frac{Q_{yy/aa}}{Q_{yy}}\right] \qquad (2\text{-}8)$$

Thus, Eq. 2-7 becomes the following:

$$Q = Q_{ay1} \cdot Q_{ay2} \cdot \left[\frac{Q_{yy/aa}}{Q_{yy}}\right]^{1/2} \cdot \left[\frac{Q_{aa/yy}}{Q_{aa}}\right]^{1/2} \qquad (2\text{-}9)$$

where $Q_{yy/aa}$ is the coupling for the homotropic interaction between allosteric sites with both equivalents of Fru-6-P bound.

The coupling for the homotropic interaction between two bound ligands of A can be measured directly when [Y] = 0 using the following equation (Reinhart, 1988):

$$Q_{aa} = \left[\frac{n_H}{2 - n_H}\right]^2 \qquad (2\text{-}10)$$

where n_H is the Hill number obtained from the individual Fru-6-P saturation profile used in determining the $K_{1/2}$ value for the high affinity active sites when [Y] = 0. One may use the same equation to also obtain $Q_{aa/yy}$ if n_H is determined when [Y] is saturating. Moreover, Q_{yy} and $Q_{yy/aa}$ may also be determined using Eq. 2-10 by measuring the Hill number for PEP binding using activity assays (see Chapter VI), and extrapolating to [A] = 0 or [A] = ∞, respectively. It should be noted however, that an apparent positive cooperativity results from the partial saturation of the heterotropic ligand that does not depend on true

homotropic interactions (Reinhart, 1988). Consequently, the determination of the values $Q_{aa/yy}$ and $Q_{yy/aa}$ requires the extrapolation to true saturation of the heterotropic ligand (see Chapter VI).

Eq. 2-9 can simplify to Eq. 2-11 when considering either of the following two cases: (1) when all the homotropic couplings are equal to 1 or (2) when there is no net change in the Hill number upon saturation of the opposing ligand:

$$Q = Q_{ay1} \cdot Q_{ay2} \qquad (2\text{-}11)$$

and with using Eq. 2-6, Eq. 2-11 becomes:

$$\Delta G = \Delta G_{ay1} + \Delta G_{ay2} \qquad (2\text{-}12)$$

where ΔG equals the coupling free energy for the 2:2 hybrid, and ΔG_{ay1} and ΔG_{ay2} represent the coupling free energies for the individual heterotropic interactions respectively.

CHAPTER III

ISOLATION AND CHARACTERIZATION OF TWO OF THE FOUR POSSIBLE HETEROTROPIC INTERACTIONS FOUND WITHIN PHOSPHOFRUCTOKINASE FROM *Bacillus stearothermophilus*

Introduction

Over several decades, the mechanism by which allosteric regulation occurs in oligomeric proteins has long been an issue of debate and many models proposed. The most popular models, the concerted (MWC) model (Monod et al., 1965) and the sequential (KNF) model (Koshland et al., 1966), consider an enzyme (or the individual subunits of an enzyme) existing in two conformational states, an active state (R-state, "relaxed") or an inactive state (T-state, "tense"), with the substrate and the allosteric effector(s) altering the equilibrium between these two states.

Applying these two models to a homotetramer containing one active site and one allosteric site per subunit, several presumptions can be made about the first binding equivalent of an allosteric effector, in our case an inhibitor, to the observed allosteric response in the subunits of the enzyme. The concerted model would predict that all four subunits would undergo the allosteric transition upon binding, while the sequential model would predict that only the subunit that bound the inhibitor would undergo the allosteric transition (Fig. 3-1). Due to these contrasting predictions, isolating the first binding event would differentiate between the validity of these models or their insufficiencies in describing an observed allosteric effect.

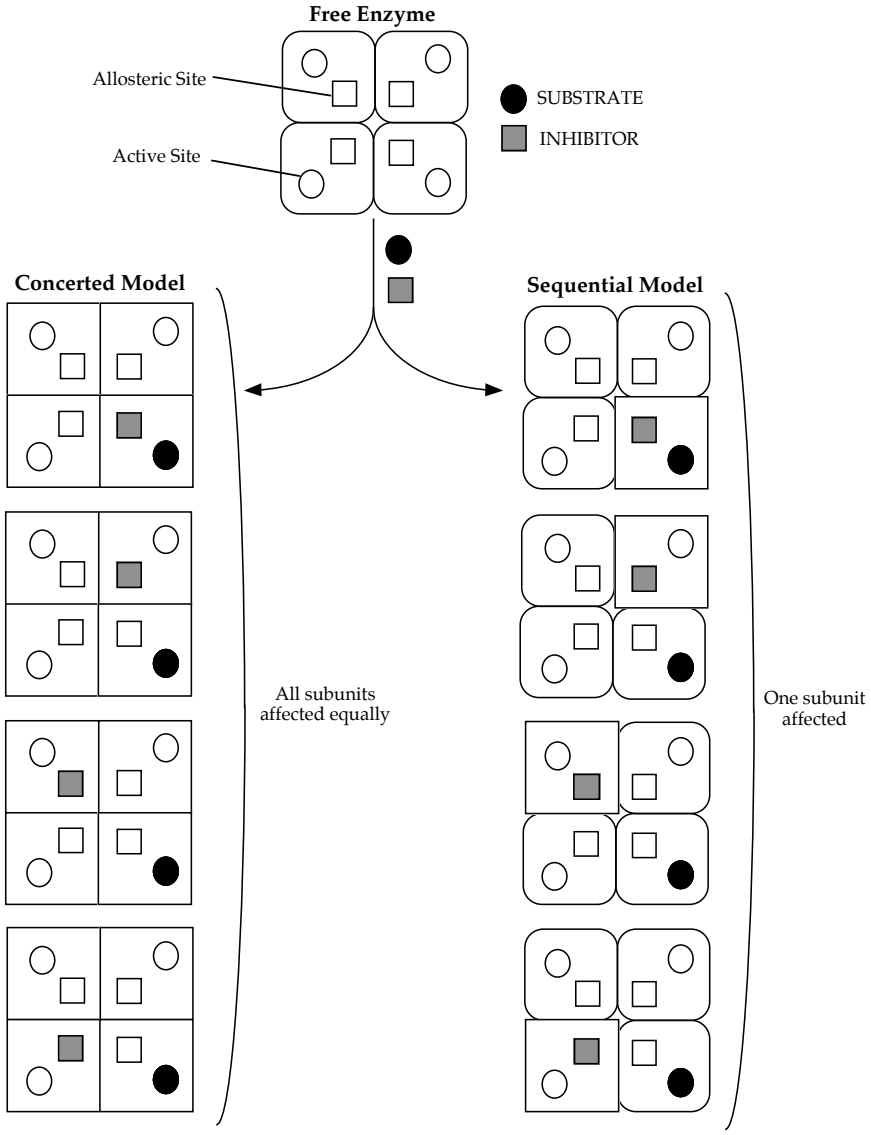

FIGURE 3-1 A two-dimensional schematic of the concerted and sequential models representing contrasting predictions regarding the influence of the binding of a single allosteric ligand upon the binding of the substrate at a single active site. The allosteric site is represented by an open square and an active site is represented by an open circle. In the concerted model, binding of the inhibitor to any of the four allosteric sites influences the binding at the active site to the same degree as is evident by the change in the conformation of all four subunits. In the sequential model, binding the inhibitor to only one site influences the binding of the substrate at only the active site which is contained within the same subunit that bound the inhibitor. Again, this effect is seen as a change in the conformation of the subunits, however this time only one of the four subunits change conformation.

However, before considering only these two models, a more systematic approach in determining the mechanism of allosteric regulation needs to be considered in which the enzyme is not limited to two conformational states. Instead, one needs to consider the enzyme as a network of communication pathways between binding sites in which each binding site affects one another in a reciprocal manner. This idea of linkage was first proposed by Wyman (1964 and 1967), and later modified by Weber (1972 and 1975) to consider the observed allosteric effect in free energy terms. Reinhart (1983 and 1988) then applied these ideas to predict the observed allosteric response in both a single substrate-single modifier system (monomer) and also in a symmetrical dimer. Applying this linkage approach to the aforementioned homotetramer, the potential for four unique allosteric heterotropic interactions exist between an individual allosteric site and each of the four active sites (Fig. 3-2). Upon binding one equivalent of inhibitor, one can envision its allosteric effect traversing throughout the enzyme to each of the four active sites via these four communication pathways and *vice versa* upon binding one equivalent of substrate. The question then arises, not regarding what the conformation of the subunits themselves are after inhibitor binding, but rather what are the relative contributions of each of the four heterotropic interactions in producing the observed allosteric effect upon inhibitor binding?

Applying this systematic approach to the concerted and sequential models, predictions can be made about these relative contributions if each of the four interactions and hence each of the four possible first binding events, were

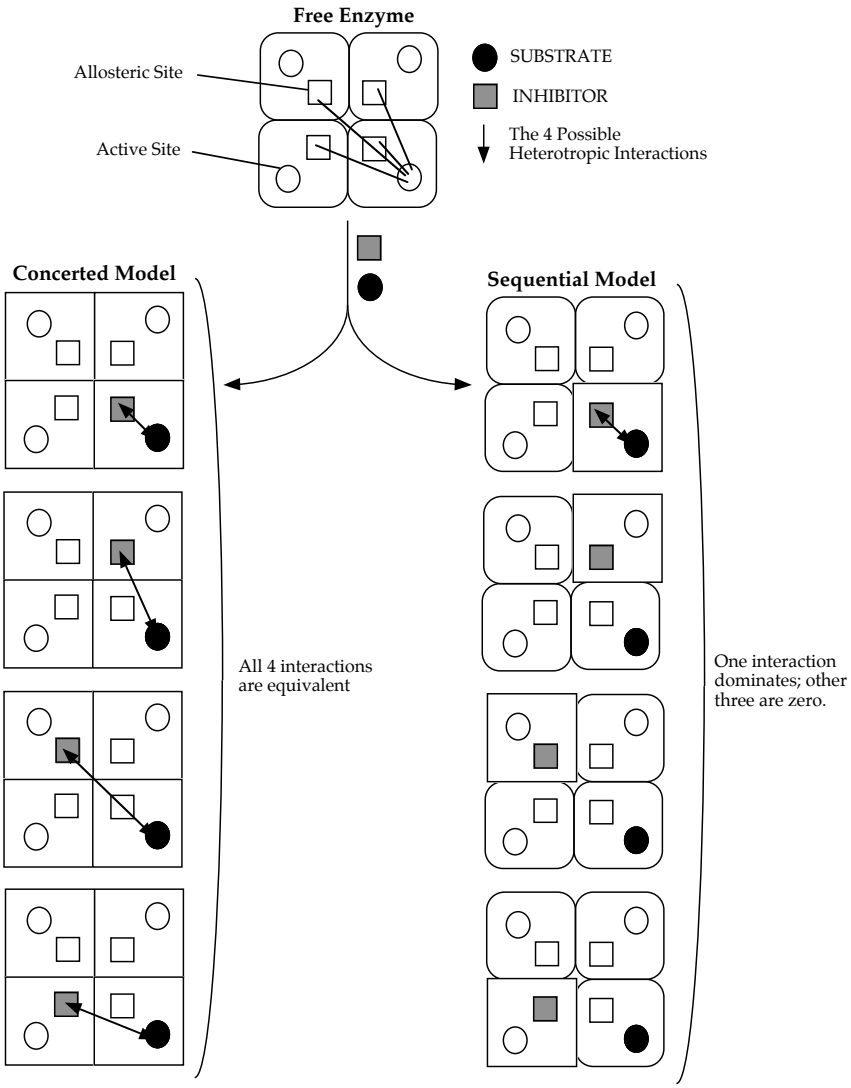

FIGURE 3-2 A two-dimensional schematic of the concerted and sequential models representing contrasting predictions regarding the influence of the binding of a single allosteric ligand upon the binding of the substrate at a single active site as it pertains to the measured allosteric effect for each of the four heterotropic interactions. Applying the idea of isolating the individual heterotropic interactions, predictions can be made regarding the magnitude of each heterotropic interaction upon binding one equivalent of inhibitor and substrate. The concerted model would predict equivalent contributions to the measured allosteric effect, while the sequential model would predict that only one of the four heterotropic interactions would possess any measurable allosteric effect (the other three would be zero). The arrows between binding sites represent the interactions that would be observed (and thus have a measurable allosteric effect) upon binding only one equivalent of inhibitor and one equivalent of substrate based upon these two models.

isolated individually. The concerted model would predict that binding one equivalent of inhibitor would influence binding at each of the four active sites equally, thus all four interactions would be equivalent in their relative magnitudes and would measure 100% of the allosteric effect; whereas, the sequential model would predict that binding one equivalent of inhibitor would influence biding at only one of the four active sites, resulting in only one interaction possessing the maximal allosteric effect (Fig. 3-2). Thus, to either validate or disprove the concerted or sequential models, or possibly provide credence for our "conformational free/linkage" model where each individual allosteric interaction is considered, the first binding event needs to be isolated and characterized.

PFK background. Phosphofructokinase from *Bacillus stearothermophilus* (BsPFK) is the model enzyme used for this investigation, as BsPFK is a tetramer consisting of four identical subunits, arranged as a dimer of dimers. Contained within the enzyme are four active sites and four allosteric sites, with the active sites located along one dimer-dimer interface and the allosteric sites located along the other dimer-dimer interface (Fig. 3-3 *A*) (Schirmer and Evans, 1990).

BsPFK is subject to K-type allosteric regulation, meaning the allosteric effector (activator or inhibitor) regulates BsPFK activity by binding to the allosteric sites and either increasing or decreasing the protein's affinity for the substrate, fructose-6-phosphate (Fru-6-P). One aspect of this regulation is heterotropic regulation, which involves the interaction between unlike binding sites. Since BsPFK contains four active sites and four allosteric sites, 16 total

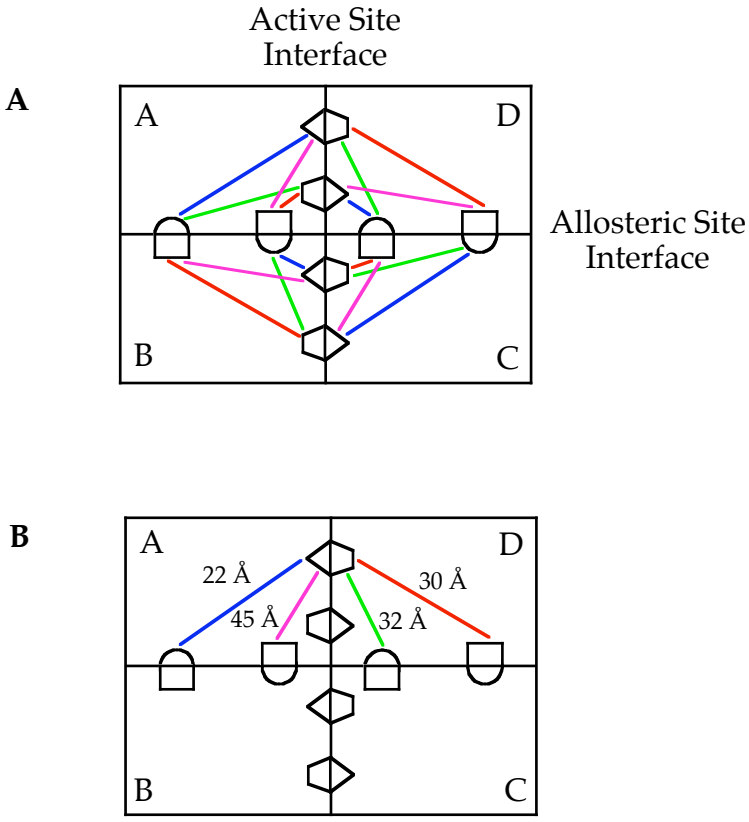

FIGURE 3-3 A two-dimensional schematic of BsPFK. (*A*) BsPFK is a homotetramer consisting of four active sites and four allosteric sites. Within this representation, the active sites are located along the vertical dimer-dimer interface, while the four allosteric sites are located along the horizontal dimer-dimer interface. Since there are four active sites and four allosteric sites, 16 pair-wise heterotropic interactions are possible between the different binding sites indicated by the colored lines drawn in between each of the active sites and allosteric sites. (*B*) Of these 16 pair-wise heterotropic interactions, four are unique to BsPFK and have been assigned a distance, which differentiates them from one another. The 22 Å interaction is blue, the 30 Å interaction is red, the 32 Å interaction is green, while the 45 Å interaction is magenta. These distances correspond to the actual distances between the binding sites within the crystal structure, but in no way imply the pathway of allosteric communication.

pair-wise heterotropic interactions are possible, 4 of which are unique as shown in Fig. 3-3 *B* (four-fold redundancy). The four heterotropic interactions have been designated as either the 22 Å, 30 Å, 32 Å or 45 Å heterotropic interactions, and these distances correspond to the distance measured within the crystal structure (Schirmer and Evans, 1990) between the phosphorous atom of the Fru-6-P molecule bound in the active site to the β-phosphorous atom of the ADP molecule bound in each of the four allosteric sites. Up until this point, the measured allosteric effect produced from the binding of an effector molecule(s) has been an average of these interactions (plus any contribution from the homotropic interactions) occurring simultaneously within the tetramer. If it is our goal to better understand the mechanism of allosteric regulation and more specifically, the mechanism of inhibition, this complexity must be reduced in order to resolve the contribution each of the four heterotropic interactions makes to the measured allosteric response of the tetramer upon binding the inhibitor phosphoenolpyruvate (PEP).

Using a method developed by Deville-Bonne et al. (1989) and Le Bras et al. (1995), and later adapted by Kimmel and Reinhart (2001), a hybrid tetramer of BsPFK containing only one copy of the 22 Å heterotropic interaction was isolated and characterized. The process began by mutating specific residues within the active site and allosteric site to discourage both the binding of the substrate Fru-6-P and the inhibitor PEP. Next, this mutant tetramer and wild-type BsPFK were dissociated into their individual subunits using KSCN. Dialysis was then used to permit the random re-association of the subunits to

generate the 7 possible enzyme species. Moreover, two lysine residues on the surface of the mutant protein, far removed from the ligand binding sites, were mutated to glutamates prior to the KSCN treatment to facilitate the separation of the various hybrid species via anion exchange chromatography. The process concluded with variable separation of the hybrid species, the subsequent identification of the 1:3 hybrid peak via native PAGE analysis and finally the characterization of the 1:3 hybrid via linked function analysis. Figure 3-4 illustrates this hybrid-making scheme used to isolate the 22 Å interaction (Kimmel and Reinhart, 2001).

The procedure outlined above is used for this current investigation to isolate the 30 Å and 32 Å interactions. In order to accomplish this, additional mutations on the opposite sides of both the active site and allosteric site need to be found that effectively decrease BsPFK's affinity for both Fru-6-P and PEP. Once achieved, the 1:3 hybrids corresponding to each interaction will be isolated and characterized in the same manner as described by Kimmel and Reinhart (2001). This characterization will then enable us to assess if either of the two, two-state models can be applied to BsPFK because if the interactions are measured and found to be equivalent, the concerted model would be supported. Conversely, if the interactions were found to have no measured allosteric effect, the sequential model would be supported since an allosteric effect was already observed for the 22 Å interaction at pH 8.0. More importantly however, if the interactions proved to be unique, our third "conformational free/linkage" model previously described would be supported.

FIGURE 3-4 A diagram showing the various steps involved in isolating the 1:3 hybrid as determined by Kimmel and Reinhart (2001) for isolating the 22 Å heterotropic interaction. First, the mutant protein must be generated in which specific sides of the binding sites are mutated to discourage ligand binding indicated by the filled-in symbols. Moreover, a surface charge tag (indicated by the "lolli-pop" on each subunit) must also be added to the protein to facilitate separation of the various hybrid species via anion exchange chromatography. Next, the proteins are mixed together and KSCN is added to dissociate the tetramers into monomers. The mixture is dialyzed, and upon removal of the KSCN, the subunits re-associate to form five different hybrid species, with the 2:2 hybrids having 3 unique orientations. The 1:3 hybrid is then separated away from the other hybrids via anion exchange chromatography and its identity confirmed via native PAGE analysis.

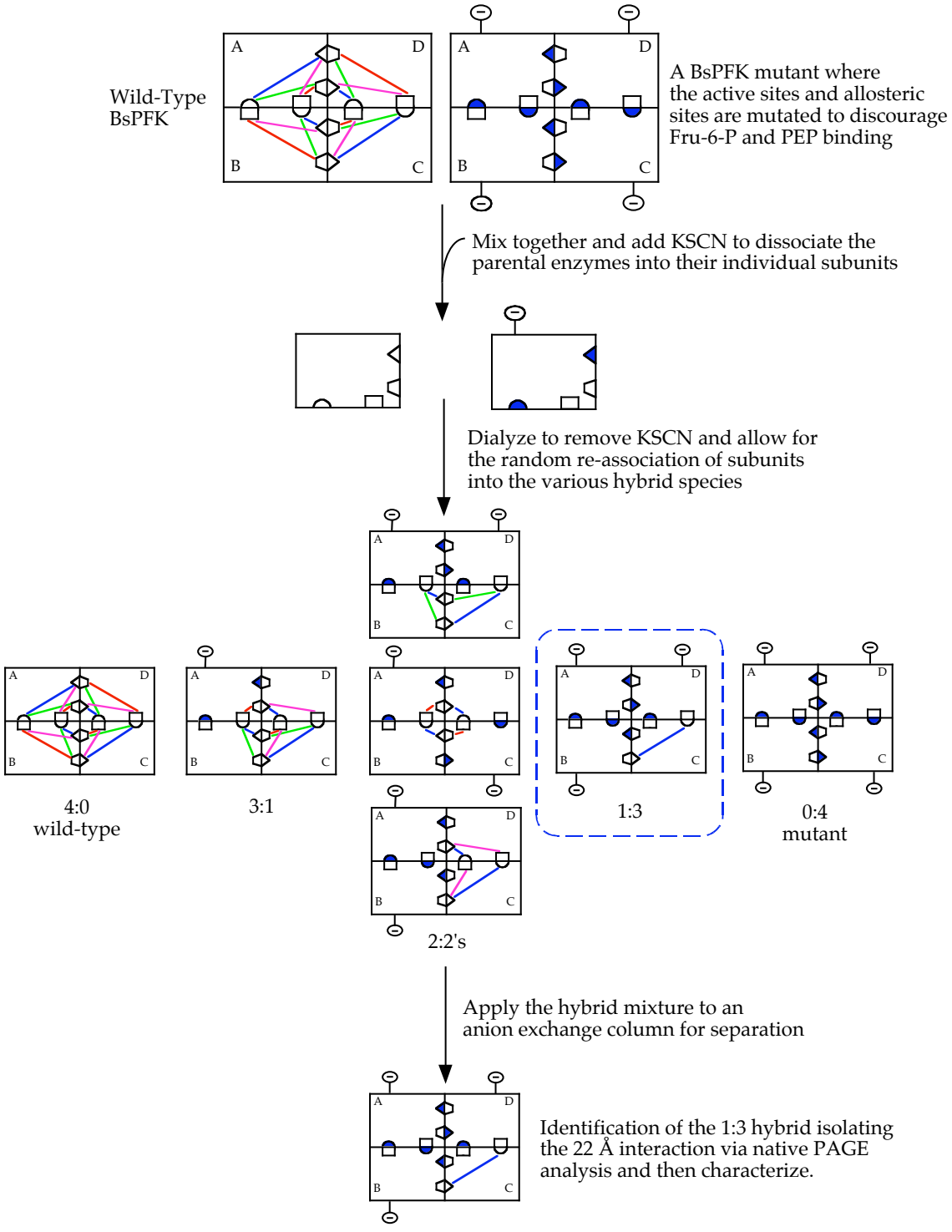
Wild-Type
BsPFK
A
D
B
C
A BsPFK mutant where
the active sites and allosteric
sites are mutated to discourage
Fru-6-P and PEP binding
Mix together and add KSCN to dissociate the
parental enzymes into their individual subunits
Dialyze to remove KSCN and allow for
the random re-association of subunits
into the various hybrid species
4:0
wild-type
3:1
2:2's
1:3
0:4
mutant
Apply the hybrid mixture to an
anion exchange column for separation
Identification of the 1:3 hybrid isolating
the 22 Å interaction via native PAGE
analysis and then characterize.

Materials and methods

The materials used for the experiments described in this chapter are the same as those described in Chapter II. Site-directed mutagenesis, protein purification, hybrid formation via monomer exchange and subsequent isolation, enzymatic activity measurements at various pH values, and data analysis were performed as described in Chapter II. Additional methods used to characterize the stability of the mutant proteins made for use in making the hybrids are described below.

Protein stability measurements. In order to assess the stability of the various mutant BsPFK proteins, KSCN denaturation profiles were performed in which BsPFK activity was monitored as a function of KSCN concentration. KSCN was dissolved in MOPS buffer containing 50 mM (MOPS), 100 mM KCl, 5 mM $MgCl_2$ and 0.1 mM EDTA at pH 7.0 to a final concentration of 10 M. The proteins assayed were diluted with MOPS buffer to have a final concentration in the eppendorf tube of 0.02 mg/mL to prevent the need for further dilution when assayed for activity. Individual eppendorf tubes were labeled from 0 M KSCN to 2.0 M KSCN in 0.1 M increments, and each tube was set up to contain the appropriate concentration of protein, buffer and KSCN with a final volume of 1 mL. The tubes were incubated at room temperature for 18 hours and then assayed for BsPFK activity at 20 mM Fru-6-P using the method described in Chapter II.

Results

Strategy. The subunits of BsPFK are organized as a dimer of dimers with the 4 active sites located along one dimer–dimer interface and the 4 allosteric sites located along the other dimer–dimer interface (Schirmer and Evans, 1990). This arrangement was previously depicted in Fig. 3-3 *A*. In considering only the heterotropic interactions, 16 pair-wise interactions are possible in which 4 of the heterotropic interactions are unique to BsPFK as shown previously in Fig. 3-3 *B*. Each interaction has been assigned a given distance unique to each interaction (22 Å, 30 Å, 32 Å or 45 Å) to provide a method of identifying and discriminating among the four heterotropic interactions.

Due to the interfacial nature of these binding sites, residues that define the binding sites originate from both participating subunits; i.e. from opposite "sides" of a subunit–subunit interface. In particular, this pertains to the numerous positively charged residues that line each binding site (each ligand is negatively charged). For example, the Fru-6-P binding site includes R162 and R243 from one subunit (a-side) and R72, H249 and R252 from the other subunit (b-side). Similarly, each allosteric site has R154, R211, and K213 from one subunit (α-side) and R21 and R25 from the other subunit (β-side). A schematic indicating the relative positions within each binding site is shown in Fig. 3-5. A nitrogen from each of these positively charged side-chains is found to make at least one close contact with, i.e. appears in the X-ray structure within 3 Å of, a negatively charged phosphate oxygen of the corresponding ligand (Fru-6-P or the PEP analog phosphoglycolate, respectively).

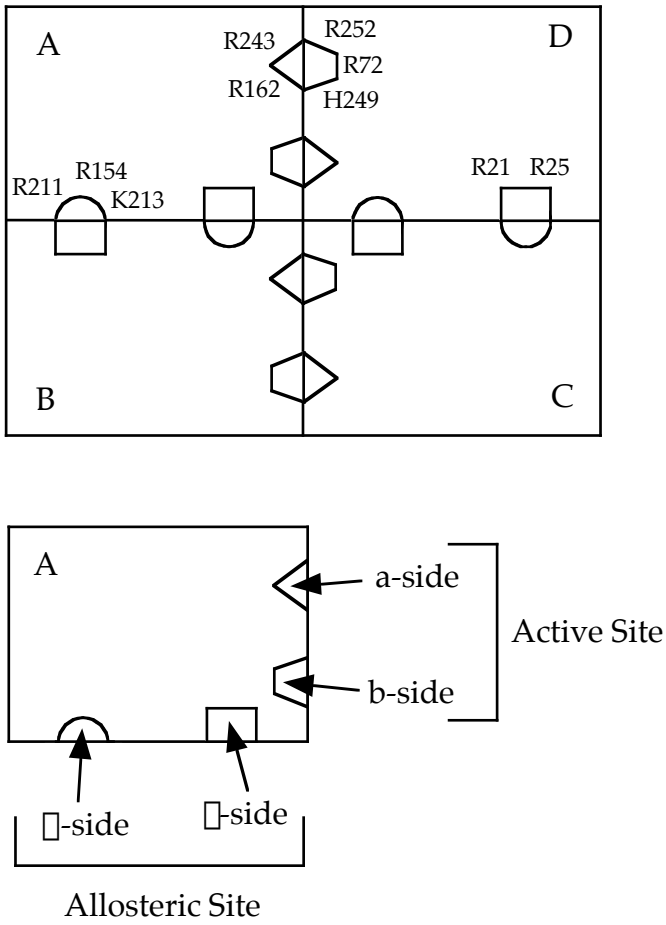

FIGURE 3-5 Schematic of the positively charged residues that line the active site and allosteric site binding pockets. Each subunit contributes a full active site and a full allosteric site but does so by contributing two half active sites and two half allosteric sites. Each "side" of the active site has been designated as either the a-side or the b-side and each "side" of the allosteric site has been designated as either the -side or the -side as shown in the bottom schematic. Different shapes are used to represent the different "sides" of each binding site, with the active sites being represented by a triangle (a-side = R162 and R243) and half-hexagon (b-side = R252, H249 and R72), and the allosteric sites by a semi-circle (-side = R211, K213 and R154) and rectangle (-side = R21 and R25). The residues contributing to their respective "sides" are shown indicated in the top schematic as well as in parentheses in the figure text (Schirmer and Evans, 1990).

These positively charged residues serve as excellent candidates for site-directed mutagenesis as one of our goals is to discourage both Fru-6-P and PEP binding at three of the four active sites and three of the four allosteric sites. Thus, it might be expected that each of these positively charged residues contribute significantly to the binding energy of these ligands, and in fact that is the case. In probing the active site, Kimmel and Reinhart (2000) observed that mutating R162 to an alanine in BsPFK increases the dissociation constant of Fru-6-P 30-fold, while the R162E mutation increases the K_d by nearly 3-orders of magnitude (Kimmel and Reinhart, 2001). Moreover, Valdez, et al. (1989) reported a 1500-fold increase in the dissociation constant for Fru-6-P upon implementing the R252A mutation at the active site. As for the allosteric site, Lau and Fersht have mutated 4 arginine residues and 1 lysine residue in the *Escherichia coli* form of the enzyme (EcPFK) and observed 30-100 fold increases in the dissociation constants for each allosteric ligand. In addition, Valdez, et al. (1989) reported a 100-fold increase in the dissociation constant for the inhibitor PEP in the R25A and R211A variants of BsPFK. Thus, one can substantially diminish ligand binding with mutations to the positively charged residues on either of the subunits that contribute to the binding site.

This ability to mutate either "side" of the binding site provides the key opportunity to individually isolate each of the four heterotropic interactions, but in this chapter, only the isolation and characterization of the 30 Å and 32Å heterotropic interactions is discussed. Figure 3-6 illustrates the basic strategy. The formation of 1:3 (1 wild-type subunit: 3 mutant subunits) hybrid tetramers

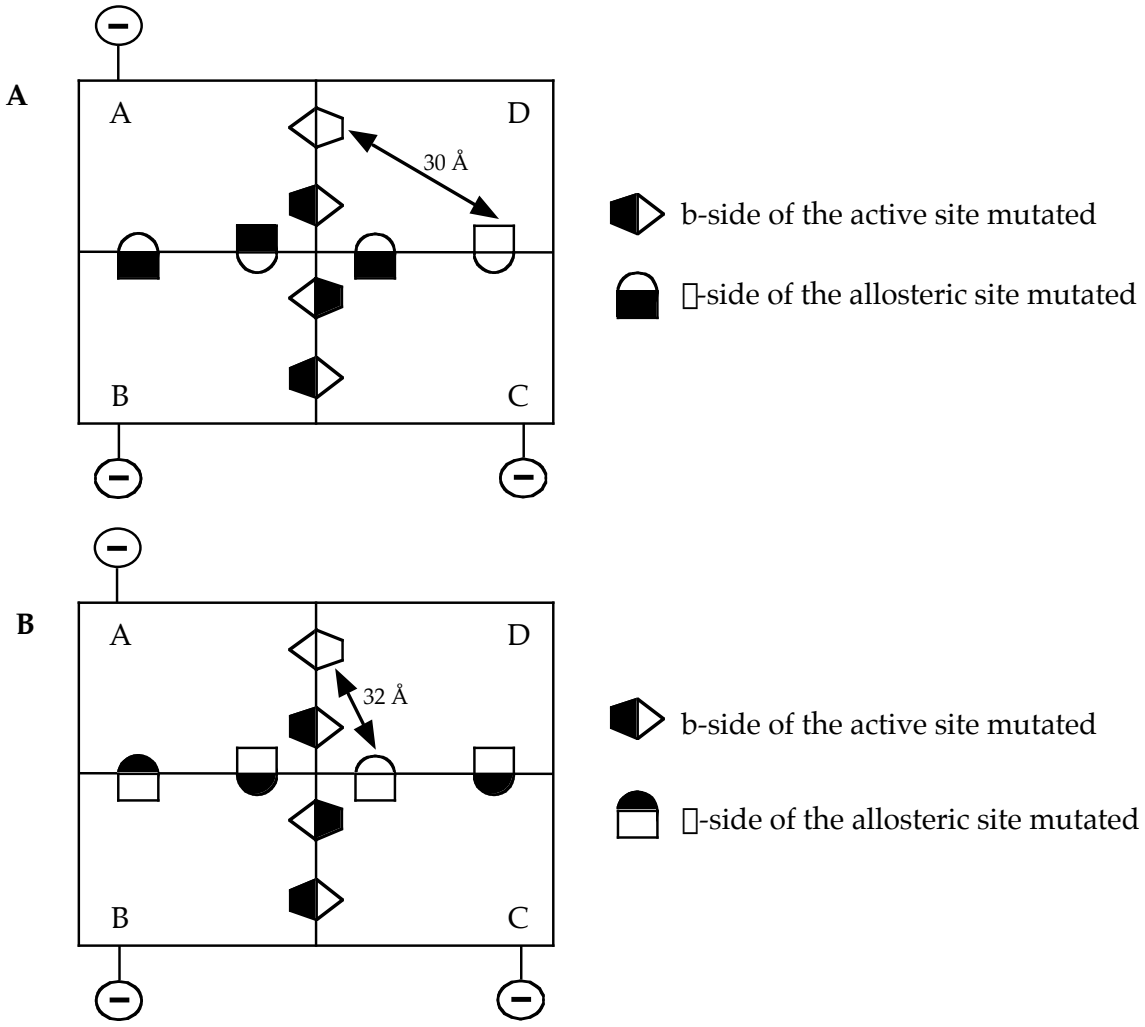

FIGURE 3-6 An illustration of the two 1:3 hybrid combinations used to isolate the 30 Å and 32 Å heterotropic interactions. The different "sides" of the active sites and allosteric sites requiring to be mutated so as to isolate that particular interaction are shown. To indicate the presence of a mutation on a specific "side" of a binding site, a closed shape is used, while the native, non-substituted binding sites remain open. The arrow drawn between the two remaining native binding sites depicts the specific heterotropic interaction isolated within each of the 1:3 hybrids. (*A*) The 1:3 hybrid that isolates the 30 Å heterotropic interaction. (*B*) The 1:3 hybrid that isolates the 32 Å interaction.

in which the mutant subunits contain modifications to positively charged residues in both the Fru-6-P and allosteric binding sites, will yield a specific unmodified Fru-6-P binding site and a specific unmodified allosteric binding site provided that the mutations are only located on a single side of the subunit interface for each site that is mutated. Thus, through mutating the b-side of the active site and the β-side of the allosteric site, the 30 Å interaction can be isolated, while mutating the b-side of the active site and the α-side of the allosteric site isolates the 32 Å interaction. Table 3-1 lists the different BsPFK variants used in this study to try to isolate the two interactions and the mutations they contain.

The active site and allosteric site mutations. In order to isolate the 30 Å and 32 Å interactions, mutations were required on the b-side of the active site. According to the crystal structure, an arginine at position 252 interacts with the phosphate group of the Fru-6-P molecule (Schirmer and Evans, 1990). Thus, to discourage Fru-6-P binding, the R252E mutation was introduced, however, the mutation dramatically affected the enzymatic turnover so a more conservative mutation was necessary. R252A was constructed, and exhibited the desired increase in the $K_{1/2}$ for Fru-6-P (approximately 1000 fold) while having no effect upon the turnover of the enzyme. Figure 3-7 shows the effects of these two mutations at the active site as compared to wild-type BsPFK.

As for the allosteric site, the mutations on the α-side had already been found (R211E/K213E by Kimmel and Reinhart, 2001) permitting use in isolating the 32 Å interaction; however, to isolate the 30 Å interaction, the β-side of the

TABLE 3-1 The BsPFK variants used in attempting to isolate the 30 Å and 32 Å interactions via their respective 1:3 hybrids

Interaction Isolated via the 1:3 Hybrid	Active Site Mutation (All on b-side)	Allosteric Site Mutation (or -side)	Charge Tag Mutation
30 Å interaction	R252A	R25E ()	K90E/K91E
	R252A	R25A ()	none
	R252A	R25A ()	K90E/K91E
	H249E	R25E ()	K90E/K91E
	H249N	R25E ()	K90E/K91E
	R252A/D12A	R25E ()	K90E/K91E
32 Å interaction	R252A	R211E/K213E ()	K90E/K91E
	R252A	R211E/K213E ()	none
	H249E	R211E/K213E ()	K90E/K91E
	H249N	R211E ()	K90E/K91E
	H249N	R211E/K213E ()	K90E/K91E
	R252A/D12A	R211E/K213E ()	K90E/K91E

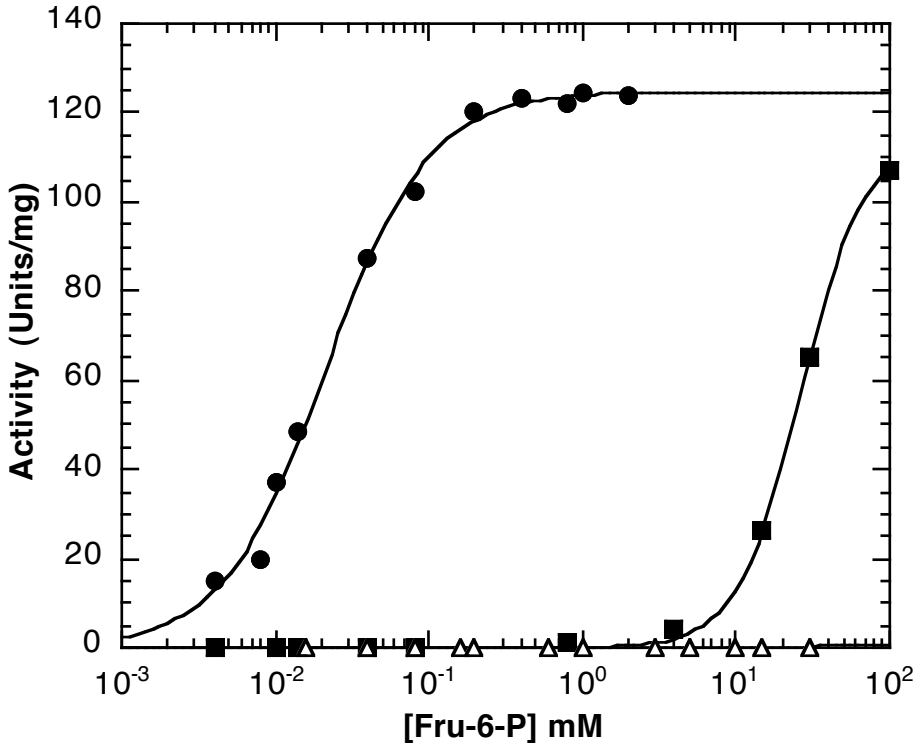

FIGURE 3-7 Fru-6-P saturation profiles for wild-type BsPFK (●) and the active site mutants proteins R252A (■) and R252E (△). MgATP concentration was 3 mM, the buffer component was MOPS-KOH (pH 7.0) and the assay temperature was 25°C. Other conditions were as described in Chapter II (Materials and methods). Curves represent the best fit to Eq. 2-1 as described in the text.

allosteric site would have to be mutated. Thus, from examining the crystal structure, an arginine at position 25 was found and mutated to a glutamate to discourage PEP binding. The effects of this mutation are summarized in Fig. 3-8. Due to the difficulties in assessing the direct binding affinity of PEP to BsPFK, an indirect method was used to elucidate the ability of PEP to inhibit the binding of Fru-6-P for both the wild-type and R25E mutant enzymes. The resulting data were fit to Eq. 2-4 in order to determine the dissociation constant of PEP for BsPFK (K_{iy}^{o}). As Fig. 3-8 shows, it requires approximately 100 mM PEP to increase the $K_{1/2}$ for Fru-6-P as compared to 0.023 mM PEP for the wild-type enzyme indicating a substantial decrease in PEP affinity. However, an increase in the $K_{1/2}$ for Fru-6-P is still observed at high concentrations of PEP, suggesting that the allosteric communication has not been destroyed by the mutation, and that binding eventually occurs. These results are analogous to the previous R211E/K213E allosteric site mutations (□-side) (Kimmel and Reinhart, 2001).

Equipped with the aforementioned active site (b-side) and allosteric site mutations (b-side), a BsPFK variant was made to isolate the 30 Å interaction that contained the following mutations: R252A, R25E and K90E/K91E, in which the surface charge tag (K90E/K91E) was added to facilitate separation of the various hybrid species via anion exchange chromatography. When this mutant protein was used to make hybrids with wild-type BsPFK, the 1:3 hybrid, as well as others, were unable to form. An example of this phenomenon can be seen in

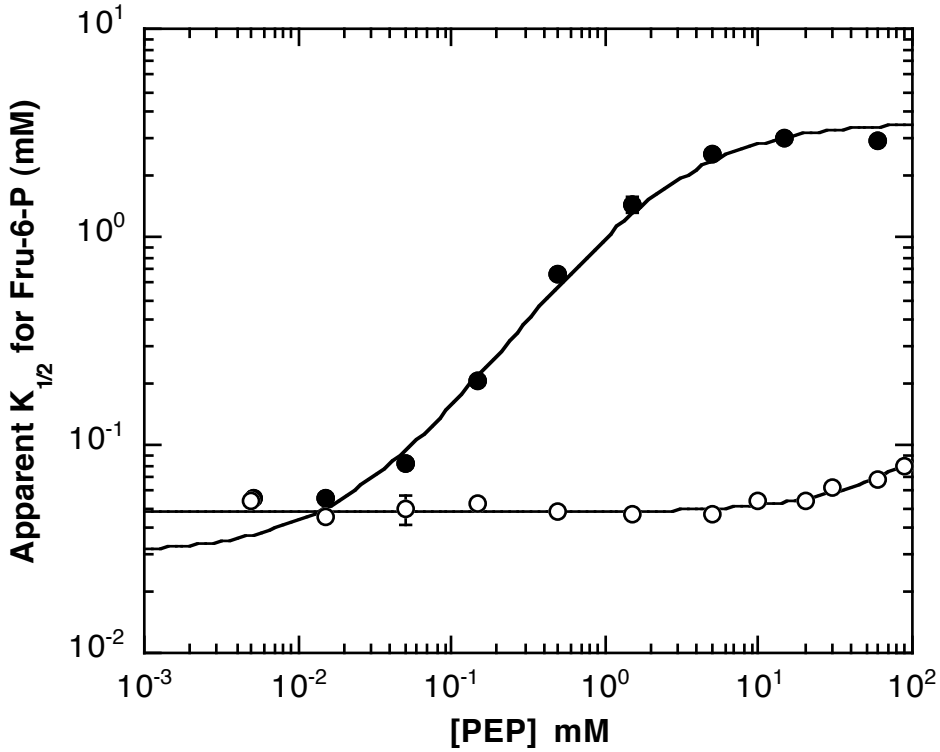

FIGURE 3-8 Dependence of the apparent $K_{1/2}$ for Fru-6-P on increasing concentrations of the inhibitor PEP for wild-type BsPFK (●) and the allosteric site mutant protein R25E (○). The $K_{1/2}$ values were obtained from individual Fru-6-P saturation profiles (performed at pH 7.0 and 25°C; data not shown but similar to Fig. 3-7) at increasing concentrations of PEP. The curves correspond to the best fit of these data to Eq. 2-4 as described in the text. Error bars represent ± the standard error and are smaller than the symbol when not evident.

lanes 2 and 3 of Fig. 3-9 where only 2 bands are observed probably corresponding to wild-type BsPFK and the 3:1 hybrid.

In an attempt to make the elusive 1:3 hybrid, the conditions used in making the hybrids were varied. Some of these variations included the following: changing the ratios of the two parent proteins used (1:1 to 50:1), altering the total protein concentration (0.5 mg/mL to 5 mg/mL) and the amount of KSCN used in making the hybrids (0.2 to 4 M), varying the time the proteins were exposed to the denaturant (seconds to hours) and the pH of the hybrid mix (pH 6.0 to pH 8.0) and using urea, guanidinium hydrochloride, and/or heat to try to dissociate the proteins. Unfortunately, none of these alterations in the hybrid making protocol produced the 1:3 hybrid.

Since this phenomenon did not occur when using the R162E mutation at the active site, it appeared that the R252A mutation was causing an unfavorable interaction at the interface not found within the native enzyme. Thus, other active site mutations on the b-side of the active site were investigated. A histidine at position 249 is adjacent to R252 and within hydrogen bonding distance of the bound Fru-6-P molecule, thus it was mutated to an alanine, an asparagine and a glutamate. The effect of each active site mutation upon the $K_{1/2}$ for Fru-6-P is shown in Fig. 3-10, (all data fit to the Eq. 2-1) and based upon the results, the H249E and H249N mutations were incorporated into the hybrid-making mutant protein(s). Unfortunately, the H249 mutants did not make the 1:3 hybrid and the same effects were observed as before (Fig. 3-11).

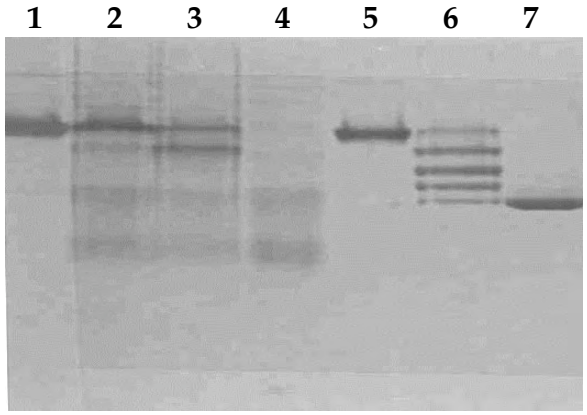

FIGURE 3-9 A 10% native PAGE gel showing the inability to form hybrids between wild-type and the R252A/R25E/K90E/K91E mutant. Lanes 1 and 5 show the wild-type protein. Lanes 2 and 3 show the results of using 1 M KSCN and 2 M KSCN to try to make hybrids between wild-type BsPFK and the R252A/R25E/K90E/K91E mutant, respectively where only 2 of the 5 hybrid species are observed. Lane 4 shows the R252A/D12A/K90E/K91E mutant protein. Lane 6 shows the result of using 2 M KSCN to make hybrids between wild-type BsPFK and the R252A/D12A/R25E/K90E/K91E mutant. All five hybrid species form as a result of incorporating the D12A mutation into the mutant protein. Lane 7 shows the R252A/D12A/R25E/K90E/K91E mutant protein. For lanes 2, 3 and 6, the samples were taken from after the dialysis step, and prior to loading unto the anion exchange column in the hybrid-making procedure. The conditions of how the gel was run were as described in Chapter II (Materials and methods).

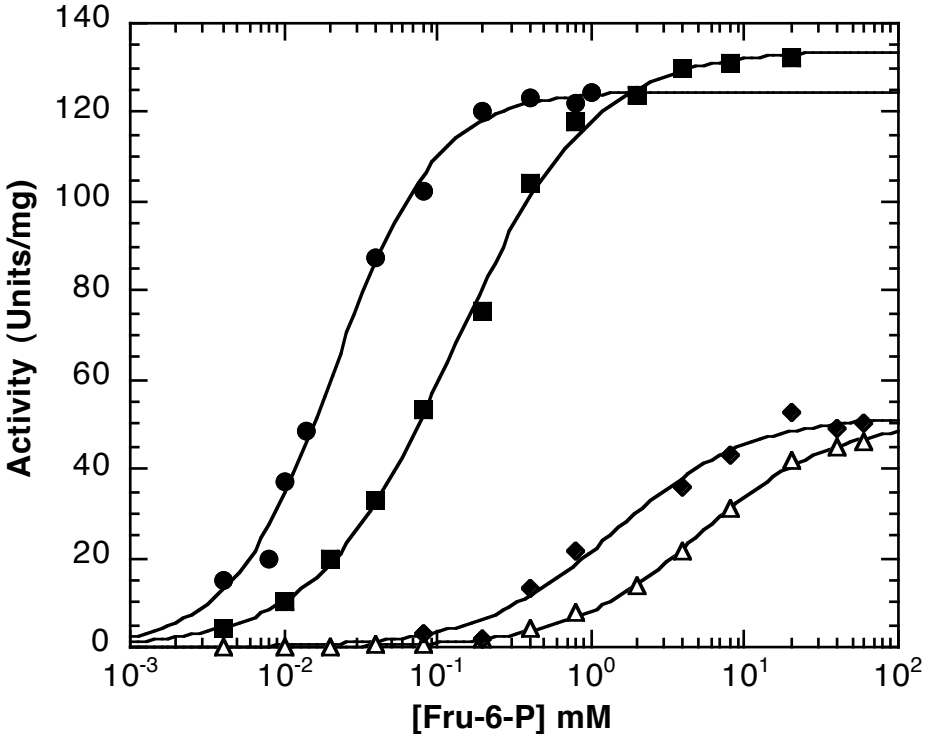

FIGURE 3-10 Fru-6-P saturation profiles for wild-type BsPFK (●) and the active site mutants proteins H249A (■), H249E (△) and H249N (◆). MgATP concentration was 3 mM, the buffer component was MOPS-KOH (pH 7.0) and the assay temperature was 25°C. Other conditions were as described in Chapter II (Materials and methods). Curves represent the best fit to Eq. 2-1 as described in the text.

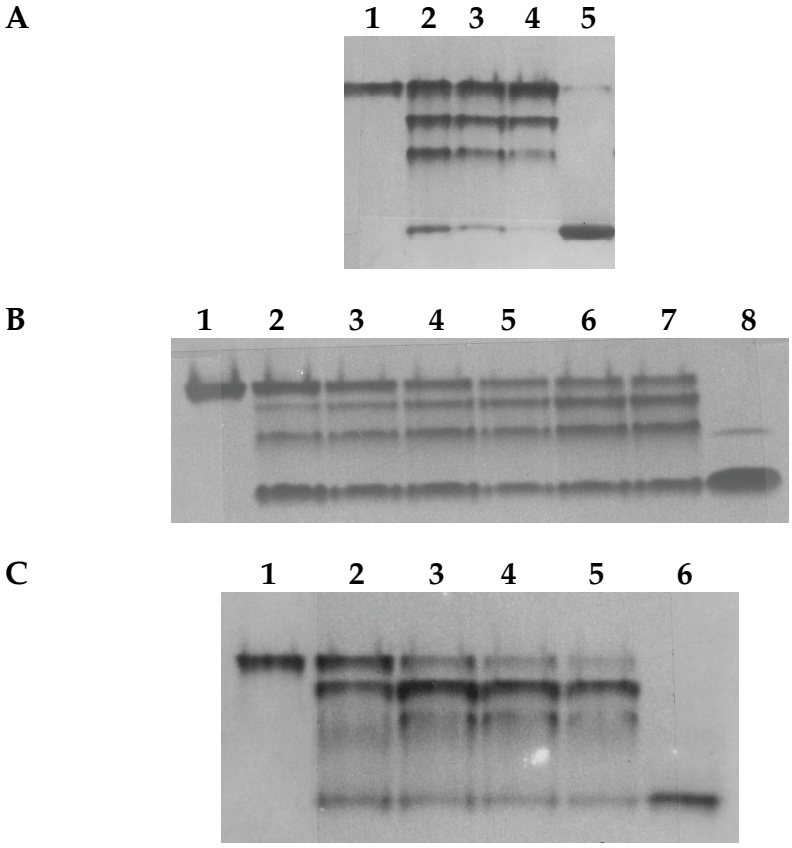

FIGURE 3-11 10% native PAGE gels showing the inability to form the 1:3 hybrid and sometimes other hybrids regardless of the conditions assayed and mutant constructs used. (*A*) Hybrids between wild-type and the R252A/R211E/K213E/K90E/K91E mutant protein. Lane 1 shows wild-type BsPFK. Lanes 2-4 show hybrids between wild-type and the R252A/R211E/K213E/K90E/K91E mutant protein varying the relative ratios of wild-type to mutant from a 2:1, 4:1 and 10:1. Lane 5 shows the R252A/R211E/K213E/K90E/K91E mutant protein. (*B*) Hybrids between wild-type and the H249N/R211E/K90E/K91E mutant protein. Lane 1 shows wild-type BsPFK. Lanes 2-7 show hybrids between wild-type and the H249N/R211E/K90E/K91E mutant protein at increasing concentrations of KSCN starting at 1 M in lane 2 and ending at 2 M in Lane 7 (0.2 M increments). Lane 8 shows the H249N/R211E/K90E/K91E mutant protein. (*C*) Hybrids between wild-type and the R252A/R25A/K90E/K91E mutant protein. Lane 1 shows wild-type BsPFK. Lanes 2-5 show hybrids between wild-type and the R252A/R25A/K90E/K91E mutant protein at increasing concentrations of KSCN starting at 1 M in lane 2 and ending at 4 M in lane 5 (1 M increments). Lane 6 shows the R252A/R25A/K90E/K91E mutant protein.

Thus, the crystal structure was examined again, but this time, instead of looking for a different b-side residue to mutate to discourage Fru-6-P binding, we looked for an amino acid that might be the cause of the unfavorable interaction when the R252(X) or H249(X) mutants were used. In the crystal structure, adjacent to the other side of R252 (outside the binding pocket) is an aspartic acid at position 12 that interacts via a hydrogen bond (inferred from the crystal structure) with R252 (Fig. 3-12). More importantly however, D12 is located at the interface of the protein across from a histidine at position 160 (within hydrogen bonding distance). Thus, we suspect that upon mutating R252 or H249, the structural integrity of the Fru-6-P binding pocket is altered in such a way that D12 interferes with the essential interfacial contacts found in the native enzyme. Consequently, D12 was mutated to an alanine in hopes of restoring the appropriate interfacial interactions when either R252 or H249 was mutated. Fig. 3-12 shows this region of interest highlighting the positions of the R252, D12 and H160 residues.

The D12A mutation was successful, as all five hybrid species formed when D12A was combined with the R252A, R25E and K90E/K91E mutations (lane 5 of Fig. 3-9). Although the entire effect of D12A is not yet fully understood, it is likely due to an enhanced quaternary stability for the aforementioned mutant proteins, which is evident when comparing lanes 4 and 7 of Fig. 3-9. In lane 4, a banding pattern is seen for the mutant protein in the absence of the D12A mutation, while in the presence of the D12A mutation a single band is observed (lane 7).

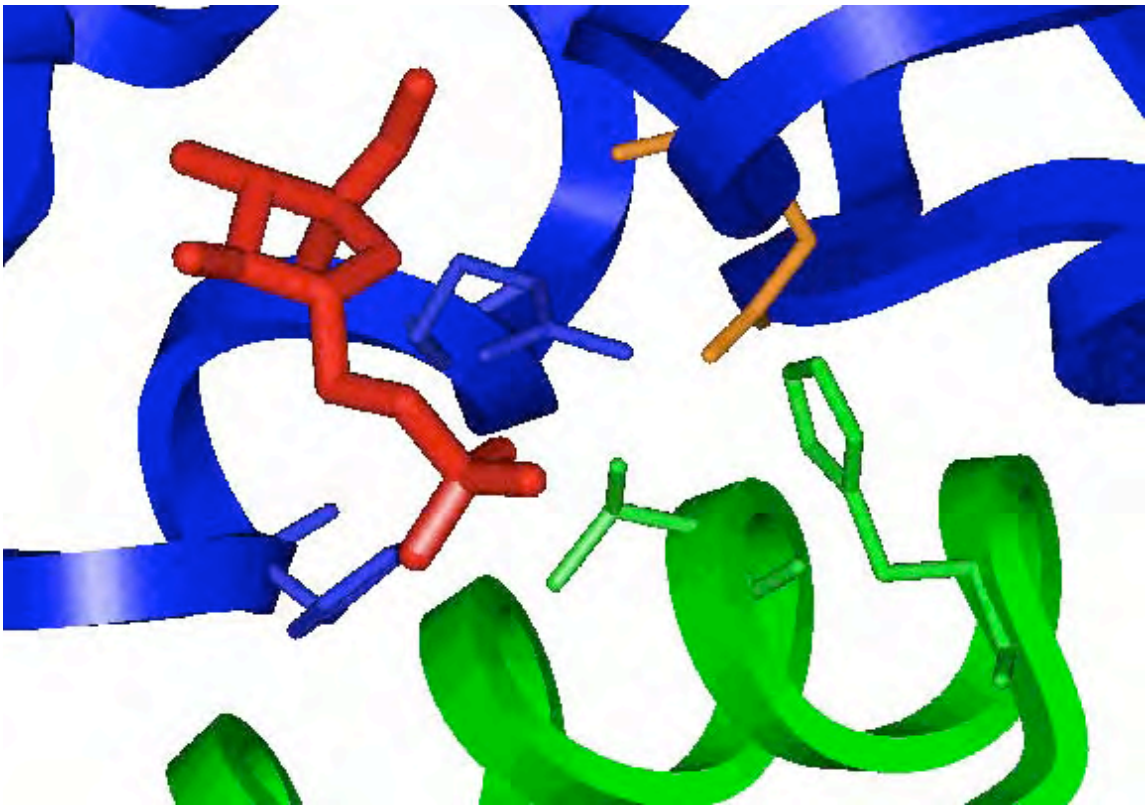

FIGURE 3-12 The x-ray crystal structure of the active site region highlighting the location of the R252, D12, and H160 residues. D12 is shown in orange (b-side of the active site), R252 and H249 are shown in blue, H160 and T156 are shown in green (from the a-side of the active site) and the Fru-6-P molecule bound in the active site is shown in red (Schirmer and Evans, 1990). It is inferred from the crystal structure that D12 makes a hydrogen bond with R252 and H160 across the interface.

To ensure the binding affinity for Fru-6-P is diminished enough in the R252A/D12A mutated protein, a Fru-6-P saturation profile was performed and Fig. 3-13 illustrates the result of incorporating these mutations at the active site. Equation 2-1 was used to fit both the wild-type and R252A/D12A mutant data, although the Hill coefficient did not vary significantly from 1. As desired, the affinity for Fru-6-P ($K_{1/2}$) is diminished by approximately 240-fold relative to that of wild-type. Moreover, the specific activity of the mutant is unaffected indicating no mechanistically significant structural perturbation of the active site. Table 3-1, described earlier, lists all of the mutant proteins constructed in trying to obtain the 1:3 hybrid and Table 3-2 summarizes all the kinetic and allosteric properties of the wild-type enzyme, the individual active site mutants, and the individual allosteric site mutants used in making the mutant proteins.

Protein stability. To further address the added stability associated with the D12A mutation as described earlier, KSCN denaturation profiles were performed in an attempt to determine which of the mutations was the cause of the inherent instability. At each KSCN concentration, BsPFK activity was measured and normalized to the percent of total activity to make it easier in comparing the various denaturation curves. Figure 3-14 summarizes the effects of various mutations on the stability, and hence the activity, of each protein.

Not surprisingly, the denaturation curve for the D12A/K90E/K91E mutant protein is virtually identical to that of wild-type, so although the D12A mutation provides an added stability in the mutant proteins, it does not provide

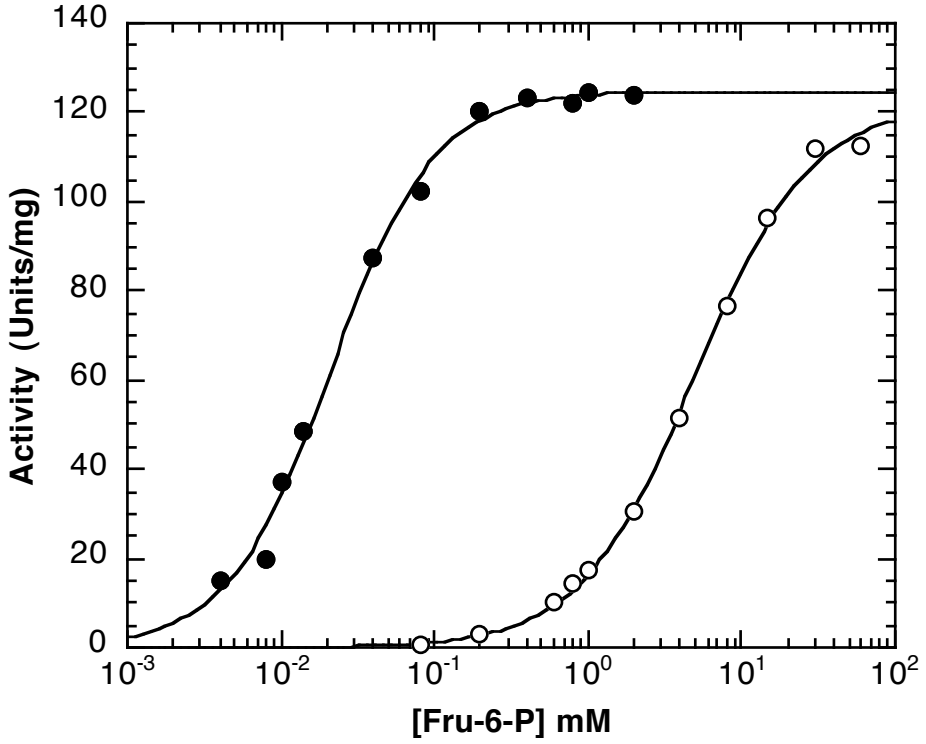

FIGURE 3-13 Fru-6-P saturation profiles for wild-type BsPFK (●) and the active site mutant protein R252A/D12A (○). MgATP concentration was 3 mM, the buffer component was MOPS-KOH (pH 7.0) and the assay temperature was 25°C. Other conditions were as described in Chapter II (Materials and methods). Curves represent the best fit to Eq. 2-1 as described in the text.

TABLE 3-2 Steady-state kinetic and thermodynamic parameters for wild-type BsPFK and the individual active site and allosteric site mutants used in constructing the mutant parent protein(s). Performed at 25°C and pH 7.0 with [MgATP] = 3 mM

Enzyme	V_{max} (Units/mg)[a]	$K_{1/2}$ (mM)[a]	n_H[a]	K^o_{iy} (mM)[b]
wild-type	125 ± 2	0.021 ± 0.001	1.30 ± 0.09	0.023 ± 0.002
R252E	ND	>100	ND	ND
R252A	114 ± 1	26.3 ± 0.5	2.11 ± 0.08	ND
H249A	134 ± 2	0.13 ± 0.01	0.98 ± 0.04	ND
H249E	51 ± 1	5.1 ± 0.3	1.02 ± 0.04	ND
H249N	52 ± 3	1.4 ± 0.3	1.00 ± 0.17	ND
R252A/D12A	122 ± 3	5.0 ± 0.3	1.17 ± 0.05	ND
R25E	91 ± 1	0.047 ± 0.002	1.27 ± 0.05	~100
R211E/K213E[c]	109 ± 1	0.058 ± 0.001	1.12 ± 0.08	~20

[a]Pertaining to Fru-6-P saturation profiles at 0 mM PEP and parameters obtained from fitting to Eq. 2-1.

[b]Obtained by fitting to Eq. 2-4 as described in Chapter II.

[c]Experiment performed under identical conditions except at pH 8.0 (Kimmel and Reinhart 2001).

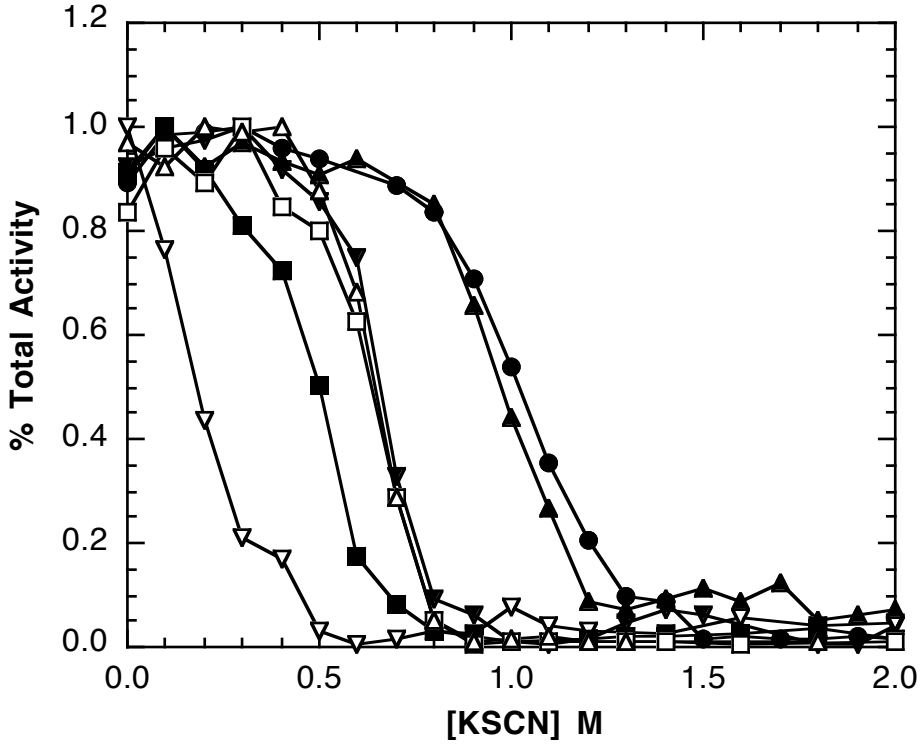

FIGURE 3-14 KSCN denaturation profiles for wild-type BsPFK and several mutant proteins. The relative activities for wild-type BsPFK (●), the D12A/K90E/K91E mutant (▲), the D12A/R25E mutant (□), the D12A/R25E/K90E/K91E mutant (△), the R252A/D12A/R25E/K90E/K91E mutant (▼), the R25E mutant (■) and the R252A/R25E/K90E/K91E mutant (▯) were determined as a function of KSCN concentration to assay protein stability. Activity measurements were performed using 20 mM Fru-6-P and as described in Chapter II at pH 7.0 and 25°C. The data pertaining to each protein were normalized to percent total activity because the differences in the specific activity of each protein made it difficult to compare the various denaturation curves.

any additional stability for the wild-type protein when using KSCN. Upon introducing the R25E allosteric site mutation to either the D12A mutant or the D12A/K90E/K91E mutant, an obvious decrease in stability is observed. The midpoint of stability, or the concentration of KSCN that eliminates 50% of the total activity, for both the D12A/R25E and D12A/R25E/K90E/K91E mutant proteins was reduced from 1.0 M (wild-type) to about 0.65 M. Notably, the presence of the K90E/K91E mutation does not change the stability of any of the mutant proteins.

However, the D12A mutation does provide some added stability for the R25E mutant as the R25E mutant protein alone has a midpoint of stability of approximately 0.5 M. The value of the D12A mutation is not truly evident however until comparing the R252A/R25E/K90E/K91E mutant protein to the R252A/D12A/R25E/K90E/K91E mutant protein, recalling that the former protein cannot form the 1:3 hybrid while the latter can. The midpoint of stability in the absence and presence of the D12A mutation changes from 0.18 M to 0.65 M respectively. It is this added stability that may aid in hybrid formation. As for the active site mutation R252A, it appears to have no effect upon protein stability as the midpoint value does not change when comparing the R252A/D12A/R25E/K90E/K91E mutant and the D12A/R25E/K90E/K91E. Thus, the allosteric site mutation(s) appears to be the main culprit of the protein instability, but how an active site mutation (D12A) can add stability at the allosteric site or it's interface is unknown. Table 3-3 summarizes the mutants investigated for this stability study and the midpoint values obtained for each

protein.

TABLE 3-3 Values obtained for the midpoint of stability in the KSCN denaturation profiles for several mutant proteins

Mutant Protein	Midpoint of Stability (M)[a]
wild-type BsPFK	1.02
D12A/K90E/K91E	0.97
R25E/D12A/K90E/K91E	0.65
R25E/D12A	0.65
R25E	0.50
R252A/D12A/R25E/K90E/K91E	0.65
R252A/R25E/K90E/K91E	0.18

[a]Best estimate obtained by examining each profile, therefore, there are no error values.

Isolating the two individual heterotropic interactions. Having identified the appropriate mutations (R252A/D12A on the b-side of the active site and R25E on the β-side of the allosteric site), and in conjunction with the previous allosteric site mutations (R211E/K213E on the β-side) discovered by Kimmel and Reinhart (2001), the 30 Å and 32 Å heterotropic interactions can be isolated via their respective 1:3 hybrids. As reported earlier, the addition of the surface charge-tag, K90E/K91E, to each of the mutant parent proteins allows for the isolation of the 1:3 hybrid from the other 6 enzyme species via anion exchange chromatography (Kimmel and Reinhart, 2001). However, the extent of

separation of the various hybrid species varied among the mutant construct used. It is presumed that this is caused by the variability in the solvent accessibility of the mutated residues, and in particular R211. Hence, the charge-tag charge change was in the same positive to negative direction as the binding site mutations, so as to not negate the chromatographic effects incurred by the charge-tag. Using the R252A/D12A, the R25E and/or the R211E/K213E mutations, the 1:3 hybrid containing either the 30 Å interaction or the 32 Å interaction was formed, isolated and identified as described earlier in Chapter II. All 1:3 hybrids were stored at 4°C and no re-hybridization between subunits was observed for at least 4 weeks as confirmed by native PAGE analysis (data not shown).

Functional properties of the 1:3 hybrid enzymes. The dependence of enzyme activity as a function of Fru-6-P concentration was determined for the wild-type enzyme, as well as the individual 1:3 hybrid enzymes at pH 6.0, 6.5, 7.0, 7.5 and 8.0. As expected, the Fru-6-P saturation profiles for the 1:3 hybrids exhibited the saturation of two different types of binding sites, corresponding to the high affinity and low affinity active sites respectively. An example of a typical saturation profile for the 1:3 hybrids containing the 30 Å interaction and 32 Å interaction at pH 7.0 is shown in Fig. 3-15. Data obtained from the Fru-6-P saturation profiles for the wild-type enzyme were fit to Eq. 2-1, while data for the 1:3 hybrids were fit to Eq. 2-2, in which two Michaelis-Menten equations are summed together.

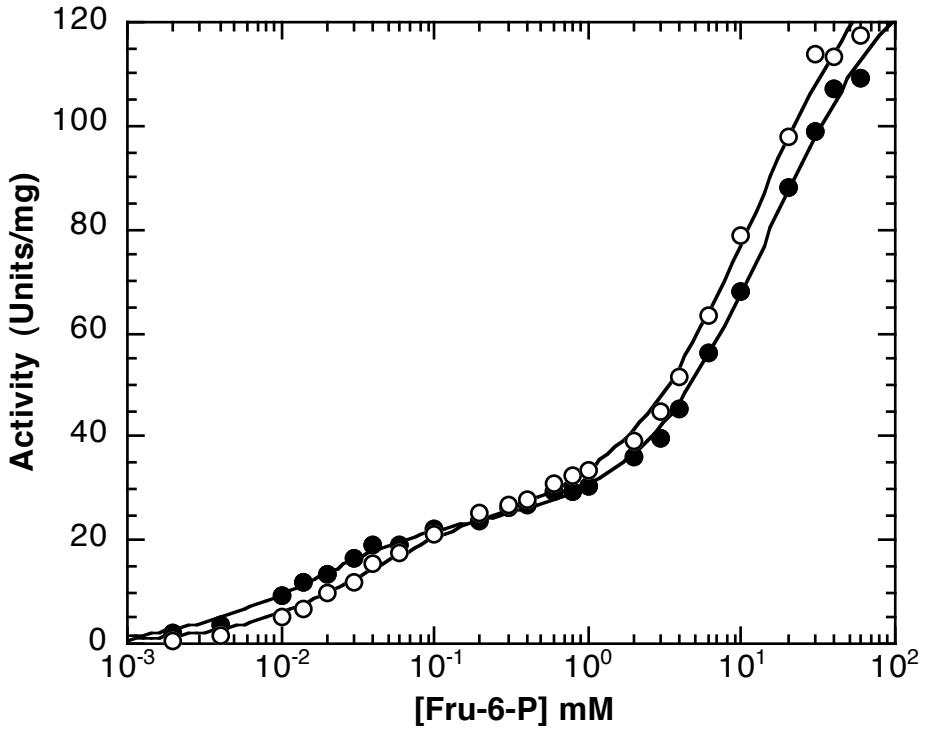

FIGURE 3-15 Fru-6-P saturation profiles for the 1:3 hybrids that isolate the 30 Å interaction (●) and 32 Å interaction (○) at pH 7.0, 25°C and in the absence of PEP. The first phase corresponds to Fru-6-P binding at the lone native active site, while the second phase corresponds to Fru-6-P binding at the mutated active sites. Activity assays were performed as described in Chapter II with the MgATP concentration equal to 3 mM. The curve represents the best fit of the data to Eq. 2-2. Similar plots were observed for either of the 1:3 hybrids at pH 6.0, 6.5, 7.5 and 8.0.

Table 3-4 summarizes the kinetic parameters obtained from these fits for wild-type BsPFK and both the high affinity (native) and low affinity (mutated) Fru-6-P binding sites found in the 1:3 hybrids. At all pH values, the maximal specific activity for the high affinity interaction (V_{max}) is approximately one-fourth that of wild-type. This result was expected, as each 1:3 hybrid contains one-fourth the number of native active sites found within the BsPFK tetramer. Also, the maximal specific activity for each of the 1:3 hybrids increases with an increase in pH, a behavior consistent with the wild-type enzyme (Tlapak-Simmons and Reinhart, 1998). Moreover, the values obtained for the $K_{1/2}$ for Fru-6-P for the high affinity active site agree, within error, with the $K_{1/2}$ values for the wild-type enzyme with the exception of the 32 Å interaction at pH 8.0. The invariability in $K_{1/2}$ was expected as little to no cooperativity between active sites in the absence of effector has been reported for the native BsPFK enzyme (Evans and Hudson, 1979).

The values obtained for the low affinity active sites also conform to expected results. The maximal specific activities for the three low affinity active sites (V'_{max}) is approximately three-fourths the V_{max} value for the mutant tetramer, which is comparable to three-fourths the V_{max} value for the wild-type enzyme since the active site mutations do not alter the enzymatic turnover of BsPFK. Furthermore, the low affinity $K_{1/2}$ values are comparable to the measured $K_{1/2}$ values for their respective active site mutant enzymes.

TABLE 3-4 Steady-state kinetic parameters for wild-type BsPFK and the two 1:3 hybrids which isolate the 30 Å interaction and the 32 Å interaction at 25°C, pH 6.0, 6.5, 7.0, 7.5 and 8.0, [MgATP] = 3 mM and [PEP] = 0 mM

Enzyme or Interaction Isolated	V_{max} (Units/mg) high affinity	$K_{1/2}$ (mM) high affinity	V'_{max} (Units/mg) low affinity	$K'_{1/2}$ (mM) low affinity
pH 6.0				
wild-type	67.1 ± 1.1	0.032 ± 0.001	n/a	n/a
30 Å	15.4 ± 0.4	0.035 ± 0.003	36 ± 1	8.0 ± 0.3
32 Å	14.5 ± 0.5	0.031 ± 0.003	46 ± 2	10.0 ± 0.8
pH 6.5				
wild-type	ND	ND	n/a	n/a
30 Å	21.0 ± 0.6	0.022 ± 0.002	59.0 ± 1.5	7.9 ± 0.3
32 Å	22.0 ± 1.1	0.026 ± 0.004	71.0 ± 3.2	8.0 ± 0.6
pH 7.0				
wild-type	125 ± 2	0.021 ± 0.001	n/a	n/a
30 Å	26.7 ± 0.7	0.020 ± 0.002	96 ± 3	12.1 ± 0.7
32 Å	30.9 ± 1.1	0.047 ± 0.005	94 ± 3	9.6 ± 0.5
pH 7.5				
wild-type	ND	ND	n/a	n/a
30 Å	40.4 ± 0.9	0.027 ± 0.002	128 ± 4	24.5 ± 2.2
32 Å	32.5 ± 1.1	0.078 ± 0.008	109 ± 5	16.6 ± 1.0
pH 8.0				
wild-type	153 ± 3	0.034 ± 0.001	n/a	n/a
30 Å	37 ± 2	0.079 ± 0.008	UD	UD
32 Å	38 ± 2	0.310 ± 0.035	UD	UD

n/a = not applicable

ND = Not Determined

UD = Undeterminable

In order to measure the allosteric effect associated with each heterotropic interaction, the $K_{1/2}$ for Fru-6-P was determined as a function of PEP concentration for each of the two 1:3 hybrids at varying pH. Ideally, this measured allosteric effect would correspond to the interaction of only the native active site and native allosteric site. However, it was previously found that the three mutated allosteric sites still have the ability to influence the measured allosteric effect for the 1:3 hybrid at high concentrations of PEP (Kimmel and Reinhart 2001), thus a control hybrid for each 1:3 hybrid was made. This control hybrid consists of one native active site, three mutated active sites and four mutated allosteric sites and is depicted schematically in Fig. 3-16 using the 30 Å interaction as an example. Using the notation introduced by Fenton and Reinhart (2002), this control hybrid is designated 1|0, where 1 equals the number of native Fru-6-P binding sites and 0 equals the number of native allosteric sites in the tetramer. Thus, the 1:3 hybrids are designated 1|1 whereas wild-type BsPFK is designated 4|4. Each of the two control hybrids were constructed in the same manner as the 1|1 hybrids except the appropriate allosteric site mutant was substituted for the wild-type parental protein. Fru-6-P titrations at pH 6.0, 6.5, 7.0, 7.5 and 8.0 were performed for each 1:3 hybrid and its corresponding control hybrid at increasing concentrations of PEP. In all cases, the measured coupling for each 1:3 hybrid was corrected for by using the following equation:

$$K_{1/2}(\text{corrected}) = \frac{K_{1/2}(1|1)}{K_{1/2}(1|0)} \qquad (3\text{-}1)$$

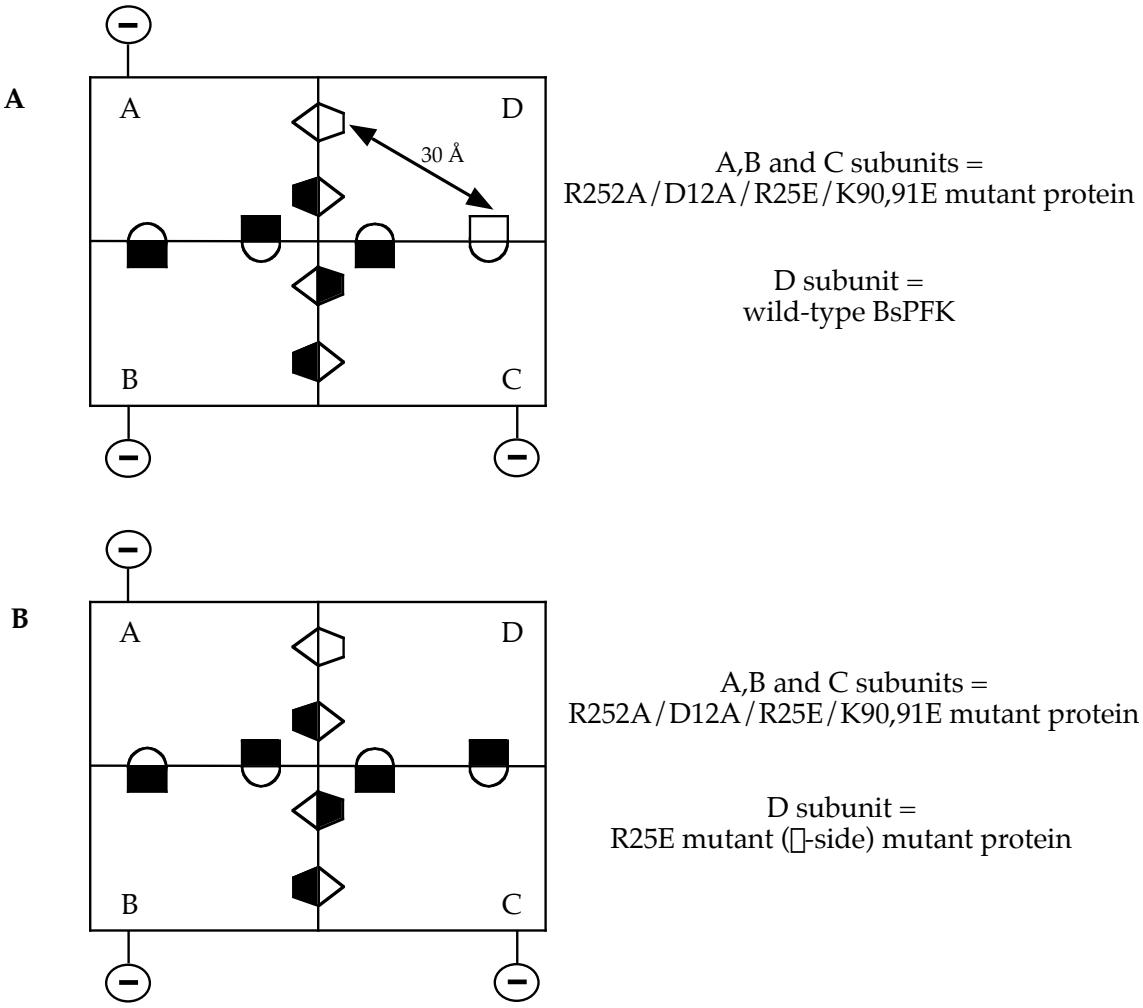

FIGURE 3-16 Two-dimensional schematics of the 1:3 hybrids corresponding to the 1|1 hybrid and 1|0 hybrid for the 30 Å interaction. (*A*) The 1:3 hybrid (1|1) used to obtain data corresponding to the magnitude of the 30 Å interaction. (*B*) The 1:3 hybrid (1|0) used to "control-subtract" the 1|1 hybrid data for the effects from PEP binding to the mutated allosteric sites.

An example of the change in Fru-6-P affinity as a function of PEP concentration for the 32 Å 1:3 hybrid (1|1) and its control hybrid (1|0) is shown in Fig. 3-17 at pH 7.0 and 25°C. The subsequent control subtracted data using Eq. 3-1 is also shown and fit to Eq. 2-4. The gray shaded region of the plot indicates the region at which the mutated allosteric sites begin to bind the inhibitor PEP, thus influencing the affinity the native active site has for Fru-6-P (occurs at around 10 mM PEP) for both the 1|1 hybrid and the 1|0 hybrid. This influence from the mutated allosteric sites results in two phases for the data corresponding to the 32 Å 1:3 hybrid (1|1), and this second phase is suitably corrected for by the control hybrid (1|0) data as seen in the plot. This control subtraction procedure was performed at all five pH values and for both of the 1:3 hybrids (1|1).

Figures 3-18 *A* and *B* show the results for the corrected apparent $K_{1/2}$ for Fru-6-P as a function of increasing concentrations of PEP for both the 30 Å and 32 Å interactions at pH 6.0, 6.5, 7.0, 7.5 and 8.0. From fitting the data to Eq. 2-4, the value of K_{ia}^{o} can be obtained which is the dissociation constant for Fru-6-P in the absence of PEP. For the 30 Å interaction, the K_{ia}^{o} is identical to wild-type and remains the same from pH 6.0 to 7.5, and increases approximately 2-fold at pH 8.0. The K_{ia}^{o} obtained for the 32 Å interaction on the other hand is affected a bit more by pH. The K_{ia}^{o} value remains like wild-type from pH 6.0 to 7.0, increases 2-fold at pH 7.5 and an additional 5-fold at pH 8.0. A minimal increase in the K_{ia}^{o} as a function of pH (less than 2-fold) has been previously reported for

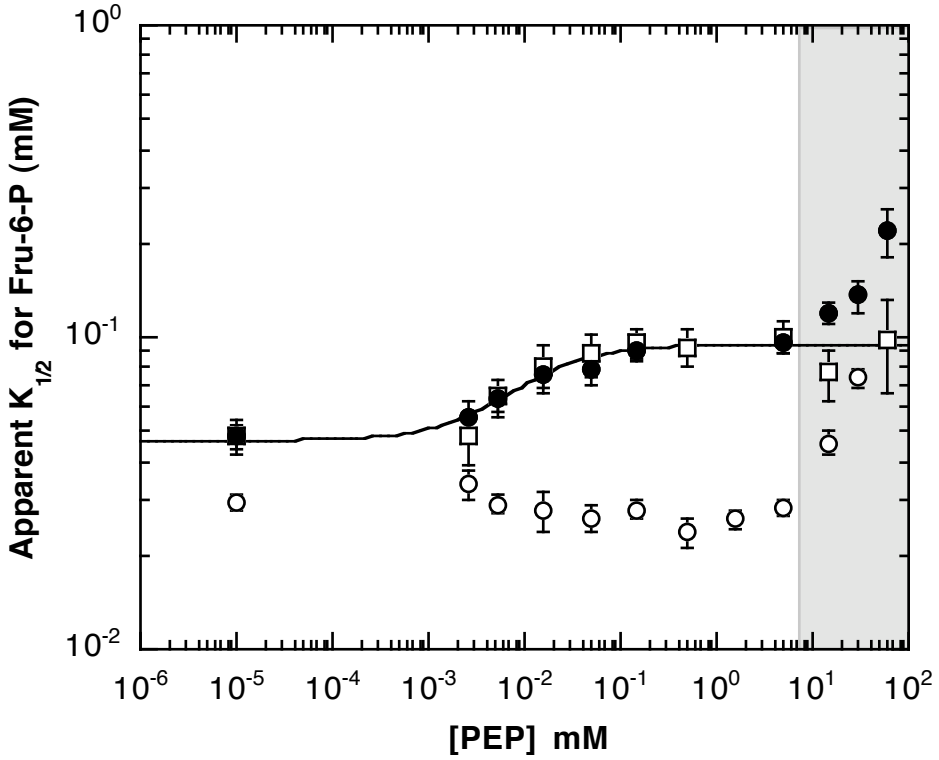

FIGURE 3-17 Dependence on the apparent $K_{1/2}$ for Fru-6-P on increasing concentrations of the inhibitor PEP for the 1|1 hybrid (●), the 1|0 control hybrid (○), and the corrected 32 Å allosteric interaction (□). The data relating to the 1|1 hybrid displays two phases where the first phase indicates the extent to which PEP binding at the native allosteric sites are influencing substrate binding at the native active sites. The second phase corresponds to the point at which PEP binding at the mutated allosteric sites influences substrate binding at the native active sites. Data for the corrected 32 Å interaction were obtained using Eq. 3-1 and Eq. 2-4 was used to generate the curve representing the best fit of those data. The shaded gray region corresponds to the point at which PEP begins binding to the mutated allosteric sites and influencing the apparent $K_{1/2}$ for Fru-6-P of the native active site in both the 1|1 and 1|0 hybrids. Error bars represent ± the standard error and are smaller than the symbol when not evident.

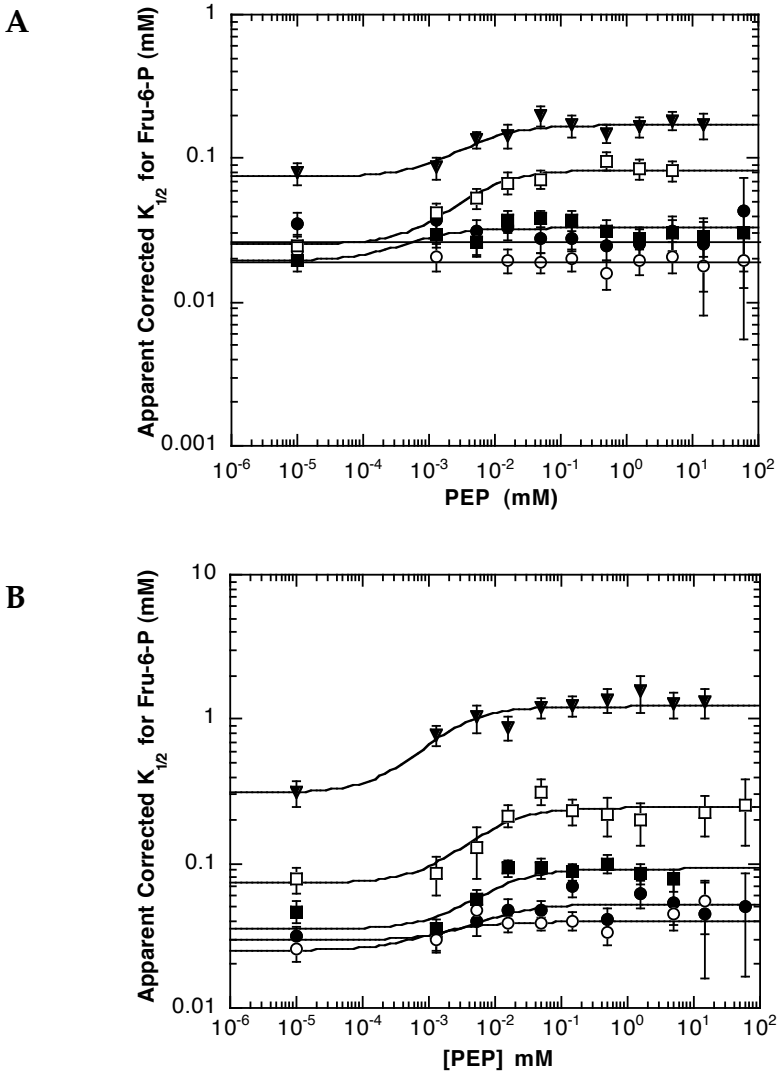

FIGURE 3-18 Dependence of the corrected apparent $K_{1/2}$ for Fru-6-P on increasing concentrations of the inhibitor PEP for the 30 Å interaction and the 32 Å interaction at pH 6.0 (●), pH 6.5 (○), pH 7.0 (■), pH 7.5 (□), and pH 8.0 (▼). The data for pH 6.0 were performed in buffer containing 50 mM MES-KOH, the data for pH 6.5. 7.0 and 7.5 were performed in buffer containing 50 mM MOPS-KOH, and the data for pH 8.0 were obtained using buffer containing 50 mM EPPS-KOH. All the curves correspond to the best fit of these data to Eq. 2-4 as described in the text. (*A*) Data corresponding to the 30 Å interaction. (*B*) Data corresponding to the 32 Å interaction.

wild-type BsPFK, but seems to be magnified inexplicably in the 30 Å and 32 Å interactions (Tlapak-Simmons and Reinhart, 1998). The dissociation constant for PEP in the absence of Fru-6-P (K^{o}_{iy}) for the 30 Å and 32 Å interactions can also be obtained from fitting the data in Figs. 3-18 *A* and *B* to Eq. 2-4. The K^{o}_{iy} values for the both the 30 Å and 32 Å interactions were found to be significantly tighter than that of wild-type BsPFK (wild-type ~ 0.030 mM) by one to two orders of magnitude with no obvious trend in the data.

The coupling constant, Q_{ay}, or the extent to which PEP inhibits the binding of Fru-6-P and *vice versa*, is also obtained from the data in Figs. 3-18 *A* and *B*. Fig. 3-18 *A* shows the corrected values for the $K_{1/2}$ for Fru-6-P plotted as a function of PEP concentration at the five pH values investigated for the 30 Å interaction. At pH 6.0 and 6.5, no coupling is measured (Q_{ay}) resulting in a coupling free energy of 0.00 ± 0.06 kcal/mol at either pH. Thus, the 30 Å interaction is "allosterically silent" at low pH. Interestingly, at pH 7.0, PEP begins to inhibit the 30 Å interaction, and this extent of inhibition increases with increasing pH (within error), a phenomenon consistent with wild-type BsPFK. At pH 7.0, 7.5 and 8.0, the measured coupling free energy (ΔG_{ay}) in kcal/mol is 0.31 ± 0.11, 0.71 ± 0.11 and 0.49 ± 0.11 respectively.

Figure 3-18 *B* shows the analogous data for the 32 Å interaction. Unlike the 30 Å interaction, the 32 Å interaction never becomes "allosterically silent" at low pH, although the extent of PEP inhibition does not change between pH 6.0 and 6.5, as seen with the 30 Å interaction. Using Eq. 2-6 to convert Q_{ay} into

coupling free energy (ΔG_{ay}), pH 6.0 and pH 6.5 have a measured coupling in kcal/mol of 0.34 ± 0.10 and 0.27 ± 0.13 respectively. The increase in inhibition arises at pH 7.0 and continues to increase with increasing pH as the couplings measured in kcal/mol proceed from 0.57 ± 0.10 at pH 7.0 to 0.71 ± 0.14 at pH 7.5 and finally to 0.82 ± 0.12 at pH 8.0. A summary of all of the thermodynamic parameters can be found in Table 3-5.

In comparing the values obtained for the coupling free energies (ΔG_{ay}) for the 30 Å and 32 Å interactions, a major similarity is evident when plotting the values obtained for ΔG_{ay} as a function of pH (Fig. 3-19). Even though the 30 Å interaction is "allosterically silent" at low pH and the 32 Å interaction has an overall greater measured allosteric effect by PEP, both interactions have an approximately identical overall change in ΔG_{ay} across the pH values investigated. This change has been denoted $\Delta\Delta G_{pH}$ and is the difference between the ΔG_{ay} measured at low pH and the ΔG_{ay} measured at high pH. Thus, from Figs. 3-19 *A* and *B*, the value of $\Delta\Delta G_{pH}$ can be estimated to be approximately 0.6 kcal/mol for both the 30 Å and 32 Å heterotropic interactions.

TABLE 3-5 Thermodynamic parameters for wild-type and the two individual allosteric interactions (control subtracted) at 25°C, pH 6.0, 6.5, 7.0, 7.5 and 8.0 and [MgATP] = 3 mM

Enzyme or Interaction Isolated	K_{ia}^{o} (mM)	K_{iy}^{o} (mM)	Q_{ay}	ΔG_{ay} (kcal/mol)
pH 6.0				
wild-type	0.032 ± 0.001	0.026 ± 0.002	0.041 ± 0.002	1.89 ± 0.03
30 Å	0.030 ± 0.002	ND	1.00 ± 0.10	0.0 ± 0.06
32 Å	0.029 ± 0.005	0.0045 ± 0.0061	0.56 ± 0.10	0.34 ± 0.10
pH 6.5				
wild-type	ND	ND	ND	ND
30 Å	0.020 ± 0.001	ND	1.00 ± 0.10	0.00 ± 0.06
32 Å	0.025 ± 0.005	0.0007 ± 0.0001	0.63 ± 0.13	0.27 ± 0.13
pH 7.0				
wild-type	0.030 ± 0.002	0.023 ± 0.002	0.0085 ± 0.0004	2.82 ± 0.03
30 Å	0.019 ± 0.004	0.0003 ± 0.0007	0.59 ± 0.11	0.31 ± 0.11
32 Å	0.035 ± 0.006	0.003 ± 0.002	0.38 ± 0.07	0.57 ± 0.10
pH 7.5				
wild-type	ND	ND	ND	ND
30 Å	0.025 ± 0.004	0.0013 ± 0.0007	0.30 ± 0.05	0.71 ± 0.10
32 Å	0.073 ± 0.015	0.0020 ± 0.0017	0.30 ± 0.07	0.71 ± 0.14
pH 8.0				
wild-type	0.027 ± 0.001	0.039 ± 0.001	0.0020 ± 0.0001	3.58 ± 0.02
30 Å	0.074 ± 0.014	0.002 ± 0.001	0.44 ± 0.08	0.49 ± 0.11
32 Å	0.31 ± 0.06	0.0004 ± 0.0003	0.25 ± 0.05	0.82 ± 0.12

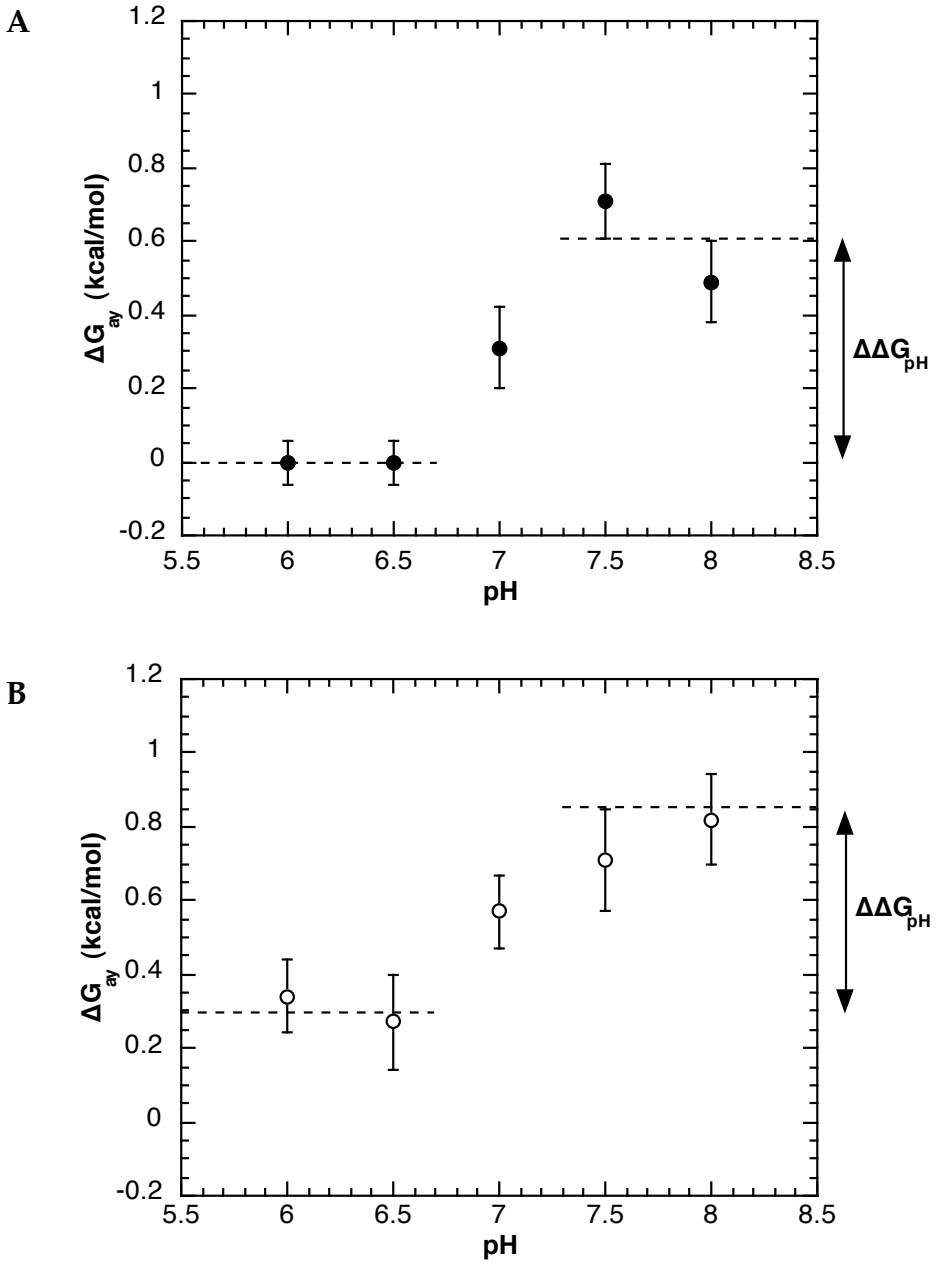

FIGURE 3-19 Determining the extent to which ΔG_{ay} changes as a function of pH for the 30 Å and 32 Å interactions. (*A*) Data pertaining to the 30 Å interaction (●). (*B*) Data pertaining to the 32 Å interaction (○).

Discussion

Phosphofructokinase from *Bacillus stearothermophilus* is a homotetramer containing four active sites and four allosteric sites, all of which are located on respective dimer-dimer interfaces within the protein. This oligomeric feature, a property common to most allosteric enzymes (Kurganov, 1982), provides many advantages to the regulatory properties of BsPFK, but it also increases the overall allosteric complexity possible between the various binding sites. For example, in BsPFK, 16 total pair-wise heterotropic interactions exist between the 8 binding sites, representing 4 occurrences each of 4 unique interactions. If our ultimate goal is to better understand the mechanism of allosteric regulation, this "web" of allosteric communication presents an interesting challenge in achieving this goal. However, when the number of native binding sites is decreased, the allosteric complexity is also decreased, eventually permitting characterization of the four heterotropic interactions individually when a particular native active site and native allosteric site remain. Moreover, by taking this divide-and-conquer approach in assessing the allosteric contributions of each of the four heterotropic interactions, we are able to better understand the allosteric properties of the enzyme as a whole. This reduction in allosteric complexity for a homotetramer, like BsPFK, containing one active site and one allosteric site per subunit is summarized in Table 3-6.

The fact that the binding sites of BsPFK are located at the interfaces of the protein is not surprising, as many allosteric enzymes possess this feature;

TABLE 3-6 Reduction in the allosteric complexity of a homotetramer containing one active site and one allosteric site per subunit upon reducing the number of wild-type subunits successively by one

Hybrid	Number of Wild-Type Subunits	Number of Native Active Sites	Number of Native Allosteric Sites	Number of Heterotropic Interactions (Unique)	Number of total Interactions (Unique)[a]
4:0 (WT)	4	4	4	16 (4)	28 (10)
3:1	3	3	3	9 (4)	15 (10)
2:2	2	2	2	4 (2)	6 (4)
1:3	**1**	**1**	**1**	**1 (1)**	**1 (1)**
0:4 (mutant)	0	0	0	0 (0)	0 (0)

[a]Includes the possible homotropic interactions between active sites and between allosteric sites.

however, it is this aspect that allows for the individual isolation of each of the four unique heterotropic interactions. In order to isolate a given interaction, a particular "side" of the active sites and allosteric sites has to be mutated to discourage both Fru-6-P and PEP binding. It was previously shown that the a-side of the active site (R162E) and the β-side of the allosteric site (R211E/K213E) could be successfully mutated to achieve these results (Kimmel and Reinhart, 2001), and we have now shown here that the b-side of the active site (R252A/D12A) and the β-side of the allosteric site (R25E) can also be mutated to substantially decrease the binding affinity for both Fru-6-P and PEP. Thus, as outlined in the strategy earlier in the chapter, mutating the b-side of the active site and the β-side of the allosteric site isolates the 30 Å interaction via it's 1:3 hybrid (1|1), and by mutating the b-side of the active site and the β-side of the allosteric site, the 32 Å interaction is isolated via it's 1:3 hybrid (1|1).

Unfortunately, a problem arose in forming hybrids when mutating the b-side of the active site, thus requiring the addition of the D12A mutation to form all the hybrid species. We surmised that the D12A mutation provides some kind of compensatory effect at the interface of the protein (possibly involving H160 across the interface) resulting in an increase in the overall quaternary stability of the tetramer as seen in both native PAGE analysis and KSCN denaturation profiles. The entire effect of the D12A mutation is not entirely understood, but is further complicated by the fact that the D12A mutation not only affects the active site, but also appears to affect the allosteric site(s). This long-range effect is evident from the KSCN denaturation profiles, which

indicates that the D12A mutation alleviates a majority of the decreased stability associated with the R25E allosteric site mutation. Furthermore, the binding affinity for the inhibitor PEP for the D12A/K90E/K91E mutant protein is at least an order of magnitude tighter as compared to wild-type as seen in Fig. 3-20. This long-range phenomenon has precedence as Valdez et al. (1989) reported a 68-fold increase in binding affinity for PEP in the R252A protein (BsPFK) relative to wild-type, while Fenton and Reinhart (2003) have also reported similar long-range effects of mutations at the active site influencing binding at the allosteric site in the *E. coli* form of the enzyme. Since an analogous mutation is not necessary when using mutations on the a-side of the active site (R162E), we believe that the R162E mutation does not create the same interfacial problems observed with mutations on the b-side of the active site.

In order to isolate the 1:3 hybrid from the other six possible enzyme species, the K90E/K91E charge tag was added to the mutated subunits (Kimmel and Reinhart, 2001). Based upon the allosteric site mutant used (R25E for the 30 Å interaction or R211E/K213E for the 32 Å interaction), the extent of separation of the seven hybrid species via anion exchange chromatography varied. This behavior is believed to be due to the solvent accessibility of R211 and this possibility will be further addressed in Chapter V. However, isolation of the 1:3 hybrid from the other enzyme species was never problematic.

With the ability to isolate the 30 Å and 32 Å interactions via the 1|1 hybrids, the couplings were determined by monitoring the apparent $K_{1/2}$ for

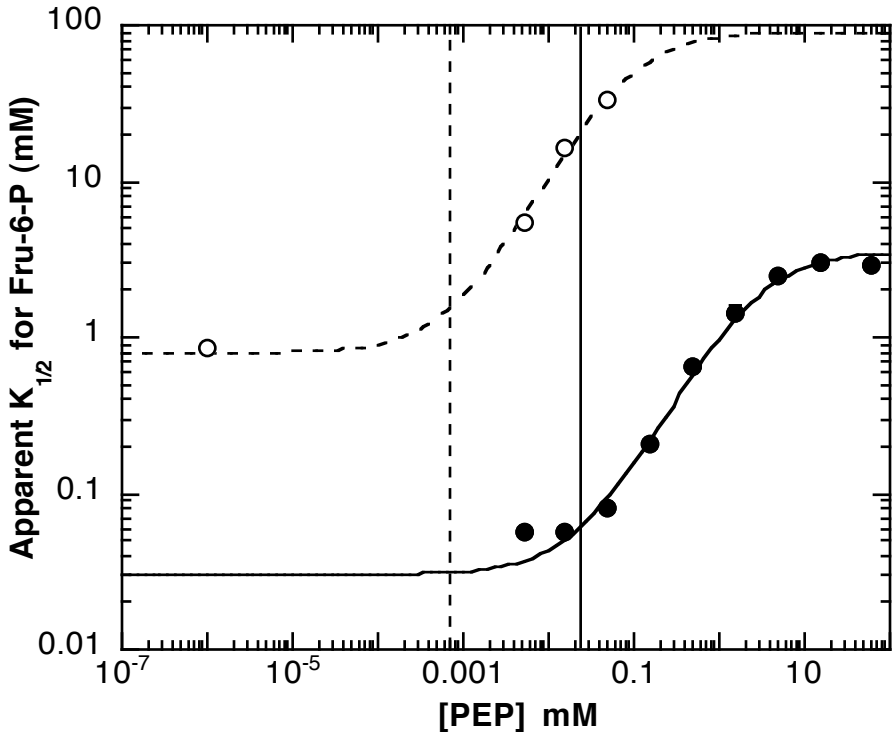

FIGURE 3-20 Comparison of the relative binding affinities for the allosteric inhibitor PEP of wild-type BsPFK (●) and the D12A/K90E/K91E mutant protein (○). The curves represent the best fit of these data to Eq. 2-4 as described in the text. The vertical lines correspond to the point at which PEP begins binding and influencing the binding of the substrate Fru-6-P for wild-type ( ) and the D12A/K90E/K91E (----) proteins. Error bars represent ± the standard error and are smaller than the symbol when not evident.

Fru-6-P at increasing concentrations of the inhibitor PEP. Not surprisingly, the individual Fru-6-P saturation profiles adhered to almost every expectation. The $K_{1/2}$ for Fru-6-P at the native active site in the absence of PEP is identical to wild-type for both interactions and at all five pH values except for some minor changes at pH 8.0 that is most likely due to the ionization of a His residue near the active site binding pocket. As for the mutated active sites, the $K_{1/2}$ for Fru-6-P is equivalent to the $K_{1/2}$ for Fru-6-P determined for their active site mutant counterparts. The V_{max} and V'_{max} values also obtained from the individual Fru-6-P saturation profiles followed expectations by equaling 25% and 75% of wild-type activity respectively.

In plotting the apparent $K_{1/2}$ for Fru-6-P against increasing concentrations of PEP, two phases are observed for both the 30 Å interaction and the 32 Å interaction, with the first phase containing the desired information regarding the interaction between the two native binding sites. The second phase, on the other hand, corresponds to the influence upon Fru-6-P affinity from the three mutated allosteric sites (see (●) data in Fig. 3-17). This second phase is easily corrected for by obtaining the analogous data with a control hybrid that contains only one native active site, three mutated active sites and four mutated allosteric sites (1|0 hybrid). The 1|1 data is then corrected for by using Eq. 3-1, and the resulting data corresponds to the influence of a particular allosteric site upon a particular active site and *vice versa*.

The individual couplings (Q_{ay}) obtained for the 30 Å and 32 Å interactions are quite different from one another. Interestingly, the 30 Å

interaction is "allosterically silent" at pH 6.0 and 6.5, meaning that PEP binding has no inhibitory effect upon the binding of Fru-6-P at that particular active site or *vice versa*. It is not until pH 7.0 that an allosteric effect is observed. As for the 32 Å interaction, an allosteric effect is measured at pH 6.0, however, it also does not change until pH 7.0. Both interactions from pH 7.0 and above behave like the wild-type enzyme in that with increasing pH, PEP became a better inhibitor for both interactions (Tlapak-Simmons and Reinhart, 1998).

Of the two interactions studied, the 32 Å interaction contributes more to the allosteric response (inhibition) as its coupling free energy (ΔG_{ay}) is 0.34 ± 0.10 kcal/mol at pH 6.0 and increases to a value of 0.82 ± 0.12 kcal/mol at pH 8.0. Whereas, the 30 Å interaction has a smaller yet significant role as it begins at a coupling free energy of 0.00 ± 0.06 and increases to a value of 0.49 ± 0.11 kcal/mol. Unexpectedly, both interactions have an almost identical overall net change in coupling free energy over the pH range examined ($\Delta\Delta G_{pH}$ ~ 0.6 kcal/mol) indicating that pH affects the two interactions equally, possibly suggesting that they share some of the same "communication pathway" within the protein.

Comparing the values for the 30 Å and 32 Å interactions to the values predicted for the concerted and sequential models, several conclusions can be made. First, the concerted model is incompatible with our data because the couplings of the 30 Å and 32 Å interactions are different at all the pH values investigated. Secondly, the sequential model is not in agreement with our data either at pH 7.0 and above because the two interactions are unique in their

relative magnitudes and are always greater than zero. However, the sequential model does hold true at pH 6.0 and 6.5 because the coupling for the 30 Å interaction is zero at those pH values. Nevertheless, the third model, the "conformational free/linkage" model described in the introduction, is consistent with the data at all pH values because the couplings are unique in magnitude regardless of the pH. However, we cannot dismiss the fact that we have introduced mutations throughout the enzyme in order to isolate each interaction, and that the mutations may be the cause of the variability in the couplings measured for the two interactions. This possibility will be addressed in the following chapter when we show how the entire allosteric effect incurred by PEP is accounted for in the native enzyme (in the absence of PEP cooperativity) by using the couplings determined here and those determined for the 22 Å and 45 Å heterotropic interactions as well.

CHAPTER IV

COMPARING THE RELATIVE ALLOSTERIC CONTRIBUTIONS OF THE FOUR UNIQUE HETEROTROPIC INTERACTIONS FOUND WITHIN PHOSPHOFRUCTOKINASE FROM *Bacillus stearothermophilus* TO THE NATIVE HOMOTETRAMER

Introduction

The basis for allosteric communication within oligomeric proteins for the most part remains an enigma. In part this is due to the inherent complications associated with the multiplicity of ligand binding sites usually present in an oligomer. Even in the simplest homotetramer containing a single active site and single allosteric site per subunit, no fewer than four possible heterotropic interactions, and six possible homotropic interactions exist by which the binding of one ligand can influence the binding of another. To illustrate the point, one might consider the question, how does the binding of an allosteric ligand at each of the four allosteric sites influence the binding of the substrate at a single active site? The popular simplifying models of allosterism, namely the concerted model of Monod, et al. (1965) and the sequential model described by Koshland, et al. (1966), provide answers to this question that represent opposite extremes (Fig. 4-1).

As discussed in Chapter III, the concerted model suggests that the initial binding of one equivalent of an allosteric inhibitor to any of the four allosteric

---

Portions of this text comprise an article that has been submitted for publication by A. Ortigosa, J. Kimmel and G. Reinhart.

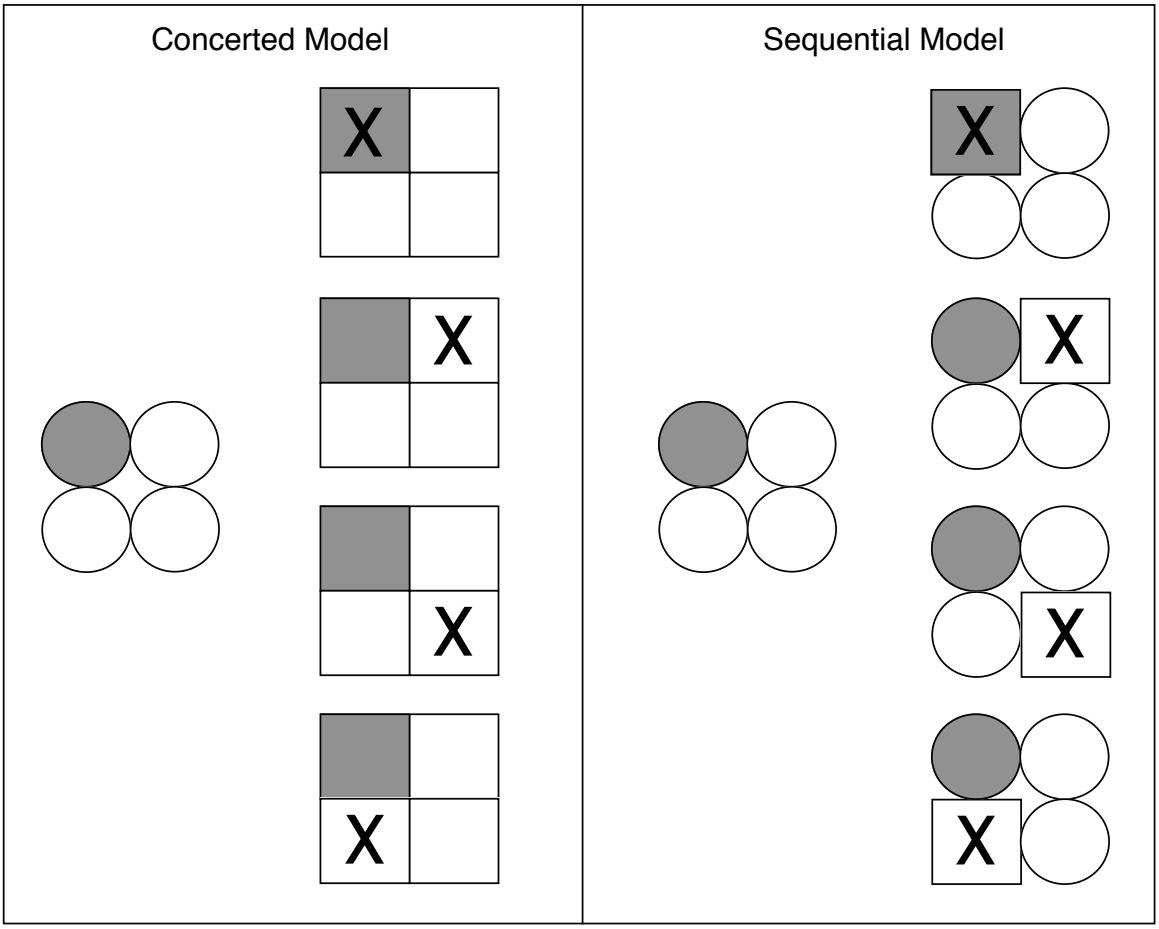

FIGURE 4-1 Contrasting predictions of the concerted and sequential models regarding the influence of the binding of a single allosteric ligand to the binding of substrate at a single active site associated with the shaded subunit. In the concerted model, binding of the allosteric ligand, X, to any site influences the binding to the active site to the same degree as commonly denoted by the change in shape from circle to square. In the sequential model, binding to only one site influences the binding of substrate at the shaded site.

sites will influence a particular active site to the same degree. The sequential model, on the other hand, suggests that the occupancy of only one of the four allosteric sites will perturb the binding of a particular active site, whereas binding to the remaining sites would have no effect. Reality, of course, may lie somewhere in between these two extremes, with the binding of an allosteric ligand to each site exerting a unique and varying influence on the binding to a particular active site. Such a circumstance would suggest that multiple allosteric routes of communications might exist.

To address this question of how enzymes are allosterically regulated, we have chosen to study phosphofructokinase from *Bacillus stearothermophilus* (BsPFK). BsPFK is a homotetramer containing on average, one active site and one allosteric site per subunit, and a schematic of how the four individual subunits and their binding sites are organized is shown in Fig. 4-2. Besides elucidating the subunit organization found within BsPFK, Fig. 4-2 also emphasizes the positively charged residues that line each of the ligand binding sites as well as the nomenclature used in identifying the individual "sides" of the active sites and allosteric sites (Schirmer and Evans, 1990). Moreover, since BsPFK contains four active sites and four allosteric sites, 16 possible heterotropic interactions exist with four of those interactions being unique. We have identified the 16 allosteric interactions in Fig. 4-2 as well as the four unique allosteric interactions, which we have designated as the 22 Å, 30 Å, 32 Å or 45 Å heterotropic interactions.

In order to determine if each heterotropic interaction plays a unique role

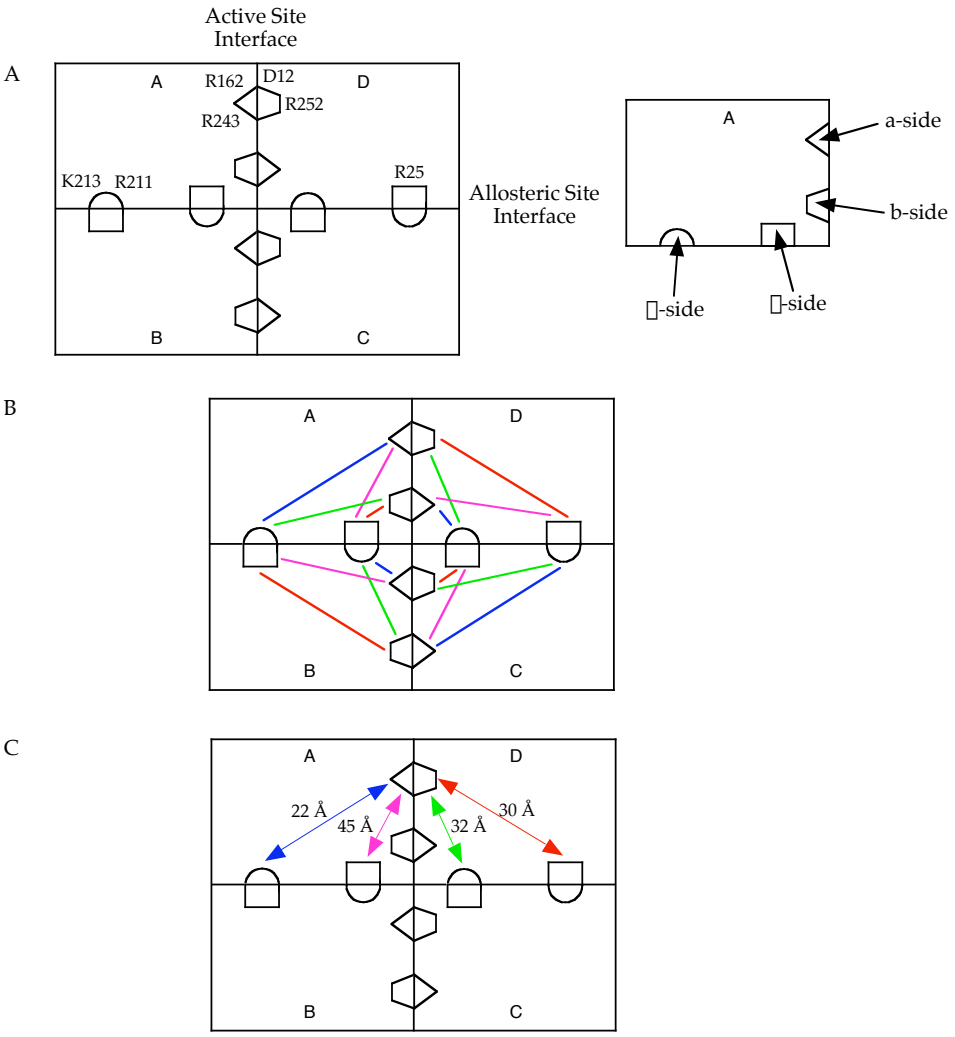

FIGURE 4-2 The subunit and binding site organization of BsPFK and the heterotropic interactions possible between the eight binding sites. (*A*) The active sites are located along one dimer-dimer interface while the allosteric sites are located along the other. Moreover, the "sides" of the binding sites have been designated as either the a-side or b-side for the active sites or the β-side or β-side for the allosteric sites. (*B*) Sixteen total pair-wise heterotropic interactions are possible between the four active sites and four allosteric sites. (*C*) Of the 16 interactions, four are unique and have been designated as the 22 Å (blue), 30 Å (red), 32 Å (green) and 45 Å (magenta) interactions. These designations correspond to the measured distances between the phosphorous atom of the Fru-6-P molecule bound in the active site to the terminal β-phosphorous atom of the ADP molecule bound in each of the four allosteric sites (Schirmer and Evans, 1990).

in the observed allosteric behavior found in the native tetramer, we needed a method for isolating each of the four heterotropic interactions so that we could quantify the allosteric effect associated with each interaction. To accomplish this we created heterotetramers of BsPFK to contain only one native active site and one native allosteric site, thus eliminating 15 of the 16 total heterotropic interactions and permitting characterization. Furthermore, by simply manipulating the particular native active site and native allosteric site that remain within a given heterotetramer, all four heterotropic interactions can be successfully isolated and characterized.

This chapter summarizes our efforts to measure the four potentially unique heterotropic allosteric interactions that exist in BsPFK, and our results suggest, perhaps not surprisingly, that neither the concerted nor the sequential models properly describe the network of allosteric communication in this enzyme. Rather, the occupancy of each allosteric site by the inhibitor introduces a unique effect on the binding of the substrate to a particular active site.

Materials and methods

The materials and methods used for the experiments described in this chapter are the same as described in Chapter II. Site-directed mutagenesis, protein purification, hybrid formation via monomer exchange and their subsequent isolation, enzymatic activity measurements at varying pH, and data analysis were performed as described in Chapter II. Preparation, isolation and data analysis pertaining to the 22 Å interaction at pH 7.0 and 8.0 and the 45 Å

interaction utilizing the R162E active site mutation at pH 6.0, 7.0 and 8.0 were performed by Kimmel (2001).

Data analysis. As mentioned in Chapter II, Q_{ay} is determined by measuring the $K_{1/2}$ for Fru-6-P at increasing concentrations of PEP and the subsequent data fit to Eq. 2-4. In order to make things easier, Eq. 2-4 has been repeated here:

$$K_{1/2} = K^{o}_{ia}\left[\frac{K^{o}_{iy} + [Y]}{K^{o}_{iy} + Q_{ay}[Y]}\right] \qquad (4\text{-}1)$$

Data pertaining to both the native tetramer and the 1:3 hybrids (1|1) have been fit with Eq. 4-1, and for either case, the single substrate, single modifier model sufficiently fits the data (Tlapak-Simmons and Reinhart, 1994, 1998; Johnson and Reinhart, 1994, 1997; Kimmel and Reinhart, 2001; Fenton and Reinhart, 2002). The legitimacy however in using Eq. 4-1 becomes questionable when the number of native active sites is not equivalent to the number of native allosteric sites. This situation arises later in the chapter when a wild-type control hybrid is constructed to address the effects of the homotropic interactions between the allosteric sites upon the observed allosteric effect in the native tetramer.

For the wild-type control hybrid (4|1), three of the allosteric sites have been mutated, eliminating the four-fold redundancy found in the native tetramer and abolishing the homotropic interactions between the allosteric sites. In order to address this discrepancy in the number of binding sites and its subsequent effect upon Q_{ay}, we can consider an analogous situation occurring in a symmetrical dimer containing two native active sites and one native allosteric

site which can be derived from the two active sites and two allosteric sites case considered by Reinhart (1988) (Weber 1972 and 1975). In this case, Eq. 4-1 becomes the following:

$$K_{1/2} = K_{ia}^{o}\left(\frac{K_{iy}^{o} + [Y]}{K_{iy}^{o} + Q_{ay}^{2}[Y]}\right)^{1/2} \qquad (4\text{-}2)$$

The apparent coupling for the dimer, Q_{app}, can then be estimated when considering the two concentration extremes for Y, zero and infinity:

$$Q_{app} = \frac{\lim_{Y \to 0} K_{1/2}}{\lim_{Y \to \infty} K_{1/2}} \qquad (4\text{-}3)$$

substituting Eq. 4-2 into Eq. 4-3 yields:

$$Q_{app} = \frac{K_{ia}^{o}}{K_{ia}^{o}\left(\frac{1}{Q_{ay}^{2}}\right)^{1/2}} \qquad (4\text{-}4)$$

which in turn implies:

$$Q_{app} = Q_{ay} \qquad (4\text{-}5)$$

Using Eq. 2-6 to convert the couplings into free energy terms, Eq. 4-5 becomes:

$$\Delta G_{app} = \Delta G_{ay} \qquad (4\text{-}6)$$

Thus, the measured coupling is equal to an average of the two heterotropic couplings that exist in the dimer in the absence of homotropic effects between the allosteric sites. Applying this result to our symmetrical tetramer, we would then assume the same phenomenon would occur leading to the measured coupling in the wild-type control hybrid (4|1) equaling an average of the four heterotropic couplings that exist in the tetramer. Thus, for the coupling free

energy determined for the wild-type control hybrid to be equivalent to the coupling free energy determined for the native tetramer in the absence of homotropic effects between the allosteric sites, the coupling free energy for the wild-type control hybrid needs to be multiplied by 4.

$$\Delta G_{tetramer} = 4 \cdot \Delta G_{(4I1)hybrid} \qquad (4\text{-}7)$$

Results

Isolation of the four heterotropic interactions via their respective 1:3 hybrids. As was previously shown by Kimmel and Reinhart (2001) and in Chapter III, the positively charged residues that make-up either the a-side or the b-side of the active site or the □-side or □-side of the allosteric site can be successfully mutated to discourage Fru-6-P and PEP binding by more than two orders of magnitude as compared to wild-type. Furthermore, by simply manipulating the "sides" of the active sites and allosteric sites that are mutated, four mutant proteins result which have been designated as the [a,□], [a,□], [b,□] and [b,□] mutants proteins where the first letter refers to the "side" of the active that is mutated while the second letter refers to the "side" of the allosteric site that is mutated. Table 4-1 summarizes the active site and allosteric site mutations that are used in this investigation to create the four mutant proteins and the heterotropic interaction that is isolated in the 1:3 hybrid (hybridization with the wild-type enzyme). The four different 1:3 hybrids are shown schematically in Fig. 4-3 indicating the "sides" of the binding sites that are mutated, and the heterotropic interaction that is isolated.

TABLE 4-1 List of the active site and allosteric site mutations used in the isolation of the four individual allosteric heterotropic interactions

Mutant Protein[a]	Active Site Mutation (a or b-side)	Allosteric Site Mutation (□ or □-side)	Heterotropic Interaction Isolated via the 1∣1 Hybrid
[a,□]	R162E (a)	R211E/K213E (□)	22 Å
[b,□]	R252A/D12A (b)	R25E (□)	30 Å
[b,□]	R252A/D12A (b)	R211E/K213E (□)	32 Å
[a,□]	R162E or R243E (a)	R25E (□)	45 Å

[a]All four mutant proteins also contain the K90E/K91E charge tag on the surface of the protein to permit isolation of the 1:3 hybrid from the other hybrid species.

FIGURE 4-3 The two-dimensional schematics of the four possible 1:3 hybrids highlighting the binding site mutations used to isolate each of the four heterotropic interactions. (*A*) The 1:3 hybrid (1 wild-type subunit: 3 [a,□] mutant subunits) that isolates the 22 Å heterotropic interaction. The R162E mutation was used in the active site, and the R211E/K213E mutations were used in the allosteric site. (*B*) The 1:3 hybrid (1 wild-type subunit: 3 [b,□] mutant subunits) that isolates the 30 Å heterotropic interaction. The R252A/D12A mutations were used in the active site, and the R25E mutation was used in the allosteric site. (*C*) The 1:3 hybrid (1 wild-type subunit: 3 [b,□] mutant subunits) that isolates the 32 Å heterotropic interaction. The R252A/D12A mutations were used in the active site, and the R211E/K213E mutations were used in the allosteric site. (*D*) The 1:3 hybrid (1 wild-type subunit: 3 [a,□] mutant subunits) that isolates the 45 Å heterotropic interaction. Either the R162E mutation or the R243E mutation was used in the active site, and the R25E mutation was used in the allosteric site.

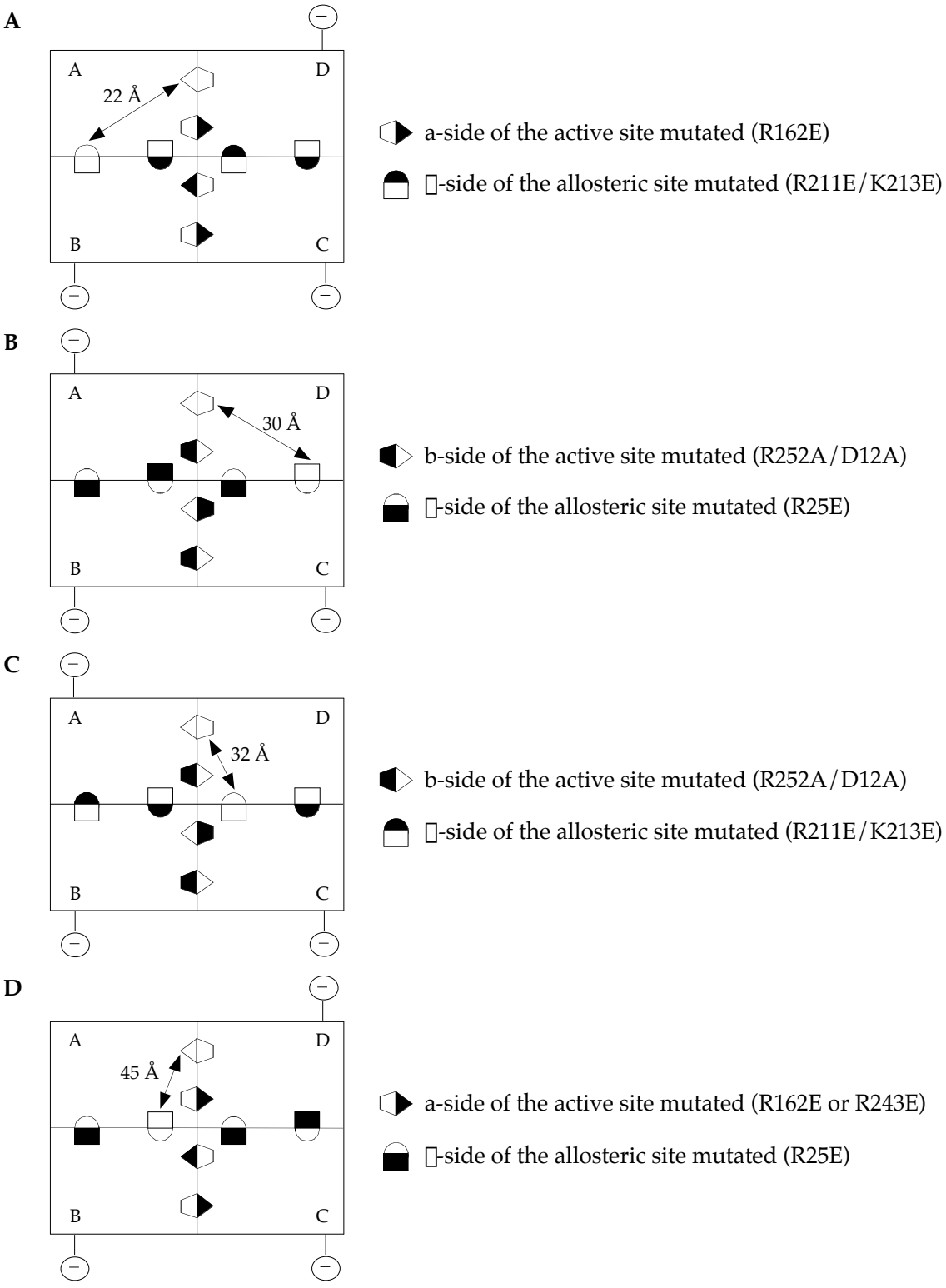
A
A
D
22 Å
B
C
a-side of the active site mutated (R162E)
β-side of the allosteric site mutated (R211E/K213E)
B
A
D
30 Å
B
C
b-side of the active site mutated (R252A/D12A)
β-side of the allosteric site mutated (R25E)
C
A
D
32 Å
B
C
b-side of the active site mutated (R252A/D12A)
β-side of the allosteric site mutated (R211E/K213E)
D
A
D
45 Å
B
C
a-side of the active site mutated (R162E or R243E)
β-side of the allosteric site mutated (R25E)

A unique case arose when investigating the allosteric properties of the 45 Å heterotropic interaction requiring an additional [a,□] mutant protein to be constructed. Instead of using the R162E mutation, R243E was used as the a-side active site mutation. R243 is adjacent to R162 and is seen in the crystal structure within hydrogen bonding distance of the bound Fru-6-P molecule at the active site (Schirmer and Evans, 1990). Characterization of the R243E active site mutation alone yielded results similar to its R162E counterpart (Kimmel, unpublished), in that it diminished Fru-6-P binding by more than two orders of magnitude compared to wild-type. A summary of the R243E steady-state kinetic data along with the data for the other active site and allosteric site mutations utilized for this investigation are found in Table 4-2.

In addition to the active site and allosteric site mutations necessary to isolate a particular interaction, a surface charge tag mutation (K90E/K91E) has also been added to the mutant subunits to facilitate separation of the 1:3 hybrid from the other six enzyme species. The charge tag is designated schematically in Fig. 4-3 as the "lolli-pop" structure on the surface of the mutant subunits. Moreover, it was also previously shown that the K90E/K91E mutations have no adverse affects upon the kinetic or allosteric properties of BsPFK and the mutations solely provide a charge differential amongst the different hybrid species to permit separation of the various enzyme species (Kimmel and Reinhart, 2001).

TABLE 4-2 Steady-state kinetic and thermodynamic coupling parameters for the wild-type, the active site mutants and the allosteric site mutants at 25°C and pH 7.0 with [MgATP] = 3 mM

Enzyme	V_{max} (Units/mg)[a]	$K_{1/2}$ (mM)[a]	n_H[a]	K^o_{iy} (mM)[b]	Q_{ay}[b]
wild-type	125 ± 2	0.021 ± 0.001	1.30 ± 0.09	0.023 ± 0.002	0.0085 ± 0.0004
R252A/D12A	122 ± 3	5.0 ± 0.3	1.17 ± 0.05	ND	ND
R162E[c]	146 ± 6	21.2 ± 1.9	1.15 ± 0.06	ND	ND
R243E[c,d]	132 ± 4	7.3 ± 0.8	0.90 ± 0.06	ND	ND
R25E	91 ± 1	0.047 ± 0.002	1.27 ± 0.05	~100	UD
R211E/K213E[c]	109 ± 1	0.058 ± 0.001	1.12 ± 0.08	~20	UD

ND = Not Determined

UD = Undetermined

[a]Pertaining to Fru-6-P saturation profiles at 0 mM PEP. Parameters determined from fitting data to Eq. 2-1.

[b]Parameters obtained by fitting to Eq. 2-4.

[c]Experiment performed under identical conditions except at pH 8.0 and utilizing EPPS buffer instead of MOPS buffer (Kimmel and Reinhart 2001).

[d]Parameters determined by Kimmel (unpublished).

Each of the four possible 1:3 hybrids shown in Fig. 4-3 were constructed and isolated in the same manner as described in Chapter II and Chapter III, utilizing the method that was originally designed for the isolation of the 22 Å interaction (Kimmel and Reinhart, 2001). All five of the isolated 1:3 hybrids (two 1:3 hybrids for isolating the 45 Å interaction) were stored at 4°C and no re-hybridization between subunits was observed for at least four weeks as confirmed by native PAGE analysis (data not shown).

Isolation of the control hybrids (1|0). As was discussed in Chapter III for the 1:3 hybrids that isolate the 30 Å and 32 Å interactions, control hybrids are necessary to correct for the influence PEP binding at the three mutated allosteric site has upon the measured allosteric effect at the lone native active site. Although the effect is minimal, it was previously shown by Kimmel and Reinhart (2001) and in Chapter III, that this correction is not only necessary, but also significant. Each control hybrid consists of one native active site, three mutated active sites and four mutated allosteric sites (1|0), and were constructed just like the 1:3 hybrids, except the appropriate allosteric site mutant was substituted for the wild-type parental protein. For the [a,□] and [b,□] mutant proteins, the R211E/K213E allosteric site mutant protein was used, whereas for the [a,□] and [b,□] mutant proteins, the R25E allosteric site mutant was used. The four different control hybrids are shown schematically in Fig. 4-4 (two control hybrids for the 45 Å interaction). All five of the isolated control hybrids were stored at 4°C and no re-hybridization between the subunits was observed for at least 4 weeks as confirmed by native PAGE analysis (data not

FIGURE 4-4 The two-dimensional schematics of the four control hybrids (1|0) constructed in order to correct for the allosteric effect incurred upon the native active site by PEP binding to the mutated allosteric sites. In all four cases, the wild-type subunit is replaced with the corresponding allosteric site mutant protein resulting in only one native active site and no native allosteric sites. (*A*) The 1:3 control hybrid (1 R211E/K213E subunit: 3 [a,□] mutant subunits) for correcting the data pertaining to the 22 Å interaction. (*B*) The 1:3 control hybrid (1 R25E subunit: 3 [b,□] mutant subunits) for correcting the data pertaining to the 30 Å interaction. (*C*) The 1:3 control hybrid (1 R211E/K213E subunit: 3 [b,□] mutant subunits) for correcting the data pertaining to the 32 Å interaction. (*D*) The 1:3 control hybrid (1 R25E subunit: 3 [a,□] mutant subunits – using either the R162E or R423E mutation in the active site) for correcting the data pertaining to the 45 Å interaction.

A

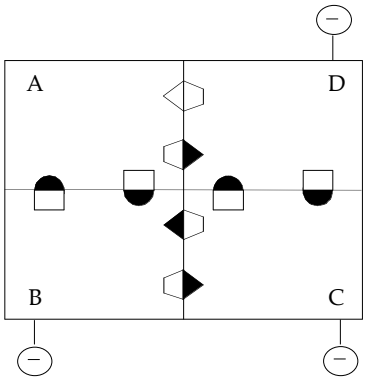

a-side of the active site mutated (R162E)

□-side of the allosteric site mutated (R211E/K213E)

B

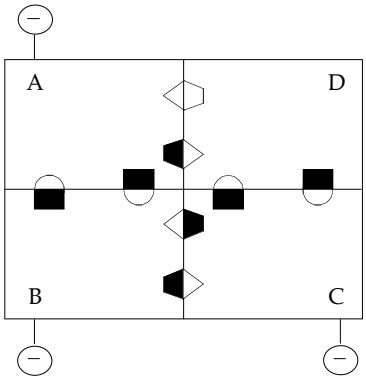

b-side of the active site mutated (R252A/D12A)

□-side of the allosteric site mutated (R25E)

C

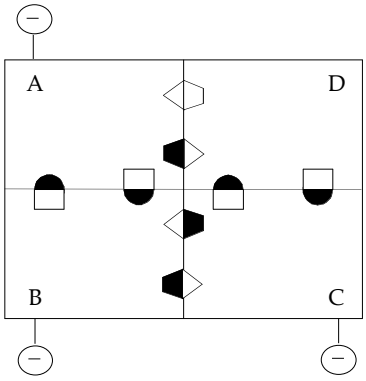

b-side of the active site mutated (R252A/D12A)

□-side of the allosteric site mutated (R211E/K213E)

D

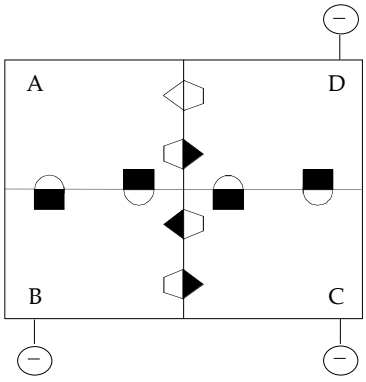

a-side of the active site mutated (R162E or R243E)

□-side of the allosteric site mutated (R25E)

shown).

Functional properties of the five 1:3 hybrid (1|1) enzymes in the absence of PEP. The dependence of enzyme activity as a function of Fru-6-P concentration was determined for the wild-type enzyme, as well as the five 1:3 hybrids at pH 6.0, 7.0 and 8.0. The Fru-6-P saturation profiles for each of the 1:3 hybrids exhibited the saturation of two different types of binding sites, corresponding to the high affinity and low affinity active sites respectively as shown in Chapter III for the 30 Å and 32 Å interactions. Data obtained from the Fru-6-P saturation profiles for the wild-type enzyme were fit to Eq. 2-1 (Hill equation), whereas the data for the 1:3 hybrids were fit to Eq. 2-2, in which two Michaelis-Menten equations are summed together.

Table 4-3 summarizes the kinetic parameters obtained from these fits for wild-type enzyme and both the high affinity (native) and low affinity (mutated) Fru-6-P binding sites found in the five 1:3 hybrids. All four parameters calculated for the five hybrids (V_{max}, $K_{1/2}$ for Fru-6-P, V'_{max} and $K'_{1/2}$ for Fru-6-P) agree primarily with one another, and more importantly, conform to expected results. At all pH values, the maximal specific activity for the high affinity interaction (V_{max}) for all five 1:3 hybrids is approximately one-fourth that of wild-type. Moreover, the maximal specific activity for each of the 1:3 hybrids increases with an increase in pH, a behavior consistent with the wild-type enzyme (Tlapak-Simmons and Reinhart, 1998). The values obtained for the $K_{1/2}$ for Fru-6-P agree, within error, with the $K_{1/2}$ values for the wild-type enzyme with the exception of the 32 Å interaction at pH 8.0.

TABLE 4-3 Steady-state kinetic parameters for wild-type BsPFK and the four 1:3 hybrids containing the four individual allosteric interactions within BsPFK at 25°C, pH 6.0, 7.0 and 8.0, [MgATP] = 3 mM and [PEP] = 0 mM

Enzyme	V_{max} (Units/mg) high affinity	$K_{1/2}$ (mM) high affinity	V'_{max} (Units/mg) low affinity	$K'_{1/2}$ (mM) low affinity
pH 6.0				
wild-type	67.1 ± 1.1	0.032 ± 0.001	n/a	n/a
22 Å interaction	22.5 ± 0.5	0.028 ± 0.002	85 ± 1	3.6 ± 0.1
30 Å interaction	15.4 ± 0.4	0.035 ± 0.003	36 ± 1	8.0 ± 0.3
32 Å interaction	14.5 ± 0.5	0.031 ± 0.003	46 ± 2	10.0 ± 0.8
45 Å interaction (R162E)	19.4 ± 1.1	0.039 ± 0.007	85 ± 1	6.2 ± 0.3
45 Å interaction (R243E)	17.6 ± 0.8	0.028 ± 0.004	50 ± 1	5.7 ± 0.5
pH 7.0				
wild-type	125 ± 2	0.021 ± 0.001	n/a	n/a
22 Å interaction	28.0 ± 1.0	0.029 ± 0.004	113 ± 2	8.6 ± 0.5
30 Å interaction	26.7 ± 0.7	0.020 ± 0.002	96 ± 3	12.1 ± 0.7
32 Å interaction	30.9 ± 1.1	0.047 ± 0.005	94 ± 3	9.6 ± 0.5
45 Å interaction (R162E)	29.2 ± 0.8	0.024 ± 0.002	114 ± 1	9.3 ± 0.4
45 Å interaction (R243E)	28.0 ± 1.3	0.017 ± 0.003	95 ± 2	6.3 ± 0.5
pH 8.0				
wild-type	153 ± 3	0.034 ± 0.001	n/a	n/a
22 Å interaction	36 ± 1	0.034 ± 0.004	90 ± 3	25 ± 2
30 Å interaction	37 ± 2	0.079 ± 0.008	UD	UD
32 Å interaction	38 ± 2	0.310 ± 0.035	UD	UD
45 Å interaction (R162E)	39 ± 1	0.038 ± 0.003	123 ±10	42 ± 6
45 Å interaction (R243E)	39 ± 2	0.024 ± 0.004	117 ± 3	8.3 ± 0.9

As for the low affinity active sites, the maximal specific activities (V'_{max}) are approximately three-fourths the V_{max} value obtained for the mutant tetramer, which is comparable to three-fourths the V_{max} value obtained for the wild-type enzyme. Furthermore, the values obtained for the $K'_{1/2}$ for Fru-6-P are comparable to the measured $K_{1/2}$ for Fru-6-P values for their respective active site mutant enzymes alone.

Measuring the allosteric effect for each of the heterotropic interactions. In order to measure the allosteric effect for each of the four heterotropic interactions, the $K_{1/2}$ for Fru-6-P was determined as a function of increasing PEP concentration for each of the five 1:3 hybrids and their corresponding control hybrids at pH 6, 7 and 8. Fru-6-P titrations at pH 6.0, 7.0 and 8.0 were performed for each 1:3 hybrid and its corresponding control hybrid at increasing concentrations of PEP. In all cases, the measured coupling for each 1:3 hybrid was corrected for by using the following equation:

$$K_{1/2}(\text{corrected}) = \frac{K_{1/2}(1|1)}{K_{1/2}(1|0)} \qquad (4\text{-}8)$$

Figure 4-5 shows the corrected values for the $K_{1/2}$ for Fru-6-P plotted as a function of PEP concentration at the three pH values investigated. With the exception of the 30 Å interaction at pH 6.0 and the 45 Å interaction at all pH values, the high affinity binding site of each of the 1:3 hybrids was found to behave like the wild-type enzyme in that the addition of PEP increased the $K_{1/2}$ for Fru-6-P in a saturable manner.

FIGURE 4-5 The dependence of the corrected apparent $K_{1/2}$ for Fru-6-P on increasing concentrations of the inhibitor PEP for the 22 Å interaction (●), the 30 Å interaction (■), the 32 Å interaction (○) and the 45 Å interaction (□). The data shown for the 45 Å interaction is from using the R243E active site mutation. The data obtained at pH 6.0 were performed in buffer containing 50 mM MES-KOH, the data for pH 7.0 were performed in buffer containing 50 mM MOPS-KOH, and the data for pH 8.0 were obtained using buffer containing 50 mM EPPS-KOH. All the curves correspond to the best fit of these data to Eq. 2-4 as described in the text. (*A*) Data corresponding to pH 6.0. (*B*) Data corresponding to pH 7.0. (*C*) Data corresponding to pH 8.0.

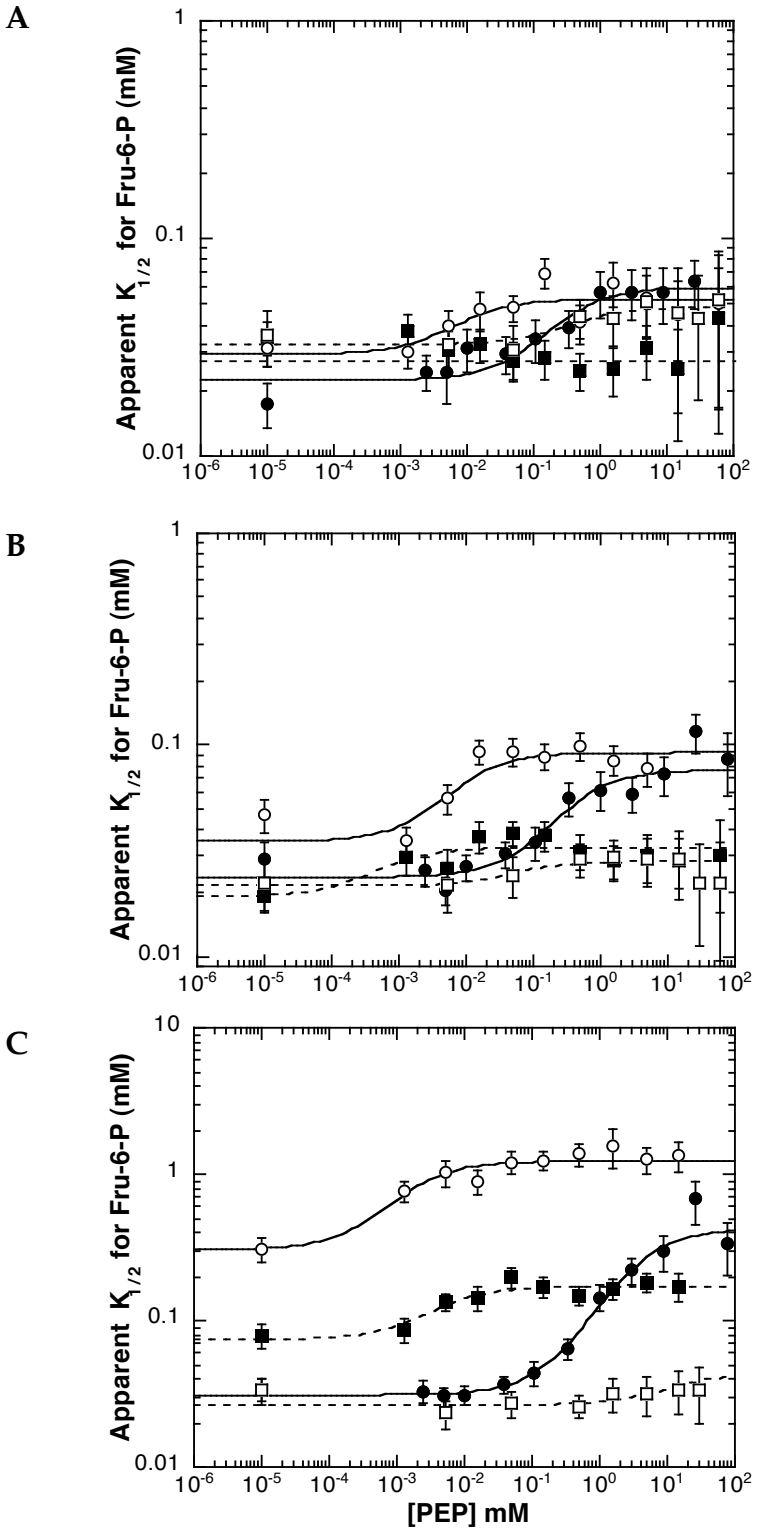
A
B
C
Apparent $K_{1/2}$ for Fru-6-P (mM)
1
0.1
0.01
10^{-6} 10^{-5} 10^{-4} 10^{-3} 10^{-2} 10^{-1} 10^{0} 10^{1} 10^{2}
10
[PEP] mM

A summary of the thermodynamic parameters obtained from fitting these data to Eq. 2-4 is found in Table 4-4. The measured coupling, Q_{ay}, for each of the 1:3 hybrids was reduced to different extents (one even becoming allosterically "silent") relative to the wild-type enzyme. Moreover, all the heterotropic interactions, with the exception of the 45Å interaction, display an increase in coupling with an increase in pH, a phenomenon consistent with the wild-type enzyme (Tlapak-Simmons and Reinhart, 1998).

Using Eq. 2-6 to convert the calculated Q_{ay} to ΔG_{ay}, it was found that the 22 Å heterotropic interaction dominated the allosteric effect incurred by the binding of PEP at all three pH values. The 22 Å interaction contributes 22 ± 5%, 23 ± 4% and 41 ± 4% to the overall coupling free energy determined for the wild-type tetramer at pH 6.0, 7.0 and 8.0 respectively. The 32 Å interaction also contributes significantly at all pH values with 18 ± 5%, 20 ± 4% and 23 ± 3% at pH 6.0, 7.0 and 8.0. Interestingly, the 30 Å interaction is the only interaction that becomes allosterically "silent" at pH 6, meaning that the binding of PEP has no effect upon the binding of Fru-6-P or *vice versa*. However, at pH 7.0 and pH 8.0 the 30 Å interaction contributes 11 ± 4% and 14 ± 3% respectively to the overall observed coupling free energy determined for the wild-type tetramer. As for the 45 Å heterotropic interaction, it was initially measured to have a coupling free energy of 0 kcal/mol at all the pH values examined using the R162E active site mutation. To confirm this phenomenon, a second [a,□] mutant protein was constructed where the active site mutation, R162E, was replaced with the R243E mutation. Upon implementing the mutation in making the 1:3 hybrids (both the

TABLE 4-4 Thermodynamic parameters for wild-type and the four individual allosteric interactions (control subtracted) at 25°C, pH 6.0, 7.0 and 8.0 and [MgATP] = 3 mM

Enzyme	K^{o}_{ia} (mM)	K^{o}_{iy} (mM)	Q_{ay}	ΔG_{ay} (kcal/mol)	% of WT
pH 6.0					
WT	0.032 ± 0.001	0.026 ± 0.002	0.041 ± 0.002	1.89 ± 0.03	-
22 Å	0.026 ± 0.002	0.091 ± 0.086	0.50 ± 0.08	0.41 ± 0.10	22 ± 5
30 Å	0.030 ± 0.002	UD	1.00 ± 0.10	0.00 ± 0.06	0
32 Å	0.029 ± 0.005	0.0045 ± 0.0061	0.56 ± 0.10	0.34 ± 0.10	18 ± 5
45 Å (R162E)	0.037 ± 0.004	UD	1.00 ± 0.15	0.00 ± 0.09	0
45 Å (R243E)	0.033 ± 0.006	0.27 ± 0.08	0.68 ± 0.18	0.23 ± 0.14	12 ± 8
pH 7.0					
WT	0.030 ± 0.002	0.023 ± 0.002	0.0085 ± 0.0004	2.82 ± 0.03	-
22 Å	0.023 ± 0.002	0.079 ± 0.047	0.33 ± 0.05	0.66 ± 0.10	23 ± 4
30 Å	0.019 ± 0.004	0.0003 ± 0.0007	0.59 ± 0.11	0.31 ± 0.11	11 ± 4
32 Å	0.035 ± 0.006	0.003 ± 0.002	0.38 ± 0.07	0.57 ± 0.10	20 ± 4
45 Å (R162E)	0.024 ± 0.001	UD	1.00 ± 0.06	0.00 ± 0.03	0
45 Å (R243E)	0.022 ± 0.005	0.04 ± 0.02	0.77 ± 0.18	0.18 ± 0.14	6 ± 5
pH 8.0					
WT	0.027 ± 0.001	0.039 ± 0.001	0.0020 ± 0.0001	3.58 ± 0.02	-
22 Å	0.031 ± 0.002	0.22 ± 0.07	0.08 ± 0.02	1.48 ± 0.15	41 ± 4
30 Å	0.074 ± 0.014	0.002 ± 0.001	0.44 ± 0.08	0.49 ± 0.11	14 ± 3
32 Å	0.31 ± 0.06	0.0004 ± 0.0003	0.25 ± 0.05	0.82 ± 0.12	23 ± 3
45 Å (R162E)	0.038 ± 0.001	UD	1.00 ± 0.04	0.00 ± 0.02	0
45 Å (R243E)	0.026 ± 0.003	2.0 ± 0.9	0.78 ± 0.24	0.17 ± 0.20	5 ± 5

1|1 hybrid and the 1|0 hybrid), and performing the characterization, a minimal amount of a coupling free energy was measured for the 45Å interaction at pH 6.0, 7.0 and 8.0 contributing 12 ± 8%, 6 ± 5% and 5 ± 5% to the overall allosteric effect measured for the tetramer.

Why this discrepancy occurred in analyzing the two different [a,□] mutant constructs that isolate the 45 Å interaction is not entirely known, but we speculate it could be due to the manner by which the data for the 1:3 hybrid (1|1) using the R162E mutant were corrected. Due to time constraints, the control hybrid was only analyzed at pH 8.0; consequently, all the data for the 1:3 hybrid (1|1) at pH 6.0, 7.0 and 8.0 were corrected with only the pH 8.0 control data (Kimmel, 2001). This differs significantly from the way the other three interactions and the alternative way to isolate the 45 Å interaction (using R243E) were characterized. In those cases, each 1:3 hybrid and its corresponding control hybrid were individually analyzed at each pH with the same experimental conditions to ensure the correction was as accurate as possible. Figure 4-6 shows the variance in the control hybrid data that isolates the 45 Å interaction using the R243E mutation at pH 6.0, 7.0 and 8.0. Although there is not a major difference between the three pH values, there is some variance between the three data sets validating the necessity to perform the control hybrid experiments using the identical conditions that were used for the 1:3 hybrid, especially when a minimal amount of coupling may be present.

When summing together all of the coupling free energies for the four heterotropic interactions at pH 6.0, 7.0 and 8.0, the entire allosteric effect

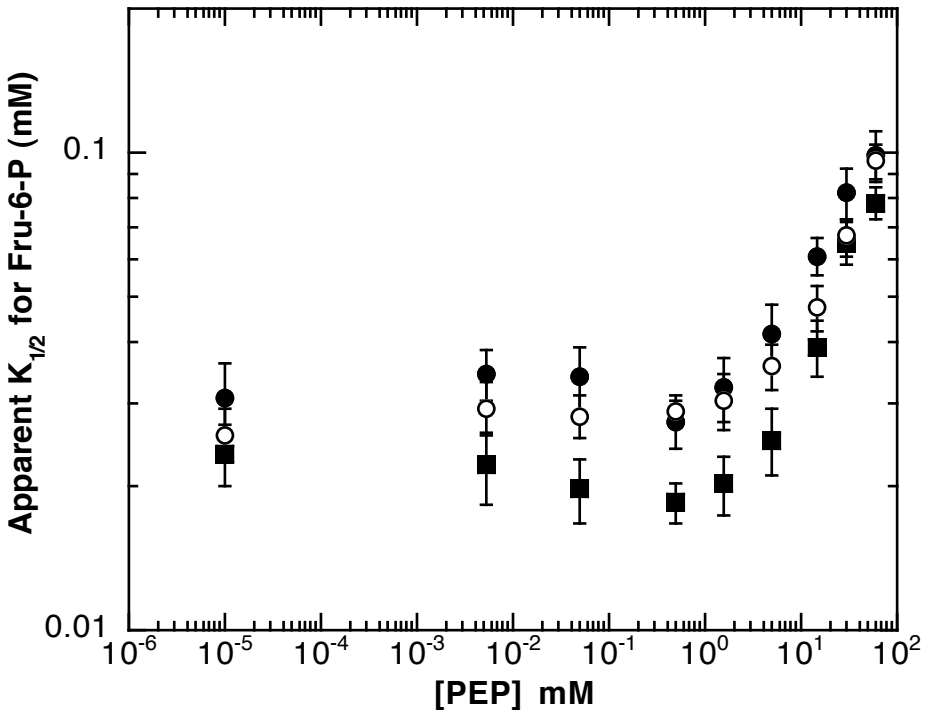

FIGURE 4-6 The dependence of the apparent $K_{1/2}$ for Fru-6-P determined for the 45 Å control hybrid (1|0) on increasing concentrations of the inhibitor PEP. The data was obtained at 25°C and at pH 6.0 (●) using 50 mM MES-KOH, at pH 7.0 (■) using 50 mM MOPS-KOH and at pH 8.0 (○) using 50 mM EPPS-KOH. The concentration of MgATP was equal to 3 mM, and the error bars represent ± the standard error.

measured for the native tetramer is never entirely accounted for by the four individual heterotropic interactions as shown in Fig. 4-7. At first we thought this was due to the mutations we had introduced throughout the binding sites and the surface of the protein in order isolate a given interaction; however, the presence of homotropic effects between the allosteric sites seemed like a more plausible explanation. This hypothesis was supported by the fact that Riley-Lovingshimer and Reinhart (2001) had measured a Hill number for PEP binding of 2.9 ± 0.3 for a tryptophan-shifted mutant of BsPFK (determined by fluorescence and in the absence of ATP and Fru-6-P).

In order to prove that cooperativity existed in the native enzyme as well and in the presence of ATP and Fru-6-P, PEP titrations were performed on the wild-type protein at pH 6.0, 7.0 and 8.0 using steady-state kinetics. Figure 4-8 summarizes the results, and as expected, a substantial amount of cooperativity was found between the PEP binding sites at low Fru-6-P (Hill number ~ 3); however, at high Fru-6-P the cooperativity is diminished greatly to approximately 1 at pH 6.0 and 7.0 and to about 1.5 at pH 8.0. With the presence of cooperativity confirmed within the native enzyme, a control hybrid was constructed to contain four native active sites, and one native allosteric site, eliminating the homotropic interactions between the allosteric sites (4|1). A schematic of this wild-type control hybrid is shown in Fig. 4-9. The control hybrid was constructed and isolated in the same manner as the other 1:3 hybrids, except the two parental proteins were wild-type BsPFK and the R211E/K213E/K90E/K91E allosteric site mutant protein. Steady-state kinetic

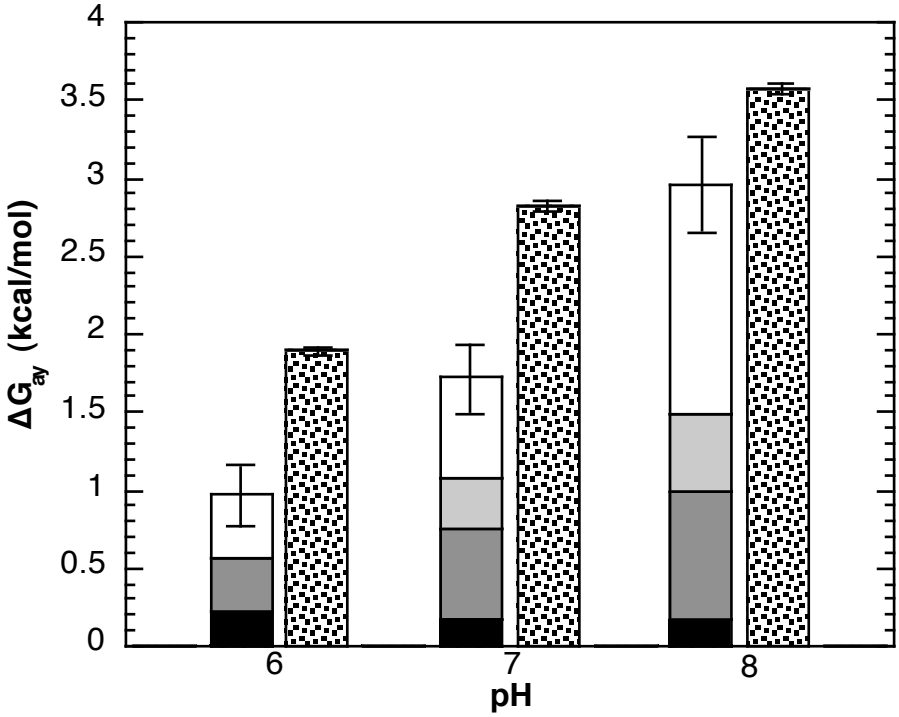

FIGURE 4-7 Comparison of the sum of the individual coupling free energies determined for the four heterotropic interactions to the coupling free energy determined for the native tetramer at pH 6.0, 7.0 and 8.0. The bar on the left at each pH corresponds to the sum of the coupling free energies determined for the 22 Å interaction (white), the 30 Å interaction (light gray), the 32 Å interaction (dark gray) and the 45 Å interaction (black), while the bar on the right at each pH corresponds to the coupling free energy determined for the wild-type enzyme (polka-dotted).

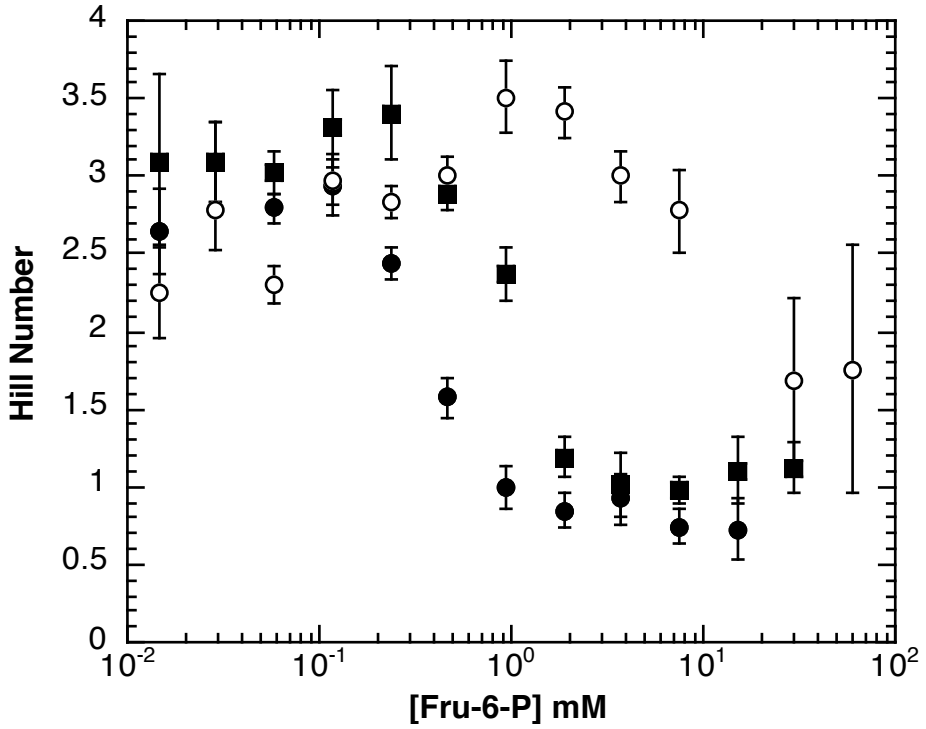

FIGURE 4-8 The dependence upon the Hill number (n_H) determined for PEP binding as a function of increasing concentrations of Fru-6-P for the wild-type enzyme. The data was obtained at 25°C and at pH 6.0 (●) using 50 mM MES-KOH, at pH 7.0 (■) using 50 mM MOPS-KOH and at pH 8.0 (○) using 50 mM EPPS-KOH. The concentration of MgATP was equal to 3 mM, and the error bars represent ± the standard error.

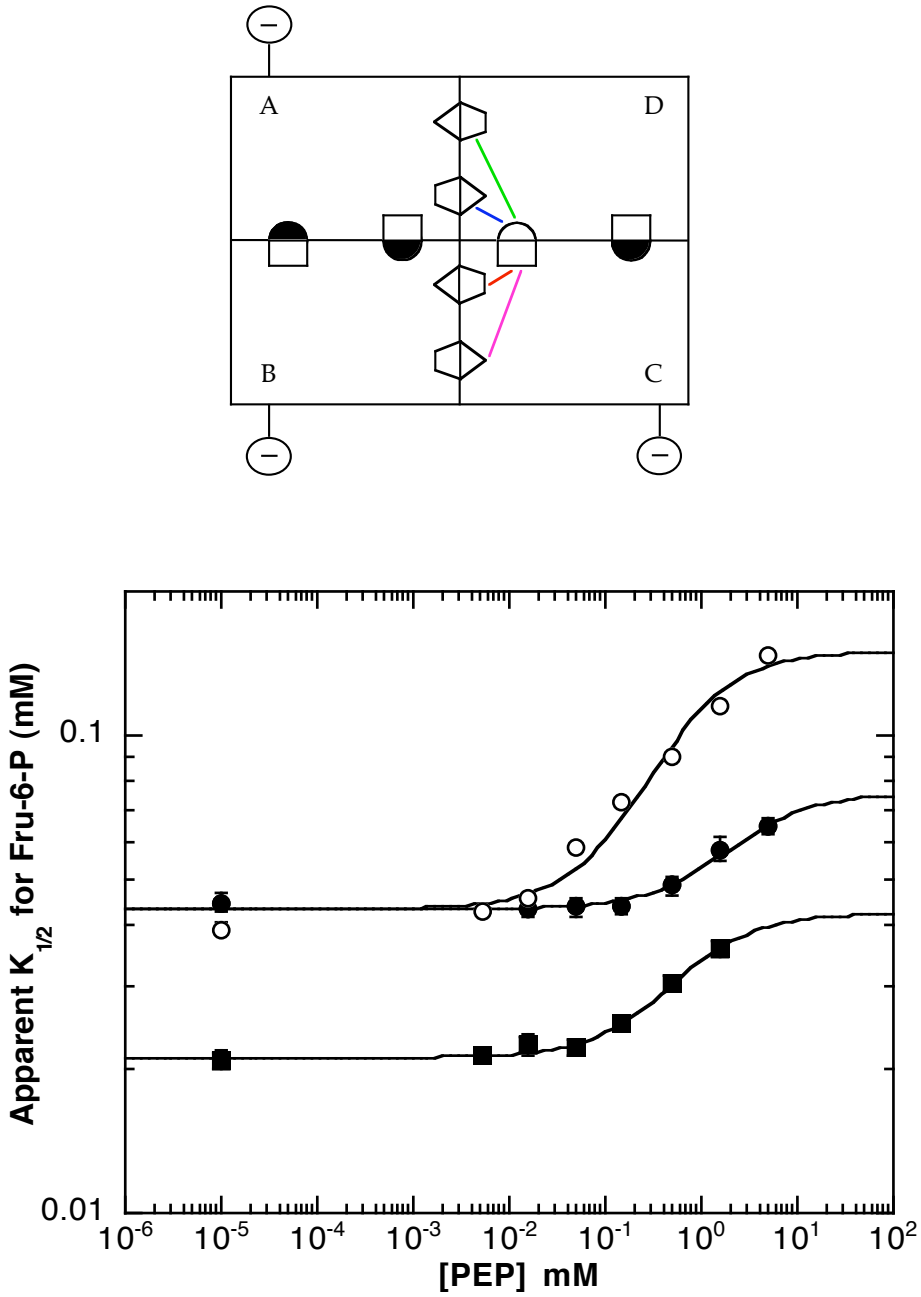

FIGURE 4-9 A two-dimensional schematic of the wild-type control hybrid (4|1) and the steady-state characterization of its allosteric properties at pH 6.0 (●), 7.0 (■) and 8.0 (○). The data was obtained at 25°C and using 50 mM MES-KOH at pH 6.0, 50 mM MOPS-KOH at pH 7.0 and 50 mM EPPS-KOH at pH 8.0. The concentration of MgATP was equal to 3 mM, and the error bars represent ± the standard error.

analysis was performed to measure the effect of PEP binding upon Fru-6-P binding and the data are shown in Fig. 4-9. The parameters obtained from the analysis are summarized in Table 4-5.

As was discussed earlier, Eq. 4-7 is used to equate the coupling free energy determined for the wild-type control hybrid to the coupling free energy determined for the wild-type enzyme in the absence of homotropic effects between the allosteric sites. Amazingly, the sum of the coupling free energies determined for the individual heterotropic interactions equals, within error, the coupling free energy determined (x4) for the wild-type control hybrid as seen in Fig. 4-10.

Discussion

The agreement of the sum of the measured individual couplings with the 4|1 control provides strong evidence that the individual interactions isolated in the respective 1:3 hybrids can be related directly to the corresponding interaction as it exists in the native tetramer. It is significant, therefore, that at each pH examined, the value of each of the couplings is different, indicating that the binding of a single Fru-6-P equivalent is influenced to a unique extent depending on which of the four allosteric sites is occupied by PEP. We note that our data do not indicate how a second equivalent of bound PEP might further influence the binding of that first Fru-6-P equivalent. Nonetheless, this result clearly lies in between the predictions made by either the concerted MWC model or the sequential KNF model as summarized in Fig. 4-1. It is also unlikely, given the modest magnitudes of the individual couplings even at pH 8,

TABLE 4-5 Thermodynamic parameters determined for the wild-type control hybrid (4 | 1) at 25°C, pH 6.0, 7.0 and 8.0 and [MgATP] = 3 mM

	K^{o}_{ia} (mM)	K^{o}_{iy} (mM)	Q_{ay}	ΔG_{ay} (kcal/mol)	ΔG_{ay} x 4 (kcal/mol)
pH 6.0 WT control (4 | 1)	0.043 ± 0.001	1.4 ± 0.9	0.57 ± 0.07	0.33 ± 0.08	1.32 ± 0.32
pH 7.0 WT control (4 | 1)	0.021 ± 0.001	0.34 ± 0.10	0.50 ± 0.04	0.41 ± 0.05	1.64 ± 0.20
pH 8.0 WT control (4 | 1)	0.043 ± 0.001	0.15 ± 0.01	0.29 ± 0.01	0.73 ± 0.02	2.92 ± 0.08

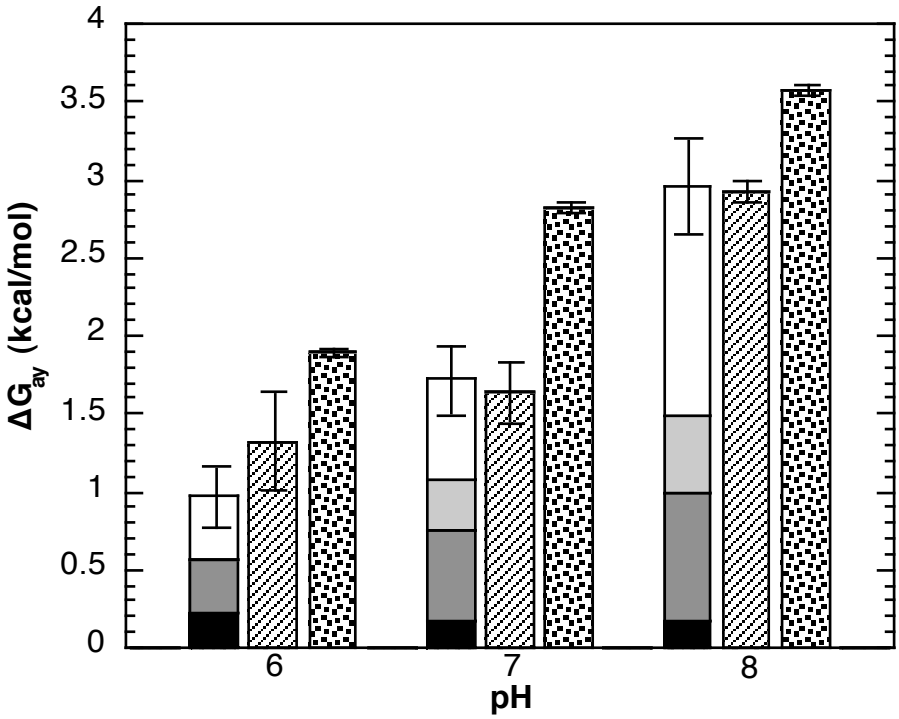

FIGURE 4-10 Comparison of the sum of the individual coupling free energies determined for the four heterotropic interactions to the coupling free energy determined for the wild-type control hybrid (4|1) and the wild-type enzyme (4|4) at pH 6.0, 7.0 and 8.0. The bar on the left at each pH corresponds to the sum of the coupling free energies determined for the 22 Å interaction (white), the 30 Å interaction (light gray), the 32 Å interaction (dark gray) and the 45 Å interaction (black). The bar in the middle at each pH corresponds to the coupling free energy determined for the wild-type control hybrid (striped), and the bar on the right at each pH corresponds to the coupling free energy determined for the wild-type enzyme (polka-dotted).

that a single species containing one bound PEP and one bound Fru-6-P would be formed in a suitable titration experiment. Although one would clearly expect the concentration of the species with Fru-6-P and PEP 45 Å apart to dominate (except at pH 6), the other species would be populated to lesser, but nonzero, extents at ambient temperatures, especially at the lower pH values. Thus a two-state view of the structural response of BsPFK to ligand binding becomes far too limiting a way of modeling its functional behavior, even in the seemingly simple case of the binding of a single equivalent of each ligand.

These results also suggest that allosteric interactions proceed by different pathways when considering how different sites are coupled. Stated another way, it is now reasonable to attempt to define the residues that are responsible for transmitting the influence between the various pairs of active and allosteric sites. Furthermore, it is unlikely that the same residues will be important for establishing the allosteric conduit in each case, although some residues may be shared. Since the hybrids isolate each individual interaction, determination of the residues that participate in the transmission of the allosteric influence would now seem to be possible, and these investigations are ongoing.

In order to isolate the 30 Å and 32 Å heterotropic interactions, the D12A mutation on the outside of the b-side binding pocket was required as discussed in Chapter III. The entire effect of D12A is still unknown however from the results presented here, we now feel confident that the mutation is not affecting the allosteric coupling between the native active site and native allosteric site because the sum of the coupling free energies of the individual heterotropic

interactions is equal to the measured allosteric coupling for the 4|1 wild-type control hybrid. However, since the binding affinity for PEP is so different between the interactions isolated in absence and presence of D12A, we do think the D12A mutation influences the binding of PEP at both the native and mutated allosteric sites. However, this long-range effect has precedence as others have also noted the same effects of mutations at the active site influencing binding at the allosteric site in both BsPFK and EcPFK (Valdez et al., 1989, Fenton and Reinhart, 2003).

With the four heterotropic interactions now isolated and characterized, almost half of the allosteric interactions found in the native tetramer have now been quantified. Thus, the six homotropic interactions remain, and it is their pair-wise isolations and characterizations that are the subjects of Chapters V and VI.

CHAPTER V

FORMATION AND ISOLATION OF THE 2:2 HYBRIDS

Introduction

Within BsPFK, the potential for twenty-eight pair-wise allosteric interactions exist between the four active sites and four allosteric sites. Of those 28 allosteric interactions, ten are unique and consist of four heterotropic interactions and six homotropic interactions. Up to this point, only the four heterotropic interactions have been individually isolated and characterized (Chapters III and IV); thus, the six homotropic interactions remain: three homotropic interactions between active sites (28 Å, 47 Å and 45 Å) and three homotropic interactions between allosteric sites (23 Å, 40 Å and 39.9 Å). As the name implies, the *homo*tropic interactions involve the allosteric communication between *like* binding sites, and in order to tell them apart, a distance has been assigned to each one which corresponds to the distance measured between the relevant binding sites within the crystal structure (Schirmer and Evans, 1990). More specifically, the active site homotropic interactions are differentiated by the distances measured in between the phosphorous atoms of the Fru-6-P molecules bound in the active sites, while the allosteric site homotropic interactions are differentiated by the distances measured between the □-phosphorous atoms of the ADP molecules bound in the allosteric sites. Of the 28 possible pair-wise allosteric interactions found within BsPFK, 12 are homotropic interactions, and of those 12, 6 are unique, all of which are shown schematically in Fig. 5-1.

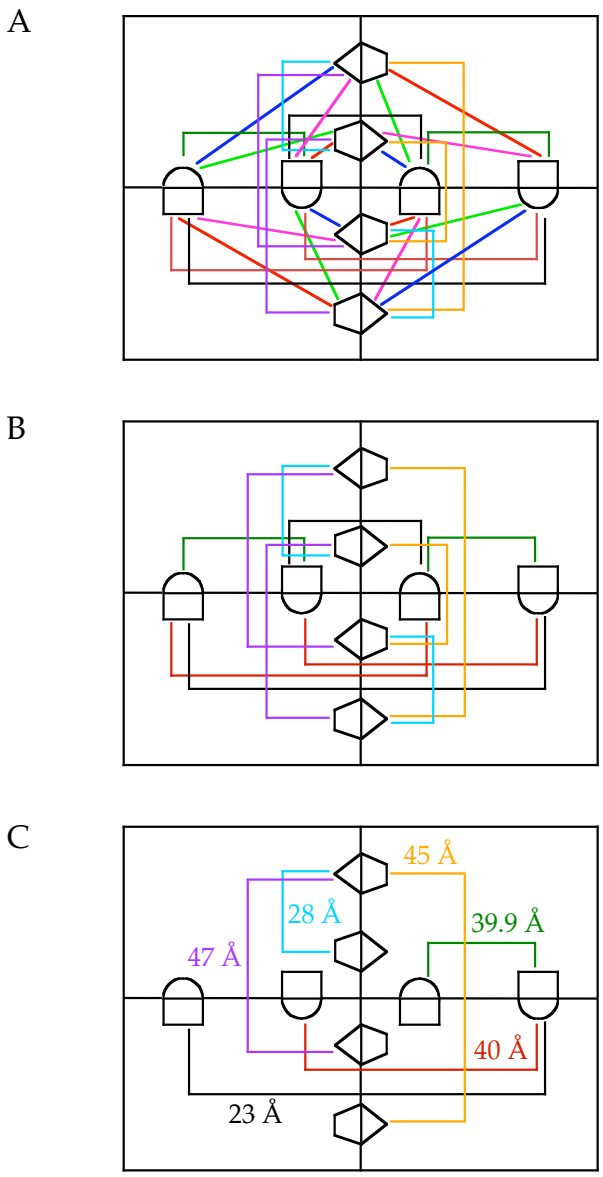

FIGURE 5-1 Three schematics depicting the pair-wise allosteric interactions possible within BsPFK. (*A*) 28 total pair-wise allosteric interactions are possible between the four active sites and four allosteric sites. (*B*) Of those 28, 12 are homotropic interactions (the interaction between like binding sites). (*C*) Of the 12 homotropic interactions, 6 are unique and have been assigned a different color and distance, which corresponds to the distance measured between the relevant binding sites within the crystal structure (Schirmer and Evans, 1990).

If our ultimate goal is to better understand the mechanism of allosteric regulation, and more specifically inhibition, then the allosteric contributions of the remaining six homotropic interactions need to be determined. However, within the native tetramer, two copies of each of the six homotropic interactions exist; thus, a reduction in the number of native binding sites, and hence the allosteric complexity is required. Utilizing the same hybrid-forming technique and mutant proteins described in Chapters III and IV, we show here the formation and isolation of the 2:2 hybrids and the ultimate characterizations of the six homotropic interactions (see Chapter VI). Two subunits of wild-type BsPFK and two subunits of either the [a,□], [a,□], [b,□] or [b,□] mutant proteins (recalling that specific "sides" of the binding sites have been mutated to discourage both Fru-6-P and PEP binding) form twelve different 2:2 hybrids, six of which are unique because of the pair-wise allosteric interactions they isolate. Each 2:2 hybrid contains two copies of two different heterotropic interactions, one copy of one homotropic interaction between active sites and one copy of one homotropic interaction between allosteric sites. A schematic of all twelve 2:2 hybrids is shown in Fig. 5-2 highlighting the interactions each 2:2 hybrid isolates and the mutant protein used to form each one.

As Fig. 5-2 shows, each of the six unique 2:2 hybrids has been designated as either the 2:2V(30&32), 2:2V(22&45), 2:2D(32&45), 2:2D(22&30), 2:2H(22&32) or 2:2H(30&45) hybrids. This notation was introduced in order to tell each of the six 2:2 hybrids apart, and utilizes two distinguishing characteristics inherent to each 2:2 hybrid. First, the letter in each "name" refers to the relative

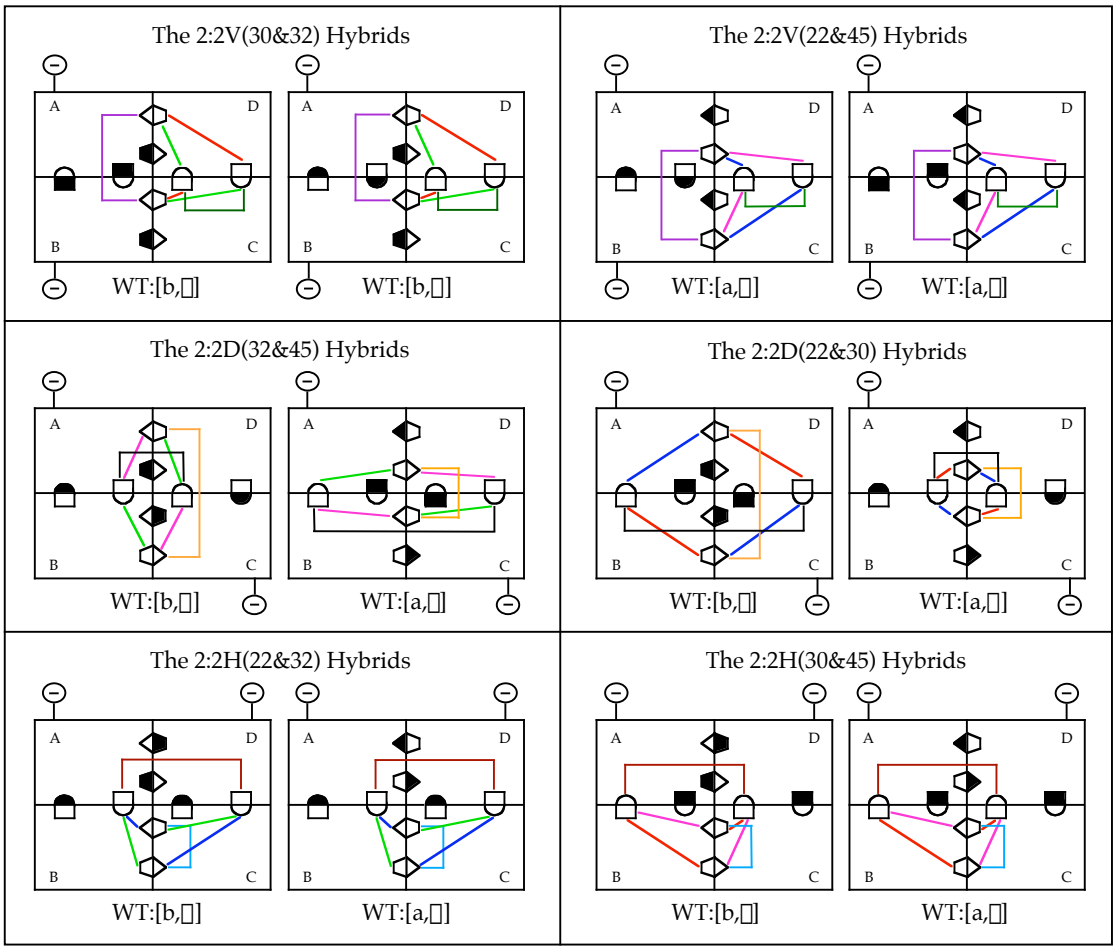

FIGURE 5-2 A schematic of the twelve 2:2 hybrids. Of the twelve 2:2 hybrids, six are unique, meaning there are two ways to form every 2:2 hybrid as shown above, with each unique pair having a specific "name" as described in the text. Furthermore, each 2:2 hybrid isolates six specific pair-wise allosteric interactions consisting of the two copies of two heterotropic interactions, a homotropic interaction between the active sites and a homotropic interaction between the allosteric sites. The "closed" symbols imply the presence of a mutation and hence the inability to bind either Fru-6-P or PEP at that particular site, while the "open" symbols are those "sides" of the binding sites that are not mutated (two paired "open" symbols are required to constitute a native binding site, while only one "closed" symbol is required to almost eliminate ligand binding as shown in Chapters III and IV).

orientations of the wild-type and mutant subunits in the two-dimensional schematic we use to depict the tetramer. Thus, the "D" refers to diagonally oriented subunits, the "H" to horizontally oriented subunits and the "V" to vertically oriented subunits. Second, the two different heterotropic interactions isolated in each 2:2 hybrid are listed in parentheses, since each of the six unique 2:2 hybrids isolates a different pair of heterotropic interactions. Hence, the 2:2V(30&32) hybrid corresponds to the 2:2 hybrid that has the wild-type and mutant subunits vertically oriented and also contains two copies each of the 30 Å and 32 Å heterotropic interactions.

Also shown in Fig. 5-2 is the fact that two different mutant proteins can be used to generate each of the six unique 2:2 hybrids, and this observation is related to the specific heterotropic interactions isolated in each 2:2 hybrid. Using the 2:2V(30&32) hybrid as an example, either the [b,□] or [b,□] mutant proteins can be used to form the 2:2V(30&32) hybrid because those two mutant proteins isolate the 30 Å and 32 Å heterotropic interactions via their individual 1:3 hybrids (1|1) respectively. Thus, if a problem arises so that a specific 2:2 hybrid cannot be formed or isolated, the alternative mutant protein can be used to possibly circumvent these difficulties.

Since the relative contributions of the four individual heterotropic interactions have already been determined (Chapters III and IV), we can then characterize the various 2:2 hybrids and in principle determine the roles played by the individual homotropic interactions in the inhibition process. However, before we are able to characterize the 2:2 hybrids, we need to devise a method

for isolating each of the 2:2 hybrids, and that is the topic of this chapter. The functional characterizations of the isolated 2:2 hybrids will be described in Chapter VI.

As discussed in Chapters III and IV, the K90E/K91E charge tag was added to the mutated subunits in order to separate the 1:3 hybrid from the other six enzyme species that form during the monomer exchange process. However, besides just separating the 1:3 hybrid, we discovered that the K90E/K91E charge tag also caused one of the three 2:2 isomers to be retarded in its elution off the Mono-Q anion exchange column relative to the other 2:2 isomers. Upon examining the crystal structure, we inferred that this separation was the result of the different distances between the K90E/K91E charge tags on each of the three 2:2 isomers. The lysines that are mutated for the K90E/K91E charge tag are relatively close together on the 2:2D isomer, only about 50 Å apart, while on the other two isomers the lysines that are mutated are on opposite ends of the protein and are approximately 82 Å and 90 Å apart (Schirmer and Evans, 1990). These distances were determined by averaging the two distances measured within the crystal structure between the four mutated residues. For example, the 50 Å distance determined for the 2:2D isomer was determined by measuring the distance between the two K90 residues and averaging that value with the distance measured between the two K91 residues. Thus, we propose that the 2:2D isomer would be retained longer on the Mono-Q anion exchange column because all four lysine to glutamate mutations could be presented more easily to the same face of an individual Mono-Q bead (particle size ~10 □M) resulting in a

stronger affinity for the resin as opposed to the other two isomers. Based on this idea, we designed two more charge tags to individually isolate the 2:2H and 2:2V isomers. Moreover, we also developed conditions that allowed dimer exchange to occur across the active site dimer-dimer interface between wild-type and the [b,□] mutant protein as an alternative means of isolating the 2:2V(30&32) hybrid.

Materials and methods

The materials and methods used for the experiments described in this chapter are as described in Chapter II. In particular, site-directed mutagenesis, protein purification, 2:2 hybrid formation via the monomer exchange procedure, enzymatic activity measurements, and data analysis were performed as described in Chapter II.

Hybrid formation, isolation and identification via dimer exchange across the active site interface. Unlike EcPFK, BsPFK does not undergo dimer exchange at room temperature (Fenton and Reinhart, 2002), thus special conditions were devised to promote exchange of the BsPFK subunits at the dimer level. Deville-Bonne et al. (1989) showed in EcPFK that the active site dimer-dimer interface was the weaker of the two interfaces, and that the addition of Fru-6-P would eliminate dimer exchange. Thus, due to the dramatic similarities between the two bacterial enzymes, we postulated that the active site dimer-dimer interface would also be the weaker of the two interfaces in BsPFK, particularly in the presence of PEP.

With this in mind, equal amounts of wild-type (1 mg/mL) and the [b,□]

mutant protein (1 mg/mL) were mixed together in the presence of 20 mM Tris-HCl (pH 8.5), 0.4 M KSCN and 4 mM PEP and incubated for 30 minutes at room temperature. A low concentration of KSCN and the addition of PEP were used to ensure subunit exchange occurred only at the dimer level and across the active site dimer-dimer interface, resulting in only one 2:2 hybrid forming, the 2:2V(30&32) hybrid.

To remove the KSCN and PEP, the hybrid mixture was dialyzed at room temperature into 20 mM Tris-HCl (pH 8.5) for 4 1/2 hours replacing the buffer every 90 minutes. The sample was then passed through a 0.22 μm membrane filter and applied onto a Mono Q HR 10/10 anion exchange column (Pharmacia) previously equilibrated with 20 mM Tris-HCl (pH 8.5). After washing the column with 3-5 bed volumes, a linear NaCl gradient (1.77 mM NaCl/mL) was used to elute the proteins. 1.5 mL fractions were collected and their absorbances at 280 nm determined. Figure 5-3 shows an elution profile for hybrids between wild-type and a mutant form of BsPFK. Three peaks are observed corresponding to wild-type BsPFK, the 2:2V(30&32) hybrid and the [b,□] mutant protein.

Native polyacrylamide gel electrophoresis analysis was used (as described in Chapter II for the monomer exchange procedure) to confirm the identity of the protein peaks and the results are shown in Fig. 5-4. The fractions exhibiting the greatest absorbance at 280 nm corresponding to the 2:2 hybrid were then pooled and stored at 4°C to prohibit any re-hybridization from occurring.

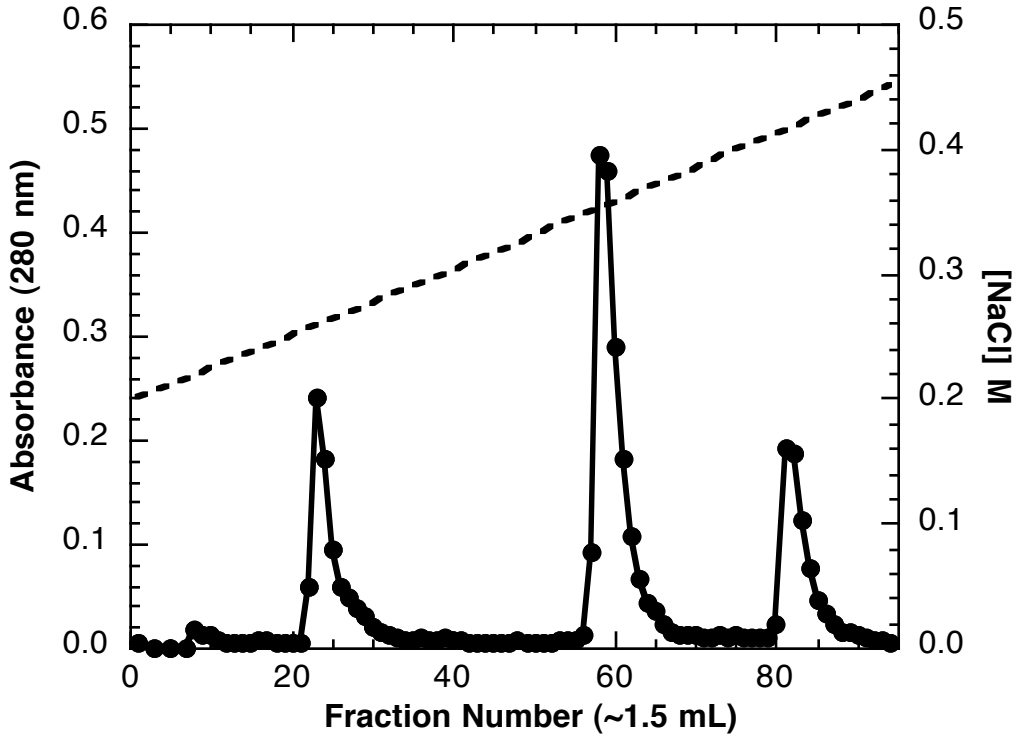

FIGURE 5-3 Elution profile for BsPFK hybrids made via dimer exchange from the Mono-Q column. Equal amounts of wild-type BsPFK and the [b,□] mutant were mixed together with 0.4 M KSCN and 4 mM PEP, and incubated for 30 minutes. The proteins were then dialyzed and loaded onto the Mono-Q column. A linear salt gradient was used to elute the proteins (1.77 mM NaCl/mL) and 1.5 mL fractions collected. Since the mutant has more net negative charge at pH 8.5, it stays on the column longer, and the wild-type protein elutes first. Absorbance at 280 nm (●) is plotted versus fraction number, and the dashed line (---) corresponds to the salt gradient used to elute the hybrid proteins from the column. Three peaks are observed with the wild-type enzyme eluting first, the 2:2V(30&32) hybrid next followed by the [b,□] mutant protein.

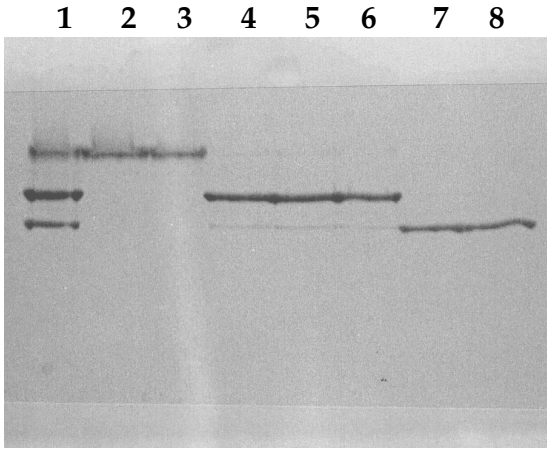

FIGURE 5-4 10% native polyacrylamide gel identifying the hybrids obtained via dimer exchange and isolated from the Mono-Q column. Samples were taken from the three peaks (Fig. 5-3) and the lanes correspond to the following: Lane 1 shows the hybrid mix prior to separation. Lanes 2 and 3 show peak 1 corresponding to wild-type BsPFK (4:0). Lanes 4, 5 and 6 show peak 2 corresponding to the 2:2V(30&32) hybrid. Lanes 7 and 8 show peak 3 corresponding to the [b,□] mutant protein (0:4).

Re-hybridization experiment. In order to confirm the identity of the isolated 2:2H(30&45) hybrid (isolated via monomer exchange and utilizing the R232E/Q233E charge tag), a subsequent re-hybridization experiment was performed between the wild-type enzyme and the 2:2H(30&45) hybrid. The two proteins were incubated in equal amounts (0.025 mg of each for a final protein concentration of 0.4 mg/mL) in 50 mM MOPS-KOH (pH 7.0) buffer containing 100 mM KCl, 5 mM $MgCl_2$, 0.1 mM EDTA and 2 mM DTT. Moreover, 30 mM PEP was also added to stabilize the allosteric site interface, and the mixture was then heated for 2 hours at 50°C. Furthermore, two experimental controls were also made, and contained the identical components as listed above except one did not contain PEP and the other was not heated. Dialysis was used to remove the PEP from the pertinent samples and then all of the samples were run on a 10% native PAGE gel using the protocol described in Chapter II.

Results

Using monomer exchange for 2:2 hybrid formation. Monomer exchange is one way to form the 2:2 hybrids (procedure outlined in Chapter II), and when this technique is utilized, three 2:2 isomers form, all of which differ in their relative orientations of the wild-type and mutant subunits and the allosteric interactions isolated. The wild-type and mutant subunits can be oriented either vertically (2:2V), diagonally (2:2D) or horizontally (2:2H), and the six pair-wise allosteric interactions that are isolated in the three 2:2 isomers vary based upon the mutant protein used. Moreover, the only interaction common to all three isomers is the heterotropic interaction that is isolated via the mutant protein's

respective 1:3 hybrid with the wild-type enzyme. Figure 5-5 illustrates schematically the three 2:2 isomers that can form when using monomer exchange to make hybrids between wild-type and either the [b,□] mutant protein or the [b,□] mutant protein, recalling that both mutant proteins produce the 2:2V(30&32) hybrid as mentioned above. Thus, in order to make any of the twelve 2:2 hybrids shown in Fig. 5-2, the same four mutant constructs ([a,□]. [a,□], [b,□] and [b.□]) used in Chapters III and IV are utilized.

Strategy for isolating the 2:2D isomer when using monomer exchange and the K90E/K91E charge tag. In order to individually characterize the 2:2 hybrids, we needed to design a method for separating the 2:2 isomers that form when using the monomer exchange procedure outlined in Chapter II. The approach we took for separating the 2:2 isomers was actually based upon our results involving the isolation of the 30 Å and 45 Å heterotropic interactions (via the 1:3 hybrids) using the K90E/K91E charge tag and either the [b,□] or [a,□] mutant proteins respectively (Chapters III and IV). Besides separating the 1:3 hybrid from the other six hybrid species, the K90E/K91E charge tag was also successful in separating the three 2:2 isomers as evidenced by seven peaks in the elution profile. Figure 5-6 shows an example of this separation for hybrids between wild-type and the [b,□] mutant protein. First, two separate peaks are observed corresponding to the wild-type enzyme and the 3:1 hybrid. Next, a doublet and a single peak are observed which were all proven to be 2:2 isomers by native PAGE analysis (data not shown). The elution profile then concludes

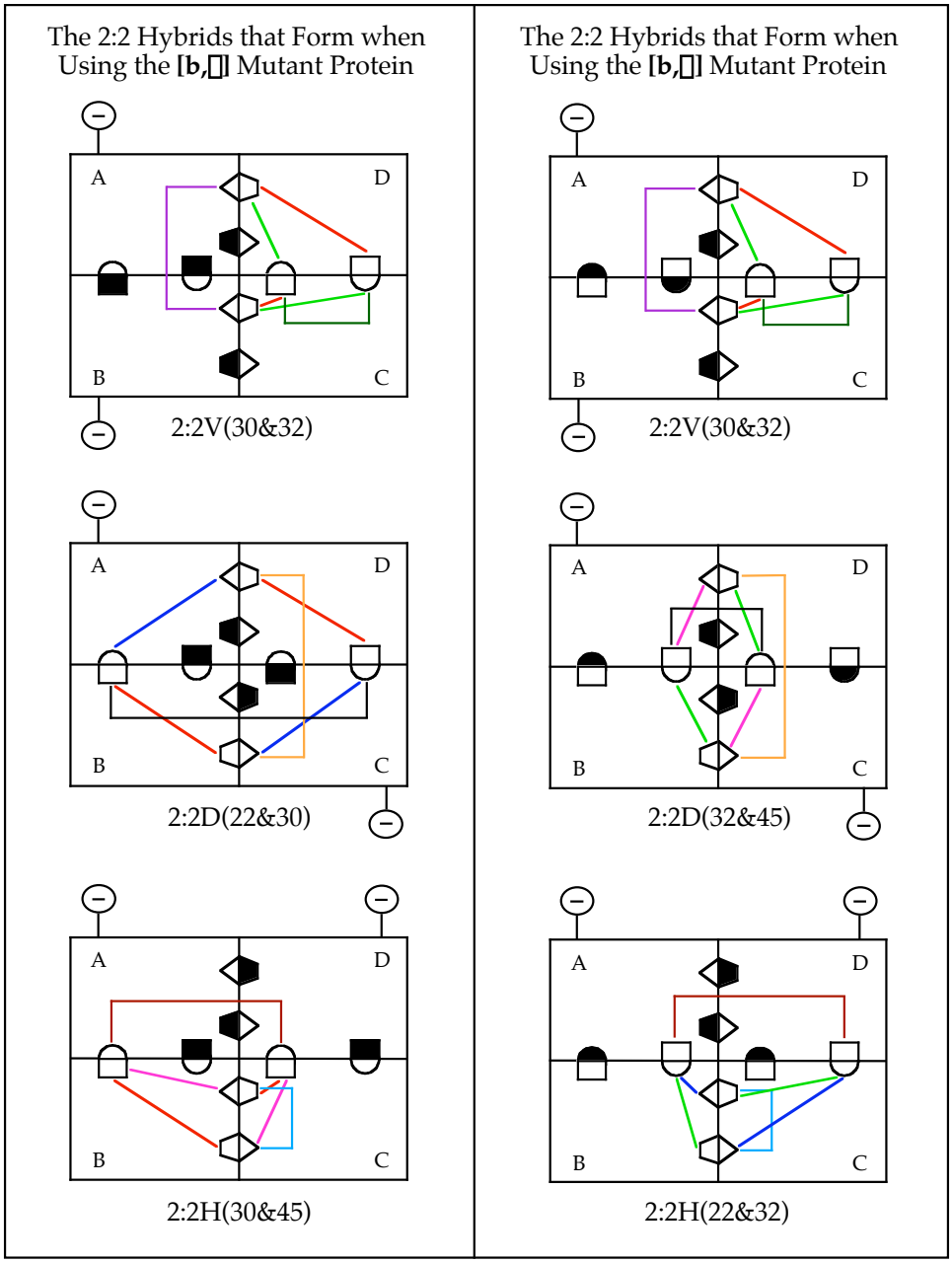

FIGURE 5-5 The three 2:2 isomers that form between wild-type BsPFK and either the [b,□] or [b,□] mutant proteins when using monomer exchange. Note that the 30 Å heterotropic interaction (red) is found in all three 2:2 isomers when using the [b,□] mutant protein, and the 32 Å interaction (bright green) is found in all three 2:2 isomers when using the [b,□] mutant protein.

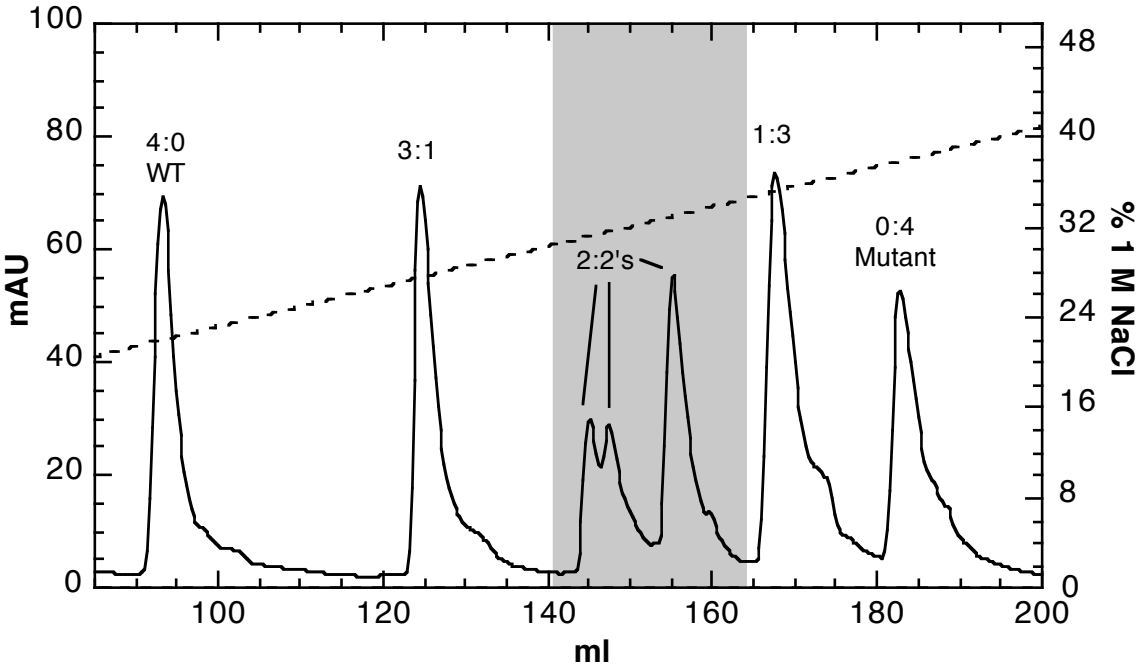

FIGURE 5-6 The elution profile for hybrids between wild-type and the [b,□] mutant protein (R252A/D12A/R25E/K90E/K91E) from the Mono-Q anion exchange column. The volume collected (each fraction contained 1.5 ml) is plotted *versus* absorbance at 280 nm (—) as well as percent 1 M NaCl (---). The gray region indicates the region of 2:2 separation. The doublet contains the 2:2H and 2:2V hybrids while the single 2:2 peak contains the 2:2D hybrid as determined from the distances between the K90E/K91E charge tag on the three isomers. The identity of the peaks (4:0, 3:1, 2:2, 1:3 or 0:4) was confirmed via native PAGE analysis (data not shown).

with individual peaks for the 1:3 hybrid (isolating the 30 Å heterotropic interaction) and the [b,□] mutant protein.

Since the three 2:2 isomers are undistinguishable from one another via native PAGE analysis, we examined the crystal structure to see where K90 and K91 were located on each of the three isomers in hopes of assigning the 2:2 isomer peaks (Schirmer and Evans, 1990). Since K90 and K91 are located on the ends of the large domain, the K90E/K91E mutations would be closest in the 2:2D isomer (~50 Å apart) and much farther away from one another in the 2:2V and 2:2H isomers (~82 Å and 90 Å respectively). Thus, we propose that the 2:2D hybrid is retained longer on the Mono-Q anion exchange column (the single peak in the gray region of Fig. 5-6), than the 2:2V or 2:2H hybrids (the doublet in the gray region of Fig. 5-6) because the negative charge tags are more likely to be presented simultaneously to the same face of an individual Mono-Q bead (particle size ~ 10 □m). This explanation has also been used to explain the separation of the 2:2 isomers for lactate dehydrogenase hybrids (Fushinobu et al., 1996) and fructose-1,6-bisphosphatase hybrids (Nelson et al., 2001), both of which are homotetrameric enzymes of approximately the same molecular weight as BsPFK. Furthermore, the functional behavior of the isolated 2:2D hybrid is also consistent with this explanation (see Chapter VI). Thus, the K90E/K91E charge tag was used to separate the 2:2D isomer from the 2:2V and 2:2H isomers, and more specifically to isolate the two 2:2D(32&45) hybrids via the [b,□] and [a,□(K213E)] mutant proteins and the 2:2D(22&30) hybrid via the [b,□] mutant protein.

The adverse chromatographic effects of the R211E mutation. Although separation of the 2:2 isomers was observed when making hybrids between wild-type and either the [a,□] or [b,□] mutant proteins, no separation of the 2:2 isomers was seen when using the [a,□] or [b,□] mutant proteins despite the K90E/K91E charge tag. Figure 5-7 *A* shows the elution profile for hybrids between wild-type and the [a,□] mutant protein (R162E/R211E/K213E/K90E/K91E), and five peaks, rather than seven are observed. This difference in hybrid separation is likely the result of the R211E/K213E (□-side) mutations in the allosteric site. It is believed that one or both of the allosteric site mutations might be solvent exposed thus interfering with the efficiency of the K90E/K91E charge tag. To provide evidence that this was in fact the case, hybrids between the R211E/K213E mutant protein and the [a,□] mutant protein (R162E/R211E/K213E/K90E/K91E) were made (Fig. 5-7 *B*). Since the R211E/K213E mutations are present in all four subunits, the effect of the K90E/K91E charge tag was not counteracted, and some separation of the 2:2 isomers is observed (two peaks) as shown in Fig. 5-7 *B*.

Next, to determine if only one of the allosteric site mutations (either R211E or K213E) was responsible for this inability to separate the 2:2 isomers, the crystal structure was examined and showed that only the side chain of R211 was exposed at the surface of the protein (Schirmer and Evans, 1990). Thus, to circumvent the adverse chromatographic effects of the R211E mutation, the K213E mutation was used instead of the R211E/K213E double mutation when necessary. Luckily, all of the other binding site residues that are mutated are

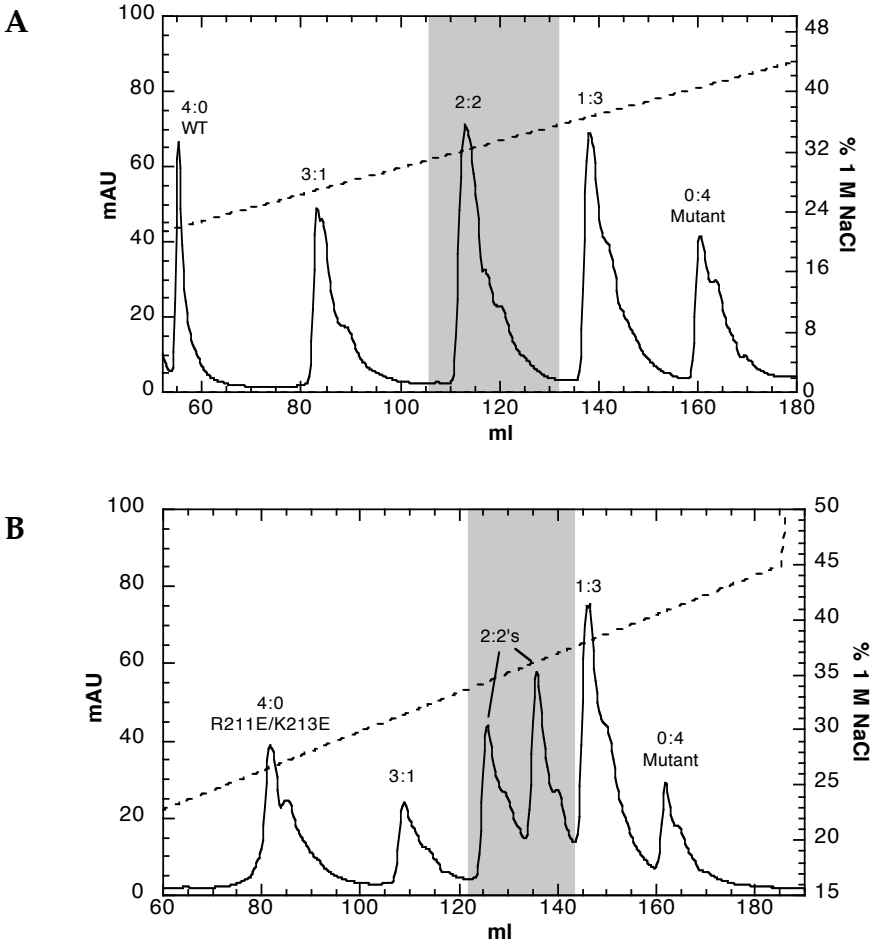

FIGURE 5-7 Two elution profiles demonstrating the influence of the R211E/K213E mutations upon resolution of the 2:2 isomers (gray region). A shoulder on the right side of every peak is observed and is thought to be a result of the column performance and not hybrid separation. The volume collected (each fraction contained 1.5 ml) is plotted *versus* absorbance at 280 nm (—) as well as percent 1 M NaCl (---). The same salt gradient is used in both experiments. (*A*) Hybrids between wild-type and the [a,□] mutant protein (R162E/R211E/K213E/K90E/K91E). No resolution of the 2:2 isomers is seen. (*B*) Hybrids between the R211E/K213E mutant protein and the [a,□] mutant protein (R162E/R211E/K213E/K90E/K91E). The 2:2D isomer is separated from the 2:2V and 2:2H isomers as evidenced by two peaks. Identification of all the peaks shown above was confirmed via native PAGE analysis.

located deep in the binding pockets prohibiting any interference with the effectiveness of the surface charge tags (Schirmer and Evans, 1990).

Characterization of the K213E allosteric site mutation. Like the R211E/K213E mutation, the K213E mutation alone needed to prohibit PEP binding by at least two orders of magnitude, thus before utilizing the K213E mutation in forming hybrids and isolating specific allosteric interactions, the mutation needed to be characterized. Using the R162E/K213E mutant protein, the effects of the K213E mutation were determined and the results shown in Fig. 5-8. Over the PEP concentrations assayed, the R162E/K213E mutant protein is essentially unresponsive to PEP, thus the K213E mutation was found to be suitable to use instead of the R211E/K213E mutations (the effects of the R162E mutation are also seen as the decreased binding affinity for Fru-6-P as compared to wild-type).

Unfortunately, when the K213E mutation was implemented for use in making hybrids, we discovered that all seven hybrid species were not able to form whenever K213E was used in conjunction with the R162E mutation (the [a,□] mutant protein) and the K90E/K91E charge tag. This phenomenon was reminiscent of the earlier problems encountered when making hybrids between wild-type and the [b,□] and [b,□] mutant proteins in the absence of the D12A mutation (Chapter III). Unfortunately, since D12 is located on the b-side of the active site and the R162E mutation is located on the a-side of the active site, we were unable to use the D12A mutation to circumvent this problem. Table 5-1 summarizes the mutant proteins that were unable to be used in forming three of

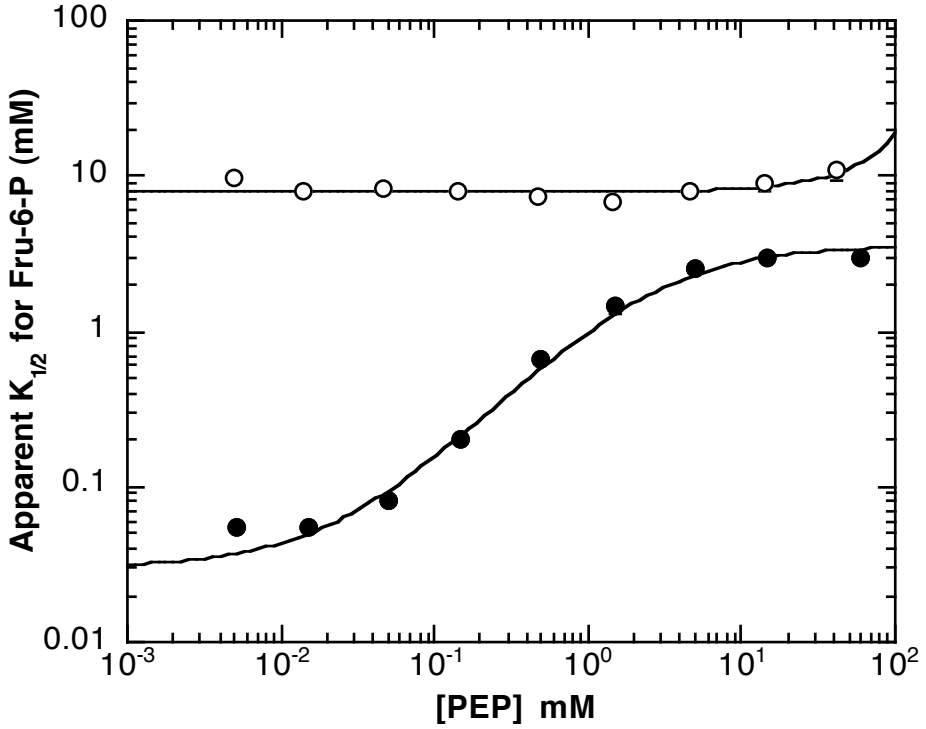

FIGURE 5-8 The dependence of the apparent $K_{1/2}$ for Fru-6-P on increasing concentrations of the inhibitor PEP for wild-type BsPFK (●) and the R162E/K213E mutant protein (○). The $K_{1/2}$ values were obtained from individual Fru-6-P saturation profiles (performed at pH 7.0 and 25°C; data not shown) at increasing concentrations of PEP. The curves correspond to the best fit of these data to Eq. 2-4 as described in the text. Error bars represent ± the standard error and are smaller than the symbol when not evident.

TABLE 5-1 The 2:2 hybrids that were unable to be formed utilizing the [a,□] mutant protein with the K213E mutation in the allosteric site

Mutant Protein	Active Site Mutation	Allosteric Site Mutation[a]	Charge Tag	2:2 Hybrid It Would Form
[a,□]	R162E	R211E/K213E (K213E)	N303E/K304E	2:2V(22&45)
[a,□]	R162E	R211E/K213E (K213E)	K90E/K91E	2:2D(22&30)
[a,□]	R162E	R211E/K213E (K213E)	R232E/Q233E	2:2H(22&32)

[a]The R11E/K213E mutations were unable to be used because of the location of R211 on the surface of the protein, thus the K213E mutation was used as an alternative.

the twelve possible 2:2 hybrids. Fortunately however, the redundant proteins were used in isolating those three 2:2 hybrids.

Strategy for isolating the 2:2H and 2:2V isomers when using monomer exchange utilizing the R232,233E and N303E/K304E charge tags. Using the same approach of separating one of the 2:2 isomers from the remaining two isomers, we set out to find two more charge tags; one to separate the 2:2H hybrid from the 2:2D and 2:2V isomers, and the other to separate the 2:2V isomer from the 2:2D and 2:2H isomers. Upon gazing at the crystal structure, we discovered that there were no pairs of positively charged residues that exhibited the same biased distance distribution as was observed for the

K90E/K91E mutations; thus, we chose one positively charged residue and one neutral residue to mutate to two glutamates for the remaining two charge tags.

The R232E/Q233E charge tag was found to be an excellent candidate for separating the 2:2H isomer from the 2:2D and 2:2V isomers because the average distance between the two R232 residues and the two Q233 residues on the 2:2H isomer was approximately 29 Å, while the average distances for the same residues on the 2:2D and 2:2V isomers were approximately 68 Å and 69 Å apart, respectively. On the other hand, to separate the 2:2V isomer from the 2:2D and 2:2H isomers, the N303E/K304E charge tag was chosen because it also met our distance criteria. The average distance between the two N303 residues and the two K304 residues on the 2:2V isomer was about 40 Å, while the average distances were approximately 64 Å and 74 Å for the 2:2H and 2:2D isomers. Figures 5-9, 5-10 and 5-11 illustrate the locations of the residues that are mutated for the three different charge tags (recalling that the K90E/K91E charge tag isolates the 2:2D isomer, the R232E/Q233E charge tag isolates the 2:2H isomer and the N303E/K304E charge tag isolates the 2:2V isomer) in the 2:2D, 2:2H and 2:V isomers respectively (Schirmer and Evans, 1990).

Implementing these two new charge tags to accomplish our goal of separating either the 2:2H or 2:2V isomers was next, and Fig. 5-12 shows the chromatographic results for utilizing either the R232E/Q233E charge tag or the N303E/K304E charge tag in the [b,□] mutant protein (R252A/D12A/R25E + Charge Tag). For the R232E/Q233E charge tagged protein, we observe a similar elution pattern to what was observed for the K90E/K91E charge tagged protein

FIGURE 5-9 The positions of K90 and K91 in the 2:2D, 2:2H and 2:2V isomers in either the two-dimensional schematic or crystal structure. In the crystal structure, K90 and K91 are colored orange. (*A*) The 2:2D isomer with a black dashed line indicating a distance of 50 Å between the charge tags. (*B*) The 2:2H isomer with a black dashed line indicating a distance of 90 Å between the charge tags. (*C*) The 2:2V isomer with a black dashed line indicating a distance of 82 Å between the charge tags.

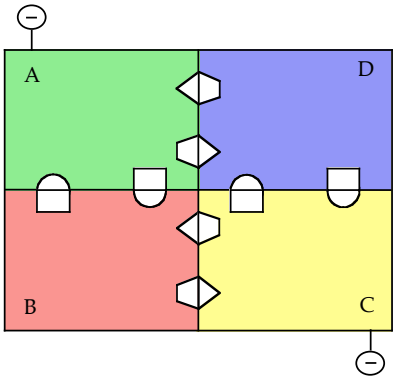

A

2:2D
K90E/K91E

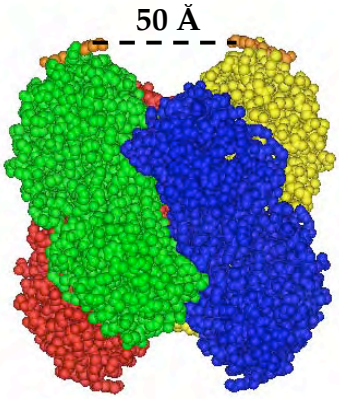

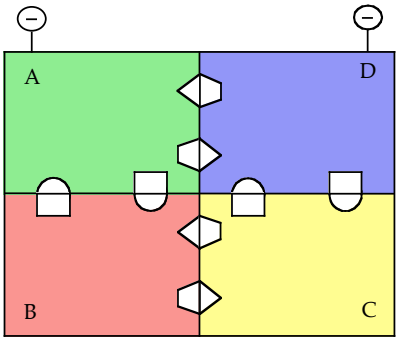

B

2:2H
K90E/K91E

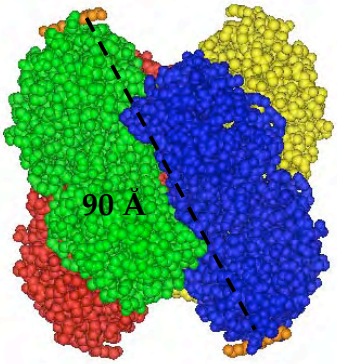

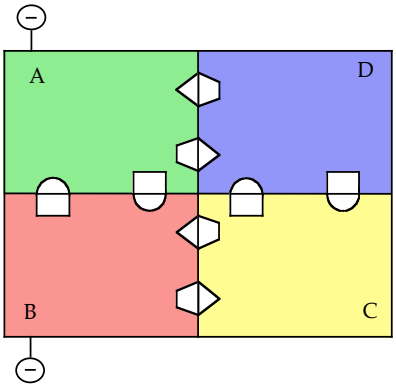

C

2:2V
K90E/K91E

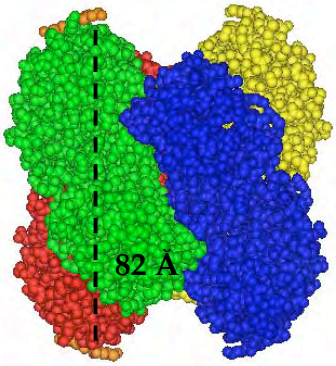

FIGURE 5-10 The positions of R232 and Q233 in the 2:2D, 2:2H and 2:2V isomers in either the two-dimensional schematic or crystal structure. In the crystal structure, R232 and Q233 are colored magenta. (*A*) The 2:2D isomer with a black dashed line indicating a distance of 68 Å between the charge tags. (*B*) The 2:2H isomer with a black dashed line indicating a distance of 29 Å between the charge tags. (*C*) The 2:2V isomer with a black dashed line indicating a distance of 69 Å between the charge tags.

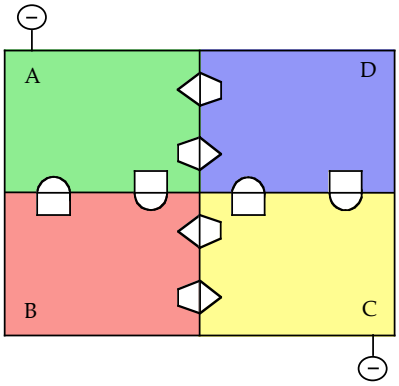

A

2:2D
R232E / Q233E

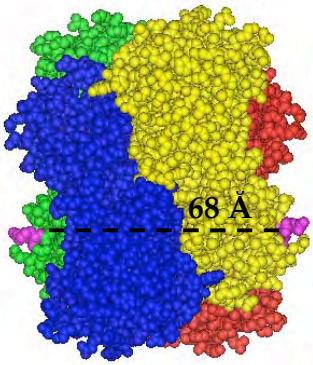

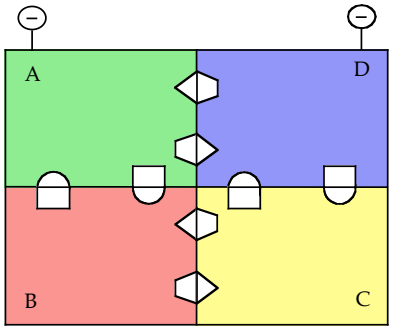

B

2:2H
R232E / Q233E

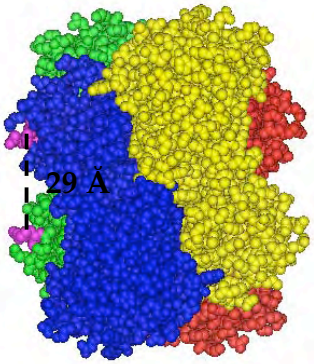

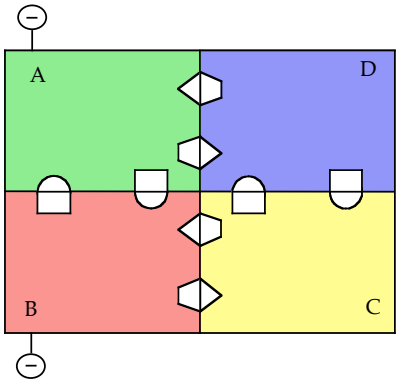

C

2:2V
R232E / Q233E

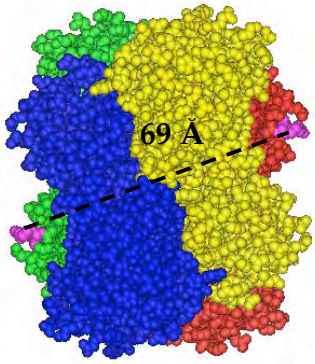

FIGURE 5-11 The positions of N303 and K304 in the 2:2D, 2:2H and 2:2V isomers in either the two-dimensional schematic or crystal structure. In the crystal structure, N303 and K304 are colored cyan. (*A*) The 2:2D isomer with a black dashed line indicating a distance of 74 Å between the charge tags. (*B*) The 2:2H isomer with a black dashed line indicating a distance of 64 Å between the charge tags. (*C*) The 2:2V isomer with a black dashed line indicating a distance of 40 Å between the charge tags.

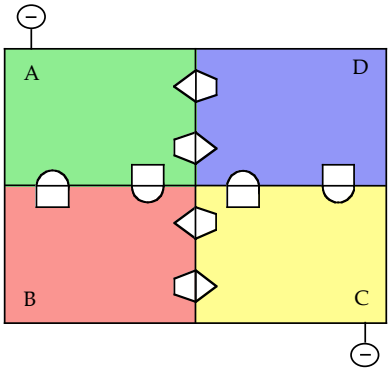

A

2:2D
N303E / K304E

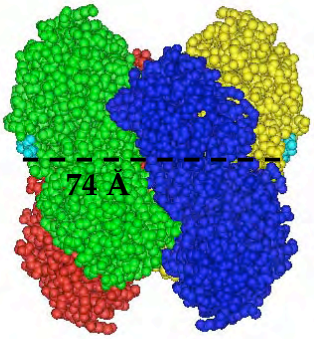

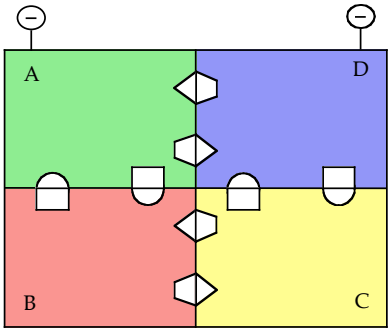

B

2:2H
N303E / K304E

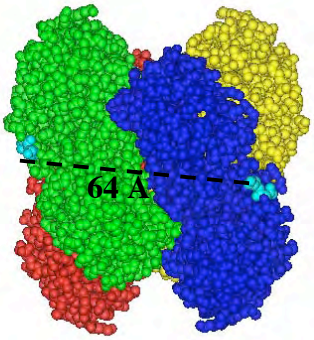

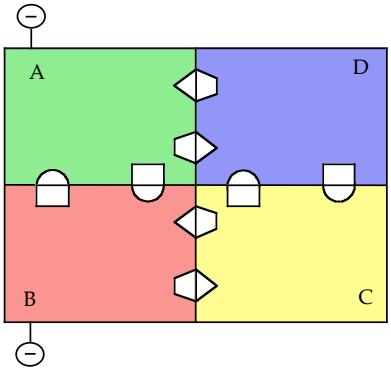

C

2:2V
N303E / K304E

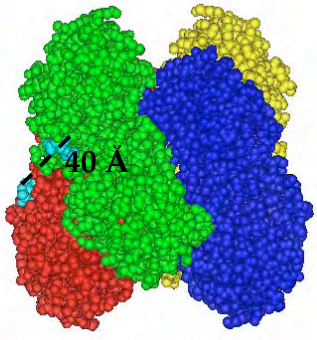

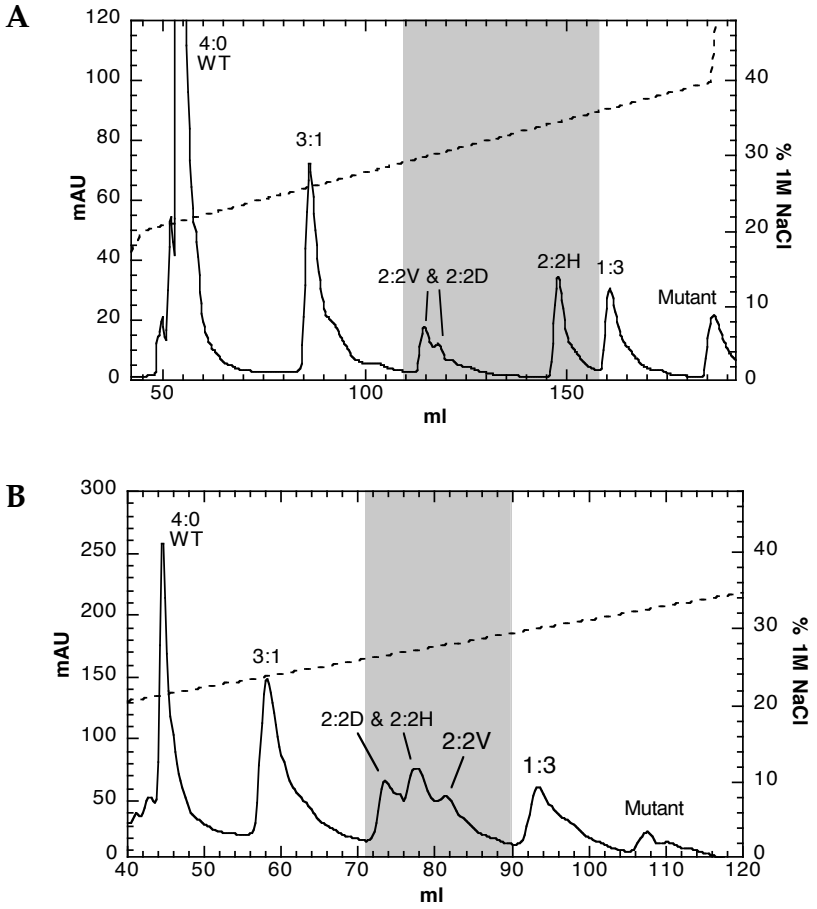

FIGURE 5-12 Two elution profiles demonstrating the influence of the R232E/Q233E and N303E/K304E charge tags upon the resolution of the 2:2 isomers (gray region). The volume collected (each fraction contained 1.5 ml) is plotted *versus* absorbance at 280 nm (—) as well as percent 1 M NaCl (---). (*A*) Hybrids between wild-type and the [b,□] mutant protein (R252A/D12A/R25E/R232E/Q233E). The 2:2 isomers separate as a doublet (2:2V and 2:2D) followed by a single peak containing the 2:2H hybrid. (*B*) Hybrids between wild-type and the [b,□] mutant protein (R252A/D12A/R25E/N303E/K304E). The 2:2 isomers are seen as a triplet peak because the charge tag distances are more similar for the three isomers (40 Å (2:2V), 64 Å (2:2H) and 74 Å (2:2D)). Identification of all the peaks shown above was confirmed via native PAGE analysis.

(compare to Fig. 5-6). For the R232E/Q233E charge tagged protein, the 2:2 isomers separate first as a doublet, followed by a single peak containing the 2:2H isomer. Thus, the R232,233E charge tag effectively isolates the 2:2H isomer from the 2:2D and 2:2V isomers and is utilized in isolating the 2:2H(22&32) hybrid utilizing the [b,□(K213E)] mutant protein and the 2:2H(30&45) hybrid using either the [b,□] or [a,□] mutant proteins.

The elution profile for the N303E/K304E charge tagged protein is also shown in Fig. 5-12 *B*, however it displays an entirely new profile. Since the relative distances between the charge tag pairs for the three 2:2 isomers are not as different as the previous two charge tags, a triplet peak is observed. Although an isolated peak is preferred, we were able to successfully obtain the 2:2V isomer by re-running the far right shoulder of the triplet peak over the Mono-Q anion exchange column again to obtain a pure peak. Figure 5-13 shows the results of this added purification. A major peak is observed with a minor contamination shoulder on the left side of the peak probably containing the 2:2H hybrid. However, to ensure the isolated 2:2 hybrid was not contaminated, only the extreme right side of the major peak was used for characterization. Thus, the N303E/K304E charge tag was successful in isolating the 2:2V isomer from the 2:2D and 2:2H isomers, and more specifically in isolating the 2:2V(30&32) hybrid via the [b,□] mutant protein, and the 2:2V(22&45) hybrid via the [a,□] mutant protein.

Isolation of the 2:2V(30&32) hybrid via dimer exchange. Besides using the monomer exchange procedure to form the 2:2 hybrids, dimer exchange

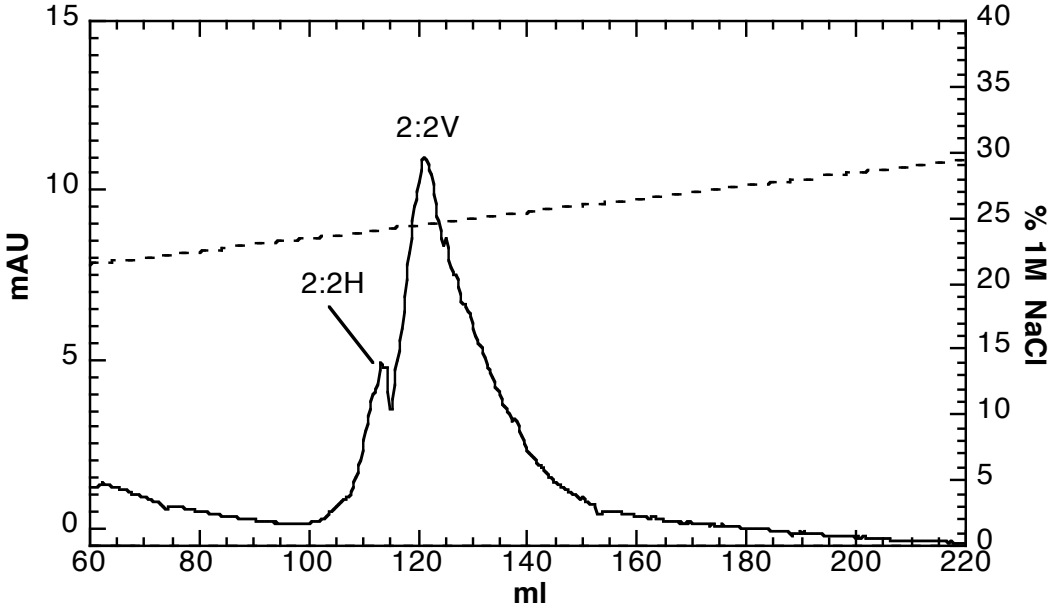

FIGURE 5-13 The elution profile for the 2:2V hybrid (with some 2:2H contamination) from the Mono-Q anion exchange column. The volume collected (each fraction contained 1.5 ml) is plotted *versus* absorbance at 280 nm (—) as well as percent 1 M NaCl (---). A doublet peak is observed, where the bigger peak is the 2:2V isomer and the left shoulder is probably the 2:2H isomer. The right side of the doublet peak was used for characterization to ensure there was no contamination from the 2:2H isomer. Identification of the 2:2 peak was confirmed via native PAGE analysis.

could also be used providing the advantage of forming only one specific 2:2 hybrid rather than three, eliminating the requirement for separating the 2:2 isomers. Unlike EcPFK, BsPFK does not undergo dimer exchange at room temperature (data not shown) thus special conditions were devised to promote exchange of BsPFK dimers. Deville-Bonne et al. (1989) showed in EcPFK that the active site dimer-dimer interface was the weaker of the two interfaces, and that the addition of Fru-6-P would eliminate dimer exchange. Thus, due to the sequence and structural similarities between the two bacterial enzymes (French and Chang, 1987), we postulated that the active site dimer-dimer interface would also be the weaker of the two interfaces in BsPFK, particularly in the presence of saturating PEP. Consequently, dimer exchange could only be used to form the 2:2V hybrids.

Exchange was attempted between wild-type and all four mutant proteins containing the K90E/K91E charge tag and surprisingly, dimer exchange only occurred between wild-type and the [b,□] mutant protein (R252A/D12A/R211E/K213E/K90E/K91E) as proven by native PAGE analysis. Since dimer exchange was successful between wild-type and the [b,□] mutant protein, the hybrid mixture was applied to the Mono-Q anion exchange column, and the elution profile shown in Fig. 5-3. As expected, three peaks are observed and native PAGE analysis confirmed the identity of all three peaks (see Materials and methods Fig. 5-4).

Furthermore, dimer exchange only occurred between wild-type and the [b,a] mutant protein in the presence of PEP as shown in Fig. 5-14. In the absence

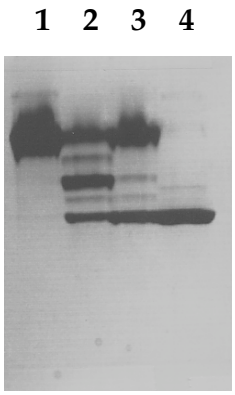

FIGURE 5-14 A 10% native PAGE gel illustrating the importance of PEP in the dimer exchange procedure. Lane 1 shows wild-type BsPFK. Lane 2 shows dimer exchange performed in the presence of 0.4 M KSCN and 5 mM PEP. Lane 3 shows dimer exchange performed only in the presence of 0.4 M KSCN. Lane 4 shows the [b,□] mutant protein.

of PEP, only the parent proteins are observed (lane 3, 2 major bands), while in the presence of PEP (5 mM PEP), dimer exchange is successful between wild-type and the [b,□] mutant protein (lane 2, 3 major bands). Some residual monomer exchange is observed with either condition, but in negligible amounts when compared to the amount of the parent proteins or the 2:2V(30&32) hybrid visualized in the gel. Thus, PEP not only potentially stabilizes the allosteric site interface, but it also seems to destabilize the allosteric site interface. This phenomenon will be revisited later, but more importantly, dimer exchange was successful in the presence of PEP and a low concentration of KSCN in producing and isolating the 2:2V(30&32) hybrid.

Interestingly, dimer exchange did not occur with the other three mutant proteins. Temperature, the concentrations of KSCN and PEP, as well as the incubation time were all varied, but with no success. Either no exchange or varying degrees of monomer exchange was always observed (data not shown). Why dimer exchange did not occur for the [a,□], [a,□] and [b,□] mutant proteins is unknown, however we believe that it is a result of the several binding site mutations introduced at the interfaces of the protein which results in an overall decrease in the quaternary stability of the protein (as shown in Chapter III for the [b,□] mutant protein in the absence of D12A). Fortunately, we were able to use monomer exchange to isolate a majority of the 2:2 hybrids. Figure 5-15 summarizes the conditions and the mutant proteins used to successfully isolate nine of the possible twelve 2:2 hybrids.

Kinetic characterization of the three charge tags. The three charge tags

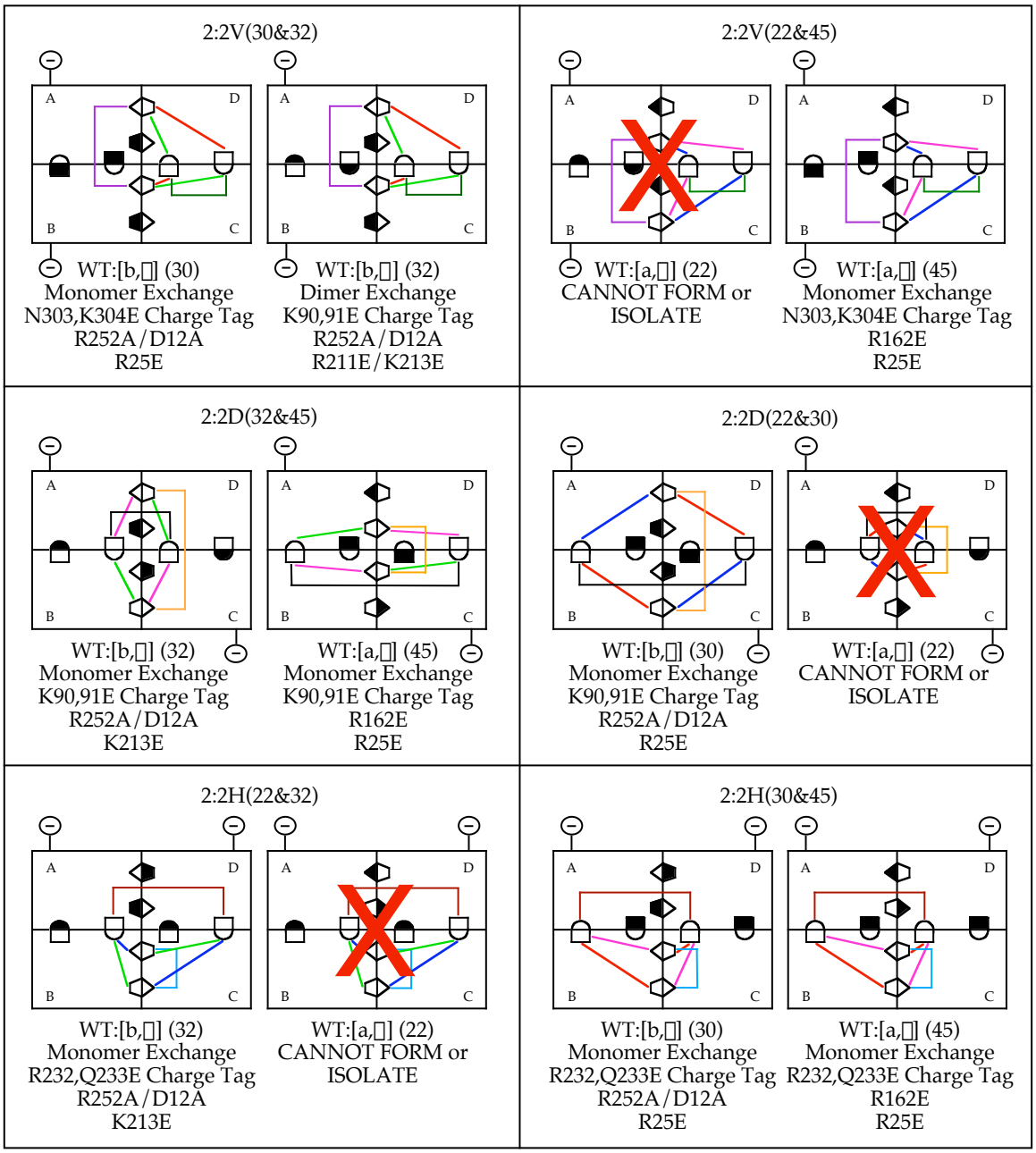

FIGURE 5-15 The nine of the twelve 2:2 hybrids that were able to be formed and isolated using strategically placed charge tags and either monomer exchange or dimer exchange with the wild-type enzyme.

were chosen primarily because of their utility in isolating either the 1:3 or 2:2 hybrids, but they were also chosen because the residues that are mutated for these surface charge tags are far removed from both the active sites and the allosteric sites. They were chosen in this manner to reduce the risk of the charge change mutations altering the binding or allosteric properties of the enzyme. To ensure this was the case, steady-state kinetic characterization was performed for each of the charge tags at pH 7.0. Kimmel and Reinhart (2001) have previously shown that the K90E/K91E charge tag has no effect upon the behavior of the enzyme. However, that characterization was performed at pH 8.0, therefore it was repeated here at pH 7.0 to be consistent with the other data.

Figure 5-16 shows the results of the allosteric characterization for the three charge tags and the wild-type enzyme at pH 7.0. Of the three charge tags, the R232E/Q233E charge tag is the only one that deviates somewhat from wild-type behavior. The binding affinity for PEP (K^{o}_{iy}) is an order of magnitude tighter than wild-type and the coupling for the R232E/Q233E mutant, Q_{ay}, is somewhat diminished. Thus, although the R232E/Q233E charge tag is approximately 26 Å and 21 Å from the two closest active sites and about 21 Å and 51 Å away from the two closest allosteric sites, it still has some effect upon the allosteric behavior of the enzyme (Schirmer and Evans, 1990). However, this is not consequential because the charge tag is on the mutated subunits, and the allosteric behavior is measured for the wild-type subunits. A summary of all the kinetic and thermodynamic parameters obtained from the analysis is found in Table 5-2.

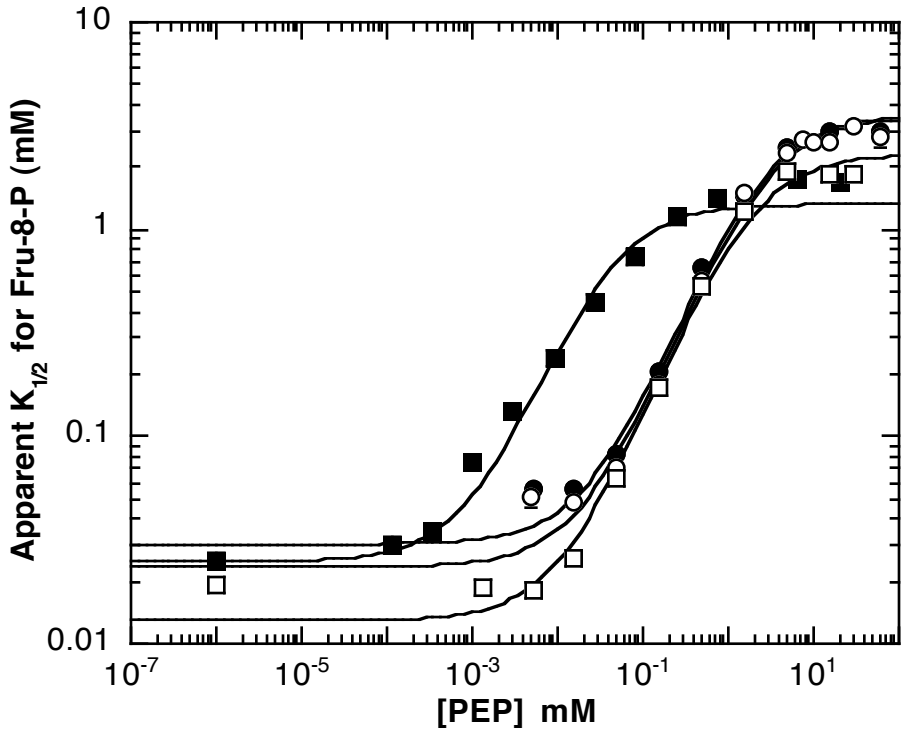

FIGURE 5-16 The dependence of the apparent $K_{1/2}$ for Fru-6-P upon increasing concentrations of the inhibitor PEP for wild-type BsPFK (●), the K90E/K91E charge tag mutant (○), the R232E/Q233E charge tag mutant (■) and the N303E/K304E charge tag mutant (□) at pH 7.0. The $K_{1/2}$ values were obtained from individual Fru-6-P saturation profiles (performed at pH 7.0 and 25°C; data not shown) at increasing concentrations of PEP. The curves correspond to the best fit of these data to Eq. 2-4 as described in the text. Error bars represent ± the standard error and are smaller than the symbol when not evident.

TABLE 5-2 Kinetic and thermodynamic parameters determined for the wild-type enzyme and the three charge tag proteins at 25°C, pH 7.0 and the [MgATP] = 3 mM

Protein	K^{o}_{ia} (mM)	K^{o}_{iy} (mM)	Q_{ay}	ΔG_{ay} (kcal/mol)
wild-type	0.030 ± 0.002	0.023 ± 0.002	0.0085 ± 0.0004	2.82 ± 0.03
K90E/K91E	0.024 ± 0.002	0.019 ± 0.002	0.0068 ± 0.0007	2.95 ± 0.07
R232E/Q233E	0.025 ± 0.002	0.00088 ± 0.00001	0.019 ± 0.001	2.34 ± 0.04
N303E/K304E	0.013 ± 0.001	0.011 ± 0.001	0.0056 ± 0.0002	3.06 ± 0.03

Utilizing dimer exchange to verify the identity of the isolated 2:2H isomer. Using the [a,□] mutant protein and the R232E/Q233E charge tag, the 2:2H(30&45) hybrid is presumed to be separated away from the 2:2V and 2:2D isomers based upon the proximity of the added negative charges between the subunits described earlier. Since all three 2:2 isomers migrate identically on a native PAGE gel, a subsequent re-hybridization experiment was performed in hopes of confirming the identity of the 2:2H(30&45) hybrid. Hybrids between the wild-type enzyme and the 2:2H isomer were attempted using conditions that allowed subunit exchange to occur only across the active site dimer-dimer interface. If the isolated 2:2 isomer is truly the 2:2H(30&45) isomer, then upon

re-hybridization, four proteins should form: the wild-type protein, the 3:1 hybrid, and the 2:2D and 2:2H isomers as shown in Fig. 5-17 *A*. On the other hand, if the hybrid was in the 2:2V orientation re-hybridization would not produce any additional species. Upon performing this experiment, and the controls, we observed three bands on a native PAGE gel verifying the identity of the 2:2 isomer as being either the 2:2H or 2:2D isomer (Fig. 5-17 *B*), as the 2:2D isomer would produce the same results. Although this procedure does not provide definitive results, it does provide further support to our distance dependence argument made earlier regarding the identification of the isolated 2:2 isomers.

Furthermore, only two bands were observed for the experimental control that was heated in the absence of PEP (lane 2 of Fig. 5-17 *B*). This is the second occasion in which PEP seems to not only stabilize the allosteric site dimer-dimer interface, but also destabilize the active site dimer-dimer interface. A destabilization of the active site interface has also been reported for a BsPFK tryptophan-shifted mutant, W179Y/Y164W. (Riley-Lovingshimer and Reinhart, 2002). It was shown in that case that upon the addition of PEP, the mutant enzyme dissociated into inactive dimers, a result consistent with our previous observations in the two preceding dimer exchange experiments. Furthermore, Schirmer and Evans (1990) have also noted a 7° shift or rotation of the active site dimer-dimer interface in a crystal structure solved with only 2-phosphoglycolate (PEP analog) bound in the allosteric sites. This conformational change at the active site dimer-dimer interface is also consistent with our data, but whether

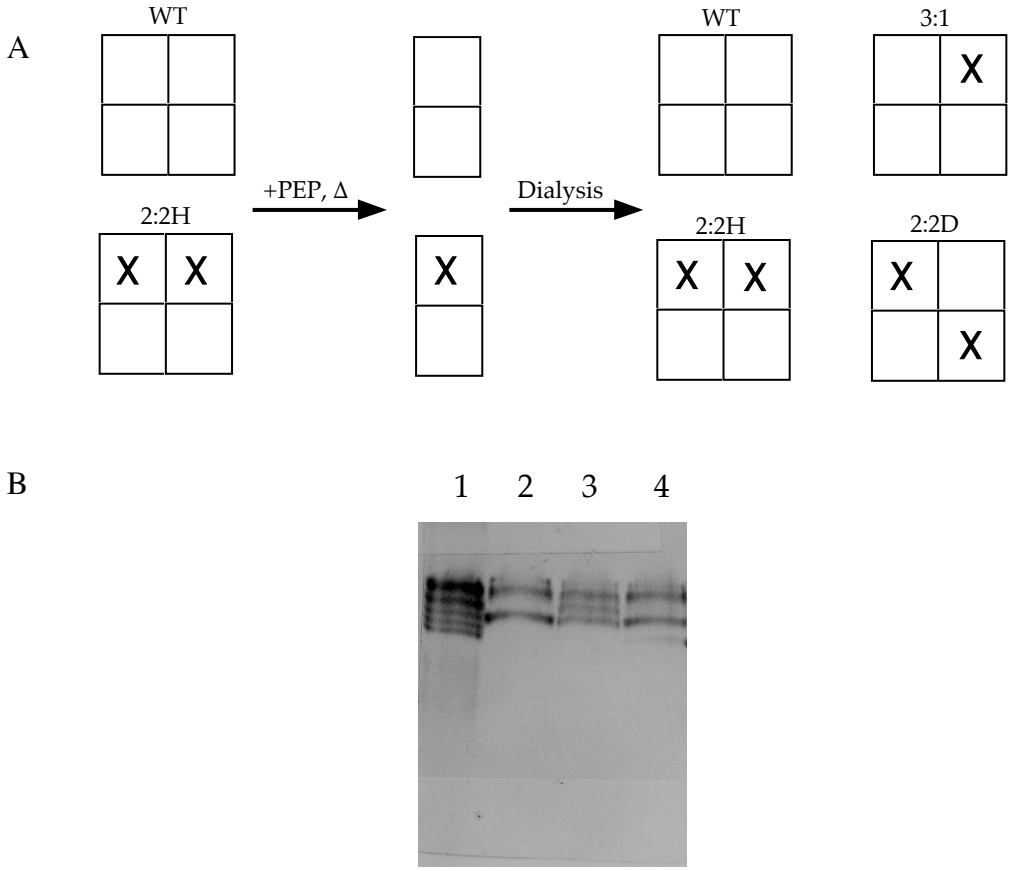

FIGURE 5-17 A schematic showing the possible proteins that can form when performing dimer exchange between wild-type and the 2:2H(30&45) hybrid, and a 10% native PAGE gel verifying the expected results. (*A*) A schematic illustrating the dimer exchange procedure as well as the expected outcome if the starting proteins are wild-type and the 2:2H(30&45) hybrid. (*B*) A 10% native PAGE gel confirming the expected results shown in A. Three bands are only observed when performing dimer exchange between wild-type and the 2:2H(30&45) hybrid when both PEP and heat are used. Lane 1 shows monomer exchange of wild-type and the [a,□] mutant protein. Lane 2 shows dimer exchange between wild-type and the 2:2H(30&45) hybrid in the absence of PEP, but in the presence of heat. Lane 3 shows dimer exchange between wild-type and the 2:2H(30&45) hybrid in the presence of both PEP and heat. Lane 4 shows dimer exchange between wild-type and the 2:2H(30&45) hybrid in the presence of PEP, but in the absence of heat.

this "destabilization" may be involved in the transmission of the allosteric signal is not evident.

Characterization of the two 2:2V(30&32) hybrids. As was previously shown, the 2:2V(30&32) hybrid can be formed and isolated with using either monomer exchange between the wild-type protein and the [b,□] mutant protein (R252A/D12A/R25E/N303E/K304E) or by using dimer exchange between the wild-type protein and the [b,□] mutant protein (R252A/D12A/R211E/K213E/K90E/K91E). Either way, the same six pair-wise allosteric interactions are isolated (refer to either Figs. 5-2 or 5-13). Thus, if our distance dependence hypothesis is correct regarding the relative separations and subsequent identification of the 2:2 isomers via monomer exchange, then the allosteric couplings (Q_{ay} or ΔG_{ay}) determined at pH 6.0, 7.0 and 8.0 for both of the aforementioned 2:2V(30&32) hybrids should be identical, thus supporting our theory.

Figures 5-18 *A*, *B* and *C* show the results for this characterization, and the measured couplings for both the dimer exchanged and monomer exchanged 2:2V hybrids are identical, within error, at pH 6.0, 7.0 and 8.0. Some minor differences are evident regarding the binding affinities of both Fru-6-P and PEP (K^{o}_{ia} and K^{o}_{iy}) at pH 6.0 and 8.0, but more importantly, the overall measured couplings are the same. Thus, the charge tag rationale used for isolating eight of the 2:2 hybrids has been further validated. Table 5-3 summarizes the parameters obtained from the above characterization.

FIGURE 5-18 The dependence of the apparent $K_{1/2}$ for Fru-6-P upon increasing concentrations of the inhibitor PEP for the 2:2V(30&32) hybrid obtained by monomer exchange utilizing the N303E/K304E charge tag (●) and the 2:2V(30&32) hybrid obtained by dimer exchange utilizing the K90E/K91E charge tag (○) at pH 6.0, 7.0 and 8.0. The $K_{1/2}$ values were obtained from individual Fru-6-P saturation profiles (at 25°C and the concentration of MgATP equal to 3 mM; data not shown) at increasing concentrations of PEP. The curves correspond to the best fit of these data to Eq. 2-4 as described in the text. Error bars represent ± the standard error and are smaller than the symbol when not evident. (*A*) pH 6.0. (*B*) pH 7.0. (*C*) pH 8.0.

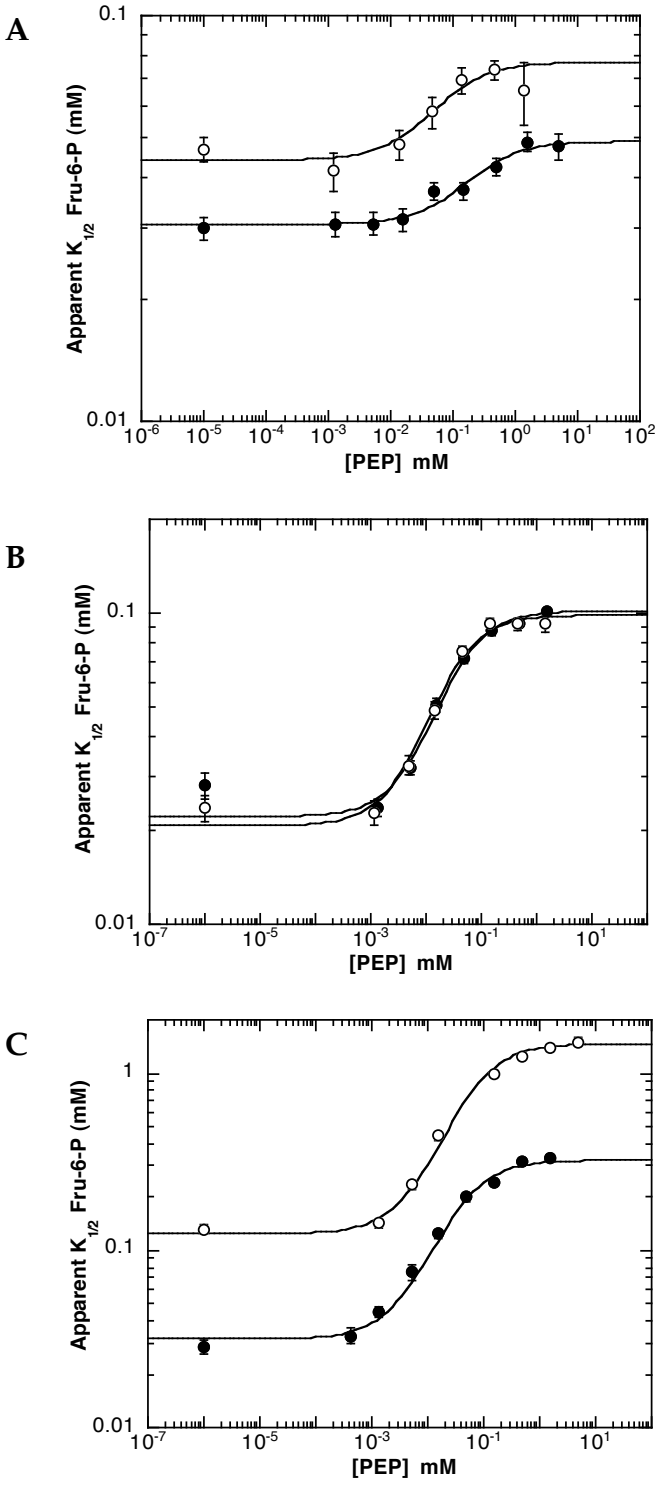
A
0.1
0.01
Apparent $K_{1/2}$ Fru-6-P (mM)
10^{-6} 10^{-5} 10^{-4} 10^{-3} 10^{-2} 10^{-1} 10^{0} 10^{1} 10^{2}
[PEP] mM
B
0.1
0.01
Apparent $K_{1/2}$ Fru-6-P (mM)
10^{-7} 10^{-5} 10^{-3} 10^{-1} 10^{1}
[PEP] mM
C
1
0.1
0.01
Apparent $K_{1/2}$ Fru-6-P (mM)
10^{-7} 10^{-5} 10^{-3} 10^{-1} 10^{1}
[PEP] mM

TABLE 5-3 Kinetic and thermodynamic parameters determined for the two 2:2V(30&32) hybrids isolated via the [b,□] or [b,□] mutant proteins at 25°C, pH 6.0, 7.0, 8.0 and [MgATP] = 3 mM

Mutant Protein Used[a]	K^{o}_{ia} (mM)	K^{o}_{iy} (mM)	Q_{ay}	ΔG_{ay} (kcal/mol)
pH 6.0				
[b,□]	0.031 ± 0.001	0.13 ± 0.06	0.62 ± 0.04	0.28 ± 0.04
[b,□]	0.044 ± 0.003	0.036 ± 0.02	0.57 ± 0.05	0.33 ± 0.05
pH 7.0				
[b,□]	0.022 ± 0.001	0.007 ± 0.001	0.22 ± 0.01	0.90 ± 0.03
[b,□]	0.021 ± 0.002	0.005 ± 0.001	0.21 ± 0.02	0.92 ± 0.06
pH 8.0				
[b,□]	0.032 ± 0.002	0.004 ± 0.001	0.098 ± 0.01	1.37 ± 0.01
[b,□]	0.12 ± 0.01	0.005 ± 0.001	0.085 ± 0.005	1.46 ± 0.04

[a]Monomer exchange was used for the [b,□] mutant protein utilizing the N303E/K304E charge tag. Dimer exchange was used for the [b,□] mutant protein utilizing the K90E/K91E charge tag.

Discussion

Often bacterial enzymes are chosen over their eukaryotic counterparts to study because they are less complex structurally, and in the realm of allosterism, are often regulated by fewer molecules. This is the case for phosphofructokinase (Bloxham and Lardy, 1973; Blangy et al., 1968), however even the bacterial form of the enzyme from *Bacillus stearothermophilus* still has the potential for 28 total pair-wise allosteric interactions (10 of which are unique) between its four active

sites and four allosteric sites. Thus, the allosteric complexity of even this simple homotetramer had to be reduced in order to address the question of how allosteric regulation occurs in proteins, and more specifically, what the roles of each of the 10 unique allosteric interactions are in the inhibitory response of BsPFK.

In order to characterize four of the ten allosteric interactions, 1:3 hybrids (1|1) were previously constructed to contain only one native active site and one native allosteric site. By doing this and alternating which active site and allosteric site remained native, we were able to successfully isolate the four heterotropic interactions found in the tetramer and determine their relative contributions to the inhibitory process (Chapters III and IV). Thus, to address the roles of the six remaining homotropic interactions, the same approach is taken, however instead of using the 1:3 hybrids, the 2:2 hybrids (2|2) are used which contain two native active sites and two native allosteric sites. Again, by alternating which two active sites and which two allosteric sites remain native, six unique 2:2 hybrids can form, with each 2:2 hybrid isolating a different set of six pair-wise allosteric interactions. Two of these six isolated interactions are two of the six pair-wise homotropic interactions found in the tetramer (one for each ligand), and by isolating two at a time via the 2:2 hybrids, we are able to characterize their individual roles in the inhibitory response (see Chapter VI). Moreover, two different mutant proteins (either [a,□], [a,□], [b,□], or the [b,□] mutant protein) can be used to form each 2:2 hybrid, resulting in a total of twelve possible 2:2 hybrids, all of which were shown in Fig. 5-2. Thus, it was the

goal of this chapter to describe how we formed and isolated these twelve 2:2 hybrids, and the subsequent chapter summarizes their allosteric characterizations (Chapter VI).

Just like the 1:3 hybrids, a charge tag (either K90E/K91E, R232E/Q233E or N303E/K304E) was added to the surface of the mutant subunits to isolate the 2:2 hybrids; however, an important determinant in the efficiency of the charge tag in separating the three 2:2 isomers that form when using the monomer exchange procedure was the solvent accessibility of the R211E/K213E mutations in the allosteric site (□-side). We arrived at this conclusion because separation of the 2:2 isomers was only observed when making hybrids between wild-type and the [a,□] or [b,□] mutant proteins, and not with the [a,□] or [b,□] mutant proteins. However, separation was observed for the latter two mutant proteins when the R211E/K213E mutations were added to the wild-type subunits. Thus, we determined that the 2:2 isomers separated because of the differences in the overall distances between each pair of charge tags on the three 2:2 isomers. Furthermore, since 2:2 isomer separation was not observed when using either the [a,□] or [b,□] mutant proteins, we determined that the solvent accessibility of the R211E/K213E mutations on the □-side of the allosteric sites were interfering with the landscape of charges on the surface of the protein, and prohibiting separation of the three 2:2 isomers.

The crystal structure was then examined to determine if the R211E/K213E mutations were near the surface of the protein, and upon inspection, the side-chain of the R211 residue is in fact at the edge of the binding

pocket and at the surface of the protein (Schirmer and Evans, 1990). Thus, we surmised that the R211E mutation was interfering with the effectiveness of the charge tag. Therefore, we used the K213E mutation alone instead of the R211E/K213E double mutation eliminating the adverse effects previously encountered with the double mutation.

Using steady-state kinetics, the K213E mutation was shown to be suitable in deterring PEP binding by over two orders of magnitude when compared to wild-type, thus it was utilized in making hybrids. Unfortunately, the 2:2 hybrids (and others) were unable to form when the K213E mutation was used in conjunction with the R162E mutation in the active site (the [a,□] mutant protein), a problem reminiscent to the one encountered in forming hybrids between wild-type and the [b,□] or [b,□] mutant proteins in the absence of the D12A mutation. Since D12 is located on the b-side of the active site and R162 is located on the a-side of the active site, the D12A mutation was unable to be used because it would have been in the wild-type subunits, complicating the allosteric characterizations. Thus, because each 2:2 hybrid can be formed two different ways, we were able to form the three relevant 2:2 hybrids by using the other mutant protein, and we just disregarded the problems encountered in forming hybrids with the K213E/R162E mutant protein.

With nine of the twelve possible the 2:2 hybrids now successfully formed, including at least one of each of the six unique 2:2 hybrids, the next formidable task was figuring out a way to separate each one of them individually so that we could characterize the homotropic interactions. From previous results using the

K90E/K91E charge tag to isolate the 1:3 hybrids, we found that the K90E/K91E charge tag successfully separated the 2:2D isomer away from the 2:2H and 2:2V isomers because of the relative positions of the lysine to glutamate mutations on the three different 2:2 isomers. As the crystal structure revealed (Schirmer and Evans, 1990), the positions of the lysines that were mutated for the K90E/K91E charge tag were on the same ends of the protein in the 2:2D isomer, approximately 50 Å apart, allowing all four lysine to glutamate mutations to present their negative charges to the positively charged Mono-Q bead at the same time. The 2:2H and 2:2V isomers on the other hand, have the lysine to glutamate mutations on the opposite ends of the protein allowing only two of the four negative charges to be presented to any given positively charged Mono-Q bead. Thus, the 2:2D isomer was retained longer on the column because of the shorter distance between it's pair of charge tags, providing the necessary separation and subsequent isolation of the 2:2D(32&45) and 2:2D(22&30) hybrids.

Using this same rationale, we constructed two additional charge tags, the R232E/Q233E charge tag and the N303E/K304E charge tag, to separate the 2:2H and 2:2V isomers respectively. The R232E/Q233E charge tag performed similarly to that of the K90E/K91E charge tag in producing a doublet and a single peak in the elution profile for separating the 2:2 isomers. More importantly however, the R232E/Q233E charge tag was shown to be successful in isolating the 2:2H isomer. More specifically, the R232E/Q233E charge tag isolated the 2:2H(22&32) and 2:2H(30&45) hybrids.

The 2:2V isomer was isolated using the N303E/K304E charge tag. However, since the distances between each pair of N303E/K304E charge tags on the three isomers are not as different from one another like they are for the K90E/K91E and R232E/Q233E charge tagged proteins, the separation is reduced, and an additional purification step was required to ensure no contamination of the other isomers occurred in isolating the 2:2V isomer. With the N303E/K304E charge tag, we were able to isolate both the 2:2V(30&32) hybrid and the 2:2V(22&45) hybrid. In summary, by using the monomer exchange procedure and the three different strategically placed charge tags (K90E/K91E, R232E/Q233E and N303E/K304E), we were able to successfully isolate and identify all six of the unique 2:2 hybrids, plus two additional 2:2 hybrids for a total of eight.

In order to further support our charge tag distance-dependence theory, we devised an additional exchange procedure that exchanged dimers instead of monomers. Unfortunately, due to the decreased quaternary stability of the mutant proteins and other unknown factors, the dimer exchange procedure was only successful when applied to the wild-type enzyme and the [b,□] mutant protein. With the addition of saturating PEP during the exchange process, exchange occurred only across the active site dimer-dimer interface, thus the 2:2V isomer was the only 2:2 hybrid that could form. Furthermore, we specifically formed the 2:2V(30&32) hybrid, a hybrid we had also obtained using the monomer exchange procedure with the [b,□] mutant protein and the N303E/K304E charge tag. The fact that the functionalities of both of these

hybrids are nearly identical helps to validate the rationale we have used for the separation and identification of the other 2:2 hybrids.

An additional experiment was performed to further corroborate these results and involved using a dimer exchange re-hybridization experiment of the 2:2H(30&45) hybrid and the wild-type enzyme. Three bands were observed on a native PAGE gel after the re-hybridization which corresponded to the wild-type enzyme, the 3:1 hybrid and a mixture of the 2:2D(32&45) and 2:2V(30&45) hybrids. Although the 2:2D(32&45) hybrid would produce the identical results, the experiment only substantiates our earlier conclusions regarding the identity of our isolated 2:2 hybrids using the monomer exchange process and the distance-dependence theory regarding the strategic placement of the three different charge tags. Thus, with nine of the 2:2 hybrids now isolated and their identities known, the allosteric characterizations of the six homotropic interactions can now be performed and the roles of the six homotropic interactions in the inhibition process determined.

CHAPTER VI

THE ALLOSTERIC CHARACTERIZATIONS OF THE 2:2 HYBRIDS

Introduction

Phosphofructokinase from *Bacillus stearothermophilus* (BsPFK) is a homotetramer containing four active sites and four allosteric sites, all of which are located along respective dimer-dimer interfaces of the protein (Schirmer and Evans, 1990). Due to this composition, twenty-eight pair-wise allosteric interactions are possible, ten of which are unique. There are four heterotropic interactions (22 Å, 30 Å, 32 Å and 45Å – 4 copies of each), three homotropic interactions between active sites (47 Å, 45 Å and 28 Å – 2 copies of each), and three more homotropic interactions between allosteric sites (39.9 Å, 23 Å and 40 Å – 2 copies of each). With this allosteric complexity it is impossible to define the role each of these allosteric interactions plays in the inhibitory response within the native tetramer. To begin to dissect these roles, we previously created and isolated BsPFK heterotetramers (1:3 hybrids) in which only one active site and one allosteric site possess high affinity for both substrate and inhibitor. This allowed us to quantify the allosteric effect associated with each of the four unique heterotropic interactions individually (Chapters III and IV). However, the 1:3 hybrids did not provide any direct information regarding the six remaining homotropic interactions found in the tetramer or how multiple allosteric interactions combine and influence one another in an oligomeric protein.

In this chapter we again use heterotetramers, however this time they

contain two native active sites and two native allosteric sites (2:2 hybrids). By increasing the number of native active sites and allosteric sites by one, we have increased the allosteric complexity to that of a dimer, requiring the analysis of six allosteric interactions at a time: one homotropic interaction between active sites, one homotropic interaction between allosteric sites and two copies of two different heterotropic interactions. We report here the allosteric characterizations of nine of the twelve possible 2:2 hybrids; those that form between the wild-type enzyme and three mutant proteins ([a,□], [b,□] or [b,□]), all of which have been previously formed, isolated and identified in Chapter V.

Deciphering the role of the homotropic interactions. From the allosteric characterizations of these nine 2:2 hybrids, we will be able to address a number of issues, the first of which being the role each of the six unique homotropic interactions play in the inhibition process. This is achieved by measuring the Hill numbers for both Fru-6-P binding and PEP binding in the absence and saturating presence of the heterotropic ligand, and using these values to calculate the allosteric couplings for the homotropic interactions in both the absence and saturating presence of the heterotropic ligand (Q_{aa}, $Q_{aa/yy}$, Q_{yy} and $Q_{yy/aa}$) with the following equation:

$$Q_{homo} = \left(\frac{n_H}{2 - n_H} \right)^2 \qquad (6\text{-}1)$$

where Q_{homo} is either Q_{aa} (coupling between Fru-6-P binding sites in the absence of PEP), $Q_{aa/yy}$ (coupling between Fru-6-P binding sites in the saturating presence of PEP), Q_{yy} (coupling between PEP binding sites in the absence of

Fru-6-P) or $Q_{yy/aa}$ (coupling between PEP binding sites in the saturating presence of Fru-6-P) and n_H is equal to the Hill number measured for either Fru-6-P or PEP binding at the appropriate heterotropic ligand concentration. Finally, the couplings are substituted appropriately into Eq. 6-2 to determine the contributions of the homotropic interactions to the measured coupling determined for the 2:2 hybrid (Reinhart, 1988).

$$Q_{2:2\,hybrid} = Q_{ay1} \cdot Q_{ay2} \cdot \left(\frac{Q_{yy/aa}}{Q_{yy}}\right)^{1/2} \cdot \left(\frac{Q_{aa/yy}}{Q_{aa}}\right)^{1/2} \qquad (6\text{-}2)$$

where $Q_{2:2\,hybrid}$ is equal to the measured coupling (Q_{ay}) for the 2:2 hybrid of interest, Q_{ay1} and Q_{ay2} are the couplings measured for the two heterotropic interactions isolated within that particular 2:2 hybrid (measured previously via the 1:3 hybrids), and Q_{aa}, $Q_{aa/yy}$, Q_{yy} and $Q_{yy/aa}$ are the couplings calculated for the two homotropic interactions isolated within that particular 2:2 hybrid in the absence and saturating presence of the heterotropic ligand. Equation 6-2 can also be considered in coupling free energy terms by simply using the Gibbs free energy equation to convert all of the allosteric couplings into coupling free energies (Eq. 2-6).

$$\Delta G_{2:2\,hybrid} = \Delta G_{ay1} + \Delta G_{ay2} + \Delta G_{homo\_allos} + \Delta G_{homo\_active} \qquad (6\text{-}3)$$

where $\Delta G_{2:2\,hybrid}$ is equal to the measured coupling free energy for the 2:2 hybrid of interest, ΔG_{ay1} and ΔG_{ay2} are the coupling free energies measured for the two heterotropic interactions isolated within that particular 2:2 hybrid, ΔG_{homo_allos} is the coupling free energy contribution measured for the homotropic interaction

between allosteric sites and ΔG_{homo_active} is the coupling free energy contribution measured for the homotropic interaction between active sites. Moreover, ΔG_{homo_allos} and ΔG_{homo_active} are further defined to be equal to the following:

$$\Delta G_{homo\_allos} = \frac{\Delta G_{yy/aa} \cdot \Delta G_{yy}}{2} \qquad (6\text{-}4)$$

$$\Delta G_{homo\_active} = \frac{\Delta G_{aa/yy} \cdot \Delta G_{aa}}{2} \qquad (6\text{-}5)$$

Thus, in order for the homotropic interactions to augment the inhibitory effect (ΔG_{homo_allos} and $\Delta G_{homo\_active} > 0$), the homotropic couplings in the absence of the heterotropic ligand (Q_{yy} and Q_{aa}) must be greater than the homotropic couplings in the saturating presence of the heterotropic ligand ($Q_{yy/aa}$ and $Q_{aa/yy}$). However, if Q_{yy} and Q_{aa} are less than $Q_{yy/aa}$ and $Q_{aa/yy}$ (ΔG_{homo_allos} and $\Delta G_{homo\_active} < 0$), then the homotropic interactions will diminish the inhibitory effect. Thus, the net change in the Hill numbers measured for Fru-6-P and PEP binding must diminish saturation of the other ligand to augment the apparent heterotropic inhibition. Conversely, if the Hill numbers increase upon saturation of the heterotropic ligand, heterotropic inhibition will diminish.

Subsaturating heterotropic cooperativity. Another issue we will be able to address from the allosteric characterizations of the 2:2 hybrids is subsaturating heterotropic cooperativity. This phenomenon was first noted by Weber (1972 and 1975) and further developed by Reinhart (1988) to describe the apparent positive cooperativity measured for ligand binding at subsaturating concentrations of the heterotropic ligand when the heterotropic couplings of the

two heterotropic interactions are not equal to 1 (Q_{ay1} and $Q_{ay2} \neq 1$). However, before we explain why subsaturating heterotropic cooperativity occurs, one needs to recall the following: (1) the binding of Fru-6-P influences the binding of PEP to the same extent as PEP binding influences Fru-6-P binding and (2) Fru-6-P and PEP antagonize each other's binding. Consequently, subsaturating heterotropic cooperativity occurs because in the presence of a subsaturating amount of PEP, the binding of the first equivalent of Fru-6-P decreases the degree of saturation of PEP binding, making it easier for the second equivalent of Fru-6-P to bind leading to an apparent positive cooperativity in Fru-6-P binding. This apparent positive cooperativity will continue to increase until a maximum Hill number is reached at which point the apparent positive cooperativity will decrease with increasing concentrations of PEP (Reinhart, 1988). The concentration of PEP that produces the greatest amount of Fru-6-P cooperativity is also related to the overall coupling measured for the 2:2 hybrid ($Q_{2:2\,hybrid}$) as well as the K^o_{iy} (Reinhart, 1988). Thus, if the K^o_{iy} is relatively high and the coupling is small, detecting subsaturating heterotropic cooperativity within our PEP concentration range becomes less feasible. Moreover, if one of the heterotropic couplings is equal to 1 ($Q_{ay1} = 1$ or $Q_{ay2} = 1$; i.e. the 30 Å heterotropic interaction at pH 6.0), then no subsaturating heterotropic cooperativity will occur. This is because in the absence of one of the heterotropic couplings, each pair of one active site and one allosteric site function independently of each other, with the first binding equivalent of Fru-6-P only affecting one allosteric site instead of two (affects two when Q_{ay1} and

$Q_{ay2} \neq 1$), eliminating the possibility of an apparent positive cooperativity at subsaturating levels of PEP.

How the pair-wise allosteric interactions combine in an oligomer. The third and most important issue we will be able to address from characterizing the 2:2 hybrids is how the six allosteric interactions combine in each of the nine isolated 2:2 hybrids. With the contributions of the four heterotropic interactions previously determined, and after measuring the individual couplings for each of the 2:2 hybrids and the contributions of the six homotropic interactions, we will be equipped with the means to determine which allosteric model most accurately describes the observed allosteric behavior for each of the nine 2:2 hybrids. Therefore, we will be able to establish the validity of not only the most popular models used to describe allosteric behavior, but also to determine for the first time experimentally if the predictions made by Reinhart (1988) regarding the allosteric response of a symmetrical dimer (analogous to the 2:2 hybrid) are accurate.

The two most widely accepted models used to describe an allosteric effect are the concerted (Monod et al., 1965) and sequential models (Koshland et al., 1966). The concerted or MWC model assumes that the conformation of all the subunits in an oligomer are identical and are subject to a concerted conformational change upon the binding of an allosteric ligand. Thus, when invoking the concerted model, an oligomeric protein at no time can contain two or more conformationally distinct subunits. The sequential or KNF model on the other hand, does allow for multiple conformational states within an

oligomer. Furthermore, as the name implies, the sequential model assumes that the binding of an allosteric ligand to an oligomer induces a conformational change localized mainly to that ligand-bound subunit, and subsequent binding events are necessary to complete the entire allosteric transition.

Applying these models to a dimeric enzyme, we can make several predictions regarding the observed allosteric effect as shown in Fig. 6-1. If the dimer contains one active site and one allosteric site per subunit (the two active sites are denoted A and B while the two allosteric sites are denoted X and Y, with A and X on one subunit and B and Y on the other), and one equivalent of PEP binds to either X or Y, then the concerted model would predict an equivalent influence upon Fru-6-P binding at A regardless of the location of PEP binding. Furthermore, the second equivalent of PEP binding to the enzyme would provide no additional allosteric effect on Fru-6-P binding to A because the entire allosteric effect was already realized upon the first binding equivalent of PEP. However, the average measured allosteric effect of both binding events would be equivalent to the measured allosteric effect for the first binding event.

The sequential model would predict that only binding PEP to X would incur an allosteric effect on Fru-6-P binding to A, while no allosteric effect would be measured for Fru-6-P binding to A if PEP was bound to Y. Moreover, if the latter case occurred, then the second equivalent of PEP binding to X would produce the entire allosteric effect upon binding Fru-6-P to A, and would be equivalent to the allosteric effect measured for Fru-6-P binding to A if the first equivalent of PEP bound to X. Thus, the average allosteric effect measured for

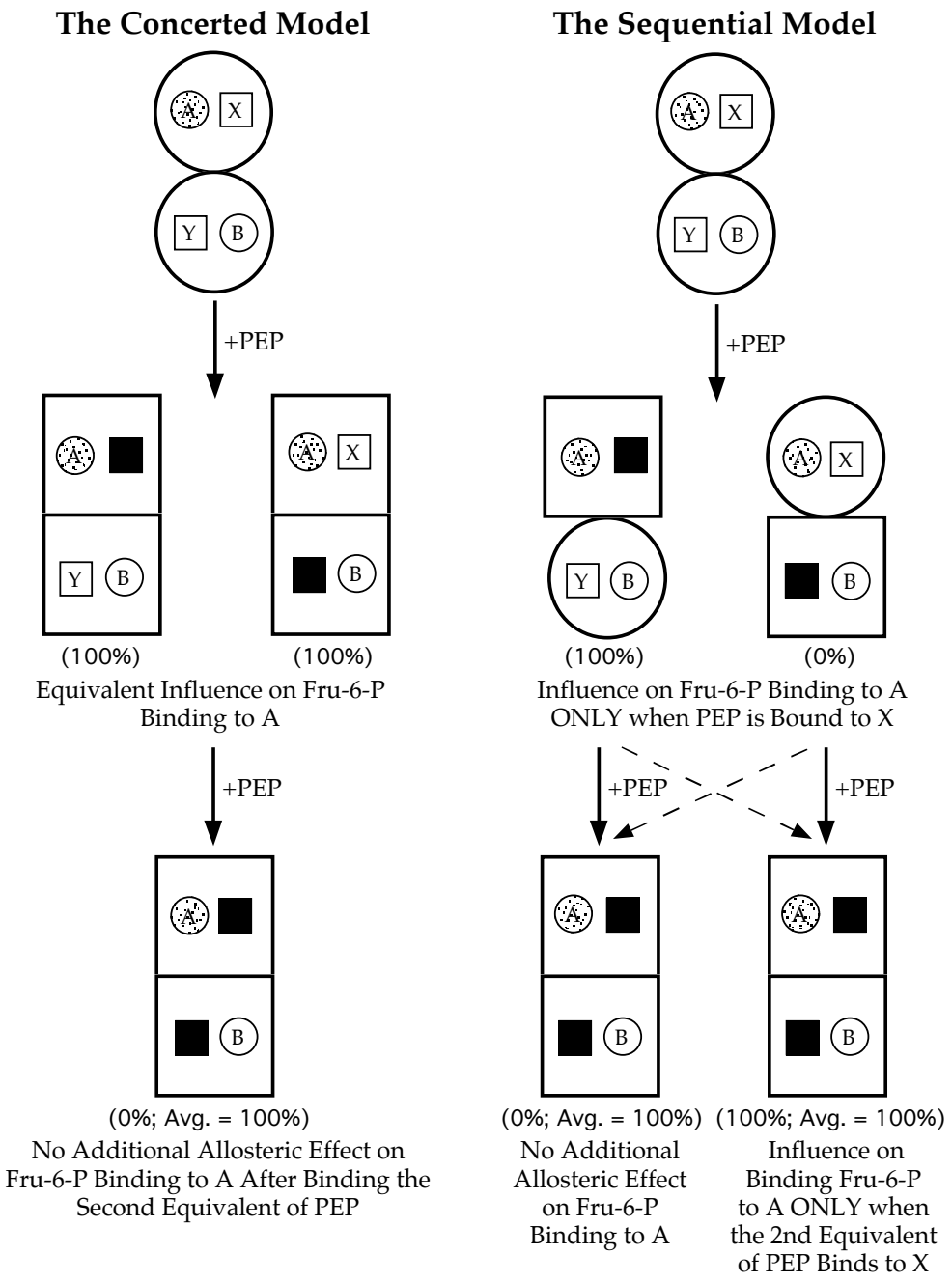

FIGURE 6-1 A schematic depicting the predictions regarding the observed allosteric effect in either the concerted or sequential models on the binding of one equivalent of Fru-6-P to the A site.

both binding events is equivalent, regardless of the pathway of binding, to the measured allosteric effect that occurred if PEP initially bound to X.

Taking it one step further and applying these predictions to the 1:3 and 2:2 hybrids and more specifically the case of the 2:2V(30&32) hybrid, the concerted model would predict that the coupling free energies measured for the 30 Å and 32 Å heterotropic interactions would be equivalent (first binding event measured via the 1:3 hybrids), and that the coupling free energy measured for the 2:2V(30&32) hybrid would not be any different than the couplings measured for the heterotropic interactions ($\Delta G_{30} = \Delta G_{32} = \Delta G_{2:2V(30\&32)}$). The sequential model on the other hand would predict that the coupling free energy of one of the two heterotropic interactions would be zero, while the other coupling free energy would be equivalent to the coupling free energy measured for the 2:2V(30&32) hybrid ($\Delta G_{30} = 0;\ \Delta G_{32} = \Delta G_{2:2V(30\&32)}$ or $\Delta G_{32} = 0;\ \Delta G_{30} = \Delta G_{2:2V(30\&32)}$). These scenarios regarding the expected data are shown in Fig. 6-2 *A*.

The biggest advantage for both of these models is their simplistic nature in describing the allosteric effect, however it is this advantage that is also their downfall. In considering only a finite number of conformationally active or inactive states, and hence an "all-or-none" type of allosteric effect, the overall allosteric freedom allowed for an oligomeric protein is constrained and oversimplified. A more suitable model would consider any number of ligand-bound states with the potential for each of those states to be distinct both in their overall conformation and in their allosteric properties. These objectives are achieved when using a linked function approach in analyzing the allosteric

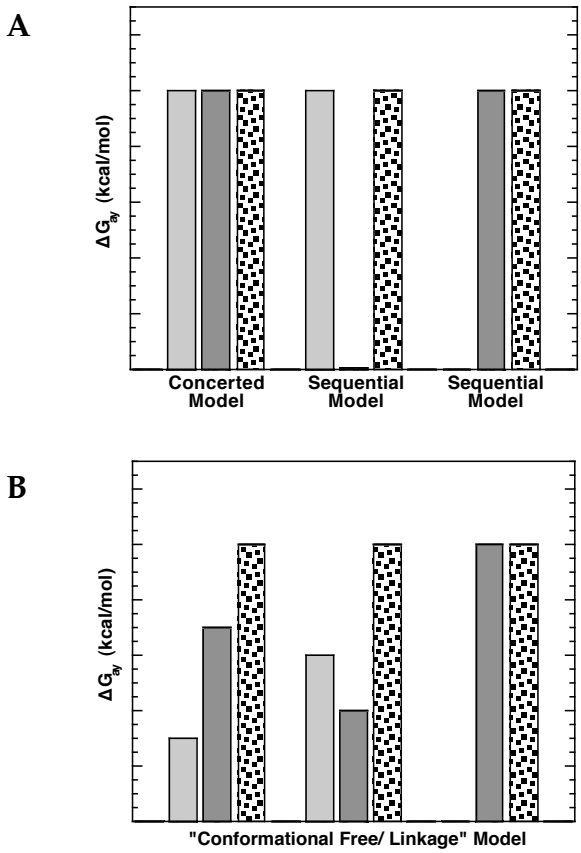

FIGURE 6-2 The data predictions for the concerted, sequential and conformational free/linkage models as they pertain to the 2:2V(30&32) hybrid. The light gray bar represents the expected measured coupling free energy for the 1:3 hybrid isolating the 30 Å heterotropic interaction (ΔG_{30}). The dark gray bar represents the expected measured coupling free energy for the 1:3 hybrid isolating the 32 Å heterotropic interaction (ΔG_{32}). The polka-dotted bar represents the expected measured coupling free energy for the 2:2V(30&32) hybrid ($\Delta G_{2:2V(30\&32)}$). (*A*) Far left: The predictions of the concerted model ($\Delta G_{30} = \Delta G_{32} = \Delta G_{2:2V(30\&32)}$). Middle and Far Right: The predictions of the sequential model ($\Delta G_{30} = 0$; $\Delta G_{32} = \Delta G_{2:2V(30\&32)}$ or $\Delta G_{32} = 0$; $\Delta G_{30} = \Delta G_{2:2V(30\&32)}$). (*B*) The conformational free/linkage model predictions ($\Delta G_{30} + \Delta G_{32} = \Delta G_{2:2V(30\&32)}$).

effect (the "conformational free/linkage" model), and predicts two major things; (1) that the coupling free energies are unique in magnitude, and (2) that the sum of the heterotropic coupling free energies and the coupling free energy contribution from the homotropic interactions is always equal to the overall coupling free energy measured for the protein (Eq. 6-3). Applying these statements to the same aforementioned 2:2V(30&32) hybrid, the coupling free energies of the 30 Å and 32 Å heterotropic interactions could be anything (even zero), but their sum in the absence of any homotropic contributions would be equal to the coupling free energy measured for the 2:2V(30&32) hybrid ($\Delta G_{30} + \Delta G_{32} = \Delta G_{2:2V(30\&32)}$). This prediction for the data is shown in Fig. 6-2 *B*.

From our work regarding the 1:3 hybrids and the wild-type control hybrid (4|1), we already know that the concerted and sequential models are insufficient in describing the observed allosteric effect between Fru-6-P and PEP and *vice versa* because the coupling free energies measured for each of the four heterotropic interactions are unique in magnitude (Chapters III and IV). However, with the information gained from characterizing the 2:2 hybrids, we will be able to determine what kind of role the homotropic interactions play in the allosteric response (specifically inhibition) and also show experimentally if the predictions made by Reinhart (1988) regarding the expected allosteric behavior of a symmetrical dimer are substantiated.

Materials and methods

The materials and methods used for the experiments described in this chapter are as described in Chapter II. The Fru-6-P enzymatic activity

measurements and data analysis were performed as described in Chapter II. The formation, isolation and identification of the nine 2:2 hybrids were performed as described in Chapter V.

Experimental determination of PEP cooperativity. As previously mentioned, the relative couplings for the homotropic interactions between both the active sites and the allosteric sites can be determined from the Hill number (n_H) obtained between the pertinent binding sites in both the absence and saturating presence of the heterotropic ligand. For determining Q_{aa} and $Q_{aa/yy}$, no additional experiments are required as the relevant data are already collected from determining Q_{ay} for each of the nine 2:2 hybrids. The Hill numbers obtained from the first phase of the individual Fru-6-P saturation profiles in the absence and saturating presence of PEP are fit to Eqs. 6-6 and 6-7 to determine Q_{aa} and $Q_{aa/yy}$ respectively.

$$Q_{aa} = \left(\frac{n_H}{2 - n_H}\right)^2 \qquad (6\text{-}6)$$

$$Q_{aa/yy} = \left(\frac{n_H}{2 - n_H}\right)^2 \qquad (6\text{-}7)$$

To determine the cooperativity between the allosteric sites, an additional experiment is required. Instead of measuring the $K_{1/2}$ for Fru-6-P at increasing concentrations of PEP, the $K_{1/2}$ for PEP is determined at increasing concentrations of Fru-6-P. The same experimental procedure outlined in Chapter II for assaying enzymatic activity as a function of PEP concentration is used in determining the $K_{1/2}$ for PEP, except the Fru-6-P and PEP components

are switched. Furthermore, since Fru-6-P is a substrate of PFK, the number of phases observed in the individual PEP saturation profiles differs upon the concentration of Fru-6-P used. At low Fru-6-P only one phase in the data is observed because a small amount of Fru-6-P is bound to the high affinity active sites; thus, upon the addition of PEP, only the effect from binding PEP to the high affinity allosteric sites is observed because there is so little PFK activity to begin with. Therefore, to determine the $K_{1/2}$ for PEP and the Hill number for the native allosteric sites, these data are fit to the following equation:

$$v = \left[\frac{\left[\text{Max}\Delta \cdot [Y]^{n_H} + V_o \cdot {K_{1/2}}^{n_H} \right] + V_o \cdot [Y]^{n_H}}{{K_{1/2}}^{n_H} + [Y]^{n_H}} \right] \qquad (6\text{-}8)$$

where v equals the steady-state rate of turnover, MaxΔ represents the maximal change in activity, [Y] equals the concentration of PEP, V_o equals the initial rate of turnover at a particular Fru-6-P concentration, $K_{1/2}$ is the concentration of PEP resulting in half maximal activity also at that particular concentration of Fru-6-P, and n_H is the Hill coefficient.

At higher Fru-6-P concentrations, the binding of PEP to the mutated allosteric sites can now be observed, due to the initially greater activity, resulting in two phases in the data. The first phase corresponds to the effect on PFK activity from PEP binding to the high affinity allosteric sites, while the second phase corresponds to the effect on PFK activity from PEP binding to the low affinity (mutated) allosteric sites. These data are fit to the Eq. 6-9 to determine the binding affinities of both types of allosteric sites, however often, the second phase is not well defined and the Hill number has to be removed

from the second half of the equation to obtain a decent fit of all the data.

$$v = \left[\frac{\left[\mathrm{Max}\Delta \cdot [Y]^{n_H} + V_o \cdot K_{1/2}{}^{n_H} + V_o \cdot [Y]^{n_H}\right]}{K_{1/2}{}^{n_H} + [Y]^{n_H}}\right] + \left[\frac{\left[\mathrm{Max}\Delta' \cdot [Y]^{n'_H} + V'_o \cdot K'_{1/2}{}^{n'_H} + V'_o \cdot [Y]^{n'_H}\right]}{K'_{1/2}{}^{n'_H} + [Y]^{n'_H}}\right] \qquad (6\text{-}9)$$

where MaxΔ′, V'_o, $K'_{1/2}$ and n'_H refer to the maximal change in activity, the initial rate of turnover, apparent dissociation parameter for PEP and the Hill coefficient for the low affinity (mutated) allosteric site population, respectively.

At saturating levels of Fru-6-P, the data returns to one phase again because now the Fru-6-P is bound to more than just the native active sites, thus more PEP is required to inhibit the enzyme. Therefore, only inhibition from the native allosteric sites is observed, not because the mutated allosteric sites are unable to inhibit the enzyme, but rather due to the inability to use high enough levels of PEP to observe the allosteric effect. Thus, in these cases the data are fit to Eq. 6-8 to determine the binding affinity for PEP at the high affinity allosteric sites. Figure 6-3 displays these three trends in the data based upon the concentration of Fru-6-P used and the necessity to alter the equations used to fit the resulting data.

The couplings for the homotropic interactions between the allosteric sites, Q_{yy} and $Q_{yy/aa}$, are determined from the Hill numbers obtained from the individual PEP saturation profiles in the absence and saturating presence of Fru-6-P using the following equations:

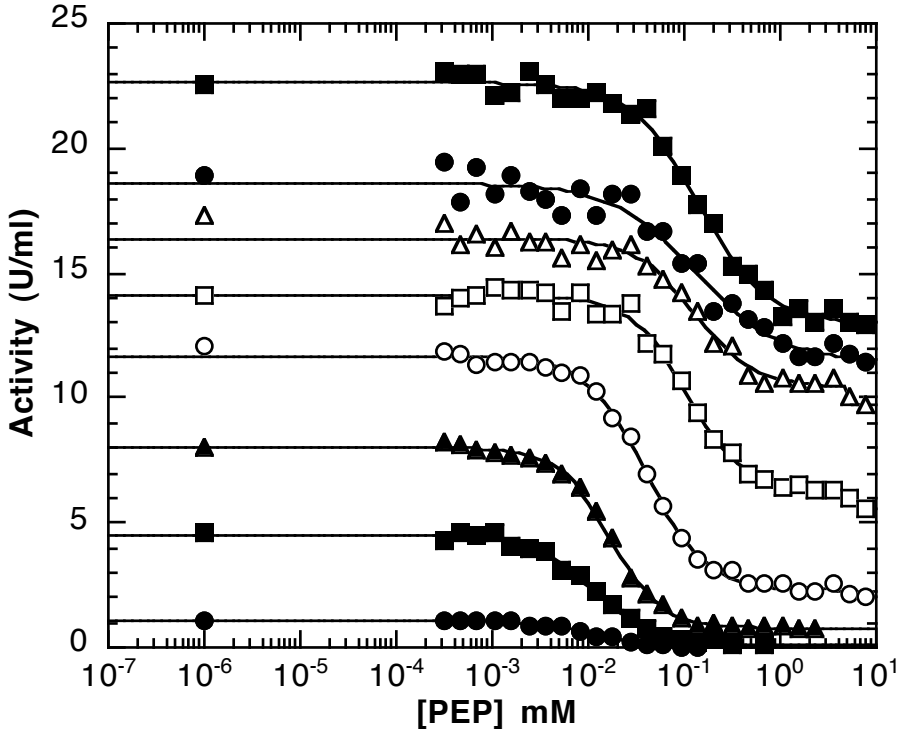

FIGURE 6-3 The PEP saturation profiles determined for the 2:2D(22&30) hybrid at pH 7.0 and increasing concentrations of Fru-6-P. At low Fru-6-P, only one phase in the data is observed and these data are fit to Eq. 6-8. As the concentration of Fru-6-P increases, and additional phase begins to be seen, thus these data were fit to Eq. 6-9 to account for the binding affinity of the mutated allosteric sites. Finally, at high Fru-6-P, the data returns to one phase because of the limitations in adding additional PEP to observe the second phase, and these data are fit once again to Eq. 6-8 as described in the text. The various concentrations of Fru-6-P are as follows: 0.0023 mM (●), 0.0069 mM (■), 0.0206 mM (▲), 0.0617 mM (○), 0.185 mM (□), 0.556 mM (△), 1.67 mM (●) and 5 mM (■).

$$Q_{yy} = \left(\frac{n_H}{2 - n_H} \right)^2 \quad (6\text{-}10)$$

$$Q_{yy/aa} = \left(\frac{n_H}{2 - n_H} \right)^2 \quad (6\text{-}11)$$

However, Q_{yy} cannot be determined explicitly because Fru-6-P is one of the substrates of PFK. Moreover, $Q_{yy/aa}$ is difficult to measure because at high Fru-6-P concentration, the binding affinity for PEP is so low that the PEP saturation profile is unable to reach saturation within the limits of the experiment. Thus, the Hill numbers for those two extremes have to be extrapolated from the data at intermediate concentrations of Fru-6-P. For those cases in which the Hill number is at or near 1 at both low Fru-6-P and high Fru-6-P, a value of 1 is assumed for the Hill numbers in the absence and saturating presence of Fru-6-P, resulting in a coupling of 1 for both Q_{yy} and $Q_{yy/aa}$ respectively. Moreover, if the Hill number for PEP binding does not change as a function of Fru-6-P concentration, then the Hill number is obtained from an average of all the Hill numbers measured. However, if the Hill number is at a value greater than 1 at low Fru-6-P and returns to 1 at high Fru-6-P, the following equation is used to obtain the Hill number in the absence of Fru-6-P:

$$n_H = \left[\frac{\text{Max}\Delta \cdot [Y] + (1 - \text{Max}\Delta) \cdot n_{H_{1/2}} + (1 - \text{Max}\Delta) \cdot [Y]}{n_{H_{1/2}} + [Y]} \right] \quad (6\text{-}12)$$

where MaxΔ now represents the maximal change in the Hill number and (1-MaxΔ) is equivalent to the Hill number in the absence of Fru-6-P. By substituting the latter parameter into Eq. 6-10, Q_{yy} is determined. The $n_{H_{1/2}}$

parameter found in Eq. 6-12 is the concentration of PEP resulting in half the maximal Hill number value, which for all intents and purposes is an irrelevant parameter. By using Eq. 6-12 to fit the data, the Hill number at saturating Fru-6-P is always equal to 1, thus the $Q_{yy/aa}$ is always equal to 1. This constraint placed upon the data is reasonable because in every case the trend is towards a final value of 1 as seen in the Results section.

Results

Characterization of the 2:2V hybrids. As previously described in Chapter V, the 2:2V(30&32) and 2:2V(22&45) hybrids were formed and isolated using three different mutant proteins and two different methods. The two 2:2V(30&32) hybrids were formed and isolated by using either dimer exchange with the [b,□] mutant protein (R252A/D12A/R211E/K213E/K90E/K91E), or by using monomer exchange with the [b,□] mutant protein (R252A/D12A/R25E/N303E/K304E). In either case, the same six allosteric interactions are isolated in each respective 2:2V(30&32) hybrid, four of which are unique and are as follows: the 30 Å heterotropic interaction, the 32 Å heterotropic interaction, the 47 Å homotropic interaction between active sites and the 39.9 Å homotropic interaction between allosteric sites.

The 2:2V(22&45) hybrid also isolates the 47 Å and 39.9 Å homotropic interactions, but was formed and isolated by using monomer exchange with the [a,□] mutant protein (R162E/R25E/N303E/K304E). However, instead of isolating the 30 Å and 32 Å heterotropic interactions like the aforementioned 2:2V hybrids, the 2:2V(22&45) hybrid isolates two copies of the 22 Å and 45 Å

heterotropic interactions. Thus, all three 2:2V hybrids isolate the same homotropic interactions, but two different pairs of heterotropic interactions depending upon the mutant protein used.

The allosteric couplings, Q_{ay}, for the three 2:2V hybrids were determined at pH 6.0, 7.0 and 8.0 and the results are shown in Figs. 6-4 of *A*, *B* and *C*. Not surprisingly, the couplings for the 2:2V(30&32) hybrids are identical within error (as discussed in Chapter V) since the two 2:2 hybrids contain the same allosteric interactions. Moreover, the coupling free energies increase with an increase in pH, a phenomenon consistent with the wild-type enzyme (Tlapak-Simmons and Reinhart, 1988). The only difference between the two 2:2V(30&32) hybrids is the binding affinity for Fru-6-P at pH 8.0. The 2:2V(30&32) hybrid obtained using the [b,□] mutant protein (isolates the 32 Å heterotropic interaction via its 1:3 hybrid) has a lower Fru-6-P binding affinity compared to the 2:2V(30&32) hybrid obtained using the [b,□] mutant protein (isolates the 30 Å heterotropic interaction via its 1:3 hybrid). This result is consistent with the Fru-6-P binding affinities measured previously for the respective 1:3 hybrids (see Chapter III).

As for the 2:2V(22&45) hybrid, the coupling also increases with an increase in pH, however, the binding affinity for PEP (K^{o}_{iy}) is substantially decreased. Due to this influence, the upper plateaus at both pH 7.0 and 8.0 are not as well defined in Fig. 6-4 *C* as the previous 2:2V hybrids (*A* and *B*) and leads to the possibility of the mutated allosteric sites influencing the measured coupling for the 2:2V(22&45) hybrid. In turn, this causes the apparent coupling to be greater than the actual coupling found between the four native binding

FIGURE 6-4 The two-dimensional schematics of the three 2:2V hybrids isolated and the steady-state characterization of their allosteric properties at pH 6.0 (●), 7.0 (□) and 8.0 (▲). The data was obtained at 25°C and using 50 mM MES-KOH at pH 6.0, 50 mM MOPS-KOH at pH 7.0 and 50 mM EPPS-KOH at pH 8.0. The concentration of MgATP was equal to 3 mM. All the curves correspond to the best fit of these data to Eq. 2-4 and the error bars represent ± the standard error. (*A*) The 2:2V(30&32) hybrid obtained by using the [b,□] mutant protein (via dimer exchange) and its allosteric characterization. (*B*) The 2:2V(30&32) hybrid obtained by using the [b,□] mutant protein (via monomer exchange) and its allosteric characterization. (*C*) The 2:2V(22&45) hybrid and its allosteric characterization.

A

2:2V(30&32)
[b,□]

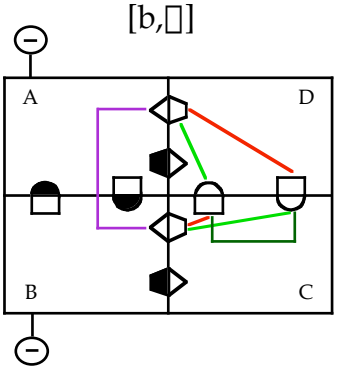

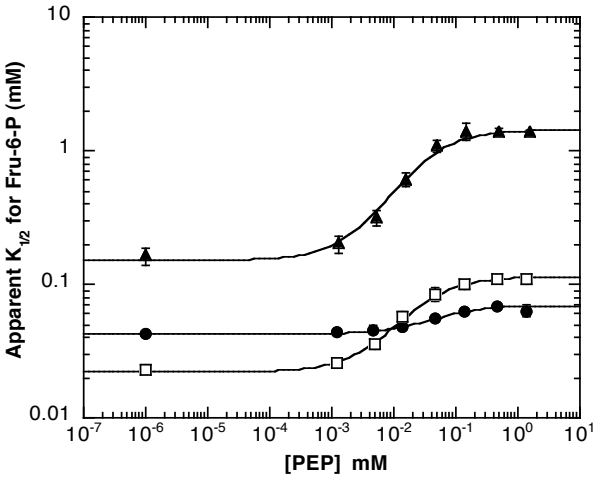

B

2:2V(30&32)
[b,□]

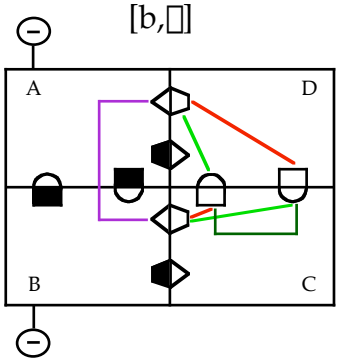

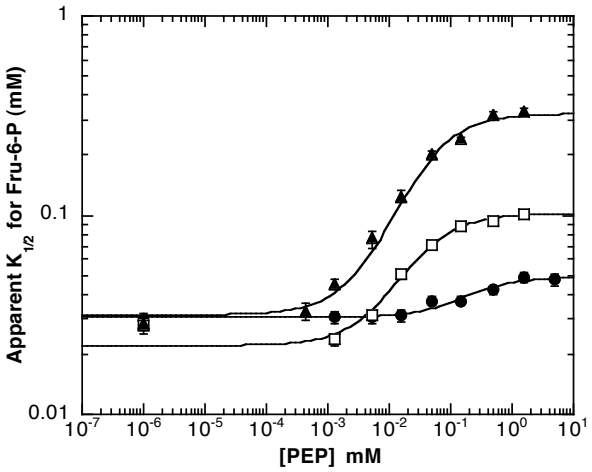

C

2:2V(22&45)
[a,□]

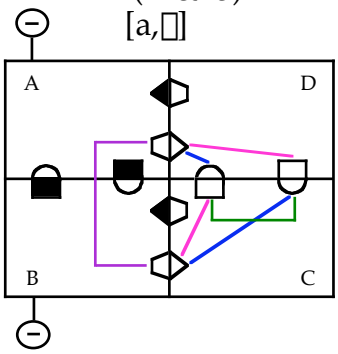

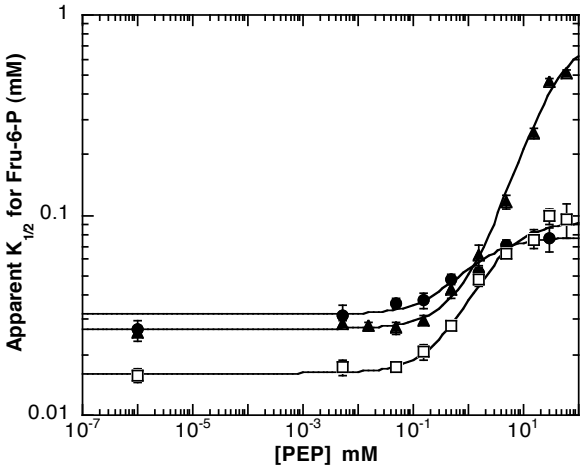

sites. A summary of all the kinetic and thermodynamic parameters obtained for the three 2:2V hybrids is found in Table 6-1, and the Gibbs free energy equation (Eq. 2-6) was used to convert all of the couplings (Q_{ay}) into coupling free energy terms (ΔG_{ay}).

Characterization of the 47 Å homotropic interaction between active sites via the 2:2V hybrids. In order to determine the allosteric contribution of the 47 Å homotropic interaction (between active sites) to the measured coupling for each of the three 2:2V hybrids, the Hill numbers for Fru-6-P binding were determined at increasing concentrations of PEP for all three 2:2V hybrids at pH 6.0, 7.0 and 8.0. The results are shown in Fig. 6-5 *A, B* and *C*. For the 2:2V(30&32) hybrid obtained by dimer exchange (using the [b,□] mutant protein), the Hill number at pH 6.0 does not change over the course of the PEP concentrations assayed as seen in Fig. 6-5 *A*. This observation can be explained by the fact that the coupling for the 30 Å heterotropic interaction equals 1 at pH 6.0 ($Q_{30\text{Å}} = 1$; Chapter III). At pH 7.0, subsaturating heterotropic cooperativity is observed, but at pH 8.0, no real trend in the Hill numbers is seen. Interestingly, the Hill numbers in the absence and saturating presence of PEP increase with increasing pH. A somewhat different pattern in Fru-6-P cooperativity is seen for the 2:2V(30&32) hybrid obtained by monomer exchange (using the [b,□] mutant protein) (Fig. 6-5 *B*). At both low and high Fru-6-P, the Hill numbers are approximately 1 at all three pH values (no pH effect observed like the other2:2V(30&32) hybrid); however, subsaturating heterotropic cooperativity is

TABLE 6-1 A summary of the kinetic and thermodynamic parameters obtained for the 2:2V hybrids at 25°C, pH 6.0, 7.0 and 8.0 and [MgATP] = 3 mM

2:2 Hybrid	K^{o}_{ia} (mM)	K^{o}_{iy} (mM)	Q_{ay}	ΔG_{ay} (kcal/mol)
pH 6.0				
2:2V(30&32) Dimer X-Δ ([b,□])	0.042 ± 0.001	0.031 ± 0.013	0.61 ± 0.03	0.29 ± 0.04
2:2V(30&32) Monomer X-Δ ([b,□])	0.031 ± 0.001	0.13 ± 0.06	0.62 ± 0.04	0.28 ± 0.04
2:2V(22&45)	0.032 ± 0.002	0.44 ± 0.03	0.41 ± 0.03	0.52 ± 0.05
pH 7.0				
2:2V(30&32) Dimer X-Δ ([b,□])	0.022 ± 0.001	0.0051 ± 0.0013	0.19 ± 0.02	0.97 ± 0.05
2:2V(30&32) Monomer X-Δ ([b,□])	0.022 ± 0.001	0.0069 ± 0.0012	0.22 ± 0.01	0.90 ± 0.04
2:2V(22&45)	0.016 ± 0.001	0.46 ± 0.07	0.17 ± 0.01	1.03 ± 0.05
pH 8.0				
2:2V(30&32) Dimer X-Δ ([b,□])	0.15 ± 0.02	0.0030 ± 0.0008	0.11 ± 0.01	1.33 ± 0.08
2:2V(30&32) Monomer X-Δ ([b,□])	0.032 ± 0.002	0.0039 ± 0.0005	0.098 ± 0.005	1.37 ± 0.03
2:2V(22&45)	0.027 ± 0.001	1.1 ± 0.1	0.033 ± 0.002	2.02 ± 0.04

FIGURE 6-5 The characterization of the 47 Å homotropic interaction between active sites by following the dependence of the Hill number (n_H) determined for Fru-6-P binding as a function of increasing concentrations of PEP for the 2:2V hybrids. The data was obtained at 25°C and at pH 6.0 (●) using 50 mM MES-KOH, at pH 7.0 (□) using 50 mM MOPS-KOH and at pH 8.0 (▲) using 50 mM EPPS-KOH. The concentration of MgATP was equal to 3 mM, and the error bars represent ± the standard error. (*A*) The 2:2V(30&32) hybrid obtained by using the [b,□] mutant protein (via dimer exchange). (*B*) The 2:2V(30&32) hybrid obtained by using the [b,□] mutant protein (via monomer exchange). (*C*) The 2:2V(22&45) hybrid.

A

2:2V(30&32)
[b,□]

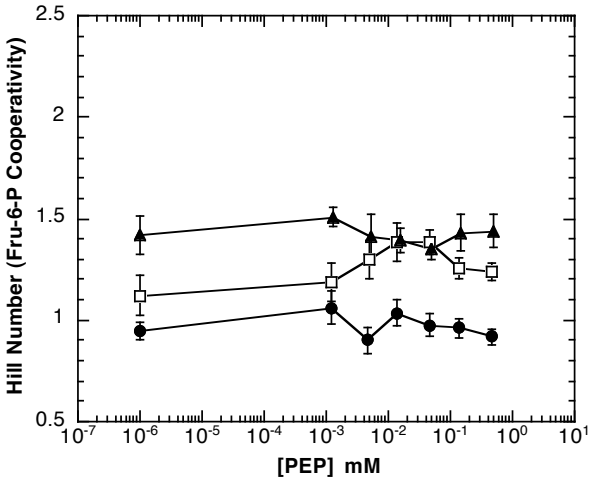

B

2:2V(30&32)
[b,□]

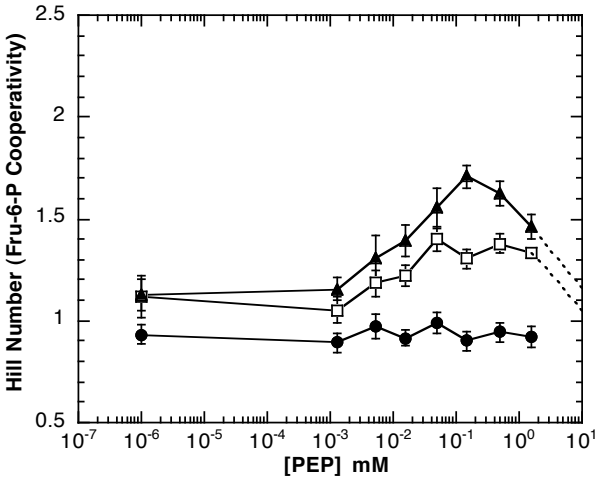

C

2:2V(22&45)
[a,□]

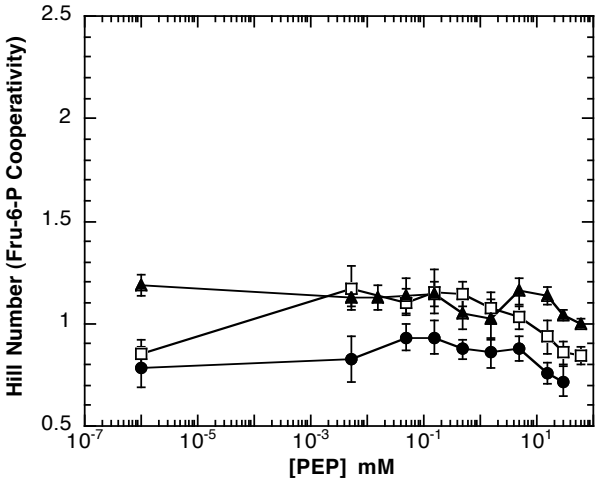

apparent at both pH 7.0 and 8.0 and absent from pH 6.0, consistent again with $Q_{30\text{Å}} = 1$. Furthermore, a greater maximal Hill number is attained at pH 8.0 than pH 7.0 because of the increased coupling ($Q_{2:2V(30\&32)}$) at pH 8.0 as compared to pH 7.0 (see Table 6-1). As for the third 2:2V hybrid (2:2V(22&45)), the Hill numbers are approximately 1 at all three pH values and at all PEP concentrations (Fig. 6-5 *C*).

Since there is no overall net change in the Hill numbers for Fru-6-P binding in the absence and saturating presence of PEP for any of the 2:2V hybrids, Q_{aa} is equal to $Q_{aa/yy}$ (according to Eqs. 6-6 and 6-7) for all three 2:2V hybrids and at all three pH values investigated (Fig. 6-5). Furthermore, because $Q_{aa} = Q_{aa/yy}$, the 47 Å homotropic interaction contributes nothing to the overall allosteric effect measured for the 2:2V hybrids based upon the prediction made earlier by Eq. 6-2, repeated here for convenience (Reinhart, 1988):

$$Q = Q_{ay1} \cdot Q_{ay2} \cdot \left[\frac{Q_{yy/aa}}{Q_{yy}}\right]^{1/2} \cdot \left[\frac{Q_{aa/yy}}{Q_{aa}}\right]^{1/2} \qquad (6\text{-}13)$$

Characterization of the 39.9 Å homotropic interaction between allosteric sites via the 2:2V hybrids. Using the same conditions, but determining the binding affinity for PEP as a function of Fru-6-P concentration enabled us to measure the cooperativity in PEP binding between the two native allosteric sites and hence determine the allosteric contribution of the 39.9 Å homotropic interaction to the overall measured coupling for the 2:2V hybrids. Figures 6-6 *A*, *B* and *C* summarize these results. All three 2:2V hybrids behave similarly, and the Hill number is always at or near 1 at both low and high Fru-6-P concentration for all

FIGURE 6-6 The characterization of the 39.9 Å homotropic interaction between allosteric sites by following the dependence of the Hill number (n_H) determined for PEP binding as a function of increasing concentrations of Fru-6-P for the 2:2V hybrids. The data was obtained at 25°C and at pH 6.0 (●) using 50 mM MES-KOH, at pH 7.0 (□) using 50 mM MOPS-KOH and at pH 8.0 (▲) using 50 mM EPPS-KOH. The concentration of MgATP was equal to 3 mM, and the error bars represent ± the standard error. (*A*) The 2:2V(30&32) hybrid obtained by using the [b,□] mutant protein (via dimer exchange). (*B*) The 2:2V(30&32) hybrid obtained by using the [b,□] mutant protein (via monomer exchange). (*C*) The 2:2V(22&45) hybrid.

A

2:2V(30&32)
[b,□]

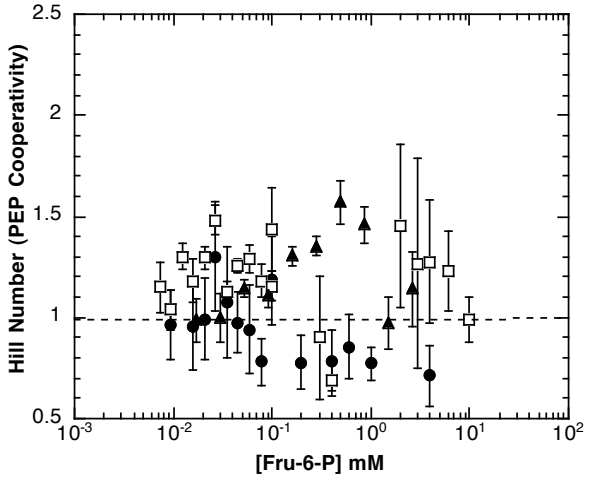

B

2:2V(30&32)
[b,∏]

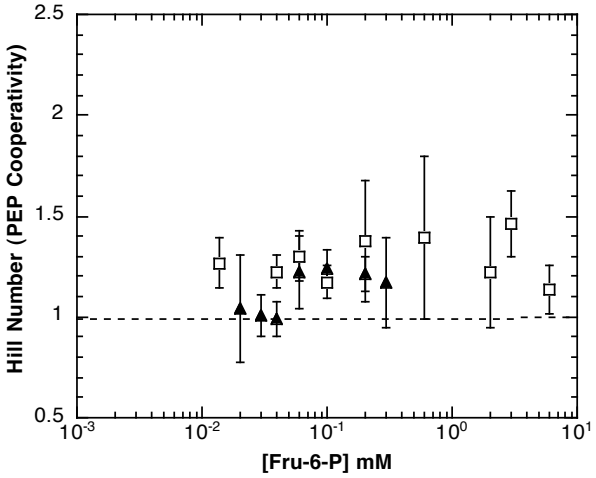

C

2:2V(22&45)
[a,□]

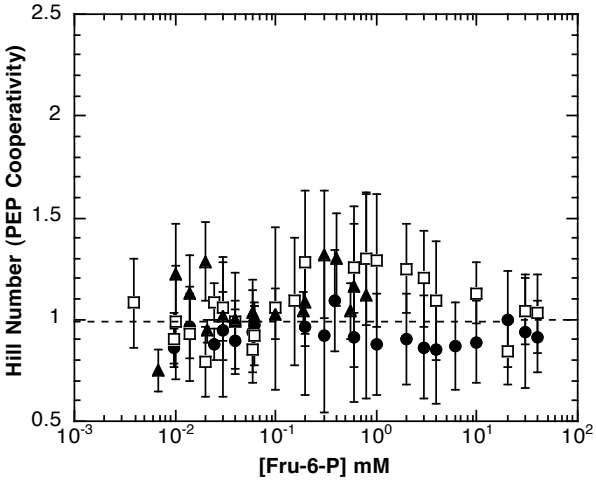

three pH values investigated. In some instances the Hill number increases somewhat at subsaturating levels of Fru-6-P (subsaturating heterotropic cooperativity), but it always returns to 1 at high Fru-6-P. Unfortunately, a limited amount of data was collected regarding PEP cooperativity for the 2:2V(30&32) hybrid, thus the number of points is decreased (Fig. 6-6 *B*).

For all three 2:2V hybrids, a value of 1 was assumed for the Hill numbers in both the absence and saturating presence of Fru-6-P leading to a coupling of 1 for both Q_{yy} and $Q_{yy/aa}$ (Eqs. 6-10 and 6-11). Furthermore, since the there is no net change in PEP cooperativity in the absence and saturating presence of Fru-6-P, the 39.9Å homotropic interaction contributes nothing to the overall measured allosteric effect in each of the three 2:2V hybrids. Thus, both homotropic interactions in the 2:2V hybrids are not involved in transmitting the allosteric signal between Fru-6-P and PEP or *vice versa*.

How the allosteric interactions combine in the 2:2V hybrids. Next, all the coupling free energies (ΔG_{ay}) measured for the four individual allosteric interactions found within each 2:2V hybrid were compared to the coupling free energy measured for each corresponding 2:2V hybrid (Figs. 6-7, *A* and *B*). Since both the 47 Å homotropic interaction between active sites (Fru-6-P cooperativity) and the 39.9 Å homotropic interaction between allosteric sites (PEP cooperativity) were found to contribute nothing to the measured allosteric effect of the 2:2V hybrids, they were not included in the analysis. For both of the 2:2V(30&32) hybrids, the measured coupling free energy for each 2:2 hybrid is equal to the sum of the individual coupling free energies (within error)

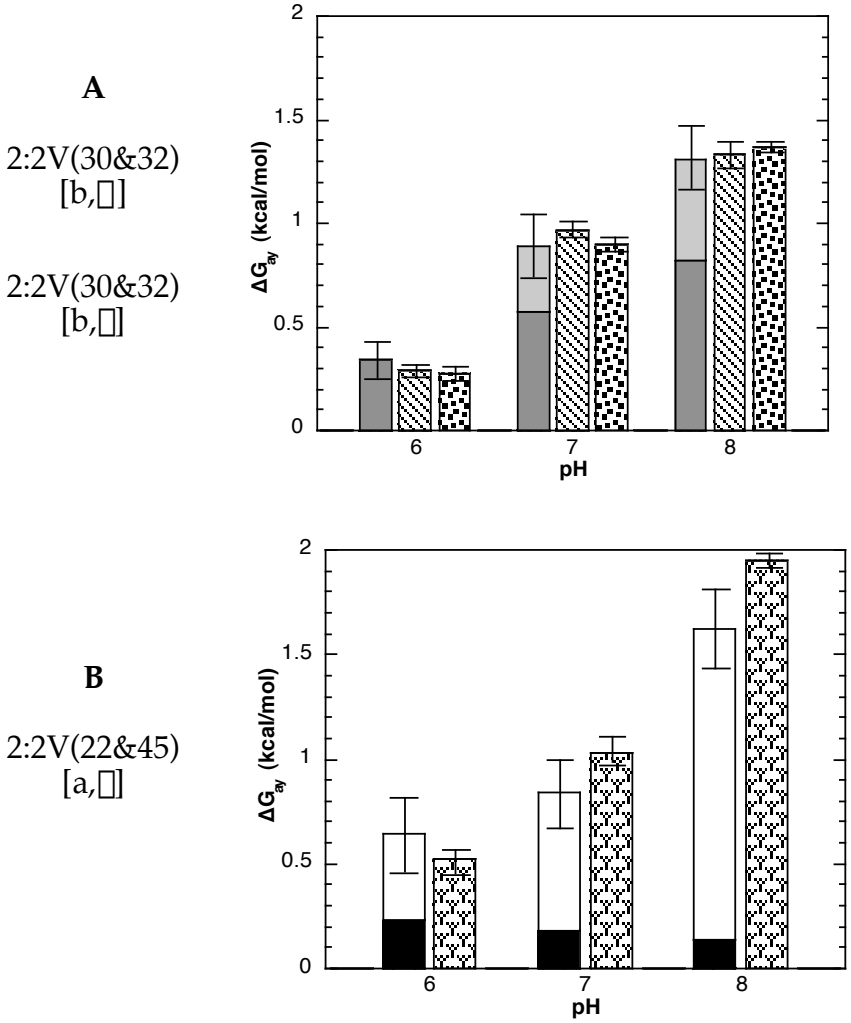

FIGURE 6-7 The comparison of the sum of the individual coupling free energies determined for the heterotropic interactions to the coupling free energy determined for the 2:2V hybrids at pH 6.0, 7.0 and 8.0 in the absence of any homotropic contribution. (*A*) The bar on the left at each pH corresponds to the sum of the coupling free energies determined for the 30 Å interaction (light gray) and the 32 Å interaction (dark gray), the bar in the middle corresponds to the coupling free energy determined for the 2:2V(30&32) hybrid obtained by using the [b,□] mutant protein (stripes), and the bar on the right corresponds to the coupling free energy determined for the 2:2V(30&32) hybrid obtained by using the [b,□] mutant protein (polka-dots). (*B*) The bar on the left at each pH corresponds to the sum of the coupling free energies determined for the 22 Å interaction (white) and the 45 Å interaction (black), and the bar on the right corresponds to the coupling free energy determined for the 2:2V(22&45) hybrid (bricks).

calculated for the 30 Å and 32 Å heterotropic interactions respectively at all three of the pH values investigated (Fig. 6-7 *A*). Thus, even as the relative contributions of the 30 Å and 32 Å heterotropic interactions change with pH, the coupling free energies measured for both of the 2:2V(30&32) hybrids changes as well to still equal the sum of the individual coupling free energies for the 30 Å and 32 Å heterotropic interactions.

As for the 2:2V(22&45) hybrid (Fig. 6-7 *B*), the coupling free energy measured at pH 6.0 also equals the sum of the coupling free energies (within error) determined for the 22 Å and 45 Å heterotropic interactions, but is not the case at pH 7.0 and 8.0. At pH 7.0 and 8.0 the coupling free energy calculated for the 2:2V(22&45) hybrid is somewhat greater than the sum of the coupling free energies measured for the 22 Å and 45 Å heterotropic interactions; this discrepancy is most likely due to the influence upon the apparent coupling of PEP binding to the mutated allosteric sites. Unlike the 1:3 hybrids, a "control" hybrid was not constructed for each individual 2:2 hybrid and assayed to determine the point at which the mutated allosteric sites begin to influence the measured allosteric coupling (see Chapters III and IV). However, from experience with the 1:3 control hybrids, the mutated allosteric sites are estimated to begin binding PEP at around 5 mM PEP. Thus, if saturation is not reached by 5 mM PEP, as is the case at pH 7.0 and 8.0 (Figs. 6-4, *B* and *C*), the measured coupling will contain partial influence from PEP binding at the two mutated allosteric sites. Unfortunately this is difficult to prove since we were unable to form and characterize the redundant form of the 2:2V(22&45) hybrid utilizing

the [a,□] mutant protein.

Characterization of the 2:2D hybrids. The three 2:2D hybrids were all formed and isolated as described in Chapter V via the monomer exchange procedure described in Chapter II utilizing the K90E/K91E charge tag and three different mutant proteins. The two 2:2D(32&45) hybrids were formed using either the [b,□] mutant protein (R252A/D12A/K213E/K90E/K91E) or the [a,□] mutant protein (R162E/R25E/K90E/K91E) respectively, while the 2:2D(22&30) hybrid was formed using the [b,□] mutant protein (R252A/D12A/R25E/K90E/K91E). All three 2:2D hybrids isolate the 45 Å homotropic interaction between active sites and the 23 Å homotropic interaction between allosteric sites, but as the names describe, the 2:2D(32&45) hybrids also isolate two copies each of the 32 Å and 45 Å heterotropic interactions (Figs. 6-8, *A* and *B*), whereas the 2:2D(22&30) hybrid isolates two copies each of the 22 Å and 30 Å heterotropic interactions respectively (Fig. 6-8 *C*).

The allosteric characterizations of the three 2:2D hybrids at pH 6.0, 7.0 and 8.0 are shown in Figs. 6-8 *A*, *B* and *C* with the parameters derived from this analysis summarized in Table 6-2. All three 2:2D hybrids responded to the change in pH in the expected manner, with the coupling (Q_{ay}) increasing with increasing pH. However, the 2:2D(32&45) hybrid obtained by using the [b,□] mutant protein (Fig. 6-8 *A*) displayed a decrease in Fru-6-P affinity with increasing pH, a phenomenon consistent with the allosteric behavior of the 2:2V(30&32) hybrid obtained using the [b,□] mutant protein discussed earlier, with the only mutational difference being the addition of the R211E allosteric

FIGURE 6-8 The two-dimensional schematics of the three 2:2D hybrids isolated and the steady-state characterization of their allosteric properties at pH 6.0 (●), 7.0 (□) and 8.0 (▲). The data was obtained at 25°C and using 50 mM MES-KOH at pH 6.0, 50 mM MOPS-KOH at pH 7.0 and 50 mM EPPS-KOH at pH 8.0. The concentration of MgATP was equal to 3 mM. All the curves correspond to the best fit of these data to Eq. 2-4 and the error bars represent ± the standard error. (*A*) The 2:2D(32&45) hybrid obtained by using the [b,□] mutant protein and its allosteric characterization. (*B*) The 2:2D(32&45) hybrid obtained by using the [a,□] mutant protein and its allosteric characterization. (*C*) The 2:2D(22&30) hybrid and its allosteric characterization.

A

2:2D(32&45)
[b,□]

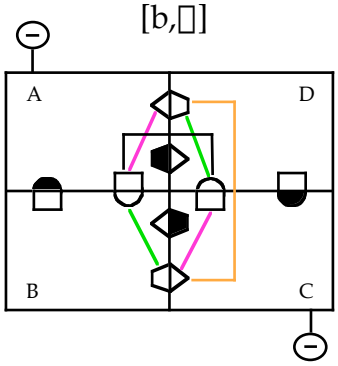

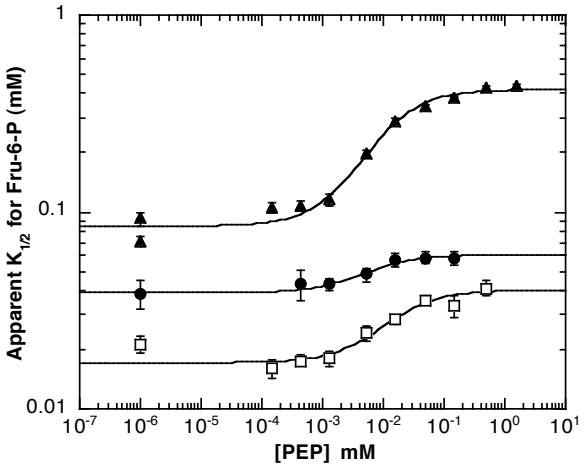

B

2:2D(32&45)
[a,□]

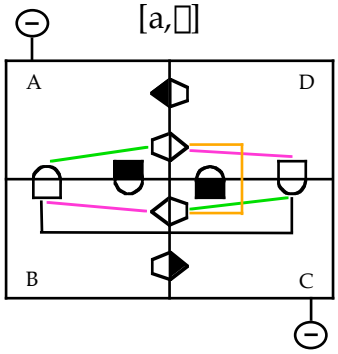

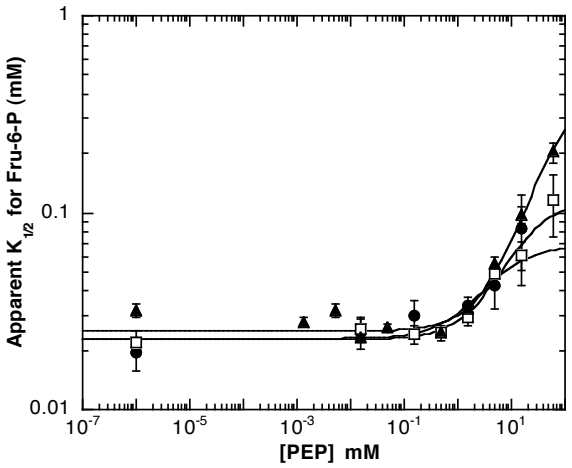

C

2:2D(22&30)
[b,□]

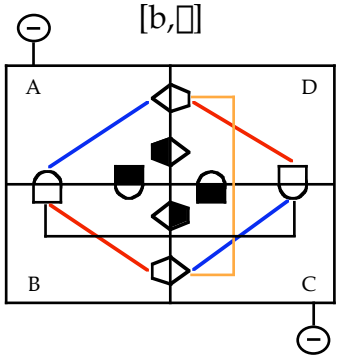

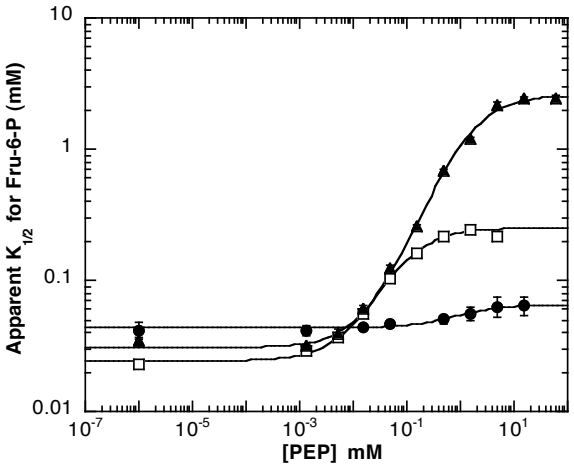

TABLE 6-2 A summary of the kinetic and thermodynamic parameters obtained for the 2:2D hybrids at 25°C, pH 6.0, 7.0 and 8.0 and [MgATP] = 3 mM

2:2 Hybrid	K_{ia}^{o} (mM)	K_{iy}^{o} (mM)	Q_{ay}	ΔG_{ay} (kcal/mol)
pH 6.0				
2:2D(32&45) ([b,□])	0.039 ± 0.004	0.0035 ± 0.0025	0.64 ± 0.07	0.26 ± 0.07
2:2D(32&45) ([a,□])	0.023 ± 0.003	1.6 ± 0.7	0.34 ± 0.24	0.64 ± 0.52
2:2D(22&30)	0.044 ± 0.002	0.65 ± 0.07	0.67 ± 0.11	0.24 ± 0.09
pH 7.0				
2:2D(32&45) ([b,□])	0.017 ± 0.001	0.0065 ± 0.0025	0.43 ± 0.03	0.50 ± 0.05
2:2D(32&45) ([a,□])	0.023 ± 0.002	3.0 ± 1.3	0.20 ± 0.08	0.96 ± 0.25
2:2D(22&30)	0.024 ± 0.001	0.0091 ± 0.0010	0.097 ± 0.005	1.38 ± 0.03
pH 8.0				
2:2D(32&45) ([b,□])	0.085 ± 0.003	0.0022 ± 0.0002	0.20 ± 0.01	0.94 ± 0.02
2:2D(32&45) ([a,□])	0.025 ± 0.001	4.5 ± 0.7	0.054 ± 0.020	1.72 ± 0.23
2:2D(22&30)	0.031 ± 0.001	0.018 ± 0.001	0.012 ± 0.001	2.62 ± 0.05

site mutation in the latter mutant protein. The other major difference between Figs. 6-8 *A, B* and *C* is the decreased binding affinity for PEP (K^{o}_{iy}) measured for the 2:2D(32&45) hybrid obtained by using the [a,□] mutant protein (Fig. 6-8 *B*). Due to this effect, none of the data reaches saturation at pH 6.0, 7.0 or 8.0 potentially allowing PEP to bind at the mutated allosteric sites and influence the apparent measured coupling. Interestingly, this observation of decreased PEP binding affinity was also made and discussed previously regarding the 2:2V(22&45) hybrid, which also used the [a,□] mutant protein (same binding site mutations but different charge tag).

In order to determine if PEP binding at the mutated allosteric sites was influencing the measured coupling of the 2:2D(32&45) hybrid obtained by using the [a,□] mutant protein, we compared the coupling free energies calculated for the two 2:2D(32&45) hybrids because the same allosteric interactions are isolated in both hybrids. The coupling free energy calculated for the 2:2D(32&45) hybrid with the elevated K^{o}_{iy} is greater than the other 2:2D(32&45) hybrid by approximately 2-fold, thus it seems that our argument regarding PEP binding at the mutated allosteric sites and influencing the measured coupling free energy for the 2:2D(32&45) hybrid isolated by using the [a,□] mutant protein is substantiated.

Characterization of the 45 Å homotropic interaction between active sites via the 2:2D hybrids. To determine the contribution of the 45 Å homotropic interaction to the measured allosteric effect of the three 2:2D hybrids, the Hill number for Fru-6-P binding was measured as a function of PEP concentration and the

results are shown in Figs. 6-9 *A*, *B* and *C*. The Hill numbers measured for the 2:2D(32&45) hybrid obtained by using the [b,□] mutant protein (Fig. 6-9 *A*) behave similarly to the previously mentioned 2:2V(30&32) hybrid obtained by using the [b,□] mutant protein (the former mutant protein has the K213E mutation, while the latter has the R211E/K213E double mutation) in that the Hill numbers themselves increase with increasing pH, but always beginning and ending at the same value. Subsaturating heterotropic cooperativity is not evident at pH 6.0 or 7.0 as the Hill number does not change dramatically over the course of the PEP concentrations assayed. At pH 8.0, subsaturating heterotropic cooperativity may be evident.

The Hill numbers measured for the other 2:2D(32&45) hybrid obtained by using the [a,□] mutant protein (Fig. 6-9 *B*), "bounce" around a little with subsaturating heterotropic cooperativity occurring at the higher concentrations of PEP for all three pH values which is consistent with the elevated K_{iy}^{o} value determined earlier for this particular 2:2 hybrid. The data regarding pH 6.0 however are somewhat inconsistent because the maximum Hill number measured at pH 6.0 should not be greater than the maximum Hill number measured at pH 7.0 and 8.0 because the coupling is lowest at pH 6.0. More importantly however, the Hill numbers begin and end at approximately the same value. The final 2:2D hybrid, the 2:2D(22&30) hybrid obtained by using the [b,□] mutant protein (Fig. 6-9 *C*), also displays subsaturating heterotropic cooperativity, but only at pH 7.0 and 8.0 (with the maximum Hill number occurring at pH 8.0) and behaves quite similarly to the 2:2V(30&32) hybrid

FIGURE 6-9 The characterization of the 45 Å homotropic interaction between active sites by following the dependence of the Hill number (n_H) determined for Fru-6-P binding as a function of increasing concentrations of PEP for the 2:2D hybrids. The data was obtained at 25°C and at pH 6.0 (●) using 50 mM MES-KOH, at pH 7.0 (□) using 50 mM MOPS-KOH and at pH 8.0 (▲) using 50 mM EPPS-KOH. The concentration of MgATP was equal to 3 mM, and the error bars represent ± the standard error. (*A*) The 2:2D(32&45) hybrid obtained by using the [b,□] mutant protein. (*B*) The 2:2D(32&45) hybrid obtained by using the [a,□] mutant protein. (*C*) The 2:2D(22&30) hybrid and its allosteric characterization.

A

2:2D(32&45)
[b,□]

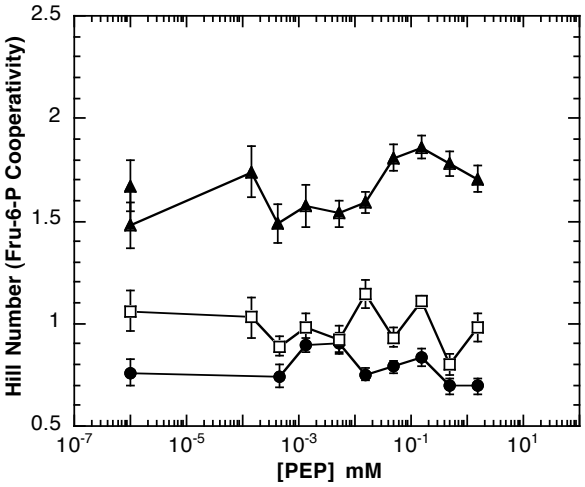

B

2:2D(32&45)
[a,□]

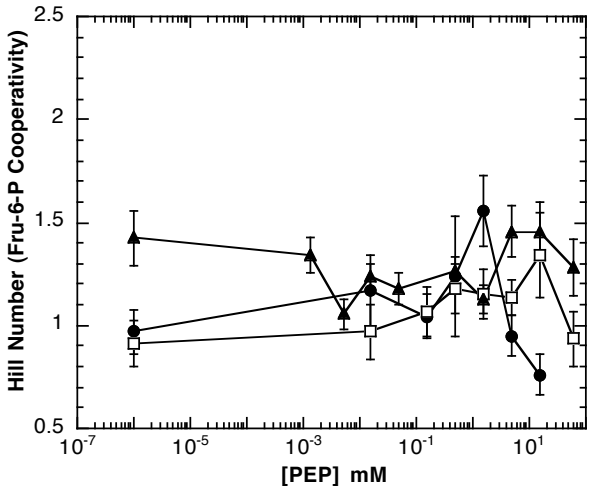

C

2:2D(22&30)
[b,□]

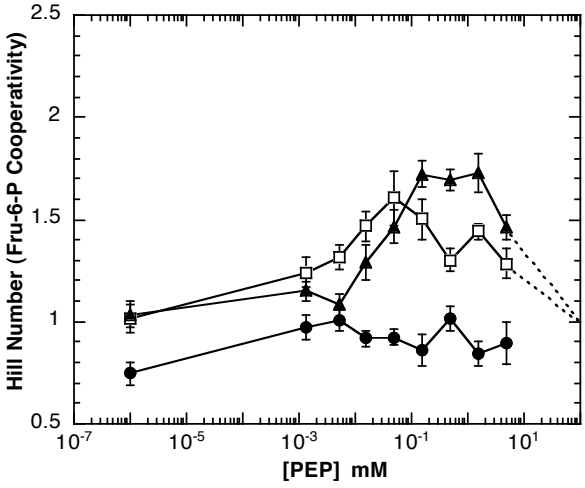

obtained by using the [b,□] mutant protein (the latter mutant protein uses the N303E/K304E charge tag instead of the K90E/K91E charge tag). The lack of subsaturating heterotropic cooperativity occurring at pH 6.0 is consistent with $Q_{30\text{Å}} = 1$. More importantly however, the Hill numbers are (within error) the same value in the limits of low and high concentrations of PEP. Thus, since $Q_{aa} = Q_{aa/yy}$, the 45 Å homotropic interaction (between active sites) contributes nothing to the apparent heterotropic coupling (Q_{ay}) measured for each of the three 2:2D hybrids.

Characterization of the 23 Å homotropic interaction between allosteric sites via the 2:2D hybrids. The other homotropic interaction isolated within the 2:2D hybrids, the 23 Å homotropic interaction between allosteric sites, proved to be much more challenging to characterize than the previous 39.9 Å homotropic interaction between allosteric sites. Of the three 2:2D hybrids, only the Hill numbers for PEP binding to the 2:2D(22&30) hybrid were measured, but for two different reasons. Unfortunately, not enough data were collected for the 2:2D(32&45) hybrid obtained by using the [b,□] mutant protein to generate quality PEP saturation profiles. Consequently, the Hill numbers for PEP binding were not measured for that particular 2:2 hybrid. On the other hand, accurate Hill numbers for PEP binding to the other 2:2D(32&45) hybrid were impossible to measure due to the decreased binding affinity for PEP. Since the K^{o}_{iy} is so high for that particular 2:2 hybrid, the individual PEP saturation profiles could not define the lower plateau preventing any kind of accurate fit to the data. Thus, the Hill numbers for PEP binding were undeterminable for the

2:2D(32&45) hybrid obtained by using the [a,□] mutant protein.

The remaining 2:2D hybrid, the 2:2D(22&30) hybrid, was characterized and the Hill numbers for PEP binding determined as a function of Fru-6-P concentration are shown in Fig. 6-10. Unlike any other homotropic interaction characterized to this point, the Hill numbers measured for PEP binding to the 2:2D(22&30) hybrid begin at a value greater than 1 at low Fru-6-P and proceed to a value of 1 at high Fru-6-P. Moreover, the initial Hill number value at low Fru-6-P increases with increasing pH. The data were fit to Eq. 6-12 to extrapolate the Hill number value in the absence of Fru-6-P at pH 6.0, 7.0 and 8.0 and their values are summarized in Table 6-3. Furthermore, Eq. 6-10 was used to calculate Q_{yy} and since the Hill numbers returned to 1 at high Fru6-P, $Q_{yy/aa}$ is equal to 1 at all pH values (Eq. 6-11).

To determine the allosteric contribution of the 23 Å homotropic interaction to the measured allosteric effect for the 2:2D(22&30) hybrid, the square root of the ratio of $Q_{yy/aa}$ to Q_{yy} was calculated as called for in Eq. 6-2 and is the ratio presented in Table 6-3. $Q_{yy/aa}$ and Q_{yy} were determined from the respective Hill coefficients at high and low concentrations of Fru-6-P using Eqs. 6-12 and 6-1. Moreover, this ratio can also be expressed as a coupling free energy, as indicated in Table 6-3. Thus, of the two homotropic interactions isolated by the 2:2D hybrids, the 23 Å homotropic interaction plays a significant role in the inhibition process, with the 45 Å homotropic interaction between active sites contributing nothing to the allosteric effect.

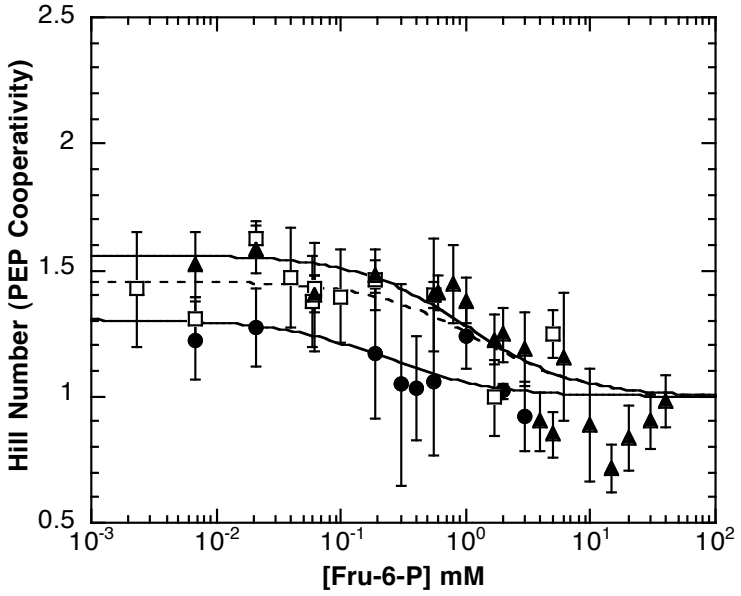

FIGURE 6-10 The characterization of the 23 Å homotropic interaction between active sites by following the dependence of the Hill number (n_H) determined for PEP binding as a function of increasing concentrations of Fru-6-P for the 2:2D(22&30) hybrid. The data was obtained at 25°C and at pH 6.0 (●) using 50 mM MES-KOH, at pH 7.0 (□) using 50 mM MOPS-KOH and at pH 8.0 (▲) using 50 mM EPPS-KOH. The concentration of MgATP was equal to 3 mM, and the error bars represent ± the standard error.

TABLE 6-3 A summary of the kinetic and thermodynamic parameters obtained in characterizing the 23 Å homotropic interaction between allosteric sites

pH	n_H	Q_{yy}	$\left(\frac{Q_{yy/aa}}{Q_{yy}}\right)^{1/2}$	$\Delta G_{23Å}$* (kcal/mol)
6.0	1.29 ± 0.11	3.30 ± 1.17	0.55 ± 0.10	0.35 ± 0.10
7.0	1.48 ± 0.04	8.10 ± 1.32	0.35 ± 0.03	0.62 ± 0.05
8.0	1.55 ± 0.05	11.86 ± 2.74	0.29 ± 0.03	0.73 ± 0.06

$$*\Delta G_{23Å} = \frac{1}{2}\left(\Delta G_{yy/aa} - \Delta G_{yy}\right) = -RT\ln\left(\frac{Q_{yy/aa}}{Q_{yy}}\right)^{1/2}$$

How the allosteric interactions combine in the 2:2D hybrids. Figures 6-11 *A, B* and *C* compare the sum of the coupling free energies measured for the individual heterotropic interactions found within a particular 2:2D hybrid and the coupling free energy contribution of the 23 Å allosteric site homotropic interaction to the coupling free energy calculated for each of the three 2:2D hybrids. For the 2:2D(32&45) hybrid obtained by using the [b,□] mutant protein (Fig. 6-11 *A*), the coupling free energy measured for the 2:2 hybrid (third bar) is substantially less than the sum of the individual 32 Å and 45 Å heterotropic interactions plus the contribution measured for the 23 Å homotropic interaction determined via the 2:2D(22&30) hybrid (first bar) at pH 6.0, 7.0 and 8.0. However, the coupling free energy for the 2:2D(22&30) hybrid is equivalent within error, except at pH 6.0, to the sum of the individual heterotropic

FIGURE 6-11 The comparison of the sum of the individual coupling free energies determined for the heterotropic interactions and the 23 Å homotropic contribution to the coupling free energy determined for the 2:2D hybrids at pH 6.0, 7.0 and 8.0. (*A*) The bar on the left at each pH corresponds to the sum of the coupling free energies determined for the 32 Å interaction (dark gray), the 45 Å interaction (black), and the 23 Å homotropic interaction measured via the 2:2D(22&30) hybrid (*hatches). The bar in the middle corresponds to the sum of the coupling free energies determined for only the 32 Å interaction (dark gray) and the 45 Å interaction (black). The bar on the right corresponds to the coupling free energy measured for the 2:2D(32&45) hybrid obtained by using the [b,□] mutant protein (stripes). (*B*) The bar on the left at each pH corresponds to the sum of the coupling free energies determined for the 32 Å interaction (dark gray), the 45 Å interaction (black), and the 23 Å homotropic interaction measured via the 2:2D(22&30) hybrid (*hatches) and the bar on the right corresponds to the coupling free energy measured for the 2:2D(32&45) hybrid obtained by using the [a,□] mutant protein (polka-dots). (*C*) The bar on the left at each pH corresponds to the sum of the coupling free energies determined for the 22 Å interaction (white), the 30 Å interaction (light gray), and the 23 Å homotropic interaction (hatched), while the bar on the right corresponds to the coupling free energy determined for the 2:2D(22&30) hybrid (bricks).

A

2:2D(32&45)
[b,□]

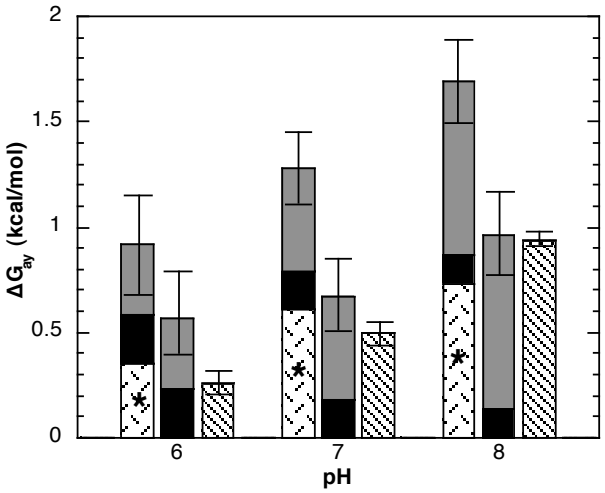

B

2:2D(32&45)
[a,□]

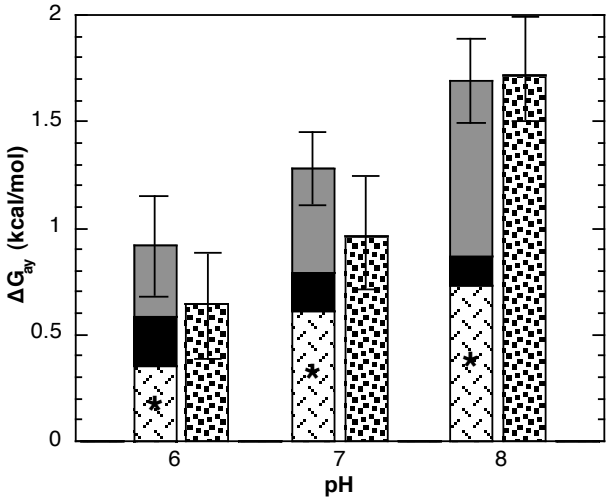

C

2:2D(22&30)
[b,□]

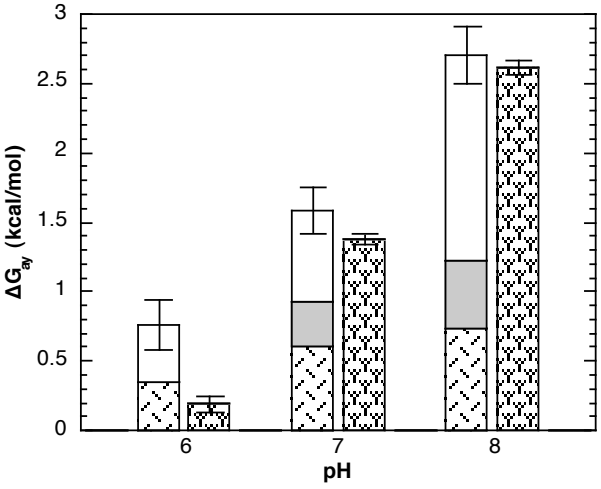

interactions in the absence of any homotropic contribution. Thus, it seems that one or more of the binding site or charge tag mutations introduced in the [b,□] mutant protein (R252A/D12A/K213E/K90E/K91E) is potentially interfering with the transmission of the 23 Å homotropic signal. The discrepancy at pH 6.0 also occurs for several other 2:2 hybrids (always with the coupling free energy measured for the 2:2 hybrid less than the sum), and is a phenomenon that cannot be explained.

On the other hand, the coupling free energy calculated for the 2:2D(32&45) hybrid obtained by using the [a,□] mutant protein (R162E/R25E/K90E/K91E – Fig. 6-11 *B*) is equivalent within error to the sum of the individual 32 Å and 45 Å heterotropic interactions plus the 23 Å homotropic component determined in the 2:2D(22&30) hybrid. Thus, it seems the reason why the coupling free energies for the two 2:2D(32&45) hybrids are different is because of the absence and presence of the 23 Å homotropic component (comparing Figs. 6-11, *A* and *B*).

The coupling free energy calculated for the third 2:2D hybrid, the 2:2D(22&30) hybrid, is found to be equivalent at pH 7.0 and 8.0 to the sum of the coupling free energies determined for the 22 Å and 30 Å heterotropic interactions plus the contribution from the 23 Å homotropic interaction as seen in Fig. 6-11 *C*. However, at pH 6.0, the coupling free energy measured for the 2:2D(22&30) hybrid is less than the sum, and at this point we have no explanation for this discrepancy except that this phenomenon also occurs for some of the other 2:2 hybrids as well (i.e. the 2:2D(32&45) – Fig. 6-11 *A*). Thus,

in two of the 2:2D hybrids, the entire allosteric effect is accounted for by the both of the heterotropic interactions plus the contribution from the 23 Å homotropic interaction, while the 2:2D(32&45) hybrid obtained by using the [b,□] mutant protein is equal to just the sum of the 32 Å and 45 Å heterotropic interactions.

Characterization of the 2:2H hybrids. The three 2:2H hybrids were formed and isolated as described in Chapter V using three different mutant proteins and the monomer exchange procedure discussed in Chapter II, with two of the three 2:2H hybrids (the 2:2H(30&45) hybrids) isolating the same six pair-wise allosteric interactions. The 2:2H(30&45) hybrids were made by using either the [b,□] mutant protein (R252A/D12A/R25E/R232E/Q233E – Fig. 6-12 *A*) or the [a,□] mutant protein (R162E/R25E/R232E/Q233E – Fig. 6-12 *B*), and in either case the following interactions were isolated: two copies each of the 30 Å and 45 Å heterotropic interactions, one copy of the 28 Å homotropic interaction between active sites, and one copy of the 40 Å homotropic interaction between allosteric sites. The third 2:2H hybrid, the 2:2H(22&32) hybrid formed by using the [b,□] mutant protein (R252A/D12A/K213E/R232E/Q233E – Fig. 6-12 *C*), also isolates the 28 Å and 40 Å homotropic interactions, however it isolates two copies each of the 22 Å and 32 Å heterotropic interactions instead of the 30 Å and 45 Å heterotropic interactions.

The allosteric characterizations of each of the three 2:2H hybrids at pH 6.0, 7.0 and 8.0 are shown in Figs. 6-12, *A*, *B* and *C*, and a summary of all the parameters determined by this analysis is found in Table 6-4. Of the three 2:2H

FIGURE 6-12 The two-dimensional schematics of the three 2:2H hybrids isolated and the steady-state characterization of their allosteric properties at pH 6.0 (●), 7.0 (□) and 8.0 (▲). The data was obtained at 25°C and using 50 mM MES-KOH at pH 6.0, 50 mM MOPS-KOH at pH 7.0 and 50 mM EPPS-KOH at pH 8.0. The concentration of MgATP was equal to 3 mM. All the curves correspond to the best fit of these data to Eq. 2-4 and the error bars represent ± the standard error. (*A*) The 2:2H(30&45) hybrid obtained by using the [b,□] mutant protein and its allosteric characterization. (*B*) The 2:2H(30&45) hybrid obtained by using the [a,□] mutant protein and its allosteric characterization. (*C*) The 2:2H(22&32) hybrid and its allosteric characterization.

A

2:2H(30&45)
[b,□]

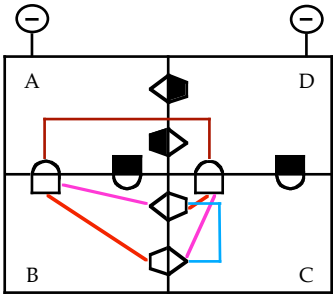

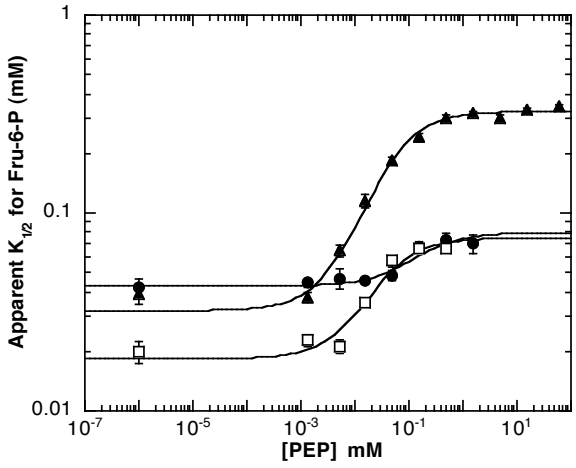

B

2:2H(30&45)
[a,□]

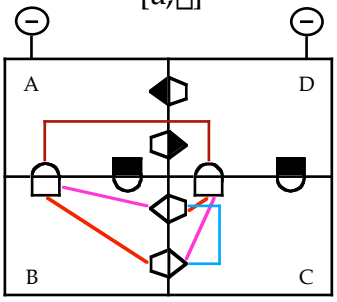

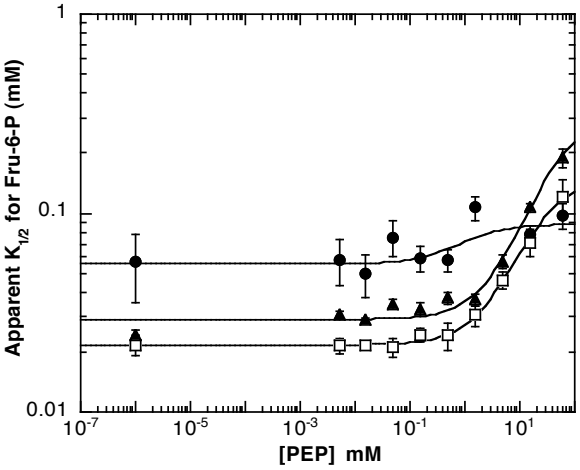

C

2:2H(22&32)
[b,□]

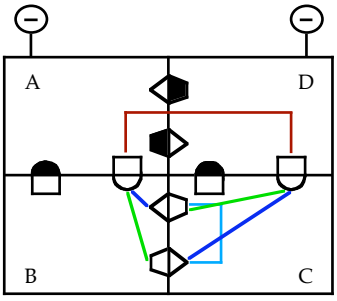

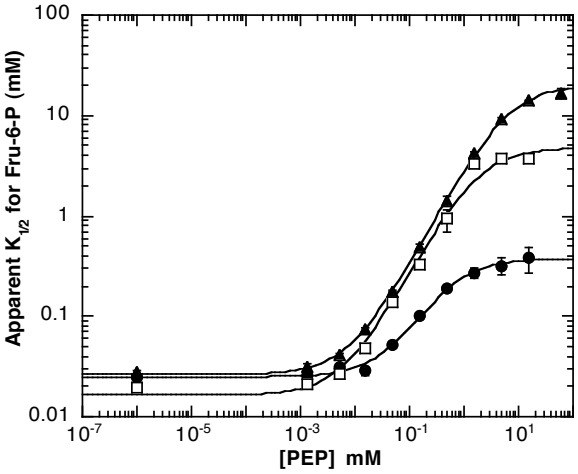

TABLE 6-4 A summary of the kinetic and thermodynamic parameters obtained for the 2:2H hybrids at 25°C, pH 6.0, 7.0 and 8.0 and [MgATP] = 3 mM

2:2 Hybrid	K_{ia}^{o} (mM)	K_{iy}^{o} (mM)	Q_{ay}	ΔG_{ay} (kcal/mol)
pH 6.0				
2:2H(30&45) ([b,□])	0.043 ± 0.002	0.087 ± 0.046	0.54 ± 0.05	0.36 ± 0.06
2:2H(30&45) ([a,□])	0.055 ± 0.007	0.55 ± 0.45	0.59 ± 0.09	0.31 ± 0.09
2:2H(22&32)	0.025 ± 0.001	0.038 ± 0.004	0.067 ± 0.007	1.60 ± 0.07
pH 7.0				
2:2H(30&45) ([b,□])	0.018 ± 0.001	0.0088 ±0.0020	0.25 ± 0.02	0.83 ± 0.05
2:2H(30&45) ([a,□])	0.022 ± 0.001	3.1 ± 0.9	0.15 ± 0.05	1.14 ± 0.14
2:2H(22&32)	0.016 ± 0.001	0.0083 ± 0.0001	0.0035 ± 0.0002	3.35 ± 0.05
pH 8.0				
2:2H(30&45) ([b,□])	0.032 ± 0.002	0.0046 ± 0.0006	0.099 ± 0.006	1.37 ± 0.04
2:2H(30&45) ([a,□])	0.029 ± 0.001	3.9 ± 0.6	0.094 ± 0.021	1.40 ± 0.14
2:2H(22&32)	0.026 ± 0.001	0.0083 ± 0.0004	0.0013 ± 0.0001	3.92 ± 0.03

hybrids, only the 2:2H(30&45) hybrid isolated by using the [a,□] mutant protein (Fig. 6-12 *B*) displays a decreased binding affinity for PEP (K_{iy}^{o}) when compared to the other two 2:2H hybrids. This observation has also been made for the 2:2V(22&45) hybrid and the 2:2D(32&45) hybrid, both of which use the [a,□] mutant protein, but with different charge tags. Due to this decreased binding affinity, the data are unable to reach saturation before 5 mM PEP at pH 7.0 and 8.0, thus binding of PEP at the mutated allosteric sites may influence the measured coupling for this particular 2:2H(30&45) hybrid resulting in an increased apparent coupling at pH 7.0 and 8.0. This possible effect from PEP binding to the mutated allosteric sites is substantiated by the fact that the coupling free energy for the 2:2H(30&45) hybrid obtained by using the [a,□] mutant protein is somewhat greater than the other 2:2H(30&45) hybrid at pH 7.0 and 8.0 (see Table 6-4).

Characterization of the 28 Å homotropic interaction between active sites via the 2:2H hybrids. Figures 6-13 *A, B* and *C* summarize the results regarding the cooperativity in Fru-6-P binding determined for the 28 Å homotropic interaction between active sites for the three 2:2H hybrids. Once again we see the same overall pattern in the Hill number. For all three 2:2H hybrids, the Hill numbers for Fru-6-P binding in the absence and saturating presence of PEP are equivalent, and in this case are all equal to approximately 1. Therefore, $Q_{aa} = Q_{aa/yy}$ and the homotropic interaction between active sites does not contribute to the overall heterotropic allosteric effect for these 2:2 hybrids.

FIGURE 6-13 The characterization of the 28 Å homotropic interaction between active sites by following the dependence of the Hill number (n_H) determined for Fru-6-P binding as a function of increasing concentrations of PEP for the 2:2H hybrids. The data was obtained at 25°C and at pH 6.0 (●) using 50 mM MES-KOH, at pH 7.0 (□) using 50 mM MOPS-KOH and at pH 8.0 (▲) using 50 mM EPPS-KOH. The concentration of MgATP was equal to 3 mM, and the error bars represent ± the standard error. (*A*) The 2:2H(30&45) hybrid obtained by using the [b,□] mutant protein. (*B*) The 2:2H(30&45) hybrid obtained by using the [a,□] mutant protein. (*C*) The 2:2H(22&32) hybrid.

A

2:2H(30&45)
[b,□]

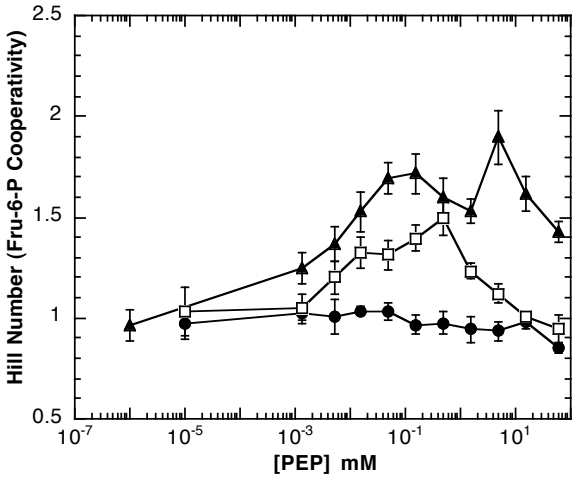

B

2:2H(30&45)
[a,□]

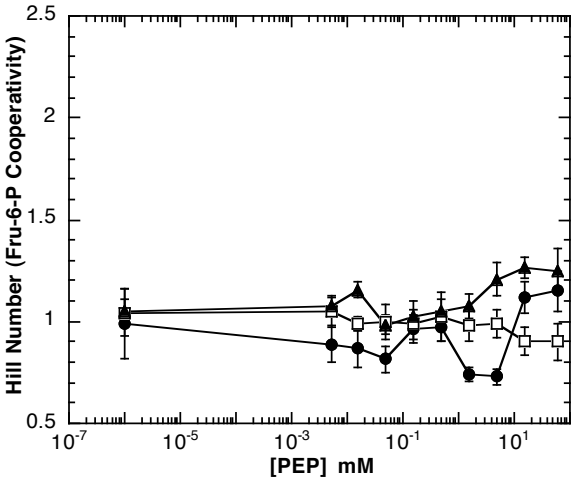

C

2:2H(22&32)
[b,□]

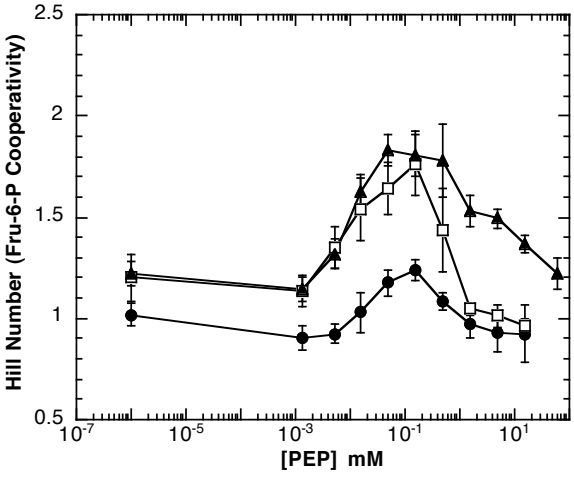

More specifically, the Hill numbers for Fru-6-P binding measured for the 2:2H(30&45) hybrid obtained by using the [b,□] mutant protein (Fig. 6-13 *A*) behave just like the other 2:2 hybrids obtained by using the same mutant protein (the 2:2V(30&32) and 2:2D(22&30) hybrids). The Hill numbers begin and end at 1 displaying subsaturating heterotropic cooperativity at pH 7.0 and 8.0, but not at 6.0 because the coupling (Q_{ay}) measured for the 30 Å heterotropic interaction is equal to 1 at pH 6.0. The other 2:2H(30&45) hybrid obtained by using the [a,□] mutant construct (Fig. 6-13 *B*) also behaves like the other 2:2 hybrids obtained from using that particular mutant protein (the 2:2V(22&45) and 2:2D(32&45) hybrids). The Hill numbers essentially stay at 1 until the higher concentrations of PEP at which point evidence of subsaturating heterotropic cooperativity possibly occurs. This behavior is consistent with the elevated K^{o}_{iy} value for this 2:2 hybrid, and the Hill number is assumed to return to a value of 1 since that is the case for all of the other 2:2 hybrids investigated. The final 2:2H hybrid, the 2:2H(22&32) hybrid obtained from using the [b,□] mutant protein (Fig. 6-13 *C*), is the only 2:2 hybrid that does not conform to the previous hybrids made utilizing the [b,□] mutant protein. The Hill number begins and ends at 1 while displaying subsaturating heterotropic cooperativity at all three pH values, whereas the Hill numbers for the other 2:2 hybrids formed utilizing the [b,□] mutant protein stayed constant as a function of PEP concentration. However, the subsaturating effect observed for the 2:2H(22&32) hybrid is consistent with the fact that both of the couplings (Q_{ay}) measured for the 22 Å and 32 Å heterotropic interactions are less than 1 at all three pH values and that the

maximum Hill number is measured at pH 8.0.

Characterization of the 40 Å homotropic interaction between allosteric sites via the 2:2H hybrids. The 40 Å homotropic interaction between allosteric sites is the last allosteric interaction to characterize, and the results from measuring the Hill number for PEP binding as a function of Fru-6-P concentration are shown in Figs. 6-14 *A* and *B*. Due to the elevated K^{o}_{iy} value for the 2:2H(30&45) obtained by using the [a,□] mutant protein, the individual PEP saturation profiles were unable to define a lower plateau within the range of PEP concentrations available, thus the 40 Å homotropic interaction was unable to be characterized for that particular 2:2 hybrid. Fortunately however, we were able to characterize the 40 Å homotropic interaction for the other 2:2H(30&45) hybrid obtained by using the [b,□] mutant protein and the results are shown in Fig. 6-14 *A*. The Hill number for PEP binding at pH 7.0 and 8.0 begins at a value greater than 1 at low Fru-6-P and proceeds to 1 at high Fru-6-P, conforming to the same behavior observed for the 23 Å homotropic interaction discussed previously. Unfortunately, the Hill numbers were difficult to determine for the 2:2H(30&45) hybrid obtained by using the [b,□] mutant protein (similar to the problem encountered for the 2:2V(30&32) hybrid discussed earlier using the same mutant protein), thus the number of points is decreased, and data were even unable to be collected at pH 6.0. However, even with the limited amount of data, Eq. 6-12 was used to determine the Hill numbers in the absence of Fru-6-P at pH 7.0 and8.0, and those results are summarized in Table 6-5 (the Hill number in the saturating presence of Fru-6-P was assumed to be 1; $Q_{yy/aa} = 1$). Furthermore,

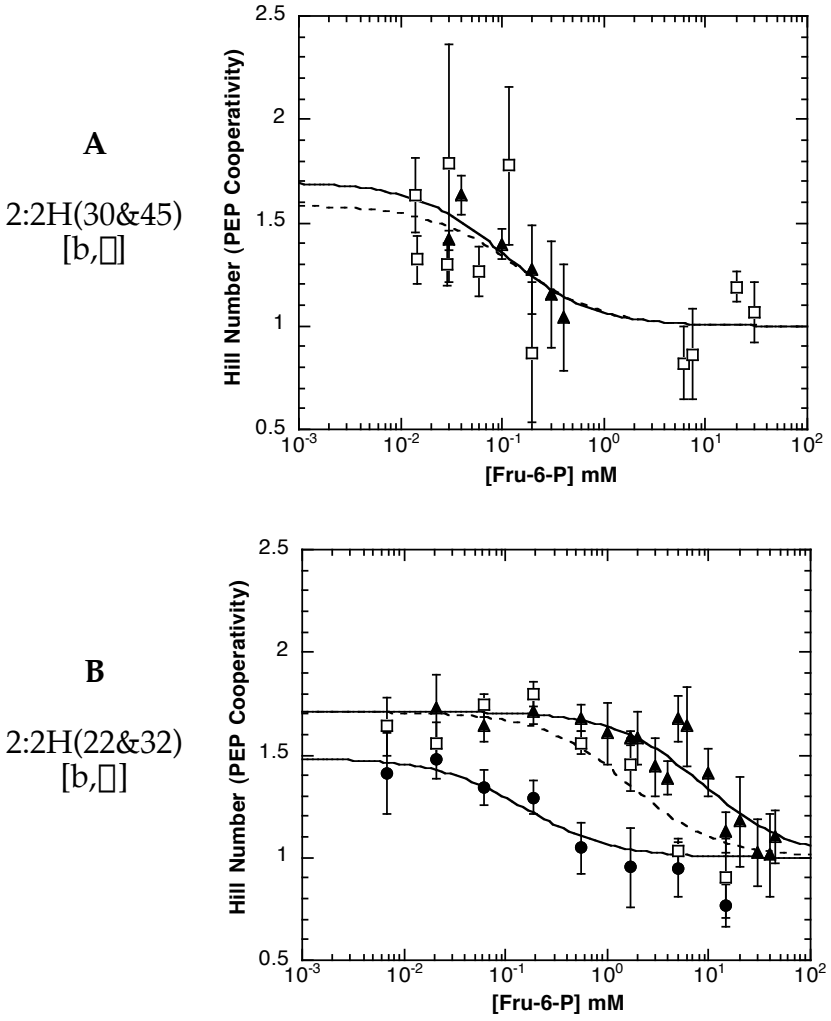

FIGURE 6-14 The characterization of the 40 Å homotropic interaction between allosteric sites by following the dependence of the Hill number (n_H) determined for PEP binding as a function of increasing concentrations of Fru-6-P for two of the 2:2H hybrids. The data was obtained at 25°C and at pH 6.0 (●) using 50 mM MES-KOH, at pH 7.0 (□) using 50 mM MOPS-KOH and at pH 8.0 (▲) using 50 mM EPPS-KOH. The concentration of MgATP was equal to 3 mM, and the error bars represent ± the standard error. (*A*) The 2:2H(30&45) hybrid obtained by using the [b,□] mutant protein. (*B*) The 2:2H(22&32) hybrid.

TABLE 6-5 A summary of the kinetic and thermodynamic parameters obtained in characterizing the 40 Å homotropic interaction between allosteric sites

Hybrid and pH	n_H	Q_{yy}	$\left(\frac{Q_{yy/aa}}{Q_{yy}}\right)^{1/2}$	$\Delta G_{40Å}$* (kcal/mol)
2:2H(30&45)				
7.0	1.58 ± 0.24	14.14 ± 16.70	0.27 ± 0.16	0.78 ± 0.35
8.0	1.70 ± 0.19	32.15 ± 41.35	0.18 ± 0.11	1.03 ± 0.38
2:2H(22&32)				
6.0	1.51 ± 0.11	9.49 ± 4.48	0.32 ± 0.08	0.67 ± 0.14
7.0	1.77 ± 0.05	59.23 ± 25.97	0.13 ± 0.03	1.21 ± 0.13
8.0	1.71 ± 0.04	34.77 ± 9.73	0.17 ± 0.02	1.05 ± 0.08

$$^{*}\Delta G_{40Å} = \frac{1}{2}\left(\Delta G_{yy/aa} - \Delta G_{yy}\right) = -RT\left(\frac{Q_{yy/aa}}{Q_{yy}}\right)^{1/2}$$

Equation 6-10 was used to calculate Q_{yy}, and the reciprocal of that value raised to the one-half power was used to determine the contribution of the 40 Å homotropic interaction to the coupling measured for the 2:2H(30&45) hybrid. The Gibbs free energy equation (Eq. 2-6) was then used to convert the coupling contribution into free energy terms. Thus, the 40 Å interaction was found to contribute approximately 0.8 kcal/mol at pH 7.0 and about 1 kcal/mol at pH 8.0 to the overall inhibition measured for the 2:2H(30&45) hybrid.

The 2:2H(22&32) hybrid also displayed the same trend in PEP cooperativity, and the same data analysis was performed to determine the

contribution of the 40 Å homotropic interaction in the 2:2H(22&32) hybrid at pH 6.0, 7.0 and 8.0. The results are also summarized in Table 6-5 and agree within error to the contribution measured for the same interaction found in the 2:2H(30&45) hybrid.

At pH 6.0, the 40 Å interaction contributes approximately 0.7 kcal/mol, at pH 7.0 about 1.2 kcal/mol and at pH 8.0 approximately 1.0 kcal/mol. Thus, for the 2:2H hybrids, the 28 Å homotropic interaction between active sites contributes nothing while the 40 Å interaction contributes significantly to the observed allosteric effect measured in the 2:2H hybrids.

How the allosteric interactions combine in the 2:2H hybrids. A comparison of the coupling free energies calculated for each 2:2H hybrid to the sum of the individual heterotropic interactions found within each 2:2 hybrid plus the 40 Å homotropic interaction is made in Figs. 6-15 *A, B* and *C*. The coupling free energy calculated for the 2:2H(30&45) hybrid obtained by using the [b,□] mutant protein is equivalent (within error) to the sum of the individual coupling free energies measured for the 30 Å and 45 Å heterotropic interactions and the contribution calculated for the 40 Å homotropic interaction at pH 7.0 and 8.0 (Fig. 6-15 *A*). However, since the contribution of the 40 Å homotropic interaction was not able to be calculated at pH 6.0, the contribution determined for the 40 Å homotropic interaction from the 2:2H(22&32) hybrid was used instead, and the coupling free energy determined for the 2:2 hybrid is less than the sum of the individual coupling free energies. Although this phenomenon is unexplained, the results are consistent with other 2:2 hybrids.

FIGURE 6-15 The comparison of the sum of the individual coupling free energies determined for the heterotropic interactions and the 40 Å homotropic contribution to the coupling free energy determined for the 2:2H hybrids at pH 6.0, 7.0 and 8.0. (*A* and *B*) The bar on the left at each pH corresponds to the sum of the coupling free energies determined for the 30 Å interaction (light gray), the 45 Å interaction (black), and the 40 Å homotropic interaction (horizontal lines, asterisks means it was measured via the 2:2H(22&32) hybrid). The bar on the right corresponds to the coupling free energy measured for either the 2:2H(30&45) hybrid obtained by using the [b,□] mutant protein (diagonal stripes - *A*) or the 2:2H(30&45) hybrid obtained by using the [a,□] mutant protein (polka-dots - *B*). (*C*) The bar on the left at each pH corresponds to the sum of the coupling free energies determined for the 22 Å interaction (white), the 32 Å interaction (dark gray), and the 40 Å homotropic interaction (horizontal lines), while the bar on the right corresponds to the coupling free energy determined for the 2:2H(22&32) hybrid (bricks).

A

2:2H(30&45)
[b,□]

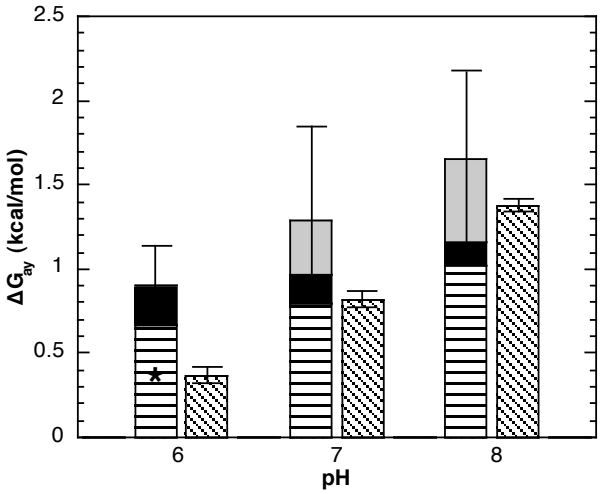

B

2:2H(30&45)
[a,□]

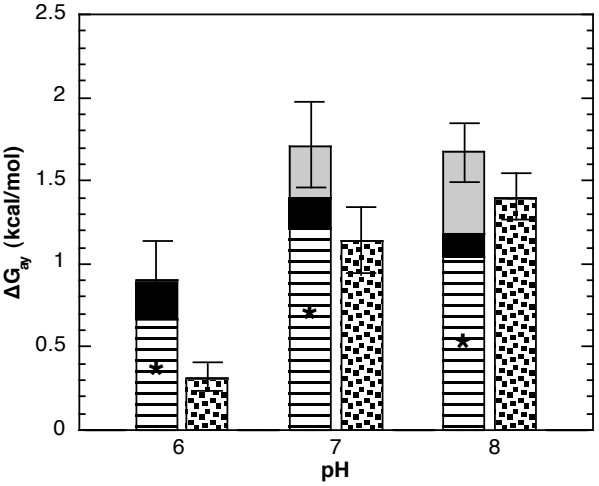

C

2:2H(22&32)
[b,□]

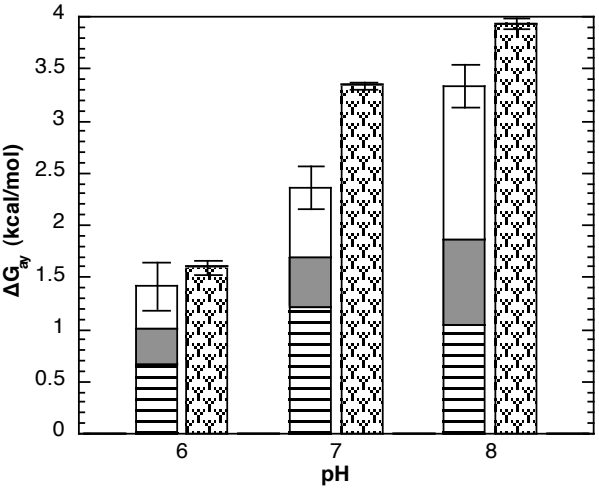

As for the 2:2H(30&45) hybrid obtained by using the [a,□] mutant protein, the same trend is seen as the coupling free energy for the 2:2 hybrid is equivalent to the sum at pH 7.0 and 8.0, but less than the sum at pH 6.0 (Fig. 6-15 *B*); however, all the data pertaining to the contribution of the 40 Å homotropic interaction was obtained from the 2:2H(22&32) hybrid.

The remaining 2:2H hybrid, the 2:2H(22&32) hybrid, was also found to have a coupling free energy equivalent (within error) to the sum of the coupling free energies measured for its individual allosteric interactions, but only at pH 6.0 as seen in Fig. 6-15 *C*. At 7.0 and 8.0, the coupling free energy for the 2:2H(22&32) hybrid is actually greater than the sum of the coupling free energies of the 22 Å and 32 Å heterotropic interactions and the contribution measured for the 40 Å homotropic interaction, with the greatest discrepancy occurring at pH 7.0 (~ 1 kcal/mol, only ~ 0.5 kcal/mol at pH 8.0). Of all the 2:2 hybrids investigated, this is the only case in which the data does not agree with the expected results.

Discussion

At the beginning of this chapter, we set out to address three different issues through the characterization of the 2:2 hybrids. The first of these issues was determining the contributions of each of the six unique homotropic interactions to the inhibition measured for each 2:2 hybrid. In each of the 2:2 hybrids, two homotropic interactions are isolated (besides the two copies of two heterotropic interactions), and consist of one homotropic interaction between active sites and one homotropic interaction between allosteric sites.

Furthermore, three different pairs of homotropic interactions are isolated in the various 2:2 hybrids characterized. The 2:2V hybrids isolate the 47 Å homotropic interaction between active sites and the 39.9 Å homotropic interaction between allosteric sites, the 2:2D hybrids isolate the 45 Å homotropic interaction between active sites and the 23 Å homotropic interaction between allosteric sites, and the 2:2H hybrids isolate the 28 Å homotropic interaction between active sites and the 40 Å homotropic interaction between allosteric sites.

From measuring the cooperativity in Fru-6-P binding as a function of PEP concentration, we were able to calculate the contributions each of the three homotropic interactions between active sites make to the apparent heterotropic allosteric effect measured for the 2:2 hybrids. For all three homotropic interactions between active sites (47 Å, 45 Å and 28 Å), the net change in the Hill number measured for Fru-6-P binding in the absence and saturating presence of PEP is zero, thus Q_{aa} and $Q_{aa/yy}$ are equivalent for all three homotropic interactions between active sites. Consequently, none of the homotropic interactions between active sites contribute to the measured allosteric effect between Fru-6-P and PEP since the contribution to the allosteric effect is determined from the ratio of $Q_{aa/yy}$ to Q_{aa} (Eq. 6-2).

By performing the reverse experiment and determining the cooperativity in PEP binding as a function of Fru-6-P concentration, we were able to calculate the contributions each of the homotropic interactions between allosteric sites makes to the heterotropic allosteric effect measured for the 2:2 hybrids. For the 39.9 Å homotropic interaction, the net change in the Hill number measured for

PEP binding in the absence and saturating presence of Fru-6-P was zero, thus Q_{yy} and $Q_{yy/aa}$ are equal to one another, resulting in no net allosteric effect from the 39.9 Å homotropic interaction. On the other hand, the net change in the Hill number for PEP binding in the absence and saturating presence of Fru-6-P was negative for both the 23 Å and 40 Å homotropic interactions. Thus, Q_{yy} is greater than $Q_{yy/aa}$ resulting in an augmentation in the allosteric effect measured for the 2:2 hybrids ($\Delta G_{homo\_allos} > 0$). In summary, of the six homotropic interactions possible in the native enzyme, we determined that 4 of the homotropic interactions contribute nothing to the observed allosteric effect between Fru-6-P and PEP, and 2 of the homotropic interactions between allosteric sites (23 Å and the 40 Å) contribute between 0.4 kcal/mol to 1.2 kcal/mol depending on if it is the 23 Å or 40 Å homotropic interaction and the pH at which the contribution is measured.

The second issue we wanted to address at the outset of this chapter was subsaturating heterotropic cooperativity (in Fru-6-P binding), and for the most part, the expectations agreed with the experimental results. When both heterotropic couplings were greater than 1, subsaturating heterotropic cooperativity occurred with the largest maximum Hill number measured at pH 8.0, consistent with how pH affects Fru-6-P-PEP coupling. However, most of the unexplainable data regarding the Hill number for Fru-6-P binding were obtained from the hybrids constructed using the [a,β] mutant protein (isolates the 45 Å heterotropic interaction in its 1|1 hybrid with wild-type). For the 2:2V(22&45) and 2:2H(32&45) hybrids, the Hill number essentially stays at 1

regardless of the PEP concentration or pH. This implies that one of the heterotropic interactions has a coupling equal to 1, but for the 2:2H(32&45) hybrid obtained using the [b,□] mutant protein, subsaturating heterotropic cooperativity is observed. Thus, the mutations used in making the [a,□] mutant protein more than likely interfere with the transmission of the allosteric signal for the 45 Å interaction since that is the common link among the 2:2 hybrids displaying this strange behavior in Fru-6-P binding.

Finally, how the pair-wise allosteric interactions combine in the simplest of oligomers, a dimer, is the final issue we wanted address with the allosteric characterizations of not only the 2:2 hybrids (2|2), but the 1:3 hybrids as well (1|1). From our previous work with the 1:3 hybrids, we calculated the coupling free energies for the four heterotropic interactions (22 Å, 30 Å, 32 Å and 45 Å) at pH 6.0, 7.0 and 8.0, and from our current investigation we calculated the allosteric contributions of the six homotropic interactions as well as the overall coupling free energy measured for each of the nine 2:2 hybrids at pH 6.0, 7.0 and 8.0. With all of the necessary parameters determined ($\Delta G_{2:2\ hybrid}$, ΔG_{ay1}, ΔG_{ay2}, $\Delta G_{homo\text{-}allos}$ and $\Delta G_{homo\text{-}active}$) we are equipped to assess which of the allosteric models previously described are accurate in describing the observed allosteric effect for each of the nine 2:2 hybrids.

For the most part, at pH 7.0 and 8.0, the "conformational free/linkage" model more adequately describes the measured allosteric effect for BsPFK since the coupling free energy for the nine 2:2 hybrids is within 0.5 kcal/mol (or less) to the sum of the coupling free energies determined for the individual

heterotropic interactions and the homotropic contribution. Only the 2:2D(32&45) hybrid obtained using the [b,□] mutant protein behaves in a manner not predicted by the conformational free/linkage" model since the measured coupling free energy for the 2:2 hybrid is significantly less (about 0.5 – 1.0 kcal/mol) than the sum of the coupling free energies determined for the individual heterotropic interactions and the homotropic contribution. However, neither the concerted or sequential models adequately describe this behavior either. The minor discrepancies observed at pH 7.0 and 8.0 for the other eight 2:2 hybrids we believe can be explained by one of two factors. The first factor is the possible influence from PEP binding to the mutated allosteric sites and influencing the coupling free energy measured for the 2:2 hybrid. In a few cases when measuring Q_{ay} (monitoring the $K_{1/2}$ for Fru-6-P as a function of PEP concentration), an upper plateau is not suitably reached prior to about 5 mM PEP, and we believe this allows the binding of PEP at the mutated allosteric sites to potentially influence the allosteric effect measured for the 2:2 hybrid, leading to a greater apparent coupling free energy. Unfortunately, control hybrids for these 2:2 hybrids were unable to be made to determine exactly at what point PEP binding to the mutated allosteric sites occurs. However, in some cases when both the K^{o}_{iy} and coupling for the 2:2 hybrid ($Q_{2:2\ Hybrid}$) are relatively small, the point at which PEP binds to the mutated allosteric sites can be defined experimentally. This is shown in Fig. 6-16 using the allosteric characterization of the 2:2V(30&32) hybrid as an example. At all three pH values, the upper plateau, defining K^{o}_{ia}, is reached well before 1 mM PEP, however at about 5 mM

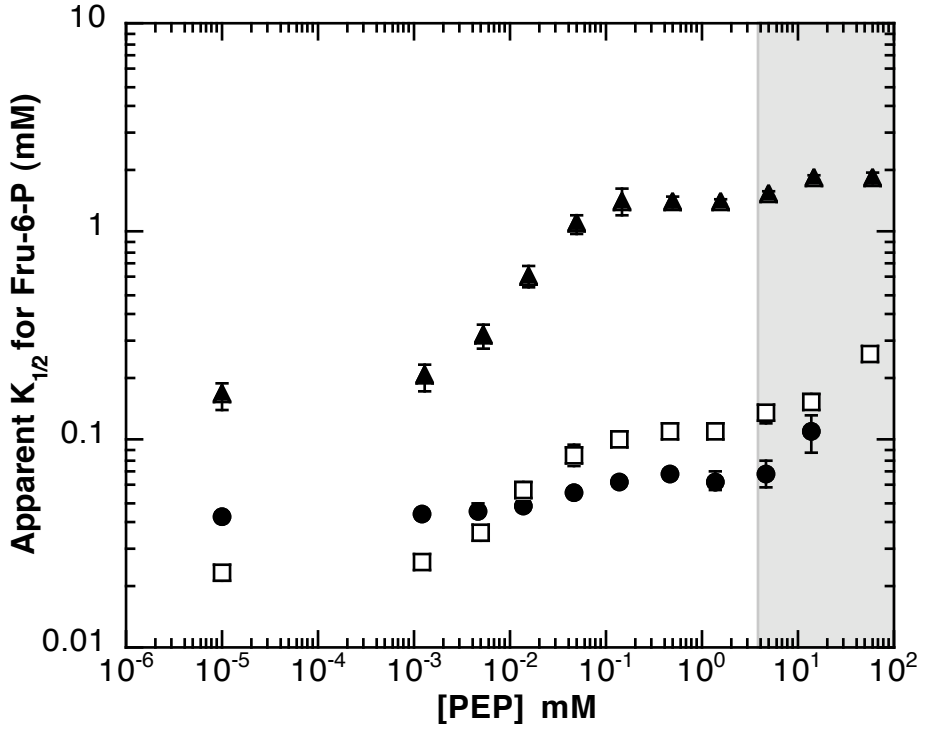

FIGURE 6-16 The dependence upon the apparent $K_{1/2}$ for Fru-6-P as a function of PEP concentration for the 2:2V(30&32) hybrid obtained from using the [b,□] mutant protein. The gray region indicates the point at which PEP binds at the mutated allosteric sites and begins to influence the apparent $K_{1/2}$ for Fru-6-P (~5 mM). The steady-state characterization was performed at pH 6.0 (●), 7.0 (□) and 8.0 (▲), and at 25°C using 50 mM MES-KOH at pH 6.0, 50 mM MOPS-KOH at pH 7.0 and 50 mM EPPS-KOH at pH 8.0. The concentration of MgATP was equal to 3 mM and the error bars represent ± the standard error.

PEP the apparent $K_{1/2}$ for Fru-6-P begins to edge upwards, increasing with increasing concentrations of PEP at all three pH values. These points identify the concentration of PEP in which PEP binds to the mutated allosteric sites and begins to influence Fru-6-P affinity at the native active sites. In our original analysis when this second phase was observed, those data points were just simply removed from the analysis. From these results and several others just like Fig. 6-16, we believe that PEP binding at the mutated allosteric sites is a suitable explanation for why the coupling free energy determined for some of the 2:2 hybrids is greater than the sum of the coupling free energies of the individual allosteric interactions.

The other possible explanation to why the coupling free energy for some of the 2:2 hybrids is somewhat different than the sum of the allosteric interactions isolated within a given 2:2 hybrid is the uncertainty in the coupling free energy determined for the 45 Å heterotropic interaction, and the possibility of its contribution being eliminated in those 2:2 hybrids formed by using the [a,□] mutant protein. Due to the very minimal amount of coupling present in the 45 Å heterotropic interaction, it was especially challenging to measure an accurate Q_{ay} for the 45 Å heterotropic interaction, as evidenced by the level of error in both Q and ΔG (Chapter IV). Thus, if the contribution for the 45 Å heterotropic interaction is removed from the analysis of the pertinent 45 Å heterotropic-interaction-containing 2:2 hybrids, then the coupling free energy measured for the relevant 2:2 hybrids is equivalent to the sum of the coupling free energies for the individual allosteric interactions (minus the 45 Å

contribution).

Another phenomenon observed in our data when comparing the coupling free energies of the individual 2:2 hybrids to the sum of the coupling free energies determined for the allosteric interactions isolated within that given 2:2 hybrid, is that at pH 6.0 the coupling free energy for the 2:2 hybrid is sometimes lower than the sum for a few of the 2:2 hybrids. Unfortunately, we have no explanation to why this occurs, but in most instances the 45 Å heterotropic interaction is involved so that may explain part of the problem. However, in the case of the 2:2D(22&30) hybrid, we have no explanation for the possible reasons why the coupling for the 2:2 hybrid is so low.

All in all however, considering all of the mutations we have introduced at the binding sites and on the surface, we feel that the "conformational free/linkage" model most accurately describes the observed allosteric effect between Fru-6-P and PEP and *vice versa* for all nine of the 2:2 hybrids investigated. Furthermore, by taking our divide-and-conquer approach and gaining a better understanding of how inhibition occurs in not only the 2:2 hybrids, but the 1:3 hybrids as well, we now hope to address how inhibition occurs in the native tetramer, and more specifically to identify the structural aspects of how inhibition occurs in the native tetramer.

CHAPTER VII

CONCLUSIONS

At the onset of this investigation, our major goal was to resolve the allosteric contributions of the 10 unique pair-wise allosteric interactions found within BsPFK to the inhibition by PEP binding. In order to accomplish this goal, we created numerous hybrid tetramers of BsPFK to contain a specific number of native binding sites and mutated binding sites in known structural relationships, such that the mutated binding sites could not bind Fru-6-P or PEP. Upon isolating and characterizing these various hybrid tetramers, the contributions of all 10 unique allosteric interactions were measured permitting us to "map" the entire inhibition landscape in BsPFK.

The first hybrid tetramers constructed and characterized were the 1:3 hybrids (1|1, 1|0 and 4|1), and they were utilized for several purposes. First and foremost, the four 1|1 hybrids individually isolated each of the four heterotropic interactions permitting the characterization of each heterotropic interaction one at a time. Next, the 1|0 hybrids were used to "correct" for the contributions to these apparent couplings (Q_{ay}) of PEP binding to the mutated allosteric sites. Lastly, a wild-type control hybrid (4|1) was required to compare the values obtained for the "corrected" contributions of the four heterotropic interactions to the inhibition measured for the wild-type enzyme in the absence of homotropic cooperativity between allosteric sites. Thus, although the three different 1:3 hybrids isolate a different number of native allosteric interactions (one, none and four respectively), the 1:3 hybrids enabled us to address

questions otherwise impossible to address in the native tetramer.

Next, the 2:2 hybrids (2|2) were characterized to determine the relative contributions of each of the six homotropic interactions found within the native enzyme. Based upon the 2:2 hybrid investigated, a different set of six pair-wise allosteric interactions were isolated: 2 copies of two different heterotropic interactions, 1 copy of one homotropic interaction between active sites and 1 copy of one homotropic interaction between allosteric sites. By simply measuring both Fru-6-P and PEP cooperativity for the 2:2 hybrid, the coupling free energies as well as the allosteric contributions of the two isolated homotropic interactions were determined (Reinhart, 1988). Moreover, different 2:2 hybrids were then investigated to determine the contributions of all six homotropic interactions to the inhibitory response in BsPFK.

None of the pair-wise allosteric interactions would have been characterized without the addition of the surface charge tags to the mutated subunits (K90E/K91E, R232E/Q233E, or N303E/K304E). Each charge tag was responsible for the isolation and identification of either a 1:3 hybrid or a specific 2:2 hybrid/isomer from the other hybrid species. Without the use of the three different charge tags, deciphering the roles of the individual allosteric interactions would have been impossible. Fortunately, all of the previously mentioned hybrid species were formed and isolated using either the monomer or dimer exchange procedure and anion exchange chromatography. A summary of the coupling free energies determined from the allosteric characterizations of all 10 pair-wise allosteric interactions are found in Table 7-1.

TABLE 7-1 The coupling free energies (ΔG_{ay}, ΔG_{yy} or ΔG_{aa}) in kcal/mol determined from the allosteric characterizations of the 10 pair-wise allosteric interactions via the 1:3 and 2:2 hybrids at 25°C and [MgATP] = 3 mM

Interaction	pH 6.0	pH 7.0	pH 8.0
ΔG_{ay} (heterotropic)			
22 Å	0.41 ± 0.10	0.66 ± 0.10	1.48 ± 0.15
30 Å	0.00 ± 0.06	0.31 ± 0.11	0.49 ± 0.11
32 Å	0.34 ± 0.10	0.57 ± 0.10	0.82 ± 0.12
45 Å	0.23 ± 0.14	0.18 ± 0.14	0.17 ± 0.20
ΔG_{yy} (homotropic)			
23 Å	-0.71 ± 0.21	-1.24 ± 0.10	-1.46 ± 0.14
39.9 Å	0	0	0
40 Å	-1.33 ± 0.28	-2.41 ± 0.26	-2.09 ± 0.17
ΔG_{aa} (homotropic)			
28 Å	0	0	0
45 Å	0	0	0
47 Å	0	0	0

One major finding from this investigation, and the investigation of Kimmel and Reinhart (2001), is the fact that the four heterotropic interactions are unique in magnitude and vary in their individual contributions to the inhibitory response depending upon pH. Moreover, when we compared the coupling free energies measured for each interaction to the coupling free energy determined for the wild-type enzyme (4|4), the entire allosteric effect was not accounted for

at any of the pH values investigated. Initially we attributed this to the mutations introduced at both the active and allosteric sites and on the surface of the protein. However, upon further consideration we discovered that the homotropic interactions between the allosteric sites are also involved in PEP inhibiting the enzyme. This was confirmed by constructing a 4|1 hybrid in which the cooperativity between the allosteric sites was removed. Thus, when comparing the coupling free energy measured for the 4|1 hybrid to the sum of the coupling free energies determined for the four heterotropic interactions, we ended up accounting for the entire allosteric response incurred by PEP! This result verified that our approach of isolating each of the four heterotropic interactions found within BsPFK via the 1:3 hybrids only affects Fru-6-P and PEP binding and not the allosteric coupling between the remaining native binding sites. More importantly however, the fact that each heterotropic interaction is unique in magnitude instantly discounts the ability of the concerted and sequential models to explain the observed allosteric effect in BsPFK.

The characterizations of the homotropic interactions also yielded very exciting results. Of the six homotropic interactions found in the native tetramer, four were found to be entirely uninvolved in the inhibitory response, including all three of the homotropic interactions between active sites. This result only validated our previous data involving the 4|1 wild-type control hybrid because, if the homotropic interactions between active sites *were involved* in the inhibition process, then the coupling free energy measured for the 4|1 hybrid would *not*

have equaled the sum of the coupling free energies measured for the four heterotropic interactions. However, two of the six homotropic interactions, the 23 Å and 40 Å homotropic interactions between allosteric sites, were found to participate in the PEP inhibition of the enzyme because the Hill number for PEP binding decreased in the saturating presence of Fru-6-P. Thus, PEP's effects are augmented by the 23 Å and 40 Å homotropic interactions (Reinhart, 1988). In summary, of all 10 interactions, 6 play a role in the inhibition process revealing an asymmetric response in PEP binding to this symmetrical enzyme. Furthermore, using the various hybrid tetramers of BsPFK and taking a divide-and-conquer approach, we have been able to take a convoluted mess of allosteric communication pathways and resolve what role each interaction plays in the inhibition process.

The other major goal we wanted to address was how the individual allosteric interactions combine in the simplest of oligomers, a dimer. Using all of the data obtained from the characterizations of both the 1:3 and 2:2 hybrids, we addressed this very issue. In Chapter VI, we showed for the first time that the predictions set forth by Reinhart (1988) regarding the allosteric behavior of a symmetrical dimer were correct. Essentially we showed that the entire heterotropic effect between two heterotropic ligands could be accounted for in a symmetrical dimer (containing one active site and one allosteric site per subunit) by the individual contributions of the two heterotropic interactions and a ratio of the contributions from both the homotropic interactions in the saturating presence and absence of the heterotropic ligand. Moreover, the contributions of

these interactions could vary to any extent from one interaction dominating the allosteric effect, to all of the interactions participating equally in the inhibition process. Regardless of these contributions, our data showed quite convincingly that the entire allosteric effect could be accounted for using the predictions made by Reinhart (1988).

The predictions made by Reinhart are based on a linked-function analysis. Thus, this entire investigation provides support that this approach in characterizing an allosteric effect is the more appropriate method for understanding how an effector molecule regulates enzyme activity. In addition, it is the formation of the ternary complex (enzyme with both substrate and effector bound) that is the key to understanding an entire allosteric effect, whereas the formation of the ternary complex is not even considered by the two-state models. The data regarding the 2:2 hybrid characterizations only provides further evidence (besides what was already presented regarding the 1:3 hybrids) that the predictions set forth by both the concerted and sequential models are not accurate for describing the inhibition of BsPFK by PEP.

Where would I like this investigation to go next? First, I would want the structural aspect of allosteric regulation elucidated in BsPFK. With the contributions of the 10 allosteric interactions now defined, it would be my hope that certain regions of the protein or even key residues could be identified as being responsible for transmitting the inhibitory signal for certain allosteric interactions. This is already starting to be addressed in both EcPFK and BsPFK by using single point mutations at locations identified by either a sequence

alignment with a non-allosteric PFK or regions of the protein identified from the crystal structure as possibly being involved due to their locations between binding sites.

Another aspect of BsPFK's regulation that needs to be addressed is the identification of the residues that are ionized with the change in pH. This would only provide further information into the possible structural components involved in the transmission of the allosteric signal.

I would also like to see a dimeric enzyme that is allosterically regulated characterized using the same overall approach to compare with the results we have obtained with the 1:3 and 2:2 hybrids. I believe this would only substantiate further the requirement for the linked-function approach to be utilized whenever an allosteric effect is characterized. All in all, I think a better understanding of allosteric regulation has been gained from this investigation, and I only hope those that follow in this work will build upon the foundation I have laid as well as the foundation laid by those before me.

REFERENCES

Ackers, G. K., P. M. Dalessio, G. H. Lew, M. A. Daugherty, and J. M. Holt. 2002. Single residue modification of only one dimer within the hemoglobin tetramer reveals autonomous dimer function. *Proc. Natl. Acad. Sci. USA*. 99:9777-9782.

Ackers, G. K., M. L. Doyle, D. Myers, and M. A. Daugherty. 1992. Molecular code of cooperativity in hemoglobin. *Science*. 255:54-63.

Ackers, G. K., J. M. Holt, Y. Huang, Y. Grinkova, A. L. Klinger, and I. Denisov. 2000. Conformation of a unique intra-dimer cooperativity in the human hemoglobin $\alpha_1\beta_1$ half-oxygenated intermediate supports the symmetry rule model of allosteric regulation. *Prot. Struct. Func. Gene. Suppl.* 4:23-43.

Babul, J. 1978. Phosphofructokinase from *Escherichia coli*. Purification and characterization of the nonallosteric isozyme. *J. Biol. Chem.* 253:4350-4355.

Blangy, D., H. Buc, and J. Monod. 1968. Kinetics of the allosteric interactions of phosphofructokinase from *Escherichia coli*. *J. Mol. Biol.* 31:13-35.

Bloxham, D. P., and H. A. Lardy. 1973. Phosphofructokinase. *In* The Enzymes, 3rd ed, Vol. 8. P. Boyer, editor. Academic Press, New York. 239-278.

Botts J., and M. Morales. 1953. Analytical description of the effects of modifiers and of enzyme multivalency upon steady-state catalyzed reaction rate. *Trans. Faraday Soc.* 49:696-707.

Braxton, B. L., V. L. Tlapak-Simmons, and G. D. Reinhart. 1994. Temperature induced inversion of allosteric phenomena. *J. Biol. Chem.* 269:47-50.

Bullock, W. O., J. M. Fernandez, and J. M. Short. 1987. XL1-blue: A high efficiency plasmid transforming *rec*A es. *Biotechniques*. 5:376-379.

Byrnes, M., W. Hu, E. S. Younathan, and S. H. Chang. 1995. A chimeric bacterial phosphofructokinase exhibits cooperativity in the absence of heterotropic regulation. *J. Biol. Chem*. 2170:3828-3835.

Byrnes, M., X. Zhu, E. S. Younathan, and S. H. Chang. 1994. Kinetic characteristics of phosphofructokinase from *Bacillus stearothermophilus*: MgATP nonallosterically inhibits the enzyme. *Biochemistry*. 33:3424-3431.

Chang, S. H., and R. G. Kemp. 2002. Role of Ser530, Arg292 and His662 in the allosteric behavior of rabbit muscle phosphofructokinase. *Biochem. Biophys. Res. Comm.* 290:670-675.

Cleland, W. W. 1963a. The kinetics of enzyme-catalyzed reactions with two or more substrates or products. I. Nomenclature and rate equations. *Biochim. Biophys. Acta.* 67:104-137.

Cleland, W. W. 1963b. The kinetics of enzyme catalyzed reactions with two or more substrates or products. II. Inhibition: nomenclature and theory. *Biochim Biophys. Acta.* 67:137-187.

Cohen, S. N., A. C. Y. Chang, and L. Hsu. 1972. Nonchromosomal antibiotic resistance in bacteria: Genetic transformation of *Escherichia coli* by R-factor DNA. Proc. Natl. Acad. Sci. 69:2110-2115.

Currie, P. D., and D. T. Sullivan. 1994. Structure and expression of the gene encoding PFK in *Drosophila melanogaster. J. Biol. Chem.* 269:24679-24687.

Daldal, F. 1983. Molecular cloning of the gene for phosphofructokinase-2 of *Escherichia coli* and the nature of a mutation, pfkB1, causing a high level of the enzyme. *J. Mol. Biol.* 168:285-305.

Decker, H., and R. Sterner. 1990. Nested allostery of arthropodan hemocyanins: The role of protons. *J. Mol. Bio.* 211:281-293.

Deville-Bonne, D., G. Le Bras, W. Teschner, and J. R. Garel. 1989. Ordered disruption of subunit interfaces during stepwise reversible dissociation of *Escherichia coli* phosphofructokinase with KSCN. *Biochemistry*. 28:1917-1922.

Eigen, M. 1967. Kinetics of reaction control and information transfer in enzymes and nucleic acids. *Nobel Symp*. 5:333-369.

Eroglu, B., and S. G. Powers-Lee. 2002. Unmasking a functional allosteric domain in an allosterically nonresponsive carbamoyl-phosphate synthetase. *J. Biol. Chem.* 277:45466-45472.

Evans, P. R., G. W. Farrants, and P. J. Hudson. 1981. Phosphofructokinase: Structure and control. *Phil. Trans. R. Soc.* Lond. B. 293:53-62.

Evans, P. R., G. W. Farrants, and M. C. Lawrence. 1986. Crystallographic structure of allosterically inhibited phosphofructokinase at 7 Å resolution. *J Mol. Biol*. 191:713-720.

Evans, P. R., and P. J. Hudson. 1979. Structure and control of phosphofructokinase from *Bacillus stearothermophilus*. *Nature*. 279:500-504.

Fenton, A. W., and G. D. Reinhart. 2002. Isolation of a single activating allosteric interaction in phosphofructokinase from *Escherichia coli*. *Biochemistry*. 41:13410-13416.

Fenton, A. W., and G. D. Reinhart. 2003. Identification of substrate contact residues important for the allosteric regulation of phosphofructokinase from *Escherichia coli. Biochemistry*. in press.

Freiden, C. 1964. Treatment of enzyme kinetic data. I. The effects of modifiers on the kinetic parameters of single substrate enzymes. *J. Biol. Chem.* 239:3522-3531.

Freire, E. 1999. The propagation of binding interactions to remote sites in proteins. Analysis of the binding of the monoclonal antibody D1.3 to lysozyme. *Proc. Natl. Acad. Sci. USA*. 96:10118-10122.

French, B. A., and S. H. Chang. 1987. Nucleotide sequence of the phosphofructokinase gene from *Bacillus stearothermophilus* and comparison with the homologous *Escherichia coli* gene. *Gene*. 54:65-71.

French, B. A., B. C. Valdez, E. S. Younathan, and S. H. Chang. 1987. High-level expression of *Bacillus stearothermophilus* 6-phosphofructo-1-kinase in *Escherichia coli*. *Gene*. 59:279-283.

Fushinobu, S., K. Kamata, S. Iwata, H. Sakai, T. Ohta, and H. Matsuzawa. 1996. Allosteric activation of lactate dehydrogenase analyzed by hybrid enzymes with effector-sensitive and –insensitive subunits. *J. Biol. Chem.* 271:25611-25616.

Gehnrich, S. C., N. Gekakis, and H. S. Sul. 1988. Liver (B-type) phosphofructokinase mRNA. *J. Biol. Chem*. 255:4240-4245.

Heinisch, J., G. Ritzel, R. C. von Bostel, A. Augilera, R. Rodicio, and F. K. Zimmerman. 1989. The phosphofructokinase genes of yeast evolved from two duplication events. *Gene*. 78:309-321.

Hellinga, H. W., and P. R. Evans. 1985. Nucleotide sequence and high-level expression of the major *Escherichia coli* phosphofructokinase. *Eur. J. Biochem.* 149:363-373.

Herzfeld, J., and H. E. Stanley. 1974. A general approach to cooperativity and its application to the oxygen equilibrium of hemoglobin and its effectors. *J. Mol. Bio.* 82:231-265.

Hill, A. V. 1910. The possible effects of the aggregation of the molecules of haemoglobin on its dissociation curves. *J. Physiol.* 40:iv-vii.

Hilser, V. J., T. Oas, D. Dowdy, and E. Freire. 1998. The structural distribution of cooperative interactions in proteins: Analysis of the native state ensemble. *Proc. Natl. Acad. Sci. USA*. 95:9903-9908.

Holt, J. M., and G. K. Ackers. 1995. The pathway of allosteric control as revealed by hemoglobin intermediate states. *FASEB J.* 9:210-218.

Hutchinson, C. A. 3rd, S. Phillips, M.H. Edgell, S. Gillam, P. Jahnke, and M. Smith. 1978. Mutagenesis at a specific position in a DNA sequence. *J. Biol. Chem*. 253:6551-6560.

Johnson, J. L., M. D. Lasagna, and G. D. Reinhart. 2001. Influence of a sulfhydryl cross-link across the allosteric-site interface of *Escherichia coli* phosphofructokinase. *Protein Science*. 10:2186-2194.

Johnson, J. L., and G. D. Reinhart. 1992. MgATP and fructose-6-phosphate interactions with phosphofructokinase from *Escherichia coli. Biochemistry.* 31:11510-11518.

Johnson, J. L., and G. D. Reinhart. 1994. Influence of MgADP on phosphofructokinase from *Escherichia coli*. Elucidation of coupling interactions with both substrates. *Biochemistry*. 33:2635-2643.

Johnson, J. L., and G. D. Reinhart. 1996. Effects of high pressure on the allosteric properties of phosphofructokinase from *Escherichia coli. In* High Pressure Effects in Molecular Biophysics and Enzymology. J. L. Markley, D. B. Northrop and C. A. Royer, editors. Oxford University Press, New York. 242-255.

Johnson, J. L., and G. D. Reinhart. 1997. Failure of a two-state model to describe the influence of phospho(enol)pyruvate on phosphofructokinase from *Escherichia coli*. *Biochemistry*. 36:12814-12822.

Kagawa, Y., H. Nojima, N. Nukiwa, M. Ishizuka, T. Nakajima, T. Yasuhara, T. Tanaka, and T. Oshima. 1984. High guanine plus cytosine content in the third letter of codons of an extreme thermophile. *J. Biol. Chem.* 259:2956-2960.

Kelly-Loughnana, N., and E. R. Kantrowitz. 2001. Binding of AMP to two of the four subunits of pig kidney fructose-1,6-bisphosphatase induces the allosteric transition. *Prot. Struct. Func. and Gene*. 44:255-261.

Kemp, R. G., and D. Gunasekera. 2002. Evolution of the allosteric ligand sites of mammalian phophofructo-1-kinase. *Biochemistry*. 41:9426-9430.

Kimmel, J. L. 2001. Investigation into the molecular basis for the allosteric regulation of phosphofructokinase from *Bacillus stearothermophilus*. Ph.D. Dissertation, Texas A&M University.

Kimmel, J. L., and G. D. Reinhart. 2000. Reevaluation of the accepted allosteric mechanism of phosphofructokinase from *Bacillus stearothermophilus*. *Proc. Natl. Acad. Sci. USA*. 97:3844-3849.

Kimmel, J. L., and G. D. Reinhart. 2001. Isolation of an individual allosteric interaction in tetrameric phosphofructokinase from *Bacillus stearothermophilus*. *Biochemistry*. 40:11623-11629.

Kolartz, D., and H. Buc. 1982. Phosphofructokinase from *Escherichia coli*. *Methods Enzymol*. 90:60-70.

Koshland, D. E., G. Nemethy, and D. Filmer. 1966. Comparison of experimental binding data and theoretical models in proteins containing subunits. *Biochemistry*. 5:365-385.

Kramer, B., W. Kramer, and H. J. Fritz. 1984. Different base/base mismatches are corrected with different efficiencies by the methyl-directed DNA mismatch-repair system of *E. coli*. *Cell*. 38:879-887.

Kurganov, B. I. 1982. Allosteric Enzymes Kinetic Behavior. John Wiley and Sons, New York.

Laemmli, U. K. 1970. Cleavage of structural proteins during the assembly of the head of bacteriophage T4. *Nature*. 227:680-685.

Le Bras, G., I. Auzat, and J. R. Garel. 1995. Tetramer-dimer equilibrium of phosphofructokinase and formation of hybrid tetramers. *Biochemistry*. 34:13203-13210.

Li, Y., D. Rivera, W. Ru, D. Gunasekera, and R. G. Kemp. 1999. Identification of allosteric sites in rabbit phosphofructokinase. *Biochemistry*. 38:16407-16412.

Li, Y., P. Valaitis, S. P. Latshaw, D. Kwiatkowska, R. L. Tripathi, M. C. Campbell, and R. G. Kemp. 1994. Structure and expression of cDNA for the C isozyme of phosphofructo-1-kinase from rabbit brain. *J. Biol. Chem.* 269:5781-5787.

Luque, I., and E. Freire. 2000. Structural stability of binding sites: Consequences for binding affinity and allosteric effects. *Prot. Struct. Func. Gene.* 4:63-71.

Martel, A., and J. R. Garel. 1984. Denaturation of the allosteric phosphofructokinase from *Escherichia coli. J. Biol. Chem.* 259:4917-4921.

Monod, J., J. Wyman, and J. P. Changeux. 1965. On the nature of allosteric transitions: A plausible model. *J. Mol. Biol.* 12:88-118.

Nelson, S. W., R. B. Honzatko, and H. J. Fromm. 2001. Spontaneous subunit exchange in porcine liver fructose-1,6-bisphosphatase. *FEBS Letters*. 492:254-258.

Nelson, S. W., R. B. Honzatko, and H. J. Fromm. 2002. Hybrid tetramers of porcine liver fructose-1,6-bisphosphatase reveal multiple pathways of allosteric inhibition. *J. Biol. Chem.* 277:15539-15545.

Ortigosa, A. D., J. L. Kimmel and G. D. Reinhart. 2003. Disentangling the web of allosteric communication in an oligomer: Heterotropic inhibition of phosphofructokinase from *Bacillus stearothermophilus* (Manuscript in preparation).

Pace, C. N., F. Vajdos, L. Fee, G. Grimsley, and T. Gray. 1995. How to measure and predict the molar absorption coefficient of a protein. *Prot. Science*. 4:2411-2423.

Pan, H., C. Lee, and V. J. Hilser. 2000. Binding sites in *Escherichia coli* dihydrofolate reductase communicate by modulating the conformational ensemble. *Proc. Natl. Acad. Sci. USA*. 97:12020-12025.

Pawlyk, A. C., and D. W. Pettigrew. 2002. Transplanting allosteric control of enzyme activity by protein-protein interactions: Coupling a regulatory site to the conserved catalytic core. *Proc. Natl. Acad. Sci. USA*. 99:11115-11120.

Poorman, R. A., A. Randolph, R. G. Kemp, and R. L. Heinrikson. 1984. Evolution of phosphofructokinase-gene duplication and reaction of new effector sites. *Nature*. 309:467-469.

Reinhart, G. D. 1983. The determination of thermodynamic allosteric parameters of an enzyme undergoing steady-state turnover. *Arch. Biochem. Biophys*. 224:389-401.

Reinhart, G. D. 1988. Linked-function origins of cooperativity in a symmetrical dimer. *Biophys. Chem*. 30:159-172.

Riley-Lovingshimer, M. R., and G. D. Reinhart. 2001. Equilibrium binding studies of a tryptophan-shifted mutant of phosphofructokinase from *Bacillus stearothermophilus*. *Biochemistry*. 40:3002-3008.

Riley-Lovingshimer, M. R., and G. D. Reinhart. 2002. Reversible ligand-induced dissociation of a tryptophan-shifted mutant of phosphofructokinase from *Bacillus stearothermophilus*. *Biochemistry*. 41:12967-12974.

Sanger, F., S. Nicklen, and A. R. Coulson. 1977. DNA sequencing with chain-terminating inhibitors. *Proc. Natl. Acad. Sci. USA*. 74:5463-5467.

Schirmer, T., and P. R. Evans. 1990. Structural basis of the allosteric behavior of phosphofructokinase. *Nature*. 343:140-145.

Serre, M. C., W. Teschner, and J. R. Garel. 1990. Specific suppression of heterotropic interactions in phosphofructokinase by the mutation of leucine 178 into tryptophan. *J. Biol. Chem.* 265:12146-12148.

Shirakihara, Y., and P. R. Evans. 1988. Crystal structure of the complex of phosphofructokinase from *Escherichia coli* with its reaction products. *J. Mol. Biol.* 204:973-994.

Smith, D. K., R. I. Krohn, G. T. Hermanson, A. K. Mallia, F. H. Gartner, M. D. Provenzano, N. m. Goeke, B. J. Olson, and D. C. Klenk. 1985. Measurement of protein using bicinchoninic acid. *Anal. Biochem*. 150:76-85.

Symcox, M. M., and G. D. Reinhart. 1992. A steady-state kinetic method for the verification of the rapid-equilibrium assumption in allosteric enzymes. *Anal. Biochem*. 206:394-399.

Tlapak-Simmons, V. L., and G. D. Reinhart. 1994. Comparison of the inhibition of phospho(enol)pyruvate and phosphoglycolate of phosphofructokinase from *Bacillus stearothermophilus*. *Arch. Biochem. Biophys*. 308:226-230.

Tlapak-Simmons, V. L., and G. D. Reinhart. 1998. Obfuscation of allosteric structure-function relationships by enthalpy-entropy compensation. *Biophys. J.* 75:1010-1015.

Uyeda, K. 1979. Phosphofructokinase. *Adv. Enzymol. Relat. Areas Mol. Biol*. 48:193-244.

Valdez, B. C., B. A. French, E. S. Younathan, and S. H. Chang. 1989. Site-directed mutagenesis in *Bacillus stearothermophilus* fructose-6-phosphate 1-kinase. *J Biol. Chem*. 264:131-135.

Weber, G. 1972. Ligand binding and internal equilibrium in proteins. *Biochemistry*. 11:864-878.

Weber, G. 1975. Energetics of ligand binding to proteins. *Adv. Prot. Chem*. 29:1-83.

Wyman, J. 1964. Linked functions and reciprocal effects in hemoglobin: A second look. *Adv. Protein Chem*. 19:223-286.

Wyman, J. 1967. Allosteric linkage. *J. Am. Chem. Soc*. 89:2202-2218.

Zell, R., and H. J. Fritz. 1987. DNA mismatch-repair in *Escherichia coli* counteracting the hydrolytic deamination of 5-methyl-cytosine residues. *EMBO Journal*. 6:1809-1815.

VITA

Allison Dawn (Waldenstrom) Ortigosa
2416 Northeast 12th Terrace
Pompano Beach, FL 33064

Education:

Kalamazoo College	Health Science	B.A.	1997
Texas A&M University	Biochemistry	Ph.D.	2003

Publications:

Ortigosa, A. D., J. L. Kimmel, and G. D. Reinhart. 2003. Disentangling the web of allosteric communication in an oligomer: Heterotropic inhibition of phosphofructokinase from *Bacillus stearothermophilus* (Manuscript in preparation).

Ortigosa, A, D., and G. D. Reinhart. 2003. Contributions of multiple allosteric ligands are unique and additive. (Manuscript in preparation).

Awards:

2003	Biophysical Society Student Research Achievement Award
2003	11th Annual Department of Biochemistry and Biophysics Research Competition 1st Place

Professional Societies:

Protein Society
Biophysical Society